Title
Challenging the Dogma of Canonical BMP signaling in the absence of Smad4 during Endochondral Bone Formation

Author
Rigueur, Diana

Publication Date
2016

Peer reviewed|Thesis/dissertation

UNIVERSITY OF CALIFORNIA

Los Angeles

Challenging the Dogma of Canonical BMP Signaling in the Absence of Smad4 during Endochondral Bone Formation.

A dissertation submitted in partial satisfaction

of the requirements of the

Doctor of Philosophy in Molecular, Cell, and Developmental Biology

by

Diana Rigueur

2016

ABSTRACT OF THE DISSERTATION

Challenging the Dogma of Canonical BMP Signaling in the Absence of Smad4 during Endochondral Bone Formation.

by

Diana Rigueur

Doctor of Philosophy in Molecular, Cell, and Developmental Biology

University of California, Los Angeles, 2016

Professor Karen Marie Lyons, Chair

Endochondral bone formation involves a highly coordinated program of chondrocyte differentiation, proliferation, maturation, and hypertrophy. The Bone Morphogenetic Protein (BMP) and Transforming Growth Factor beta (TGFb) and Activin signaling pathways are regulators of these processes. The importance of the BMP type I receptors had been well documented; however, the physiological role of the BMP type I receptor Activin Like Kinase 2 (ALK2/ACVR1) during the process of mammalian endochondral bone formation was unknown. The ALK2 receptor gained its infamy when activating mutations in it were discovered to cause the devastating disease fibrodysplasia ossificans progressiva (FOP), an autosomal dominant condition that causes paralysis and early death due to ossification of soft connective tissue. Early *in vivo* and *in vitro* chick studies revealed that the ALK2 receptor plays an important role in the formation of cartilage and bone. However, the physiological relevance of ALK2 in mammalian

skeletal tissues remained unknown. Furthermore, whether ALK2 receptor impacts BMP signaling in the development of skeletal tissues as strongly as and/or has overlapping functions with those of the other BMP Type I receptors ALK3/BMPR1A and ALK6/BMPR1B remained unclear. My studies addressed these unknowns.

Previous studies in the laboratory of Professor Karen Lyons had shown that the main transducers of the BMP signaling pathways in cartilage are the receptor regulated Smads (R-Smads) 1, 5, and 8. This was demonstrated by the observation that cartilage-specific knockouts of all three Smads recapitulated the phenotype seen in mice lacking the BMP receptors ALK3 and ALK6. Smad4, a co-Smad that complexes with R-Smads, was thought to be required for all transcriptional R-Smad activity. However, cartilage specific knockout of Smad4 reported by another group surprisingly rendered a viable mouse. The phenotypic analysis of pre- and postnatal Smad4 mutants was characterized, however, the mechanism by which BMP signaling persisted in the absence of Smad4 remained unclear. The studies in this thesis address the mechanisms underlying this apparent R-Smad-dependent, Smad4-independent signaling. Cartilage specific knockout of Smad4 was found to result in an accumulation of phosphorylated Smads 1/5/8 in the cell that could not be targeted for degradation. Overall these studies showed that the requirement of Smad4 for Smad1/5/8-mediated transcription is, in part, obsolete in systems with persistent BMP signaling such as the developing cartilage growth plate. However, Smad4 appears to be required in events that require temporal, rapid, and potent signaling, like that of limb bud development. Therefore, Smad4 plays a role in regulating the duration and strength of BMP signaling.

This thesis includes one published review and two original articles (one of which has been published). The known mechanisms by which BMP signaling regulates chondrogenesis and cartilage maintenance will be highlighted in Chapter One, “BMP signaling in Skeletogenesis” and Chapter Two “TGFb signaling in Cartilage Development and Maintenance”. The roles of the BMP type I receptors ALK2/ALK3/ALK6, with a focus on ALK2, will be highlighted in Chapter Three. This work has been published. The novel Smad4-independent, Smad1/5/8-dependent signaling pathway will be the subject of Chapter Four “ Challenging the Dogma of Canonical BMP signaling in the absence of Smad4 during endochondral bone formation”. Next, a short methods paper highlighting the art of skeletal tissue staining will be outlined in Chapter Five “Whole-Mount Skeletal Staining”. This work has been published. Finally, Chapter Six will discuss the overall conclusions and future directions of my thesis project.

The dissertation of Diana Rigueur is approved.

Daniel Howard Cohn

Maria Luisa Iruela-Arispe

Kristina Bostrom

Volker Hartenstein

Karen Marie Lyons, Committee Chair

University of California, Los Angeles

2016

TABLE OF CONTENTS

LIST OF FIGURES AND TABLES

ACKNOWLEDGMENTS:

I thank my past and current mentors who have shaped me into the scientist I am today: Dr. Alison Miyamoto, my first scientific mentor at CSUF (California State University, Fullerton), taught me the basics of scientific investigation and the fundamentals of scientific writing. Although I can still improve, I would not be as competent a writer without her guidance. Dr. Amybeth Cohen helped me become a competitive applicant for graduate school and without her guidance, I would not be getting a Ph.D. Dr. C.-Ting Wu, whom I worked for at Harvard, was always very supportive of my work and taught me that research in lower organisms, such as Drosophila, can help uncover many biological mysteries in the mammalian system. Lastly, Dr. Karen M. Lyons, my current mentor and advisor, has given me the room I needed to become an independent researcher. I had so much fun working and interacting with Karen that I honestly did not notice the years fly by. These last years have been the best scientific experience of my life and I hope that I have not reached my cap on fun in my scientific career. She always encouraged me to collaborate, try new scientific techniques, and to aim for well established and high impact journals, which I am sure will be essential in my future in academic research.

I also thank my current and previous lab members for their assistance and encouragement. Ghazal Bahri, a lab partner in the Miyamoto lab, taught me the importance of having a lab family and motivated me with her tireless energy and diligent work ethic to push my scientific boundaries. Teni Anbarchian, my first undergraduate student researcher during my years as a graduate student in the Lyons lab, and now at Stanford graduate school, taught me how to have patience with future students and therefore has greatly influenced my

teaching/mentoring style. To Jong Kim Kil (Charlie), Kenneth Pessino, Austin Rike, my other undergraduate students, I thank you for helping me remember the initial feeling of excitement during scientific discovery. I would also like to thank Nancy Morones and Marissa Foster, my last two undergraduate students who are going to Yale and Berkeley for graduate school, respectively, for keeping me company the last two wonderful years of my graduate career. Lastly, I thank YooJin Lee, our lab technician and manager, for bringing me smiles every day and helping me with experiments when I had my hands full. I am grateful for her input when nothing seemed to work as planned.

Most importantly I thank my parents, Maria and Chester Smith, and my siblings Jonathan, Derek, and Kevin Smith for their unconditional love and support to follow my aspirations. Lastly, I would like to thank my partner in crime, Nathan Elis Jackson, for supporting my every decision for the past 10 years. I hope that we can continue to support, inspire, and challenge each other for many years to come.

Chapter Two is a reprint of "TGFb Signaling in Cartilage and Maintenance" from *Birth Defects Research Part C: Embryo Today Reviews* Volume 102, Issue 1, Pages 37-51 with permission from John Wiley and Sons.

Chapter Three is a reprint of "The Type I BMP receptor ACVR1/ALK2 is Required for Chondrogenesis During Development" from the *Journal of Bone and Mineral Research,* Volume 4, pages 733-741 with permission from John Wiley and Sons.

Chapter Five is a reprint of "Whole-Mount Skeletal Staining" *Methods in Molecular Biology*, Volume 1130, Pages 113-21 with permission from Springer.

Appendix A is a reprint of "GATA4 Is Essential for Bone Mineralization via ERα and TGFβ/BMP Pathways" from the *Journal of Bone and Mineral Research,* Volume 29, pages 2676-2687 with permission from John Wiley and Sons.

Appendix B is a reprint of "TGFβ and BMP Dependent Cell Fate Changes Due to Loss of Filamin B Produces Disc Degeneration and Progressive Vertebral Fusions" from the online all open access journal *Plos Genetics,* Volume 12, Pages 1-22.

VITA

2005-2010	B.S. Biological Science California State University, Fullerton
2008-2010	Maximizing Access to Research Careers Scholar, National Institute of Health Research Award. California State University, Fullerton
2009	Summer Undergraduate Research Program (SHURP) Scholar, National Institute of Health Research Award Harvard Medical School
2010-2016	Ph.D. Molecular, Cell and Developmental Biology Eugene-Cota Robles Award National Institute of Health Supplement Research Award University of California, Los Angeles

PUBLICATIONS

03/2016

- J. Zieba,, K.N. Forlenza, J.S. Khatra, A. Srukhanov, I. Duran, **D. Rigueur**., K.M. Lyons, D.H. Cohn, AE Merrill., D. Krakow. "TGFβ and BMP dependent Cell Fate Changes Due to Loss of Filamin B Produces Disc Degeneration and Progressive Vertebral Fusions. *PloS Genetics.* 12(3):e1005936.. (2016). doi: 10.1371/journal.pgen.1005936

11/2014

- **D. Rigueur**, S. Brugger, T. Anbarchian, J. K. Kim, Y. Lee, K. Lyons. The type I BMP receptor ACVRI/ALk2 is required for chondrogenesis during development. *Journal of Bone and Mineral Research*. 30(4):733-41. (2015). doi: 10.1002/jbmr.2385.

10/2014

- M. Guemes, A. J. Garcia, **D. Rigueur**, S. Runke, W. Wang, G. Zhao, V.H. Mayorga, E. Atti, S. Tetradis, B. Peult, K. Lyons, G. A. Miranda-Carboni and S. A. Krum. "Gata4 is essential for bone mineralization via ER-alpha and TGFb/BMP pathways". *Journal of Bone and Mineral Research.* (2014) DOI 10.1002/jbmr.2296.

3/2014

- W. Wang, **D. Rigueur**, and K. Lyons. TGFβ signaling in cartilage development and maintenance. *Birth Defects Research Part C Embryo Today Reviews 03/2014*; 102(1). DOI 10.1002/bdrc.21058.

01/2014

- **D. Rigueur** and K. Lyons. Whole-Mount Skeletal Staining. *Methods in molecular*

biology. 1130:113-121. DOI 10.1007/978-1-62703-989-5_9.

PRESENTATIONS

03/2015

- **D. Rigueur**, K. Lyons: Challenging the dogma of canonical BMP signaling in the absence of Smad4. *Gordon Conference Cartilage Biology and Pathology 2015.* Galveston, Texas. (Oral and poster presentation).

09/2014

- **D. Rigueur**, K. Lyons. "Challenging the dogma of canonical BMP signaling in the absence of Smad4." *American Society of Bone and Mineral Research 2014.* Houston, Texas. (Plenary poster presentation).

04/2013

- **D. Rigueur,** K. Lyons. "Challenging the dogma of canonical BMP signaling in the absence of Smad4." *Gordon Conference Cartilage Biology and Pathology 2013.* Les Diablerets, Switzerland. (Poster presentation).

03/2011

- **D. Rigueur**, K. Lyons. "Challenging the dogma of canonical BMP signaling in the absence of Smad4." *Society for Developmental Biology West Coast Regional Conference 2013.* Cambria, California. (Oral and poster presentation).

04/2010

- **D. Rigueur**, A. Miyamoto, E. Garret. "Microfibril-associated Glycoprotein-2 (MAGP-2) is ectopically expressed in ovarian carcinoma cells." *Inter Club Council 2010*. California State University, Fullerton, Fullerton, CA. (Oral presentation).

04/2010

- **D. Rigueur**, A. Miyamoto, E. Garret. "The elastic fiber protein MAGP-2 is ectopically expressed in ovarian carcinoma cells." *Experimental Biology 2010.* Anaheim, CA (Poster Presentation).

10/2009

- **D. Rigueur**, A. Miyamoto, E. Garret. "Microfibril-associated Glycoprotein-2 (MAGP-2) and its role in the progression of ovarian cancer." *SACNAS National Conference 2009,* Dallas, TX. (Poster Presentation)

09/2009

- **D. Rigueur**, A. Miyamoto, E. Garret. "Microfibril-associated Glycoprotein-2 (MAGP-2) and its role in the progression of ovarian cancer." MARC Pro-seminar, CSUF, Fullerton, CA. (Oral Presentation)

07/2009

- Miyamoto, E. Garret, **D. Rigueur**. "Elastin and Elastic Fibers" *Gordon Research Conference 2009,* Biddeford, ME. (Poster Presentation)

07/2009

- **D. Rigueur**, M. Jakubic, C.-Ting Wu. "Homologous Chromosome pairing in *Drosophila melanogaster." Leadership Alliance National Symposium 2009,* Chantilly, VA (Poster Presentation

CHAPTER ONE

BMP Signaling in Skeletogenesis

Introduction

Cartilage and bone are dynamic tissues that provide mechanical support and protect essential organs, a property only attributed to the skeleton. The skeleton is essential for maintenance and homeostasis of hematopoiesis and serves as a calcium reserve in times of improper nutrition. Remodeling of the skeleton is regulated by systemic and paracrine factors, and it in turn can act as a regulator of systemic homeostasis. No more than 60 years ago, Bone Morphogenetic Proteins (BMPs) isolated from crushed bone were discovered to induce ectopic cartilage and bone formation in vivo when injected into tissues. Cloning and production of BMP like polypeptides revealed that BMPs are a subgroup of a large family of transforming factors. Therefore, these proteins were categorized under the Transforming Growth Factor beta (TGFb) Superfamily. BMPs play an essential role in patterning and the development of non-skeletal tissues. In particular BMP signaling plays strong and imperative roles in dorsal/ventral patterning, internal organ formation, muscle, and in subsets of neuronal cell fate. Other than patterning, at the molecular level, BMPs are important for cell survival and regulation of apoptosis. A brief introduction into the multiple roles BMPs and their respective receptors play in skeletal tissues is highlighted in this chapter.

1.1. BMP signaling in pre-chondrocyte condensations

BMPs

Marshall Urist reported the discovery of bone morphogenetic proteins (BMPs) in 1965 (Urist, 1965). He found that subcutaneously implanted decalcified bone could induce ectopic cartilage and bone formation. Subsequent purification of these cartilage and bone-conductive factors led to the discovery of BMPs. Found in organisms ranging from invertebrates, such as *Drosophila melanogaster*, to vertebrates, such as mice and humans, BMPs are expressed throughout embryogenesis and through adulthood in many tissues (Bandyopadhyay et al., 2013; Chu et al., 2004; Wisotzkey et al., 1998). BMPs form homo- or heterodimers linked by disulfide bonds, and bind to their respective heterodimeric complexes of type I and type II BMP receptors (Massague et al., 2005). As the name implies, BMPs can act as morphogens, inducing distinct effects according to specific protein concentrations, ultimately modulating transcription of BMP controlled genes. BMPs influence diverse cell functions including proliferation, cell fate determination, differentiation, and survival. Absence of most of these proteins leads to defects in overall development, patterning, and/or survival.

There are over 30 TGF-β superfamily ligands, of which a large portion encompasses BMPs and growth and differentiation factors (GDFs) (Ducy and Karsenty, 2000). Patterns of BMP expression reflect their potential functions in the developing embryo. BMPs are expressed in an array of tissues from all three of the primary germ layers. Examples include mesodermal cells of the amnion, chorion cells of the visceral endoderm, the lateral plate mesoderm underlying the head fold, and the ectoderm of the neural tube. Phenotypes that highlight the

developmental impact of BMP ligands are the early embryonic lethality that results from knockouts of BMPs 2 and 4, independently in mice (Winnier et al., 1995).

1.2 BMP signaling in joint formation

In the early developing limb, BMPs play a crucial role in the formation of mesenchymal condensations and the formation of the joints. For example, BMP5 expression marks a subset of mesenchymal condensations such as the genital tubercle, the ribcage sternum, thyroid cartilage, cartilage rings of the trachea, and cells forming part of the vertebrae (Storm, 1999). As is the case for TGF-β, BMPs have been shown to induce the formation of prechondrogenic condensations (Barna et al., 2007; Pizette et al., 2000). GDF5 has a critical role in joint formation. GDF5 stimulates cartilage formation and then restricts the expression of joint molecular markers to the appropriate location. GDF5 also induces the apoptosis necessary for cavitation where the future joint will form (Storm et al., 1994; Brunet et al., 1998; Storm and Kinsley, 1999; Baur et al., 2000). There are appendicular skeletal abnormalities associated with mutations with GDF5 in humans and mice, such as short limbs, altered shape and number of bones, and brachypodism; however, these mutations in GDF5 do not yield craniofacial or axial skeletal phenotypes (Francis-West and Macpherson, 1999; Provot and Schipani, 2005).

Noggin, a BMP antagonist, suppresses the formation of mesenchymal condensations, such that in the absence of noggin, cartilage primordia are enlarged. The consequences of noggin ablation reflect its role in joint formation. In the absence of noggin, no joint formation ensues due to an unbalanced GDF5 stimulation. In humans, heterozygous mutations in Noggin resulted

in either proximal symphalangism or multiple synostosis, phenotypes characterized by the display of joint fusions (Brunet, 1998).

After mesenchymal condensation, BMPs are expressed in the perichondrium of the developing cartilage primordium (Minina et al., 2001). BMPs expressed here include BMP-2, -3, -4, -5, and -7; however, some are expressed in other structures within the long bones. For example, BMP-7 is found in proliferating chondrocytes, while BMP-2 and -6 are expressed in hypertrophic chondrocytes (Minina et al., 2002). BMPs have been shown to be positive regulators of chondrocyte proliferation and alternatively, negative regulators of chondrocyte terminal differentiation (Minina et al., 2002; Provot and Schipani, 2004).

1.3 BMP Receptors in growth plate formation

The BMP type I receptors include Alk2 (ActR1/ACVR1), Alk3 (BMPR1A), and Alk6 (BMPR1B). They are activated by complexing with constitutively active BMP Type II receptors via transphosphorylation of serine/threonine residues, a process mediated by ligand binding (Massague et al, 2005). To transduce the signal, type I receptors phosphorylate intracellular Smads, which translocate to the nucleus to modulate transcription. Several BMP and GDFs ligands elicit responses through the receptors. In earlier literature, it was shown that although all of the type I BMP receptors activate a common set of Smads, the BMP type I receptors conveyed different functions, contributing to the diversity of actions during development. There was some evidence for this hypothesis. Characterization of *Bmpr1a* and *–b* expression in chick revealed low expression of *Bmpr1a* in developing limb bud mesenchyme, while *Bmpr1b* displayed expression in pre-cartilaginous condensations. Furthermore, while constitutively active forms of

BMPR1A or –B promoted chondrogenesis, only dominant negative (DN) BMPR1B and not either DN-BMPR1A or DN-ActR1, blocked chondrogenesis. This result suggested that BMPR1B was the main transducer of BMP signals in limb condensations (Lehmann et al., 2003). However, *Bmpr1b* null mice displayed a skeletal phenotype restricted to phalangeal elements, contradicting the previous conclusion and thus suggesting that perhaps BMPR1A sustains chondrogenesis through an overlapping function, or rather is the prominent receptor.

Mouse knockout studies in cartilage uncovered the *in vivo* overlapping functions of *Bmpr1a* and *–b* (Yoon et al., 2005). Double ablation of both *Bmpr1a* and *–b* resulted in severe chondrodysplasia, suggesting that the remaining ActR1 receptor cannot sustain chondrogenesis on its own, and that BMP signaling is imperative for chondrogenesis. In sum, BMPRIA and -B are functionally redundant for many aspects of chondrogenesis, working to elicit proliferation, survival, and differentiation (Retting et al., 2009; Yoon et al., 2005).

ActR1/ALK2/Acvr1 is more promiscuous than BMPR1A/ALK3 or BMPR1B/ALK6; in addition to binding to a subset of BMP ligands, including BMPs 2 and 7, it can also be activated by TGFβ ligands; however ActRI transduces a BMP signal via phosphorylation of Smads 1/5/8 (Clarke, 2001; Ehnert et al., 2012; Luo et al., 2010). Its expression pattern has been detected in the axial skeleton within vertebral column mesenchymal condensations. Mouse knockout studies in neural crest cells revealed that ActR1 plays a role in cranial development, producing cleft palate and hypotrophic mandible defects (Dudas et al., 2004). Moreover, constitutive activation of ALK2 due to a point mutation causes fibrodysplasia ossificans progressiva (FOP), a disorder characterized by progressive ossification of connective tissue as well as ectopic endochondral bone formation (Groppe et al., 2011).

There are now three mechanisms proposed for ectopic endochondral bone formation in FOP patients via the ALK2 receptor: ligand-independent constitutive activity, ligand-dependent receptor hyperactivity, and ectopic ligand-dependent hyperactivity of BMP signaling induced by Activin A, an antagonist turned agonist in FOP patients with ALK2 receptor mutations (Hino et al., 2015). These studies highlight the versatility and overlapping functions of BMP receptors; they also highlight the importance of understanding the different BMP and TGFb ligand binding properties to each type of BMP and TGFb receptor for understanding disease.

There are few developmental defects associated with aberrant ALK2 activation in FOP; thus ALK2's role in endochondral bone formation had yet to be addressed. Our lab generated a cartilage specific ALK2 deficient mouse that was used to reveal ALK2's in vivo function in the growth plate. ALK2/BMPR1A and ALK2/BMPRIB cartilage specific double knockouts were also analyzed. As will be discussed below, our studies revealed that ALK2 is required for chondrogenesis, particularly in craniofacial and axial elements, but exerts coordinated functions with both BMPR1A and BMPR1B.

Knockout studies have been fundamental in revealing the underlying roles of each receptor in cartilage. As discussed, such studies have been performed for the type I BMP receptors ALK3, and ALK6, and Chapter Three addresses the function of ALK2. The remaining type I BMP receptor is ALK1. Cartilage specific knockout of ALK1, a BMP Type I receptor that is activated by either TGFb or BMP ligands, leads to no obvious skeletal defects; however, when a compound ALK1;ALK5 cartilage knockout is generated, loss of ALK1 rescues the majority of defects caused by loss of ALK5 (data not shown; unpublished data from the Karen Lyons laboratory). Only through combinatorial compound knockouts and knock-ins will scientists

uncover the breadth of roles that BMP signaling plays in the production and maintenance of skeletal elements, cartilage and bone.

1.4 Smad-dependent roles in growth plate formation

The Smads

The Smad proteins are a set of transcription factors known to transduce the extracellular signals of BMP and TGFβ receptors. These proteins were first discovered in *Drosophila melanogaster*, the common fruit fly. These Smad proteins are conserved in vertebrate and invertebrate species. The Smads are believed to be the major signaling effectors of the TGFβ superfamily. Smad proteins can be divided into three groups: the receptor Smads (R-Smads), co-Smad (Smad4), and inhibitory Smads (I-Smads 6 and 7) (Derynck et al., 2005; Massague et al., 2005). Canonical BMP signaling is defined by the complex of Smad4 with phosphorylated Smads 1/5/8 driving transcription of BMP target genes, where as TGFβ's canonical signaling transduction involves phosphorylated Smads2/3 in a complex with Smad4 (Derynck, 2005). The R-Smads and Co-Smad4 contain two globular structures called the MH1 and MH2 domain, that are attached by a region know as the linker domain. The MH1 domain is necessary for DNA binding, while the MH2 domain is important for interactions with other Smads. The linker region is necessary for regulation of Smad activity and for target degradation (Alarcon et al., 2009; Fuentealba et al., 2007). A schema of the Smads is shown in Figure 1.

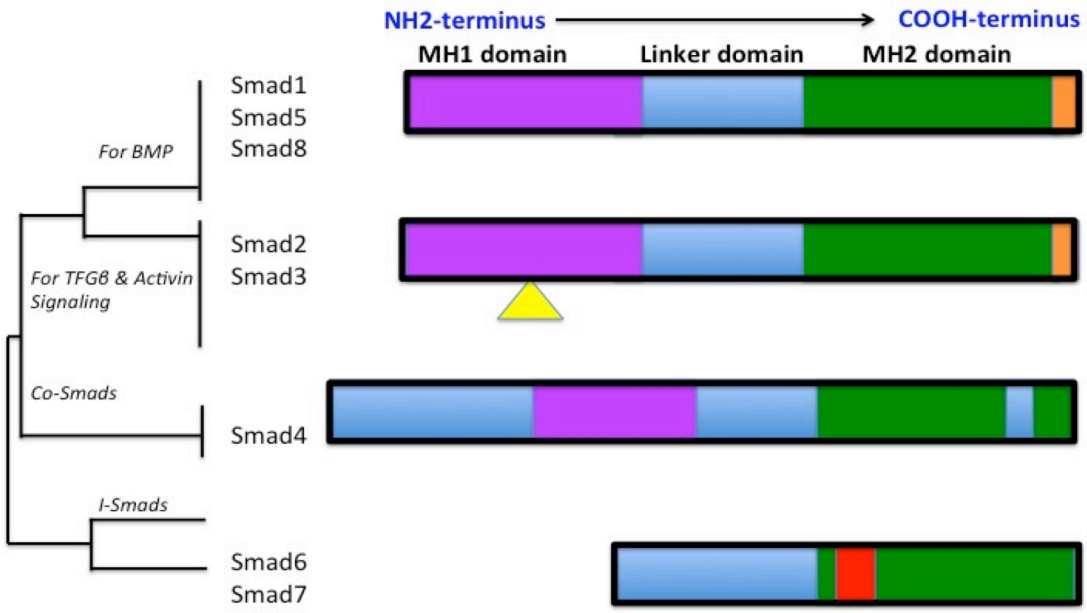

Figure 1. Dendrogram of the Smad family of proteins. Sequence homology is shown on the right. The orange represents the receptor phosphorylation sites at the C-terminus of the R-Smads. The triangle represents the alternatively spliced insert in Smad2.

Smad1/5/8 function in growth plate development

BMP signaling encompasses two main avenues for signal transduction: canonical and non-canonical. The transducers of canonical BMP signaling pathway are receptor-mediated Smads (R-Smads) 1, 5, and 8 (Retting et al., 2009). These transcription factors complex with Smad4, translocate into the nucleus and activate or repress BMP target genes. The main non-canonical pathway is mediated through activation of the MAP3K TAK1. The roles of canonical and non-canonical pathways as BMP transducers in cartilage became apparent when analyzing mouse models. Cartilage specific ablation of MAP3K (TAK1) resulted in a viable mouse, while cartilage specific knockout of Smads 1/5/8 resulted in severe lethal chondrodysplasia, a phenotype similar to that caused by absence of the two type I BMP receptors, BMPR1A and BMPR1B (Greenblatt et al., 2010; Gunnell et al., 2010; Yoon et al., 2005). These data suggested that Smad1/5/8 were the main transducers of the BMP signaling pathway (Retting et al., 2009). Transcriptional analysis of BMP target genes, i.e. *Ihh (Indian Hedgehog),* as well as non-canonical pathway genes, TAK1 and Mekk3, revealed significantly reduced expression in Smad1/5/8 deficient chondrocytes, indicating that Smads1/5/8 are required for both arms of the BMP signaling pathway, and overall for chondrocyte (Retting et al., 2009)

Smad4-dependent and independent functions in growth plate development

In the canonical BMP signaling pathway, the intracellular receptor regulated Smads (R-Smads) 1, 5 and 8 transduce the signal by complexing with co-Smad4 and migrating to the nucleus, to activate or repress BMP target genes. The majority of studies to date indicate that Smad4 is an essential component of canonical BMP signaling. However, there is some evidence in *Drosophila* that R-Smads transduce a limited amount of signaling in the absence of Smad4.

Until recently, this has not been seen in vertebrates. Recent findings provide evidence that Smad1/5-dependent, Smad4 independent BMP signaling does occur in vertebrates, and in the context of the cartilage growth plate, may be the major mode of BMP signaling. We find that cartilage-specific loss of Smads1/5/8 results in severe chondrodysplasia, yet cartilage-specific Smad4-knockout mice are viable and present with a much milder cartilage phenotype (Zhang et al, 2005; Retting et al., 2009). A well-characterized BMP target gene, *Ihh*, albeit reduced, responds to BMP stimulation in isolated Smad4 deficient primary chondrocytes (Seki and Hata, 2004; Zhang et al., 2005). Smad4, however, is required at a stage prior to establishment of chondrogenic cell fate for proper development of the zeugo- and autopodal skeletal elements (Benazet and Zeller, 2013). Overall, these data exemplify that some systems may require Smad4 for canonical BMP transduction; however, Smad4 may be dispensable for other systems or developmental events, calling for a re-evaluation of the putative BMP canonical pathway and the extent of BMP signaling.

Smad6 and Smad7 function in growth plate development

BMP signaling intensity and duration are regulated both extracellular and intracellular factors. Extracellular regulation can occur via antagonists, such as chordin, noggin, and follistatin, which sequester BMP ligands and prevent them from binding to BMP receptors. Intracellular regulation can occur through inhibitory Smads (I-Smad) 6 and 7. Smad7 inhibits both BMP and TGFβ, whereas Smad6 specifically inhibits BMP signaling (Iwai et al., 2008; Massague et al., 2005). I-Smads can block R-Smad phosphorylation by forming stable associations with activated type I receptors (Hata, 1998; Hayashi, 1997; Nakao, 1997). I-Smads are also able to recruit E3 ubiquitin ligases (Smurf1) to type I receptors and R-Smads, targeting

them for degradation (Inoue and Imamura, 2008; Murakami et al., 2003). Smad6 has also been shown to antagonize BMP signaling by directly associating with receptor activated Smad1, and thus interfering with Smad1-Smad4 complex formation (Hata, 1998; Iwai et al., 2008).

Genetic analysis of the physiological roles I-Smads 6 and 7 play during multiple aspects of chondrogenesis have been recently revealed. Although previous gain-of-function studies showed an important role for both Smad6 and 7 *in vitro*, *in vivo* loss-of-function studies honed I-Smad function during endochondral bone formation (Horiki et al., 2004). Growth plate analysis in *Smad6-/-* mice showed that Smad6 was required to limit BMP signaling for proper cartilage development, while growth plate analysis of *Smad7-/-* mice revealed that Smad7 is required for proper terminal maturation of chondrocytes in the growth plate (Estrada et al., 2011; Estrada et al., 2013; Horiki et al., 2004). Smad7 inhibits chondrocyte differentiation at multiple steps during endochondral bone formation while down regulating p38 MAPK pathways (Iwai et al., 2008).

1.5 Summary and perspectives:

With more progression toward understanding the physiological function of TGFb/BMP signaling network components and downstream pathways during cartilage development and maintenance, it is now clear that the composition of receptor complex and cross-talk between Smads and non-Smad signaling pathways determines the final outcome of cellular response to TGF-beta/BMPs. Not every signaling component is well understood in regards to their *in vivo* function in different cartilage developmental stages, for example ALK5 and Smad2 functions are still not clear. Very little is known about the physiological functions of each BMP type I receptor in the maintenance of articular cartilage. Further investigating their in vivo functions using inducible conditional knock out mice, coupled with Chromatin Immunoprecipitation (ChIP) studies will clarify gene targets and their roles. Since cell context will affect the signaling outcome, it is of great interest to know whether and how the signaling network components change in different cartilage development stages, ages, and disease conditions.

Transcriptome and proteome expression profiles of stratified cartilage zones will give us a better picture of the spatial and temporal dynamics of the emergent properties in the whole signaling network. Our knowledge is still far from allowing a comprehensive understanding of how complex interactions among cell signaling pathways work together to regulate specific gene expression and achieve various biological functions in different developmental stages of cartilage. In vivo imaging of protein dynamics and interactions, top-down proteomics analysis of protein complexes (XL-Mass Spec), ChIP-sequencing, RNA-sequencing, loss-of-function and gain-of-function analysis, use of specific inhibitors and activators, RNA interference, conditional knockout and knock-in mouse models, all will further advance our knowledge in these promising

areas. The final goal will be to unravel key molecules in cell signaling pathways or downstream target genes that could be aimed for pharmacological intervention for treatment of pathological conditions of cartilage such as osteoarthritis.

References:

Alarcon, C., Zaromytidou, A. I., Xi, Q., Gao, S., Yu, J., Fujisawa, S., . . . and Massague, J. (2009). Nuclear CDKs drive Smad transcriptional activation and turnover in BMP and TGF-beta pathways. *Cell, 139*(4), 757-769. doi:10.1016/j.cell.2009.09.035.

Bandyopadhyay, A., Yadav, P. S., & Prashar, P. (2013). BMP signaling in development and diseases: a pharmacological perspective. *Biochem Pharmacol, 85*(7), 857-864. doi:10.1016/j.bcp.2013.01.004.

Barna, M., & Niswander, L. (2007). Visualization of cartilage formation: insight into cellular properties of skeletal progenitors and chondrodysplasia syndromes. *Developmental Cell, 12*(6), 931-941. doi:10.1016/j.devcel.2007.04.016

Baur, S. T., Mai, J. J., & and Dymecki, M. (2000). Combinatorial signaling through BMP receptor IB and GDF5: shaping of the distal mouse limb and the genetics of distal limb diversity. *Development, 127*, 605-619.

Benazet, J. D., and Zeller, R. (2013). Dual requirement of ectodermal Smad4 during AER formation and termination of feedback signaling in mouse limb buds. *Genesis, 51*(9), 660-666. doi:10.1002/dvg.22412.

Brunet, L., McMahon, J.A., McMahon, A.P., Harland, R.M. (1998). Noggin, Cartilage Morphogenesis, and Joint Formation in the Mammalian Skeleton. *Science, 280*, 1455-1457.

Chu, G. C., Dunn, N. R., Anderson, D. C., Oxburgh, L., & Robertson, E. J. (2004). Differential requirements for Smad4 in TGFβ-dependent patterning of the early mouse embryo. *Development, 131*(15), 3501-3512. doi:10.1242/dev.01248.

Clarke, T. R., Hoshiya, Y., Yi, S. E., Liu, X., Lyons, K. M., and Donahoe, P. K. (2001). Mullerian inhibiting substance signaling uses a bone morphogenetic protien BMP like pathway mediated by ALK2 and induces Smad6 expression. *Molecular Endocrinology, 15*, 946-959.

Davis, B. N., Hilyard, A. C., Lagna, G., & Hata, A. (2008). SMAD proteins control DROSHA-mediated microRNA maturation. *Nature, 454*(7200), 56-61. doi:10.1038/nature07086.

Derynck, H.-H. F. a. R. (2005). Specificity and versatility in TGFβ Signaling Through Smads. *Annual Review Cell Developmental Biology, 21*, 659-693. doi:10.1146.

Dudas, M., Sridurongrit, S., Nagy, A., Okazaki, K., & Kaartinen, V. (2004). Craniofacial defects in mice lacking BMP type I receptor Alk2 in neural crest cells. *Mech Dev, 121*(2), 173-182. doi:10.1016/j.mod.2003.12.003.

Ducy, P., & Karsenty, G. (2000). The family of bone morphogenetic proteins. *Kidney Int, 57*(6), 2207-2214. doi:10.1046/j.1523-1755.2000.00081.x.

Duprez, D., Bell, E.J., Richardson, M.K., Archer, C.W., Wolpert, L., Brickell, P.M., Francis-West, P.H. (1996). Overexpression of BMP-2 and BMP-4 alters the size and shape of developing skeletal elements in chick limb. *Mechanisms of Development, 57*, 145-157.

Ehnert, S., Zhao, J., Pscherer, S., Freude, T., Dooley, S., Kolk, A., . . . Hube, R. (2012). Transforming growth factor beta1 inhibits bone morphogenic protein (BMP)-2 and BMP-7 signaling via upregulation of Ski-related novel protein N (SnoN): possible mechanism for the failure of BMP therapy? *BMC Med, 10*, 101. doi:10.1186/1741-7015-10-101.

Estrada, K. D., Retting, K. N., Chin, A. M., & Lyons, K. M. (2011). Smad6 is essential to limit BMP signaling during cartilage development. *Journal of Bone and Mineral Research, 26*(10), 2498-2510. doi:10.1002/jbmr.443.

Estrada, K. D., Wang, W., Retting, K. N., Chien, C. T., Elkhoury, F. F., Heuchel, R., & Lyons, K. M. (2013). Smad7 regulates terminal maturation of chondrocytes in the growth plate. *Dev Biol, 382*(2), 375-384. doi:10.1016/j.ydbio.2013.08.021.

P. H. Francis-West, A. Abdelfattah, P. Chen2, C. Allen, J. Parish, R. Ladher, S. Allen, & S. MacPherson, F. P. L., and C. W. Archer. (1999). Mechanisms of GDF-5 action during skeletal development. *Development, 126*, 1305-1315.

Fei, T., Xia, K., Li, Z., Zhou, B., Zhu, S., Chen, H., . . . Chen, Y. G. (2010). Genome-wide mapping of SMAD target genes reveals the role of BMP signaling in embryonic stem cell fate determination. *Genome Res, 20*(1), 36-44. doi:10.1101/gr.092114.109.

Fuentealba, L. C., Eivers, E., Ikeda, A., Hurtado, C., Kuroda, H., Pera, E. M., & De Robertis, E. M. (2007). Integrating patterning signals: Wnt/GSK3 regulates the duration of the BMP/Smad1 signal. *Cell, 131*(5), 980-993. doi:10.1016/j.cell.2007.09.027.

Greenblatt, M. B., Shim, J. H., & Glimcher, L. H. (2010). TAK1 mediates BMP signaling in cartilage. *Ann N Y Acad Sci, 1192*, 385-390. doi:10.1111/j.1749-6632.2009.05222.x.

Groppe, J. C., Wu, J., Shore, E. M., & Kaplan, F. S. (2011). In vitro analyses of the dysregulated R206H ALK2 kinase-FKBP12 interaction associated with heterotopic ossification in FOP. *Cells Tissues Organs, 194*(2-4), 291-295. doi:10.1159/000324230

Gunnell, L. M., Jonason, J. H., Loiselle, A. E., Kohn, A., Schwarz, E. M., Hilton, M. J., & O'Keefe, R. J. (2010). TAK1 regulates cartilage and joint development via the MAPK and BMP signaling pathways. *Journal of Bone and Mineral Research, 25*(8), 1784-1797. doi:10.1002/jbmr.79

Hata A., L. G., Massague J., Hemmati-Brivanlou A. (1998). Smad6 inhibits BMP:Smad1 signaling by the specifically competing with the Smad4 tumor suppressor. *Journal of Cell Biology, 389*(6651), 622-626.

Hayashi H., A. S., Qiu Y, Cai J, Xu YY, Grinnell BW, Richardson MA Jr, Wrana JL, Falb D. (1997). The mad related protein smad7 associates with the TGFβ receptor and functions as an antagonist of TGFβ signaling. *Cell, 89*(7), 1165-1173.

Hino, K., Ikeya, M., Horigome, K., Matsumoto, Y., Ebise, H., Nishio, M., . . . and Toguchida, J. (2015). Neofunction of ACVR1 in fibrodysplasia ossificans progressiva. *Proc Natl Acad Sci U S A, 112*(50), 15438-15443. doi:10.1073/pnas.1510540112

Horiki, M., Imamura, T., Okamoto, M., Hayashi, M., Murai, J., Myoui, A., . . . Tsumaki, N. (2004). Smad6/Smurf1 overexpression in cartilage delays chondrocyte hypertrophy and causes dwarfism with osteopenia. *Journal of Cell Biology, 165*(3), 433-445. doi:10.1083/jcb.200311015.

Inoue, Y., & Imamura, T. (2008). Regulation of TGF-beta family signaling by E3 ubiquitin ligases. *Cancer Science, 99*(11), 2107-2112. doi:10.1111/j.1349-7006.2008.00925.x.

Iwai, T., Murai, J., Yoshikawa, H., & Tsumaki, N. (2008). Smad7 Inhibits chondrocyte differentiation at multiple steps during endochondral bone formation and down-regulates p38 MAPK pathways. *J Biol Chem, 283*(40), 27154-27164. doi:10.1074/jbc.M801175200.

Kim, J., Johnson, K., Chen, H. J., Carroll, S., & and Laughon, A. (1997). Drosophila mad binds to DNA and directly mediates activation of vestigial by Decapentaplegic. *Nature, 388*(17), 304-308.

Kobayashi, T., Papaioannou, G., Mirzamohammadi, F., Kozhemyakina, E., Zhang, M., Blelloch, R., & Chong, M. W. (2015). Early postnatal ablation of the microRNA-processing enzyme, Drosha, causes chondrocyte death and impairs the structural integrity of the articular cartilage. *Osteoarthritis Cartilage, 23*(7), 1214-1220. doi:10.1016/j.joca.2015.02.015

Luo, J., Tang, M., Huang, J., He, B. C., Gao, J. L., Chen, L., . . . He, T. C. (2010). TGFβ/BMP type I receptors ALK1 and ALK2 are essential for BMP9-induced osteogenic signaling in mesenchymal stem cells. *J Biol Chem, 285*(38), 29588-29598. doi:10.1074/jbc.M110.130518

Massague, J., Seoane, J., & Wotton, D. (2005). Smad transcription factors. *Genes Dev, 19*(23), 2783-2810. doi:10.1101/gad.1350705

Morikawa, M., Koinuma, D., Miyazono, K., & Heldin, C. H. (2013). Genome-wide mechanisms of Smad binding. *Oncogene, 32*(13), 1609-1615. doi:10.1038/onc.2012.191

Murakami, G., Watabe, T., Takaoka, K., Miyazono, K., & Imamura, T. (2003). Cooperative inhibition of bone morphogenetic protein signaling by Smurf1 and inhibitory Smads. *Molecular Biology of the Cell, 14*(7), 2809-2817. doi:10.1091/mbc.E02-07-0441

Nakao A., A. M., Moren A., Nakayma T., Christian JL, Heuchel R., Itoh S., Kawabata M., Heldin NE., Heldin CH., Ten Dijke P. (1997). Identification of Smad7, a TGFβ inducible antagonist of TGFβ signalling. *Nature, 389*(6651), 631-635.

Pizette, S., & Niswander, L. (2000). BMPs are required at two steps of limb chondrogenesis: formation of prechondrogenic condensations and their differentiation into chondrocytes. *Dev Biol, 219*(2), 237-249. doi:10.1006/dbio.2000.9610

Provot, S., & Schipani, E. (2005). Molecular mechanisms of endochondral bone development. *Biochem Biophys Res Commun, 328*(3), 658-665. doi:10.1016/j.bbrc.2004.11.068

Retting, K. N., Song, B., Yoon, B. S., & Lyons, K. M. (2009). BMP canonical Smad signaling through Smad1 and Smad5 is required for endochondral bone formation. *Development, 136*(7), 1093-1104. doi:10.1242/dev.029926

Seki, K., & Hata, A. (2004). Indian hedgehog gene is a target of the bone morphogenetic protein signaling pathway. *J Biol Chem, 279*(18), 18544-18549. doi:10.1074/jbc.M311592200

Storm, E. E., Kingsley, D. M. (1999). GDF5 coordinates bone and joint formation during digit development. *Dev Biol, 209*, 11-27.

Wang, W., Lian, N., Li, L., Moss, H. E., Wang, W., Perrien, D. S., Elefteriou, F., Yang, X. (2009). Atf4 regulates chondrocyte proliferation and differentiation during endochondral ossification by activating Ihh transcription. *Development, 136*(24), 4143-4153. doi:10.1242/dev.043281

Winnier, G., Blessing, M., Labosky, P. A., & Hogan, B. L. (1995). Bone morphogenetic protein-4 is required for mesoderm formation and patterning in the mouse. *Genes & Development, 9*(17), 2105-2116. doi:10.1101/gad.9.17.2105

Yoon, B. S., Ovchinnikov, D. A., Yoshii, I., Mishina, Y., Behringer, R. R., & Lyons, K. M. (2005). Bmpr1a and Bmpr1b have overlapping functions and are essential for chondrogenesis in vivo. *Proc Natl Acad Sci U S A, 102*(14), 5062-5067. doi:10.1073/pnas.0500031102

Zhang, J., Tan, X., Li, W., Wang, Y., Wang, J., Cheng, X., & Yang, X. (2005). Smad4 is required for the normal organization of the cartilage growth plate. *Dev Biol, 284*(2), 311-322. doi:10.1016/j.ydbio.2005.05.036

CHAPTER TWO:

TGFβ Signaling in Cartilage Development and Maintenance

Weiguang Wang[1], Diana Rigueur[1,2], and Karen M. Lyons*[1,2,3]

Members of the transforming growth factor beta (TGFβ) superfamily of secreted factors play essential roles in nearly every aspect of cartilage formation and maintenance. However, the mechanisms by which TGFβs transduce their effects in cartilage in vivo remain poorly understood. Mutations in several TGFβ family members, their receptors, extracellular modulators, and intracellular transducers have been described, and these usually impact the development of the cartilaginous skeleton. Furthermore, genome-wide association studies have linked components of the (TGFβ) superfamily to susceptibility to osteoarthritis. This review focuses on recent discoveries from genetic studies in the mouse regarding the regulation of TGFβ signaling in developing growth plate and articular cartilage, as well as the different modes of crosstalk between canonical and noncanonical TGFβ signaling. These new insights into TGFβ signaling in cartilage may open new prospects for therapies that maintain healthy articular cartilage.

Birth Defects Research (Part C) 102:37–51, 2014.

Introduction

Members of the transforming growth factor beta (TGFβ) superfamily of secreted factors play essential roles in nearly every aspect of development, from the generation of germ cells, through gastrulation and organ formation, and into postnatal life. Mutations in several TGFβ family members, their receptors, extracellular modulators, and intracellular transducers have been described, and these commonly impact the development of the cartilaginous skeleton. Furthermore, genome-wide association studies have linked components of the (TGFβ) superfamily to susceptibility to osteoarthritis. This review focuses on recent discoveries from genetic studies in the mouse regarding the regulation of TGFβ signaling in developing growth plate and articular cartilage, as well as the different modes of crosstalk between canonical and noncanonical TGFβ signaling. These new insights into TGFβ signaling in cartilage may open new prospects for therapies that maintain healthy articular cartilage.

ENDOCHONDRAL BONE FORMATION

The skeleton is composed primarily of cartilage and bone. Throughout the axial and appendicular skeleton, with the exception of the skull, the skeleton is formed from a hyaline cartilage template. During development, cells from three distinct lineages (sclerotome, paraxial mesoderm, and neural crest) undergo chondrogenesis through a similar sequence of events to form the cartilage of the embryonic skeleton (Long and Ornitz, 2013; Pitsillides and Beier, 2011) (Fig. 1). The first overt sign of chondrogenesis is aggregation of mesenchymal chondroprogenitor cells into condensations. This process is mediated by elevated expression of various cell adhesion molecules, such as neural cadherin (N-cadherin) and neural cell adhesion molecule (NCAM). These molecules mediate crucial cell–cell interactions and are critical for maintenance of the expression of Sox9, the transcription factor currently known to act earliest in the chondrogenic program (Akiyama and Lefebvre, 2011).

GROWTH PLATE CARTILAGE FORMATION

Cells at the core of the condensations differentiate into chondrocytes. This involves a change in morphology from fibroblast-like to more spherical, along with a significant increase in synthesis of specific extracellular matrix (ECM) molecules. The Sox9 mediated transcriptional program continues, with the collaboration of the structurally related transcription factors Sox5 and 6, driving the expression of collagen types II, IX, and XI, and the major proteoglycan of cartilage, aggrecan (Karsenty et al., 2009; Kronenberg, 2003; Long and Ornitz, 2013). Cells at the periphery of the condensations retain a fibroblastic morphology, and continue to express type I collagen, giving rise to the structure known as the perichondrium (for review see, Karsenty and Kronenberg, 2009).

Chondrocytes in the cores of the condensations initially undergo rapid proliferation that leads to linear growth of the developing skeletal element. Subsequently, chondrocytes in the centers of the elements exit the cell cycle and execute a well-coordinated program of maturation. This ordered process of proliferation and differentiation leads to the formation of stratified zones of cells at different stages of the cell cycle, with continued expression of Sox9 throughout the resting and proliferating chondrocytes. From the ends of the element to the center, these zones include a layer of relatively quiescent cells (resting zone) that exhibit a round cell morphology, a zone of rapidly proliferating cells

[1]Department of Orthopaedic Surgery and Orthopaedic Institute for Children, David Geffen School of Medicine, University of California, Los Angeles, California 90095
[2]Department of Molecular, Cell and Developmental Biology, David Geffen School of Medicine, University of California, Los Angeles, California 90095
[3]Molecular Biology Institute, David Geffen School of Medicine, University of California, Los Angeles, California 90095

Key words: TGFβ signaling; cartilage; development; maintenance

*Correspondence to: Karen M. Lyons, 1Department of Orthopaedic Surgery and Orthopaedic Institute for Children, David Geffen School of Medicine, University of California, Los Angeles, CA 90095. E-mail: klyons@mednet.ucla.edu

Published online in Wiley Online Library (wileyonlinelibrary.com).
Doi: 10.1002/bdrc.21058

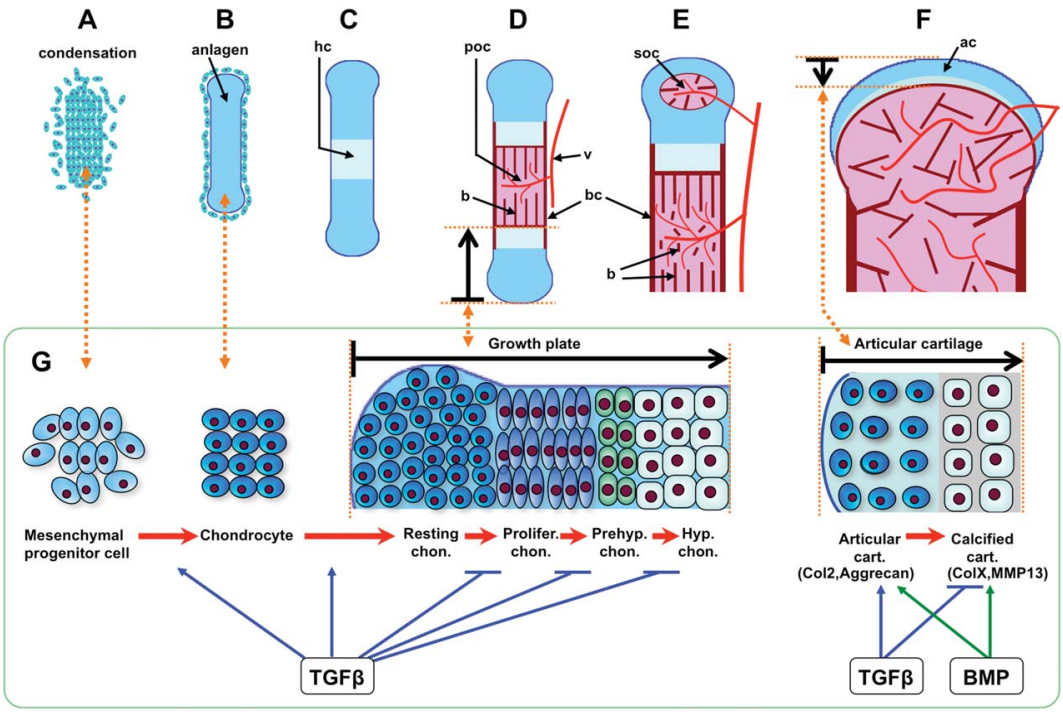

FIGURE 1. *Process of endochondral bone formation and TGFβs role during cartilage development. (**A**) Mesenchymal progenitor cells condense. (**B**) Cells of condensations become chondrocytes that synthesize a collagen II and aggrecan-rich extracellular matrix (ECM), constructing a cartilage template (anlagen) for endochondral ossification. (**C**) Chondrocytes at the center of condensation stop proliferating and become hypertrophic chondrocytes that synthesize a collagen X-rich ECM, the hypertrophic cartilage (hc) is calcified and provides the niche for vascular invasion. (**D**) Hypertrophic chondrocytes undergo apoptosis and attract blood vessels (v) that bring in precursors of osteoblasts, which secret collagen I into ECM, and build the calcified bone (b) in the primary ossification center (poc). Perichondrial cells adjacent to hypertrophic chondrocytes also become osteoblasts, forming bone collar (bc). Chondrocytes continue to proliferate and differentiate in the growth plate that drives the bone elongation. Chondrocytes differentiate into four different cell subtypes, including resting (Rc), proliferative (Plc), prehypertrophic (Phc), and hypertrophic chondrocyte (Hc). (**E**) At the end of the bone, the secondary ossification center (soc) forms through cycles of chondrocyte hypertrophy, vascular invasion, and osteoblast activity. The soc separates the epiphyseal cartilage from the growth plate cartilage. (**F**) Epiphyseal cartilage becomes articular cartilage (ac) at the end of bone. In humans the primary and secondary ossification centers fuse after puberty, whereas in adult mice a narrow region of growth plate cartilage remains. (**G**) During cartilage development, TGFβ signaling promotes mesenchymal cell condensation and differentiation into chondrocytes, and maintains resting chondrocytes in a quiescent stage. It prevents chondrocytes from further differentiating into proliferative cells, and inhibits prehypertrophic and hypertrophic differentiation. In articular cartilage, TGFβ signaling cooperates with BMP signaling to stimulate anabolic function of chondrocytes, for example, enhancing collagen II (Col2) and aggrecan expression. On the contrary, TGFβ signaling antagonizes BMP signaling to prevent calcification and catabolic gene expression, such as collagen X (ColX) and matrix metallopeptidase 13 (MMP13).*

that have a more flattened morphology and form stacks (columnar or proliferative zone), a zone of postmitotic cells that begin to enlarge and are characterized by the expression of *Indian Hedgehog* (*Ihh*) and decreased expression of *Sox9* (prehypertrophic zone), and a zone of terminal enlarged chondrocytes (hypertrophic zone). Most of these undergo cell death, leaving an ECM that is replaced by bone-forming osteoblasts (Shapiro et al., 2005). Hypertrophic chondrocytes produce a unique mineralized ECM containing type X collagen. These cells also produce matrix metalloproteinase 13 (MMP-13), which modifies the ECM to facilitate vascular invasion. The invading vasculature permits the entry of osteoprogenitors, which differentiate into osteoblasts. These cells build the bone matrix and subsequently replace the cartilage.

ARTICULAR CARTILAGE FORMATION AND MAINTENANCE

Unlike growth plate cartilage, which is eventually replaced by bone in most species, articular cartilages are permanent structures. Articular cartilage is formed during

embryonic stages at sites of joint formation, but is not replaced by bone and instead remains and develops during postnatal stages of growth (Chan et al., 2012). Articular cartilage is distinct from growth plate cartilage in terms of ECM content, cellular organization, and mechanical properties (Iwamoto et al., 2013). Briefly, there are fewer cells in this structure, and they are embedded as solitary cells within a distinct ECM that contains more collagen crosslinks than in growth plate cartilage. Mature articular cartilage has a zonal organization that is divided into a superficial layer, a mid layer, the deep layer, and the calcified layer, in order from the surface of articular cartilage toward the bone (Las Heras et al., 2012; Poole, 2003).

Within this cartilage, through mechanisms that are not well understood, the nonhypertrophic Sox trio (Sox9/5/6) program is maintained and chondrocyte differentiation is blocked, resulting in a permanent cartilage residing at the end of the long bones. However, during osteoarthritis, articular chondrocytes lose their inactive phenotype, and undertake hypertrophic chondrocyte terminal differentiation, thus expressing markers ColX and MMP-13.

The different morphologies and functions of cartilage across the lifespan are supported by the differences in proliferation and differentiation of chondrocytes, tightly controlled by many cytokines and their intracellular signaling pathways. These important cytokines include the transforming growth factor-beta (TGFβ) superfamily, Wnts, Hedgehog, Notch, and FGFs (Gao et al., 2013; Long and Ornitz, 2013; Pan et al., 2008).

OVERVIEW OF BMP/TGFβ SIGNALING

The TGFβ superfamily consists of two subfamilies. The TGFβ subfamily includes TGFβs (1, 2, and 3), Activin (A and B), Nodals, myostatin (GDF-8), and Mullerian inhibiting substance. The bone morphogenetic protein (BMP) subfamily consists of BMPs 2, 4–10, and the growth and differentiation factors (GDFs) (Gordon and Blobe, 2008; Guo and Wang, 2009; Hinck, 2012). Ligands are usually assigned to either of these subfamilies based on the utilization of the downstream signaling mediators known as the receptor-regulated Smad proteins (R-Smads). Members of the TGFβ subfamily usually transduce signals through R-Smads 2 and 3, while members of the BMP subfamily transduce signals through R-Smads 1, 5, and 8 (Burks and Cohn, 2011; Weiss and Attisano, 2013). Smad4 is a cofactor that forms a complex with the activated R-Smads from both groups; it is thought to be essential for canonical signaling. The third group includes the inhibitory Smads 6 and 7 (I-Smads), which act as inhibitors on the BMP and TGFβ signaling cascade by various mechanisms (Song et al., 2009).

TGFβ ligands initiate signaling cascades across the cell membrane by binding and assembling a receptor complex on the cell surface (Fig. 2). These complexes are assembled from serine/threonine kinase types I and II receptors (Hinck, 2012; Massague, 2012). Upon ligand binding, the type II receptor is activated and transphosphorylates the type I receptor (Song et al., 2009). The type I receptors are termed ALKs (activin receptor-like kinases), of which seven have been discovered (Hinck, 2012; ten Dijke et al., 1994; van der Kraan et al., 2009). ALK 1, 2, 3, and 6 bind BMPs and signal via the R-Smads1/5/8; ALK 4, 5, and 7 bind activins and TGFβs and signal through R-Smads2/3 (Hinck, 2012; Massague, 2012b; Weiss and Attisano, 2013). ALK5 is the canonical type I receptor for TGFβs and activates Smads2/3. However, TGFβ can also bind to ALK1 and ALK2 in some cell types to activate R-Smads 1,5,8, thus activating the BMP pathway (van der Kraan et al., 2009). There are five type II receptors, including TβRII, ActRII, ActRIIb, BMPRII, and MISRII (Hinck, 2012; Weiss and Attisano, 2013).

Upon receptor activation, TGFβ/BMPs can signal through canonical and noncanonical pathways (Qiao et al., 2005; ten Dijke et al., 2002; Yoon et al., 2004). In the canonical pathway, activated type I receptors trigger phosphorylation of specific R-Smads, which then complex with Smad4, and translocate into the nucleus to direct transcriptional responses in combination with other gene specific transcription factors (Song et al., 2009). In addition, TGFβ/BMPs signal through a variety of noncanonical, Smad-independent avenues, utilizing MAP kinases, TAK1, RhoA, and mTOR pathways (Moustakas and Heldin, 2005; Mu et al., 2012; Yamaguchi et al., 1995; Yonekura et al., 1999; Zhang, 2009).

TGFβ Signaling in Cartilage Development

TGFβs play critical roles in regulating chondrocyte differentiation from early to terminal stages, including condensation, proliferation, terminal differentiation, and maintenance of articular chondrocytes (Li et al., 2005; Serra and Chang, 2003; Serra et al., 1997; van der Kraan et al., 2009; Yang et al., 2001). All three TGFβ isoforms are expressed in mesenchymal condensations. TGFβ3 is highly expressed in ribs and vertebral cartilage, whereas TGFβ1 and TGFβ2 expression is barely detected (Pelton et al., 1991). Levels of expression of all of these ligands are reduced at later stages of development in cartilage (Pelton et al., 1990, 1991). In the perichondrium, TGFβ3 is expressed at higher levels than other TGFβs (Pelton et al., 1990, 1991). In appendicular growth plates, TGFβ1 and TGFβ3 are expressed mainly in the proliferative and hypertrophic zones, whereas TGFβ2 is expressed in all zones, but at its highest levels in the hypertrophic zone (Horner et al., 1998; Millan et al., 1991; Sandberg et al., 1988; Thorp et al., 1992).

TGFβS IN PRECHONDROCYTE CONDENSATION

There is a considerable amount of in vitro evidence to indicate that TGFβ signaling pathways promote mesenchymal condensation. In vitro data demonstrate that TGFβ1 induces mesenchymal cell condensation via up-regulation of N-

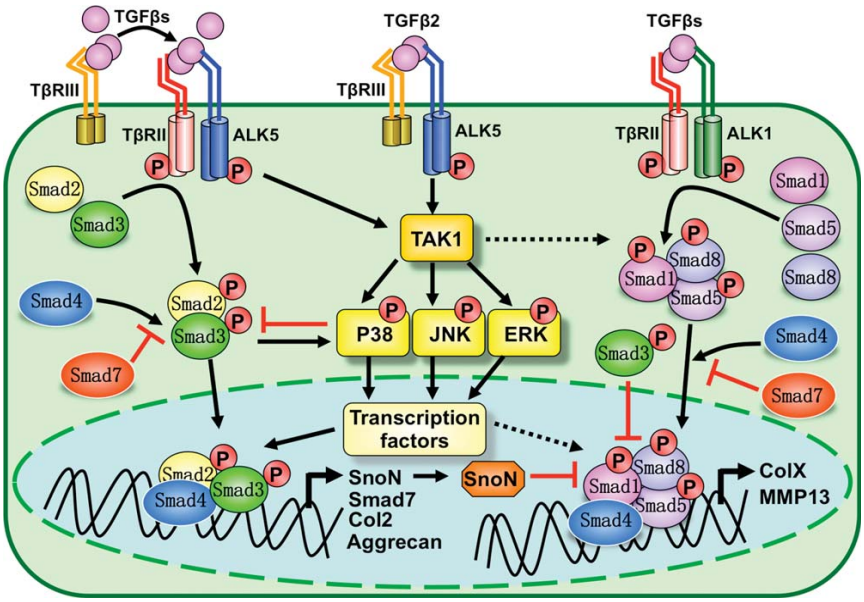

FIGURE 2. *Canonical and noncanonical TGFβ signaling pathways in cartilage formation and maintenance. Canonical Smad-dependent TGFβ signaling is initiated by TGFβ ligand binding to receptors and assembly of heteromeric complexes of type II (TβRII) and type I (ALK5) receptors. Type III (TβRII) receptor stabilizes TGFβs, particularly TGFβ2, at the cell membrane, and facilitates presentation of TGFβs to TβRII and ALK5, which are activated and then transduce signals through Smad2 and 3. Activated Smads form a complex with Smad4 and then translocate into the nucleus, where they interact with other transcription factors to regulate target gene expression. Activated ALK5 can relay signaling to noncanonical TAK1-mediated pathways, which are also the primary pathways activated by TβRIII/ALK5 complexes that do not contain TβRII. TAK1 pathways act either by converging with or repressing Smad2/3, depending on the cell context. TGFβs can also activate Smad1/5/8 (BMP) pathways through ALK1 receptor. The balance of signaling through Smad2/3 versus Smad1/5/8 thus depends on ratios of ALK1 and ALK5 expression. Smad2/3-mediated TGFβ signaling generally counteracts Sma1/5/8 (BMP) pathways through inhibiting transcriptional activity by forming mixed Smad3/Smad1/5 complexes, or though SnoN, and blocking Smad1/5/8 interaction with Smad4. TAK1 can activate and cooperate with Smad1/5/8 to regulate cartilage development, but whether and how TAK1 mediated TGFβ signaling interacts with Smad1/5/8 is still not clear.*

cadherin and fibronectin (FN) (Song et al., 2007; Tuli et al., 2003). TGFβ1 treatment initiates chondrogenesis of mesenchymal progenitor cells (Tuli et al., 2003). TGFβ2 and TGFβ3 are even more effective, causing a twofold greater accumulation of glycosaminoglycan (Barry et al., 2001). However, knockouts for individual TGFβ ligands do not exhibit phenotypes that support an essential role for TGFβs in condensation in vivo. *Tgfb1* null mice that survive to birth do not exhibit any skeletal defects, but die from diffuse inflammation (Shull et al., 1992). However, at least 50% of *Tgfβ1*$^{-/-}$ embryos die prior to the onset of skeletal development (Dunker et al., 2001), raising the possibility that this ligand could play a role in early skeletal patterning on specific genetic backgrounds. This possibility can now be addressed because a conditional allele for TGFβ1 has been generated (Azhar et al., 2009).

If TGFβs play an essential role in condensation in vivo, this should be seen in mice deficient for the TGFβ receptor ALK5, as this is the primary receptor that transduces TGFβ signals. *Alk5*$^{-/-}$ mice die at midgestation, exhibiting severe defects in vascular development in the yolk sac and placenta that preclude an analysis of skeletal formation (Larsson et al., 2001). Conditional ablation of *Alk5* using *Dermo1-Cre*, which targets skeletal progenitor cells prior to condensation, results in cartilage malformation and short limbs (Matsunobu et al., 2009). In these mice, chondrocytes proliferate and differentiate, but ectopic cartilaginous tissues protrude into the perichondrium, a phenotype related to the abnormally thin perichondrial layer. These and other studies in which the impact of TGFβ signaling has been investigated at early stages of chondrogenesis in the mouse are discussed in greater detail below, but in vivo genetic data demonstrating an essential role for TGFβ signaling in condensation stages are lacking.

TGFβ SIGNALING IN JOINT FORMATION

Several studies have revealed an essential role for TGFβ signaling through the type II receptor TβRII in appendicular and axial joint formation. Constitutive deletion of *Tgfbr2* causes defects in yolk sac hematopoiesis and vasculogenesis, resulting in embryonic lethality around 10.5 days of

gestation (Oshima et al., 1996). In *Tgfbr2;Prx-1Cre* mice, where the Prx-1 limb enhancer drives Cre recombinase expression in limb mesenchyme beginning at E9.5 and prior to condensation, loss of TβRII signaling resulted in the absence of interphalangeal joints (Spagnoli et al., 2007). The chemokine MCP-5 was recently identified as a key target for TβRII in the joint; TGFβ signaling was shown to be required to down-regulate MCP5 expression in joint interzone cells, to prevent the acquisition of a chondrogenic fate (Longobardi et al., 2012).

There are some similarities in defects in *Alk5;Dermo1-Cre* and *Tgfbr2;Prx1-Cre* conditional knockout mice. Both *Dermo1-Cre* and *Prx1-Cre* are expressed in mesenchymal progenitors, and in each case, the mice develop short-limbed dwarfism, abnormal sternums, and defects in joint formation (Seo and Serra, 2007; Spagnoli et al., 2007), suggesting that TGFβRII and ALK5 work together, likely in a complex, in mesenchymal progenitor cells. However, there is a distinction as to where joint fusion defects arise in these two mutants. *Tgfbr2;Prx1-Cre* mice develop fused phalangeal joints, while *Alk5;Dermo1-Cre* mice showed normal phalangeal joints, but partially fused knee joints (Matsunobu et al., 2009). In addition, there was a decrease in chondrocyte proliferation and a delay of late hypertrophic differentiation in *Tgfbr2;Prx1-Cre* mice that was not seen in *Alk5;Dermo1-Cre* growth plates (Matsunobu et al., 2009). The phenotypic differences in these two mouse models may result from the differences in *Prx1-Cre* and *Dermo1-Cre* expression patterns. *Prx1-Cre* is expressed earlier than *Dermo1-Cre* in limb mesenchymal progenitors (Rodda and McMahon, 2006). It is also possible that the expression levels of *Dermo1-Cre* and *Prx1-Cre* differ in mesenchyme progenitors, perichondrial cells, and chondrocytes. Finally, as discussed below, the differences between *Alk5* and *Tgfbr2* mutant mice may reflect the fact that these two receptors do not have to work together in all tissues to transduce TGFβ signals.

TGFβ SIGNALING IN THE GROWTH PLATE

As discussed above, mice lacking TGFβ1 do not exhibit an obvious growth plate phenotype (Kaartinen and Heisterkamp, 1995; Shull, 1992). Similarly, while loss of TGFβ3 leads to perinatal lethality, defects in chondrogenesis are not observed (Kaartinen and Heisterkamp, 1995; Proetzel, 1995). However, mice lacking TGFβ2 present with generalized chondrodysplasia that appears to have an onset at late gestation stages (Sanford, 1997). Furthermore, it has been shown that loss of TGFβ2 (but not loss of TGFβ3) prevents the ability of exogenous Shh (sonic hedgehog) to block hypertrophic differentiation in ex vivo metatarsal cultures (Alvarez, 2002). In summary, of the three TGFβ ligands, the evidence suggests that TGFβ2 may be the predominant one impacting chondrogenesis in vivo.

The evidence for a role for TGFβ signaling in the growth plate is clearer at the level of the receptors, although these roles are still not well understood. The majority of loss-of-function studies have been conducted using targeted deletions or overexpression of dominant-negative forms of *Tgfbr2* (the gene encoding TβRII). *Tgfbr2;Prx1-Cre* growth plates display elevated Indian hedgehog (Ihh) expression, along with a delay in the onset of hypertrophy and decrease in levels of *Col10a1* expression in hypertrophic cells (Spagnoli et al., 2007). This result is more severe than but consistent with the phenotype resulting from blockade of TGFβ signaling by the overexpression of a dominant negative form of TβRII (dnTβRII) in condensing mesenchymal cells and chondrocytes; this resulted in absence of hypertrophic chondrocytes at 14.5 dpc, suggesting impaired hypertrophic chondrocyte differentiation (Hiramatsu et al., 2011).

Interestingly, in contrast to the above results where deletion or transgenic overexpression of TβRII occurs prior to the onset of formation of differentiated (*Col2a1*-expressing) chondrocytes, conditional deletion of the TβRII in *Col2a1*-expressing chondrocytes did not lead to obvious defects in appendicular elements (Baffi et al., 2004). These findings strongly suggest that TβRII transduces TGFβ signaling at prechondrogenic stages, but may not have as substantial a role at later stages. Consistent with this speculation, defects in *Tgfbr2;Col2a1-Cre* mice were restricted to axial elements, where defective segmentation and formation of intervertebral discs was found (Baffi et al., 2004). In axial elements, *Col2a1* is activated in somites, considerably earlier than the onset of *Col2a*1 expression in chondrocytes within appendicular elements.

Given the lack of severe cartilage phenotypes in appendicular elements when *Tgfbr2* is ablated in differentiated chondrocytes, the question arises as to whether TGFβ signaling plays a substantial role in growth plate chondrocytes in vivo. This would be best addressed by studies in which the type I receptor ALK5 is ablated. ALK5 clearly has an important role in the formation of the perichondrium, as revealed in the *Alk5;Dermo1-Cre* mice discussed above (Matsunobu et al., 2009). However, the role, if any, of ALK5 in growth plate chondrocytes has not yet been investigated in vivo.

Investigating the role of TGFβ signaling at the level of ALK5 gains importance because it was shown recently that TβRII may be dispensable for TGFβ signaling in some settings; TGFβ ligands are able to elicit signals in TβRII (*Tgfbr2*) mutant mice (Iwata et al., 2012). Loss of *Tgfbr2* in cranial neural crest cells results in elevated expression of TGFβ2 and the type III TGFβ receptor (TβRIII; also known as betaglycan). TβRIII can keep TGFβ at the cell surface and can promote signaling by presenting ligand to the TβRI/TβRII complex (Shi and Massague, 2003). However, Iwata et al. (2012) demonstrated the existence of an ALK5/TβRIII-mediated, TβRII-independent signaling pathway that was essential for proliferation in the palatal mesenchyme. In palatal mesenchyme, TβRI/TβRII guides TGFβ signaling through Smad2 and Smad3, while TβRI/TβRIII transduces a signal through the noncanonical TAK1/p38 pathway (Bernabeu

et al., 2009; Iwata et al., 2012). Of interest, TβRIII has high affinity for TGFβ2, but not for TGFβ1 or TGFβ3. Thus, utilization of this TβRI/TβRIII pathway may explain why skeletal phenotypes are observed in TGFβ2-deficient mice, but not in mice lacking TGFβ1 or TGFβ3, and why loss of TβRII does not exhibit a strong phenotype in growth plate chondrocytes. Finally, it has been reported that ALK5 can form a complex with other type II receptors, such as ACTRII (Andersson et al., 2006; Rebbapragada et al., 2003; Tsuchida et al., 2008; Wu et al., 2003). Whether TGFβ relays signals through ALK5/TβRIII or ALK5/ACTRII complexes during chondrogenesis warrants further investigation.

TGFβ SIGNALING IN POSTNATAL/ARTICULAR CARTILAGE

In postnatal cartilage homeostasis, TGFβs act as inhibitors of terminal hypertrophic differentiation in chondrocytes. TGFβ1 arrests differentiation at an early stage of hypertrophy in bovine synovial explants (Shintani et al., 2013), and TGFβ3 inhibits terminal differentiation of chondrocytes from cultured mesenchymal stem cells (Mueller et al., 2010; Mueller and Tuan, 2008). In micromass culture using mouse limb bud cells, TGFß treatment delayed chondrocyte maturation and hypertrophy, and in accordance, inhibited expression of type X collagen, VEGF, MMP13, and osteocalcin (Zhang et al., 2004). TGFβ1 prevents the terminal differentiation of epiphyseal chondrocytes into hypertrophic cells (Ballock et al., 1993). These data along with the previously discussed data showing that TβRII is required for hypertrophy at early stages, indicate that TGFβ promotes the initial stages of chondrocyte differentiation, but represses terminal hypertrophic differentiation.

TβRII has profound roles in maintaining cartilage integrity. TβRII inhibits terminal differentiation and hypertrophy in articular chondrocytes. Deletion of *Tgfbr2* in early postnatal chondrocytes, achieved using tamoxifen-inducible;*Tgfbr2;Col2-CreER* mice, results in up-regulation of Runx2, Mmp13, and Adamts5 expression in articular cartilage tissue, leading to progressive development of an osteoarthritis (OA)-like phenotype (Shen et al., 2013). One caveat of these studies is that the ablation was carried out in 2-week old mice. No significant changes were reported in growth plate chondrocytes, strongly suggesting that the effects seen on formation of articular cartilage were direct. However, studies in which TGFβ signaling is ablated in adult articular cartilage will be needed to investigate the impact of these pathways on maintenance of articular cartilage.

Whether and how ALK5 acts in postnatal articular cartilage development and maintenance are not well understood and should be further investigated. ALK5 is expressed in murine and human cartilage, but its expression level decreases in normal aging and OA cartilage (Blaney Davidson et al., 2009). In vitro knockdown of ALK5 in articular chondrocytes leads to elevated expression of MMP13, a marker of terminally differentiated chondrocytes and a major cartilage-degrading enzyme in OA (Billinghurst et al., 1997; Blaney Davidson et al., 2009). These results strongly suggest that ALK5 plays an important role in inhibiting chondrocyte terminal differentiation in articular cartilage, but this remains to be confirmed in vivo.

It has been shown that TGFβ can activate canonical BMP pathways through engagement of ALK1 (Goumans et al., 2002), and that this pathway leads to activation of Smads1/5/8 in articular cartilage (van der Kraan et al., 2009). Moreover, the ALK1/ALK5 ratio is elevated in aged and OA articular chondrocytes as a consequence of an age-related decline in ALK5 expression (Blaney Davidson et al., 2009; van der Kraan et al., 2012). The increased ALK1/ALK5 ratio is correlated with a shift from Smad2/3 to Smad1/5/8 signaling during aging and OA in murine cartilage (Blaney Davidson et al., 2009; van der Kraan et al., 2012). Moreover, there is a significant correlation between ALK1 and MMP13 mRNA expression in the cartilage of human OA knee joints (Blaney Davidson et al., 2009). The effects of ALK1/Smad1/5/8 signaling on expression of many genes are opposite to those of ALK5/Smad2/3 in cartilage; thus, the outcome of TGFβ treatment will differ depending on the constellation of receptors in cartilage. The above discussion focuses on the role of TGFβ in articular chondrocytes. It is important to bear in mind that TGFβ signaling through Smad2/3 and Smad1/5 affects multiple joint tissues, including ligament, meniscus, subchondral bone, and synovium, and signaling through either pathway (Smad2/3) versus (Smad1/5/8) can have both protective and harmful effects (Plaas et al., 2011). Evaluation of the physiological significance of these effects with respect to joint health and OA will require additional in vivo studies.

Smad-Dependent TGFβ Signaling Functions in Cartilage

Smad2 and Smad3 are expressed throughout the growth plate. Smad2 is preferentially expressed in proliferative and prehypertrophic chondrocytes, whereas Smad3 is expressed at higher levels in prehypertrophic and hypertrophic chondrocytes. Smad4 is expressed in all zones (Billiar et al., 2004; Sakou et al., 1999). Smad2 and Smad3 have distinct roles in mediating TGFβ signaling. Smad3 binds DNA directly, whereas Smad2 regulates gene expression by interacting with Smad3 or other transcriptional factors (Massague et al., 2005). Smad2 is essential at early stages of embryonic development, while Smad3 may play a more important role in adult life (Song et al., 2009). *Smad2*$^{-/-}$ mice die at embryonic day 7.5–12.5 (Heyer et al., 1999; Nomura and Li, 1998; Waldrip et al., 1998; Weinstein et al., 1998). *Smad3*$^{-/-}$ mice are viable, but develop metastatic colorectal cancer, defects in the immune system, and present with OA-like symptoms (Datto et al., 1999; Li et al., 2006; Yang et al., 1999, 2001; Zhu et al., 1998). *Smad3*$^{-/-}$ mice develop degenerative joint disease resembling human OA, as characterized by increased chondrocyte hypertrophy

and the presence of type X collagen-positive cells in articular cartilage, progressive loss of the joint surface, formation of osteophytes, and decreased production of proteoglycans in synovial joints (Yang et al., 2001).

As is the case for *Tgfbr2* conditional knockout mice (*Tgfbr2;Col2-cre*) (Baffi et al., 2004), *Smad3* conditional knockout mice (*Smad3; Col2-Cre*) do not exhibit profound cartilage defects at prenatal stages (Chen et al., 2012). Depletion of *Smad3* in chondrocytes causes progressive articular cartilage degeneration, associated with increased expression of MMP13 and deficiency in key cartilage matrix constituents type II collagen and aggrecan (Chen et al., 2012).

The in vivo function of Smad2 in cartilage is still not clear. Overexpression of either Smad2 or Smad3 can block the spontaneous maturation observed in *Smad3*-deficient chondrocytes (Li et al., 2006). These data indicate that in spite of the fact that Smad2 and Smad3 regulate different sets of genes, Smad2 may partially compensate for Smad3 in preventing chondrocyte terminal differentiation. The extent to which TGFβ signaling utilizes Smad-dependent versus Smad-independent signaling in aspects of cartilage development and maintenance in vivo is as yet unclear, because direct comparisons of phenotypes using the same Cre drivers to ablate Smads versus TGFβ receptors have not been reported.

Noncanonical TGFβ Signaling in Cartilage

There exist numerous Smad-independent noncanonical pathways for transduction of TGFβ signals, including various MAPK, Rho-like GTPase, and phosphatidylinositol-3-kinase (PI3K)/AKT pathways (Moustakas and Heldin, 2005; Mu et al., 2012; Yeganeh et al., 2013; Zhang, 2009). The extent to which TGFβs mediate their effects through these pathways in cartilage in vivo is unknown, but there is solid evidence that these pathways are important for chondrogenesis.

TAK1 AND p38 IN CARTILAGE

The most extensively studied noncanonical pathways are those mediated by TGFβ activating kinase 1 (TAK1), a member of the MAPKKK family. TAK1 is activated by type I BMP and TGFβ receptors, and subsequently activates several MAP kinases (MAPKs), including p38, JNK, and ERK. Many reports have shown that MAPK activation converges with Smad signaling downstream of TGFβ to regulate cell apoptosis and epithelial–mesenchymal transition (EMT) (Holm et al., 2011; Lamouille and Derynck, 2007; Massague, 2012b; Mu et al., 2012; Wu and Hill, 2009). For example, the TAK1-JNK/p38 cascade functions in conjunction with the Smad-dependent pathway to regulate TGFβ-induced apoptosis. Moreover, siRNA knockdown of TRAF6, an upstream activator of TAK1, or treatment of cells with a chemical inhibitor of p38, efficiently blocked TGFβ-mediated apoptosis (Sorrentino et al., 2008; Yamashita et al., 2008; Yu et al., 2002). TGFβ promotes tumor growth by inducing EMT through a combination of Smad-dependent and Smad-independent effects mediated by p38 (Lee et al., 2006; Massague, 2012a; Thiery, 2003). Cooperation of Smad4 and p38 mediated signaling pathways is also required for normal tooth and palate formation (Xu et al., 2008). It is highly likely that TGFβ mediates its effects in chondrocytes through both canonical and noncanonical pathways.

In growth plate chondrocytes, TAK1 is critical for stimulating chondrocyte proliferation and differentiation. However, in developing cartilage, BMPs, rather than TGFβ, appear to be the major activators of TAK1. Whether this is the case in articular cartilage is unknown. Conditional deletion of TAK1 in cartilage (*Tak1;Col2Cre*) results in chondrodysplasia characterized by neonatal-onset runting, delayed formation of secondary ossification centers, and defects in formation of the elbow and tarsal joints (Greenblatt et al., 2010). Data from another research group showed that deletion of *Tak1* in chondrocytes resulted in multiple developmental cartilage defects, including decreased chondrocyte proliferation and survival, delayed onset of hypertrophy, reduced MMP13 expression, and a failure to maintain interzone cells of the elbow joint (Gunnell et al., 2010). These defects resemble those seen in mice deficient for BMP receptors or ligands more than they do the phenotypes of mice deficient for components of TGFβ pathways. In accordance, chondrocytes from these mice show evidence of defective BMP signaling in vivo and in vitro. Somewhat unexpectedly, deletion of TAK1 seems to affect not only activation of the p38 MAPK signaling cascade, but also activation of canonical BMP Smads1/5/8. Deletion of *Tak1* in limb mesenchyme (*Tak1*;*Prx1Cre*) resulted in widespread joint fusions, likely owing to the commitment of joint interzone cells to the chondrocyte lineage (Gunnell et al., 2010). Since TAK1 activates both p38/JNK/ERK MAPK and Smad1/5/8 pathways, the defects seen in *Tak1;Col2Cre* mice likely reflect reduced signaling through both canonical and noncanonical BMP pathways.

Although the above studies indicate that BMPs are major mediators of TAK1 pathways, TGFβ signaling also depends on TAK1 in several aspects of chondrogenesis. The most extensive data comes from studies of p38, a downstream effector of TAK1 signaling. Studies with genetically modified mice show that p38 pathways have various functions in cartilage, including inhibiting chondrocyte proliferation and differentiation, and maintaining cartilage integrity. p38 has 4 isoforms, α, β, γ, and δ, but only α, β, and γ are detectible in mouse cartilage (Li et al., 2010). Transgenic overexpression in chondrocytes of activated MKK6, a downstream mediator of TAK1 and an upstream activator of p38, resulted in dwarfism, inhibition of chondrocyte proliferation and differentiation, and a delay in primary and secondary ossification (Zhang et al., 2006). Inhibition of p38 in transgenic mice by cartilage-specific expression of a dominant-negative p38 (*Col2a1-p38-DN*) resulted in severely deficient endochondral bone formation

and reduced limb length (Namdari et al., 2008). p38-DN heterozygotes developed osteoarthritis-like symptoms, indicating that chronic p38 deficiency is harmful to articular cartilage (Namdari et al., 2008). Whether this is due to early chondrogenesis defects that affect joint shape, or to a role for p38 in adult articular cartilage, is an important unknown.

p38 also has catabolic functions in cartilage. Increased p38 phosphorylation was found in human OA cartilage (Fan et al., 2007). *Col10a1* is expressed in all hypertrophic chondrocytes, but *MMP13* expression is restricted to the most terminally differentiated hypertrophic chondrocytes (Inada et al., 2004; MacLean et al., 2003). p38 inhibits *Col10a1* expression (Li et al., 2010), but activates MMP13 expression (Chen et al., 2012). These results suggest that p38 prevents onset of chondrocyte hypertrophy, but stimulates their terminal differentiation, an effect also seen for TGFβ, as discussed above.

CROSSTALK BETWEEN SMAD3 AND P38 IN CARTILAGE

TGFβ can activate MAPK pathways through Smad-independent and Smad-dependent pathways. For example, a mutant TβRI receptor defective in Smad binding and activation, but retaining an intact kinase activity, is able to mediate TGFβ-induced activation of JNK and p38 through TAK1 (Itoh et al., 2003; Yu et al., 2002), indicating that Smads can be dispensable for TGFβ activation of JNK and p38. However, several studies have demonstrated that Smad2/3 and p38 act in concert to regulate aspects of chondrogenesis. For example, in vitro assays using chondrocytic ATDC5 cells showed that although TGFβ-dependent activation of p38 and ERK1/2 does not influence activation of R-Smads by TGFβ, inhibition of p38 or ERK1/2 inhibited TGFβ-induced transcriptional activity of both Smad2 and Smad4 (Watanabe et al., 2001). Hence, these studies suggest that TGFβ-induced activation of p38 or ERK1/2 is essential for transcriptional activation of Smad2 and Smad4, and for maximal activation of specific Smad-dependent transcriptional responses in ATDC5 cells (Watanabe et al., 2001).

Smad3 has been shown to modulate p38 activity. For example, Smad3 regulates p38 phosphorylation in chondrocytes. Assays using primary chondrocytes from *Smad3*$^{-/-}$ mice showed that loss of Smad3 promotes inactivation of p38, most likely by disrupting a pSmad3–p38 complex, thereby abrogating signaling through a TAK1/p38/ATF-2 pathway. Over-expression of ATF-2 or treatment with the p38 activator anisomycin inhibited expression of type X collagen, suggesting that Smad3 and p38 cooperate to repress the onset of hypertrophy (Li et al., 2010). p38 can also act independently of Smad3 to promote induction of MMP13 in growth plate chondrocytes (Chen et al., 2012). Smad3-mediated TGFβ signals transiently repress MMP13 expression. However, after 24 hr of TGFβ treatment, there is an increase of MMP13 expression; this induction is mediated by p38, but not Smad3 (Chen et al., 2012). Hence, a switch from Smad3-mediated signals to p38-mediated signals changes the outcome of TGFβ treatment from repression to activation of MMP13 expression. Whether this switch to a Smad3-independent effect correlates with a change in receptor utilization towards ALK1 is an interesting possibility.

In contrast to the above studies demonstrating cooperativity between Smad and p38 pathways, MAPK pathways negative regulate Smad signaling through phosphorylation of Smad linker sites (Fuentealba et al., 2007; Gao et al., 2009). The BMP and TGFβ type I receptors phosphorylate R-Smads at the C-terminal SXS site to initiate signal propagation. Subsequently, the R-Smad linker region is phosphorylated by MAPK, leading to a primed substrate for glycogen synthase kinase 3 (GSK3). GSK3 creates binding sites for the E3 ubiquitin protein ligases SMURF1 (SMAD-specific E3 ubiquitin protein ligase 1) or NEDD4L (neural precursor cell expressed developmentally downregulated protein 4-like), which target SMAD proteins for polyubiquitilation and proteasome-mediated degradation (Alarcon et al., 2009; Fuentealba et al., 2007; Gao et al., 2009). Besides MAPK pathways, PI3K/Akt pathway can also antagonize Smad-mediated effects. Akt can directly interact with Smad3 and inhibit Smad3-phosphorylation, nuclear localization, and Smad3-mediated transcription (Conery et al., 2004; Remy et al., 2004). The extent to which noncanonical pathways interact with Smad pathways in cartilage development remains poorly understood.

JNK, ERK, PI3K, AND RHO GTPASE PATHWAYS IN CARTILAGE

When compared with p38, there is less information on the functions of JNK and ERK pathways in cartilage. JNK1 and JNK2 are expressed in chondrocytes, but deletion of either isoform has not been associated with a skeletal phenotype (Beier and Loeser, 2010), suggesting that JNK1 and JNK2 may have overlapping functions in cartilage. High levels of activated JNK are seen in human OA cartilage (Clancy et al., 2001; Fan et al., 2007). In vitro experiments showed that inhibiting JNK blocks MMP13 expression in human chondrocytes (Im et al., 2007; Loeser et al., 2003), implicating JNK in the progression of OA.

Chondrocytes also express both ERK1 and ERK2. ERK1-null mice have no obvious skeletal or growth abnormalities (Pages et al., 1999), and ERK2 null mice die very early in embryogenesis as a result of defective trophoblast development (Saba-El-Leil et al., 2003). Constitutive activation of MEK1 in chondrocytes inhibits hypertrophic differentiation of growth plate chondrocytes, and negatively regulates bone growth without inhibiting chondrocyte proliferation, resulting in achondroplasia-like dwarfism (Murakami et al., 2004). Similar to p38 and JNK, ERK plays a role in stimulating MMP13 expression in human chondrocytes, and inhibiting ERK prevents MMP13 expression (Forsyth et al., 2002; Loeser et al., 2003). In vitro assay results showed that all three major MAP kinases (ERK1/2, p38a, and JNK1/2) must be activated at the same time to

TABLE 1. *Genetic Modified Mouse Models on TGFβ Signaling on Cartilage Formation and Maintaining*

Gene	Models	Defects	References
Tgfβ1	−/−	No defect in cartilage formation, 50% embryos die early	Shull et al. (1992), Dunker et al. (2001)
Tgfβ2	−/−	Generalized chondrodysplasia	Sanford et al. (1997)
Tgfβ3	−/−	No defects in chondrogenesis, perinatal lethality	Proetzel et al. (1995), Kaartinen et al. (1995)
Alk5	Flox; Dermo1-Cre	Fused knee joints, short limbs and ectopic cartilaginous protrusions	Matsunobu et al. (2009)
Tgfbr2	Flox; Prx1-Cre	Fused phalangeal joints, decreased chon. proliferation, delayed hypertrophic differentiation	Longobardi et al. (2012)
	Flox; Wnt1-Cre	Craniofacial deformities	Iwata et al. (2012)
	Flox; Col2a1-Cre	No defect in appendicular elements, defective segmentation and formation of intervertebral discs	Baffi et al. (2004)
	Flox; Col2-CreER	osteoarthritis(OA)-like phenotype	Shen et al. (2013)
DN-Tgfbr2[a]	Col11a2-promoter/ enhancer; Flox; Prx1-Cre	Hypoplasia, absence of hypertrophic chondrocytes at 14.5 dpc	Hiramatsu et al. (2011)
Smad3	−/−	Increased chondrocyte hypertrophy, osteoarthritis-like symptoms	Yang et al. (2001)
	Flox; Col2a1-Cre	No cartilage defects at prenatal stages, articular cartilage degeneration	Chen et al. (2012)
Smad4	−/−	Early embryonic lethal	Chu et al. (2004)
	Flox; Col2a1-Cre	Dwarfism, disorganized growth plate, delay in chondrocyte maturation	Zhang et al. (2005)
	Flox; Prx1-Cre	Halted limb bud development and carpal fusions	Benazet et al. (2012)
Smad7	−/−	Early postnatal lethality, retained proliferative chondrocytes, hypocellular cores, anterior/posterior transformation.	Estrada et al. (2013)
Tak1	Flox; Prx1-Cre	Survive to the weaning stag, decreased chondrocyte proliferation, delays in both the onset and progression of chondrocyte maturation, joint fusions,	Gunnell et al. (2010)
	Flox; Col2-Cre	Die before birth, decreased chondrocyte proliferation and survival, delayed onset of hypertrophy, elbow abnormalities	Gunnell et al. (2010)
	Flox; Col2a1-Cre	Survive postnatally for 2–3 weeks, neonatal-onset runting, decreased chondrocyte proliferation, delayed formation of secondary ossification centers, and defects in formation of the elbow and tarsal joints	Greenblatt et al. (2010)
	Flox; Col2-CreER	Display severe growth retardation and OA-like phenotype	Gao et al. (2013)

TABLE 1. *Continued*

Gene	Models	Defects	References
CA-MKK6[a]	Col2a1 promoter	Dwarfism, inhibition of both chondrocyte proliferation and differentiation, and a delay in primary and secondary ossification	Zhang et al. (2006)
DN-P38[a]	Col2 promoter	Dwarfism, OA-like phenotype	Namdari et al. (2008)
CA-MEK1[a]	Col2a1 promoter	Dwarfism, inhibits hypertrophic differentiation, no defect of chondrocyte proliferation	Murakami et al. (2004)
Akt1	−/−	Dwarfism, exhibit decreased calcification in the growth plate with fewer osteophyte formation in OA	Fukai et al. (2010)
Pten	Flox; Col2a1-Cre	Dyschondroplasia, defects in chondrocyte proliferation and maturation, and exhibit aberrant neoplastic cores	Yang et al. (2008)

[a]CA: Constitutive active, DN: Dominant negative.

induce MMP expression, while inhibition of any one of the three is sufficient to inhibit MMP13 expression (Forsyth et al., 2002; Loeser et al., 2003).

The PI3K pathway has various stage-specific functions in cartilage development. Transgenic overexpression of an activated form of Akt, a downstream target of PI3K, in cartilage increased chondrocyte proliferation in the resting zone, and delayed hypertrophic differentiation in the growth plate, but promoted hypertrophic differentiation in craniobasal cartilaginous elements and vertebrae (Rokutanda et al., 2009). The differential effects on hypertrophy were shown to be a result of engagement of different pathways downstream of Akt. Organ culture experiments showed that Akt relays signals through mTOR, FoxO, and GSK3 pathways. The Akt–mTOR pathway was responsible for promoting chondrocyte proliferation, maturation, and cartilage matrix production. The Akt–FoxO pathway enhanced chondrocyte proliferation, but inhibited chondrocyte maturation and cartilage matrix production, while the Akt–GSK3 pathway negatively regulated three of the cellular processes in limb skeletons but not in vertebrae, as a result of less GSK3 expression in vertebrae (Rokutanda et al., 2009).

Cartilage-specific inactivation of PTEN, the main phosphatase counteracting PI3K activity, leads to profound defects in skeletal development in mice, including skeletal overgrowth, disorganization of growth plates with increasing resting cell proliferation, and fusion of the primary and secondary ossification centers (Ford-Hutchinson et al., 2007; Hsieh et al., 2009; Yang et al., 2008). As is the case for Akt, the function of PTEN varies depending on the time and location of skeletal development. The loss of PTEN delays chondrocyte hypertrophy in embryonic growth plates (Yang et al., 2008), whereas it accelerates hypertrophic chondrocyte maturation in adult mice (Ford-Hutchinson et al., 2007). Among the Akt isoforms (Akt1, Akt2, and Akt3), Akt1 is the most highly expressed in chondrocytes. *Akt1*$^{-/-}$ mice are small and have normal proliferative and hypertrophic zones, but exhibit decreased calcification in the growth plate. *Akt1*$^{-/-}$ mice formed fewer osteophytes in medial collateral ligament transection induced OA (Fukai et al., 2010).

The in vivo functions of Rho GTPases in chondrogenesis are not clear because in vivo models are lacking (e.g., conditional knockout mice). In vitro data indicate that RhoA, one of the main prototypes of Rho GTPas families, inhibits early chondrogenesis and hypertrophic chondrocyte differentiation by repressing Sox9 expression (Woods et al., 2005; Woods and Beier, 2006; Kumar and Lassar, 2009; reviewed in Beier and Loeser, 2010).

In summary, p38, JNK, ERK, PI-3 Kinase, and Rho GTPases pathways have different functions in regulating chondrocyte proliferation and differentiation according to the development stage and type of skeletal element (Table 1). p38, ERK, and PI3K pathways both promote and inhibit chondrocyte terminal differentiation. As a result, attempts at pharmacological intervention for OA using these pathways as targets must take these temporal and spatial differences in function into consideration. The extent to which these pathways are regulated by TGFβ in vivo is unknown, as is the extent to which TGFβ transduces its signals through these pathways in cartilage.

CROSSTALK BETWEEN TGF-β SIGNALING AND BMP SIGNALING

BMP pathways control nearly every aspect of chondrogenesis (Song et al., 2009; Yoon and Lyons, 2004). Thus, understanding how BMP and TGFβ pathways intersect is fundamental to understand the mechanisms controlling cartilage formation and maintenance. TGFβ enhances BMP2-induced chondrogenesis in bovine synovial explants,

improves the hyaline-like properties of neocartilage, and arrests differentiation at an early stage of hypertrophy (Shintani et al., 2013). In undifferentiated ATDC5 cells, which represent a proliferative stage, TGFβ enhanced BMP signaling, while BMP2 significantly reduced levels of TGFβ signaling (Keller et al., 2011). These results suggest that TGFβ promotes BMP signaling during early chondrogenesis and cell proliferation.

On the other hand, in vivo data demonstrated that Smad3 can repress Smad1/5/8 activation to prevent chondrocyte hypertrophy (Li et al., 2006). In accordance, there is an increase in the level of pSmad1/5/8 activity with the loss of Smad3. *Smad3*$^{-/-}$ chondrocytes were more responsive to BMP2, exhibiting increased type X collagen expression, pSmad1/5/8 levels, and BMP-responsive luciferase reporter activity (Li et al., 2006). In vitro assays using MDA-MB-231 breast cancer cell lines showed that TGFβ inhibits BMP responses by inducing the formation of pSmad3–pSmad1/5 complexes, which bind to BMP-responsive elements and mediate TGFβ-induced transcriptional repression (Gronroos et al., 2012). In ATDC5 cells, TGFβ suppresses BMP signaling and chondrocyte hypertrophy via SnoN, a transcriptional corepressor (Kawamura et al., 2012). SnoN is induced by TGFβ signaling in maturing chondrocytes and suppresses the BMP-Smad signaling pathway to inhibit hypertrophic maturation of chondrocytes (Kawamura et al., 2012).

Summary and Perspectives

There has been considerable progress toward understanding the physiological functions of TGFβ signaling network components and downstream pathways during cartilage development and maintenance. However, many questions remain regarding the relative importance of various pathways downstream of TGFβ, the role of TGFβ as opposed to other growth factors in activating these pathways, and the mechanisms by which TGFβ-regulated canonical and noncanonical pathways intersect. It is clear that the composition of TGFβ receptor complexes and crosstalk between Smad and non-Smad signaling pathways determines the final cellular response. Not every signaling component, however, is well understood with regard to in vivo functions at different developmental stages. For example, the functions of ALK5, ALK1, Smad2, and Smad4 in mediating TGFβ actions in cartilage development and maintenance are still not clear. Given that TGFβ can transduce both canonical TGFβ (Smad2/3) and BMP (Smad1/5/8) signals that have fundamentally different and usually opposing effects in cartilage, understanding the extent to which TGFβ utilizes BMP pathways in vivo is also an important goal.

References

Akiyama H, Lefebvre V. 2011. Unraveling the transcriptional regulatory machinery in chondrogenesis. J Bone Miner Metab 29: 390–395.

Alarcon C, Zaromytidou AI, Xi Q, et al. 2009. Nuclear CDKs drive Smad transcriptional activation and turnover in BMP and TGF-beta pathways. Cell 139:757–769.

Alvarez J, Sohn P, Zeng X, et al. 2002. TGFβ2 mediates the effects of Hedgehog on hypertrophic differentiation and PTHrP expression. Development 129:1913–1924.

Azhar M, Yin M, Bommireddy R, et al. 2009. Generation of mice with a conditional allele for transforming growth factor beta 1 gene. Genesis 47:423–431.

Baffi MO, Slattery E, Sohn P, et al. 2004. Conditional deletion of the TGF-beta type II receptor in Col2a expressing cells results in defects in the axial skeleton without alterations in chondrocyte differentiation or embryonic development of long bones. Dev Biol 276:124–142.

Ballock RT, Heydemann A, Wakefield LM, et al. 1993. TGF-beta 1 prevents hypertrophy of epiphyseal chondrocytes: Regulation of gene expression for cartilage matrix proteins and metalloproteases. Dev Biol 158:414–429.

Barry F, Boynton RE, Liu B, et al. 2001. Chondrogenic differentiation of mesenchymal stem cells from bone marrow: differentiation-dependent gene expression of matrix components. Exp Cell Res 268:189–200.

Beier F, Loeser RF. 2010. Biology and pathology of Rho GTPase, PI-3 kinase-Akt, and MAP kinase signaling pathways in chondrocytes. J Cell Biochem 110:573–580.

Benazet JD, Pignatti E, Nugent A, et al. 2012. Smad4 is required to induce digit ray primordia and to initiate the aggregation and differentiation of chondrogenic progenitors in mouse limb buds. Development 139:4250–4260.

Bernabeu C, Lopez-Novoa JM, Quintanilla M. 2009. The emerging role of TGF-beta superfamily coreceptors in cancer. Biochim Biophys Acta 1792:954–973.

Billiar RB, St Clair JB, Zachos NC, et al. 2004. Localization and developmental expression of the activin signal transduction proteins Smads 2, 3, and 4 in the baboon fetal ovary. Biol Reprod 70:586–592.

Billinghurst RC, Dahlberg L, Ionescu M, et al. 1997. Enhanced cleavage of type II collagen by collagenases in osteoarthritic articular cartilage. J Clin Investig 99:1534–1545.

Blaney Davidson EN, Remst DF, et al. 2009. Increase in ALK1/ALK5 ratio as a cause for elevated MMP-13 expression in osteoarthritis in humans and mice. J Immunol 182:7937–7945.

Burks TN, Cohn RD. 2011. Role of TGF-beta signaling in inherited and acquired myopathies. Skelet Muscle 1:19.

Chen CG, Thuillier D, Chin EN, et al. 2012. Chondrocyte-intrinsic Smad3 represses Runx2-inducible matrix metalloproteinase 13 expression to maintain articular cartilage and prevent osteoarthritis. Arthritis Rheum 64:3278–3289.

Chu GC, Dunn NR, Anderson DC, et al. 2004. Differential requirements for Smad4 in TGF beta-dependent patterning of the early mouse embryo. Development 131:3501–3512.

Clancy R, Rediske J, Koehne C, et al. 2001. Activation of stress-activated protein kinase in osteoarthritic cartilage: Evidence for nitric oxide dependence. Osteoarthritis Cartilage 9:294–299.

Conery AR, Cao Y, Thompson EA, et al. 2004. Akt interacts directly with Smad3 to regulate the sensitivity to TGF-beta induced apoptosis. Nat Cell Biol 6:366–372.

Datto MB, Frederick JP, Pan L, et al. 1999. Targeted disruption of Smad3 reveals an essential role in transforming growth factor beta-mediated signal transduction. Mol Cell Biol 19:2495–2504.

Dunker N, Schuster N, Krieglstein K. 2001. TGF-beta modulates programmed cell death in the retina of the developing chick embryo. Development 128:1933–1942.

Estrada KD, Wang WG, Retting KN, et al. 2013. Smad7 regulates terminal maturation of chondrocytes in the growth plate. Dev Biol 382:375–384.

Fan Z, Soder S, Oehler S, et al. 2007. Activation of interleukin-1 signaling cascades in normal and osteoarthritic articular cartilage. Am J Pathol 171:938–946.

Ford-Hutchinson AF, Ali Z, Lines SE, et al. 2007. Inactivation of Pten in osteo-chondroprogenitor cells leads to epiphyseal growth plate abnormalities and skeletal overgrowth. J Bone Miner Res 22:1245–1259.

Forsyth CB, Pulai J, Loeser RF. 2002. Fibronectin fragments and blocking antibodies to alpha2beta1 and alpha5beta1 integrins stimulate mitogen-activated protein kinase signaling and increase collagenase 3 (matrix metalloproteinase 13) production by human articular chondrocytes. Arthritis Rheum 46:2368–2376.

Fuentealba LC, Eivers E, Ikeda A, et al. 2007. Integrating patterning signals: Wnt/GSK3 regulates the duration of the BMP/Smad1 signal. Cell 131:980–993.

Fukai A, Kawamura N, Saito T, et al. 2010. Akt1 in murine chondrocytes controls cartilage calcification during endochondral ossification under physiologic and pathologic conditions. Arthritis Rheum 62:826–836.

Gao L, Sheu TJ, Dong Y, et al. 2013. TAK1 regulates Sox9 expression in chondrocytes and is essential for postnatal development of the growth plate and articular cartilages. J Cell Sci 126:5704–5713.

Gao S, Alarcon C, Sapkota G, et al. 2009. Ubiquitin ligase Nedd4L targets activated Smad2/3 to limit TGF-beta signaling. Mol Cell 36:457–468.

Gordon KJ, Blobe GC. 2008. Role of transforming growth factor-beta superfamily signaling pathways in human disease. Biochim Biophys Acta 1782:197–228.

Goumans MJ, Valdimarsdottir G, Itoh S, et al. 2002. Balancing the activation state of the endothelium via two distinct TGF-beta type I receptors. EMBO J 21:1743–1753.

Greenblatt MB, Shim JH, Glimcher LH. 2010. TAK1 mediates BMP signaling in cartilage. Ann NY Acad Sci 1192:385–390.

Gronroos E, Kingston IJ, Ramachandran A, et al. 2012. Transforming growth factor beta inhibits bone morphogenetic protein-induced transcription through novel phosphorylated Smad1/5–Smad3 complexes. Mol Cell Biol 32:2904–2916.

Gunnell LM, Jonason JH, Loiselle AE, et al. 2010. TAK1 regulates cartilage and joint development via the MAPK and BMP signaling pathways. J Bone Miner Res 25:1784–1797.

Guo X, Wang XF. 2009. Signaling cross-talk between TGF-beta/BMP and other pathways. Cell Res 19:71–88.

Heyer J, Escalante-Alcalde D, Lia M, et al. 1999. Postgastrulation Smad2-deficient embryos show defects in embryo turning and anterior morphogenesis. Proc Natl Acad Sci USA 96:12595–12600.

Hinck AP. 2012. Structural studies of the TGF-betas and their receptors: Insights into evolution of the TGF-beta superfamily. FEBS Lett 586:1860–1870.

Hiramatsu K, Iwai T, Yoshikawa H, et al. 2011. Expression of dominant negative TGF-beta receptors inhibits cartilage formation in conditional transgenic mice. J Bone Miner Metab 29:493–500.

Holm TM, Habashi JP, Doyle JJ, et al. 2011. Noncanonical TGFbeta signaling contributes to aortic aneurysm progression in Marfan syndrome mice. Science 332:358–361.

Horner A, Kemp P, Summers C, et al. 1998. Expression and distribution of transforming growth factor-beta isoforms and their signaling receptors in growing human bone. Bone 23:95–102.

Hsieh SC, Chen NT, Lo SH. 2009. Conditional loss of PTEN leads to skeletal abnormalities and lipoma formation. Mol Carcinogen 48:545–552.

Im HJ, Muddasani P, Natarajan V, et al. 2007. Basic fibroblast growth factor stimulates matrix metalloproteinase-13 via the molecular cross-talk between the mitogen-activated protein kinases and protein kinase Cdelta pathways in human adult articular chondrocytes. J Biol Chemistry 282:11110–11121.

Inada M, Wang Y, Byrne MH, et al. 2004. Critical roles for collagenase-3 (Mmp13) in development of growth plate cartilage and in endochondral ossification. Proc Natl Acad Sci USA 101:17192–17197.

Itoh S, Thorikay M, Kowanetz M, et al. 2003. Elucidation of Smad requirement in transforming growth factor-beta type I receptor-induced responses. J Biol Chem 278:3751–3761.

Iwamoto M, Ohta Y, Larmour C, et al. 2013. Toward regeneration of articular cartilage. Birth Defects Res 99:192–202.

Iwata J, Hacia JG, Suzuki A, et al. 2012. Modulation of noncanonical TGF-beta signaling prevents cleft palate in Tgfbr2 mutant mice. J Clin Investig 122:873–885.

Kaartinen V, Voncken JW, Shuler CF, et al. 1995. Abnormal lung development and cleft palate in mice lacking TGF-b3 indicates defects of epithelial–mesenchymal interaction. Nat Genet 11: 415–421.

Karsenty G, Kronenberg HM, Settembre C. 2009. Genetic control of bone formation. Ann Rev Cell Dev Biol 25:629–648.

Kawamura I, Maeda, S, Imamura K, et al. 2012. SnoN suppresses maturation of chondrocytes by mediating signal cross-talk between transforming growth factor-beta and bone morphogenetic protein pathways. J Biol Chem 287:29101–29113.

Keller B, Yang T, Chen Y, et al. 2011. Interaction of TGFbeta and BMP signaling pathways during chondrogenesis. PloS one 6: e16421.

Kronenberg HM. 2003. Developmental regulation of the growth plate. Nature 423:332–336.

Kulkarni AB, Karlsson S. 1993. Transforming growth factor-beta 1 knockout mice. A mutation in one cytokine gene causes a dramatic inflammatory disease. Am J Pathol 143:3–9.

Kumar D, Lassar AB. 2009. The transcriptional activity of Sox9 in chondrocytes is regulated by RhoA signaling and actin polymerization. Mol Cell Biol 29:4262–4273.

Lamouille S, Derynck R. 2007. Cell size and invasion in TGF-beta-induced epithelial to mesenchymal transition is regulated by activation of the mTOR pathway. J Cell Biol 178:437–451.

Larsson J, Goumans MJ, Sjostrand LJ, et al. 2001. Abnormal angiogenesis but intact hematopoietic potential in TGF-beta type I receptor-deficient mice. EMBO J 20:1663–1673.

Las Heras F, Gahunia HK, Pritzker KP. 2012. Articular cartilage development: a molecular perspective. Orthop Clin N Am 43: 155–171.

Lee JM, Dedhar S, Kalluri R, et al. 2006. The epithelial–mesenchymal transition: New insights in signaling, development, and disease. J Cell Biol 172:973–981.

Li TF, Darowish M, Zuscik MJ, et al. 2006. Smad3-deficient chondrocytes have enhanced BMP signaling and accelerated differentiation. J Bone Miner Metab 21:4–16.

Li TF, Gao L, Sheu TJ, et al. 2010. Aberrant hypertrophy in Smad3-deficient murine chondrocytes is rescued by restoring transforming growth factor beta-activated kinase 1/activating transcription factor 2 signaling: A potential clinical implication for osteoarthritis. Arthritis Rheum 62:2359–2369.

Li TF, O'Keefe RJ, Chen D. 2005. TGF-beta signaling in chondrocytes. Front Biosci 10:681–688.

Loeser RF, Forsyth CB, Samarel AM, et al. 2003. Fibronectin fragment activation of proline-rich tyrosine kinase PYK2 mediates integrin signals regulating collagenase-3 expression by human chondrocytes through a protein kinase C-dependent pathway. J Biol Chem 278:24577–24585.

Long F, Ornitz DM. 2013. Development of the endochondral skeleton. Cold Spring Harbor Perspect Biol 5:a008334.

Longobardi L, Li T, Myers TJ, et al. 2012. TGF-beta type II receptor/MCP-5 axis: At the crossroad between joint and growth plate development. Dev Cell 23:71–81.

MacLean HE, Kim JI, Glimcher MJ, et al. 2003. Absence of transcription factor c-maf causes abnormal terminal differentiation of hypertrophic chondrocytes during endochondral bone development. Dev Biol 262:51–63.

Massague J. 2012a. TGF-beta signaling in development and disease. FEBS Lett 586:1833.

Massague J. 2012b. TGFbeta signalling in context. Nat Rev Mol Cell Biol 13:616–630.

Massague J, Seoane J, Wotton D. 2005. Smad transcription factors. Genes Dev 19:2783–2810.

Matsunobu T, Torigoe K, Ishikawa M, et al. 2009. Critical roles of the TGF-beta type I receptor ALK5 in perichondrial formation and function, cartilage integrity, and osteoblast differentiation during growth plate development. Dev Biol 332:325–338.

Millan FA, Denhez F, Kondaiah P, et al. 1991. Embryonic gene expression patterns of TGF beta 1, beta 2 and beta 3 suggest different developmental functions in vivo. Development 111:131–143.

Moustakas A, Heldin CH. 2005. Non-Smad TGF-beta signals. J Cell Sci 118:3573–3584.

Mu Y, Gudey SK, Landstrom M. 2012. Non-Smad signaling pathways. Cell Tissue Res 347:11–20.

Mueller MB, Fischer M, Zellner J, et al. 2010. Hypertrophy in mesenchymal stem cell chondrogenesis: effect of TGF-beta isoforms and chondrogenic conditioning. Cells Tissues Organs 192: 158–166.

Mueller MB, Tuan RS. 2008. Functional characterization of hypertrophy in chondrogenesis of human mesenchymal stem cells. Arthritis Rheum 58:1377–1388.

Murakami S, Balmes G, McKinney S, et al. 2004. Constitutive activation of MEK1 in chondrocytes causes Stat1-independent achondroplasia-like dwarfism and rescues the Fgfr3-deficient mouse phenotype. Genes Dev 18:290–305.

Namdari S, Wei L, Moore D, et al. 2008. Reduced limb length and worsened osteoarthritis in adult mice after genetic inhibition of p38 MAP kinase activity in cartilage. Arthritis Rheum 58:3520–3529.

Nomura M, Li E. 1998. Smad2 role in mesoderm formation, left–right patterning and craniofacial development. Nature 393:786–790.

Oshima M, Oshima H, Taketo MM. 1996. TGF-beta receptor type II deficiency results in defects of yolk sac hematopoiesis and vasculogenesis. Dev Biol 179:KC 297–302.

ORIGINAL ARTICLE

JBMR®

The Type I BMP Receptor ACVR1/ALK2 is Required for Chondrogenesis During Development

Diana Rigueur,[1] Sean Brugger,[2] Teni Anbarchian,[1,2] Jong Kil Kim,[1] YooJin Lee,[2,3] and Karen M Lyons[1,2,3]

[1]Department of Molecular, Cell and Developmental Biology, University of California, Los Angeles, Los Angeles, CA, USA
[2]Department of Orthopaedic Surgery, University of California, Los Angeles, CA, USA
[3]Orthopaedic Institute for Children, Los Angeles, CA, USA

ABSTRACT

Bone morphogenetic proteins (BMPs) are crucial regulators of chondrogenesis. BMPs transduce their signals through three type I receptors: BMPR1A, BMPR1B, and ACVR1/ALK2. Fibrodysplasia ossificans progressiva (FOP), a rare disorder characterized by progressive ossification of connective tissue, is caused by an activating mutation in *Acvr1* (the gene that encodes ACVR1/ALK2). However, there are few developmental defects associated with FOP. Thus, the role of ACVR1 in chondrogenesis during development is unknown. Here we report the phenotype of mice lacking ACVR1 in cartilage. *Acvr1*^{CKO} mice are viable but exhibit defects in the development of cranial and axial structures. Mutants exhibit a shortened cranial base, and cervical vertebrae are hypoplastic. *Acvr1*^{CKO} adult mice develop progressive kyphosis. These morphological defects were associated with decreased levels of Smad1/5 and p38 activation, and with reduced rates of chondrocyte proliferation in vertebral cartilage. We also tested whether ACVR1 exerts coordinated functions with BMPR1A and BMPR1B through analysis of double mutants. *Acvr1/Bmpr1a* and *Acvr1/Bmpr1b* mutant mice exhibited generalized perinatal lethal chondrodysplasia that was much more severe than in any of the corresponding mutant strains. These findings demonstrate that ACVR1 is required for chondrocyte proliferation and differentiation, particularly in craniofacial and axial elements, but exerts coordinated functions with both BMPR1A and BMPR1B throughout the developing endochondral skeleton. © 2014 American Society for Bone and Mineral Research.

KEY WORDS: BMP; ALK2; ACVR1; CHONDROGENESIS; MOUSE

Introduction

Bone morphogenetic proteins (BMPs) are crucial regulators of chondrogenesis. BMPs transduce their signals through three type I receptors: BMP receptor type 1 A (BMPR1A, also known as ALK3), BMPR1B (ALK6), and activin receptor type 1 A (ACVR1/ActR1/ALK2). BMPR1A and BMPR1B are structurally similar and bind BMPs.[1] ACVR1 binds to a more diverse set of ligands, including TGF-βs, activins, and multiple BMPs.[2–4]

The majority of the vertebrate skeleton forms through endochondral ossification, and BMPs play essential roles at many steps in this process. BMP signaling is required to maintain expression of Sox9, a transcription factor essential for commitment to the chondrogenic fate,[5,6] and for these cells to differentiate as chondrocytes and organize into a growth plate. The growth plate consists of zones of proliferating cells, followed by postmitotic prehypertrophic and hypertrophic chondrocytes.[7] BMP signaling is required to promote proliferation and differentiation.[8–10] Growth plates form in mice deficient in *Bmpr1a* or *Bmpr1b*, but chondrogenesis is arrested at the condensation stage in mice lacking both receptors in cartilage.[6,10,11] The function of ACVR1/ALK2 is not as well characterized. The ability of ACVR1 to promote chondrogenesis has been established in vitro.[12,13] Its importance in vivo is demonstrated by the fact that fibrodysplasia ossificans progressiva (FOP), a rare disorder characterized by progressive ossification of connective tissue,[14] is caused by an activating mutation in *Acvr1* (the gene that encodes ALK2).[15,16] Constitutively active ACVR1 can cause ectopic endochondral ossification.[17] The activating mutant can also enhance chondrogenic commitment of progenitor cells and predispose mesenchymal cells to an osteoblastic fate.[18] However, FOP patients have only subtle developmental defects.[14] Therefore, whether ACVR1 activity is required for normal chondrogenesis is unknown. Moreover, whether this receptor has unique functions in line with its unique ability to engage diverse TGF-β ligands is unknown. We generated mice lacking ACVR1 in cartilage to address these questions.

Materials and Methods

Generation of *Acvr1*^{CKO} and *Bmpr1a*^{CKO}; *Acvr1*^{CKO}, and *Bmpr1b*$^{-/-}$; *Acvr1*^{CKO} mice

Generation and genotyping of *Bmpr1b*, *Bmpr1a*, *Acvr1*, and *Col2-Cre* mice has been described.[11,19–21] To generate cartilage-

Received in original form April 9, 2014; revised form September 7, 2014; accepted October 7, 2014. Accepted manuscript online November 21, 2014.
Address correspondence to: Karen M Lyons, PhD, 510 OHRC, 615 Charles E Young Dr. South, Los Angeles, CA 90095, USA. E-mail: klyons@mednet.ucla.edu
Additional Supporting Information may be found in the online version of this article.

Journal of Bone and Mineral Research, Vol. 30, No. 4, April 2015, pp 733–741
DOI: 10.1002/jbmr.2385

specific *Acvr1* null mice, *Acvr1*$^{fx/+}$;*Col2-Cre* mice were intercrossed to generate *Acvr1*$^{fx/fx}$;*Col2-Cre* (*Acvr1*^{CKO}) mice. *Acvr1*$^{fx/-}$;*Bmpr1a*$^{fx/+}$;*Col2-Cre* mice were intercrossed to generate *Acvr1*^{CKO};*Bmpr1a*^{CKO};mice (referred to as *Acvr1/Bmpr1a*^{CKO}). An analogous scheme was used to generate *Acvr1*^{CKO};*Bmpr1b*$^{-/-}$ mice. All procedures were approved by the Institutional Animal Care and Use Committee at UCLA (IACUC protocol number 95–018).

Skeletal preparation and histology

Skeletal preparations were performed as described.[22] For histology, embryos were fixed in 4% paraformaldehyde, decalcified, and embedded in paraffin. Sections were stained with hematoxylin and eosin or Alcian blue and nuclear fast red.[23]

Immunohistochemistry

Primary antibodies were ACVR1/ALK2 (Sigma, Dallas, TX ; SAB1306388–40TST; 1:100), proliferating cell nuclear antigen (PCNA) (Invitrogen, Chicago, IL; 13–3900), phospho-SMAD1/5 (Cell Signaling Technology, Boston, MA), or p-p38 (Cell Signaling Technology; 9211,1:00). As a control for specificity, a second ACVR1 antibody (Abcam, Cambridge, MA; 155981; 1:100) was used for immunohistochemistry (IHC); similar results were obtained (data not shown). Sections were quenched in 3% H_2O_2 in methanol, blocked with 0.5% blocking reagent (TSA Biotin System; Perkin Elmer, Waltham, MA, USA; NEL700A) in TBS (100 mM Tris pH 7.5, 150 mM NaCl), incubated with primary antibody overnight at 4 °C, and then washed and incubated overnight at 4 °C with Alexa-Fluor-488-conjugated or Alexa-Fluor-555-conjugated rabbit secondary antibody (Invitrogen). Detection of antibody binding was performed using the TSA Biotin System according to the manufacturer's instructions. Fluorescence detection was conducted using Streptavidin–AlexaFluor-488 or Streptavidin–AlexaFluor-555 (Invitrogen) secondary antibodies; sections were counterstained with 4,6-diamidino-2-phenylindole (DAPI) (Invitrogen; D1306). Quantitation of pSmad1/5-positive and PCNA-positive cells was performed as described;[24] at least three sections from 5 mice per genotype were examined by individuals blinded to genotype. Total cells (DAPI-positive) and the percentage of total cells (DAPI-positive cells that were also pSmad1/5-positive) were determined and statistical significance assessed using Student's *t* test.[24]

Western blot analysis

Primary chondrocytes were isolated from costal cartilage as described[25] and seeded at $1 \times 10^{(5)}$ cells/well in 12-well plates. Cells were maintained in chondrogenic medium for 3 days. They were then washed twice with 1× PBS and treated with ACVR1/ALK2 shRNA lentivirus transmission particles (Sigma-Aldrich; SHCLNV-NM_007394; TRCN0000361057) at a multiplicity of infection (MOI) of 10 in serum-free medium for 24 hours. Cells were then maintained in chondrogenic medium for 72 hours. Cells were lysed in radioimmunoprecipitation assay (RIPA) buffer supplemented with protease and phosphatase inhibitors as described.[25] Whole-cell lysates were run on 10% SDS-polyacrylamide gels and transferred onto polyvinylidene fluoride (PVDF) membranes. The membranes were blocked with 5% milk in TBS-Tween (30 mM Tris pH 74, 300 mM NaCl, 0.2% Tween 20), incubated with primary antibody (ACVR1/ALK2; Sigma; SAB1306388–40TST;1:100) (Tubulin; Cell Signaling; 2144; 1:2000) for 1 hour at room temperature and then incubated with secondary antibody diluted in blocking buffer for 1 hour at room temperature. Binding was detected using the ECL Plus kit (GE Healthcare).

X-ray and micro–computed tomography analysis

X-ray analyses of adult mice were performed using a Faxitron as described.[11] Micro–computed tomography (μCT) analysis of neonates was performed as described.[22]

Results

Expression of ACVR1/ALK2

We examined ACVR1 protein expression in the skeletal system from E10.5 through birth (P0). Western analysis revealed that the antibody employed in these studies detected a single band of the expected size of approximately 57 kDa in primary chondrocytes; lentiviral shRNA against ACVR1 significantly reduced the detection of this band (Supporting Fig. 1). The results are consistent with and extend previous in situ hybridization studies[12,26,27] that indicated diffuse expression of *Acvr1 (Alk2)* mRNA throughout the growth plate. In craniofacial elements, expression was detected beginning at E10.5 in mesenchyme (Supporting Fig. 2), and by E12.5 in condensing cartilage (Supporting Fig. 2B). By E14.5, expression was seen in proliferating chondrocytes in the sphenoid and at lower levels in adjacent resting chondrocytes in the spheno-occipital synchondrosis (Supporting Fig. 2C). At E16.5, expression persisted in proliferating chondrocytes, and high levels of ACVR1 protein were seen in hypertrophic chondrocytes (Supporting Fig. 2D, E). This expression persisted at P0 (data not shown).

ACVR1 protein was not strongly expressed in appendicular elements until a growth plate had formed. At E13.5, ACVR1 protein was detected in proliferating chondrocytes, and at higher levels in hypertrophic chondrocytes (Supporting Fig. 2F). By E16.5, ACVR1 protein expression persisted in proliferating chondrocytes but was expressed at higher levels in hypertrophic chondrocytes (Supporting Fig. 2G). This pattern persisted through P0 (data not shown).

The highest levels and earliest onset of ACVR1 protein expression were detected in axial elements. Expression was first seen at E11.5 in sclerotomal cells (Fig. 1*A–D*). Consistent with a previous report,[28] ACVR1 protein was also expressed in the notochord at this stage (Fig. 1*C, D*). By E13.5, ACVR1 protein expression was strong in the nucleus pulposus. Expression could also be seen in proliferating chondrocytes in vertebral bodies (Fig. 1*E, F*). This pattern persisted at E15.5 (Fig. 1*G*). At P0, expression was strong in the nucleus pulposus, and persisted in the proliferating chondrocytes in cartilage endplates of vertebral bodies (Fig. 1*H*).

Although our studies of ACVR1 protein localization—indicating expression throughout midgestation stages in proliferating chondrocytes, notochord, and perichondrium—are consistent with previous in situ studies,[12,26,27] our finding of relatively higher levels of ACVR1 protein in hypertrophic chondrocytes would not be predicted from these studies. It is conceivable that ACVR1 protein produced in less mature chondrocytes persists and accumulates on the surface of maturing chondrocytes. However, we cannot rule out the possibility of cross-reactivity with an unrelated antigen in the hypertrophic zone, as discussed further below.

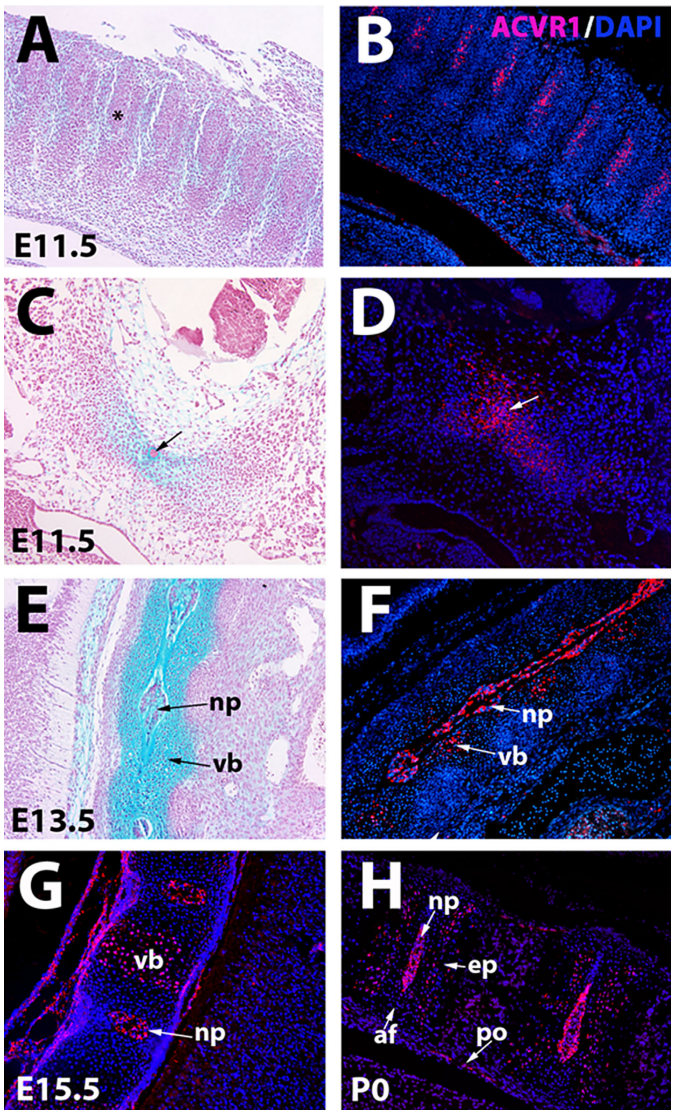

Fig. 1. ACVR1/ALK2 protein expression in axial elements. (*A*, *C*, *E*) Stained with Alcian blue-nuclear fast red. (*B*, *D*, *F*, *G*, *H*) are immunofluorescent images counterstained with DAPI. (*A*, *B*) E11.5 cervical region showing ACVR1/ALK2 protein is expressed in sclerotome (asterisk). (*C*, *D*) E11.5 cervical region showing expression in precartilaginous mesenchyme (detected by Alcian blue staining in *C*), and notochord (arrows). (*E*, *F*) Sections through E13.5 cervical spine showing expression in nucleus pulposus and chondrocytes in the vertebrae. (*G*) E15.5 cervical spine showing expression in nucleus pulposus and proliferating chondrocytes in vertebral bodies. (*H*) P0 cervical spine showing expression in endplate cartilage and nucleus pulposus. Low levels of expression are present in the periosteum of the vertebrae. af = annulus fibrosus; ep = endplate; np = nucleus pulposus; po = periosteum; vb = vertebral body.

Phenotype of mice lacking AVCR1/ALK2 in cartilage

We used a conditional allele of *Acvr1* (*Alk2*)[21] to investigate the function of ACVR1 in cartilage. To assess the efficiency of recombination and as a test of specificity of the ACVR1 antibody used to characterize ACVR1 expression, we performed IHC on *Acvr1*$^{fx/fx}$;*Col2a1-Cre* (hereafter referred to as *Acvr1*^{CKO}) growth plates (Supporting Fig. 3A, B). This analysis revealed that at least 80% of the proliferating chondrocytes had undergone efficient recombination (Supporting Fig. 3C). Immunoreactivity persisted in the nucleus pulposus as expected because this structure is not derived from *Col2a1-Cre*–expressing cells. Within *Col2a1-Cre*–expressing cells, immunoreactivity persisted in hypertrophic chondrocytes in mutants. As discussed above, we cannot rule out the possibility that this represents cross-reactivity of the antibodies we used. However, the strong reduction in ACVR1 protein observed in *Acvr1*^{CKO} vertebral chondrocytes argues that efficient recombination occurred and that the antibody used to detect ACVR1 protein displays reasonable specificity.

Acvr1^{CKO} mice were recovered in Mendelian ratios. No abnormalities were seen in heterozygotes. However, *Acvr1*^{CKO} neonates exhibited axial defects with 100% penetrance ($n = 23$). The cervical vertebral column was compressed, and cervical elements were thinner and broader than in WT littermates (Fig. 2*A*, *B*). Transverse views showed that the diameters of cervical vertebrae were enlarged in mutants (Fig. 2*C*–*E*′). The vertebral arches of cervical vertebrae C_1 (Fig. 2*C*, *C*′) and C_2 (Fig. 2*D*, *D*′) were hypoplastic and failed to fuse. Transverse processes on C_3 through C_7 were incomplete (Fig. 2*E*, *E*′, and data not shown), and the centra exhibited delayed ossification. Histological analyses did not reveal obvious defects in the sizes of condensations, or in chondrocyte differentiation in axial or appendicular elements at E13.5 (Supporting Fig. 4), suggesting either a subtle defect and/or later onset.

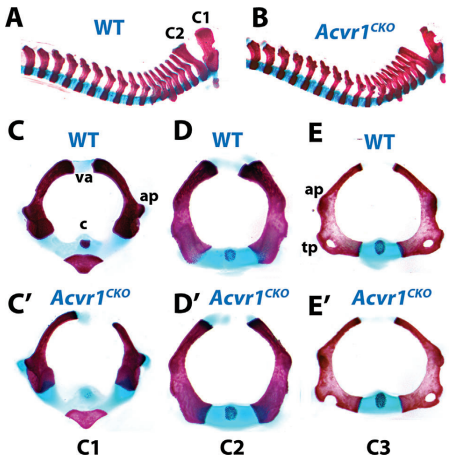

Fig. 2. Axial defects in *Acvr1*$^{fx/fx}$;*Col2a1-Cre* (*Acvr1*^{CKO}) mutants. All images are whole-mount skeletal preparations of neonatal (P0) littermates stained with Alcian blue/alizarin red. Cervical and thoracic spines of P0 WT (*A*) and *Acvr1*^{CKO} (*B*) littermates. (*C*–*E*) Transverse views of isolated WT cervical (C_1–C_3) vertebrae. (*C*′–*E*′) C_1, C_2, and C_3 vertebrae, respectively, from *Acvr1*^{CKO} P0 littermate. ap = anterior process; c = centrum; tp = transverse process; va = vertebral arch.

BMPs exert their effects through canonical (Smad) and noncanonical (eg, p38) pathways. Because a subtle defect was detected in *Acvr1*^{CKO} axial elements at P0 (Fig. 2), pSmad1/5/8 levels were assessed in vertebral bodies. A small but statistically significant decrease in the percentage of cells positive for pSmad1/5/8 was seen in *Acvr1*^{CKO} mutants at E17.5 (Fig. 3*A*, *B*), but not at E13.5 (data not shown). p-p38 levels were examined to determine whether differences in noncanonical BMP pathway activity could be detected. This analysis revealed an impairment in noncanonical pathway activity in mutants at E17.5 (Fig. 3*C*, *D*). Proliferation, assessed by PCNA, was indistinguishable between WT and mutant littermates at E13.5 (data not shown), but was reduced at E17.5 in *Alk2*^{CKO} vertebrae (Fig. 3*E*, *F*). Therefore, loss of ACVR1/ALK2 leads to decreased canonical and noncanonical signaling in axial chondrocytes, and this is correlated with reduced rates of cell proliferation.

X-ray analysis of adult mice revealed no differences between WT and heterozygotes ($n = 15$). However, 100% of *Acvr1*^{CKO} (9/9) mice developed thoracic kyphosis (Supporting Fig. 5A). Mutant cervical and upper thoracic vertebrae exhibited wedging characteristic of butterfly vertebrae (Supporting Fig. 5B). Consistent with the cervical defects seen at P0 (Fig. 2), cleared skeletal preparations revealed deformations in cervical vertebrae (Supporting Fig. 5C, D). Lumbar and sacral vertebrae were indistinguishable in adult WT and mutant littermates (data not shown). *Acvr1*^{CKO} mice also exhibited broader skulls as a result of a shortened cranial base ($n = 9/9$) (Supporting Fig. 5E). Measurements of the lengths of appendicular bones revealed no differences at any stage (data not shown).

Overlapping functions with other BMP receptors

Loss of BMPR1A in cartilage leads to generalized chondrodysplasia and perinatal lethality.[10] *Bmpr1b*$^{-/-}$ mice are viable, but exhibit appendicular skeletal defects, including brachypodism and shortened long bones.[11] The pattern of ACVR1/ALK2 expression overlaps with those of BMPR1A and BMPR1B.[10,26,29] Double mutants were constructed to test whether ACVR1 shares overlapping functions with these receptors.

Analysis of craniofacial (data not shown) and axial elements revealed a considerable degree of cooperative function between ACVR1 and BMPR1A. As discussed, C_1 and C_2 are hypoplastic in neonatal *Acvr1*^{CKO} mice (Fig. 1*A*, *B*; Fig. 4*A*–*B*′; $n = 6$). *Bmpr1a*^{CKO} mutants also exhibited axial defects ($n = 5$) (Fig. 4*C*, *C*′). In contrast to *Acvr1*^{CKO} mice, in which defects are most severe in cervical vertebrae, *Bmpr1a*^{CKO} mice exhibit more severe defects in thoracic vertebrae (Fig. 4*B*, *C*); vertebral arches are severely malformed in *Bmpr1a*^{CKO} (Fig. 4*A*′–*C*′).

In *Acvr1/Bmpr1a*^{CKO} double mutants, the entire vertebral column is severely malformed. Centra are absent, and the vertebral arches are diminished (Fig. 4*D*, *D*′, and data not shown). In the upper cervical region, there is a failure in segmentation (evidenced by the non–Alcian blue-stained center of the spinal column; arrow in Fig. 4*D*). Disorganized and incomplete ossification is seen in the lower cervical and thoracic regions (Fig. 4*D*). At E12.5, vertebral bodies in *Acvr1/Bmpr1a*^{CKO} mutants are slightly smaller than in WT littermates, and Alcian blue staining appears less intense (Supporting Fig. 6A, B). Consistent with reduced proliferation in cervical vertebrae in E17.5 *Acvr1*^{CKO} mutants (Supporting Fig. 3E, F),

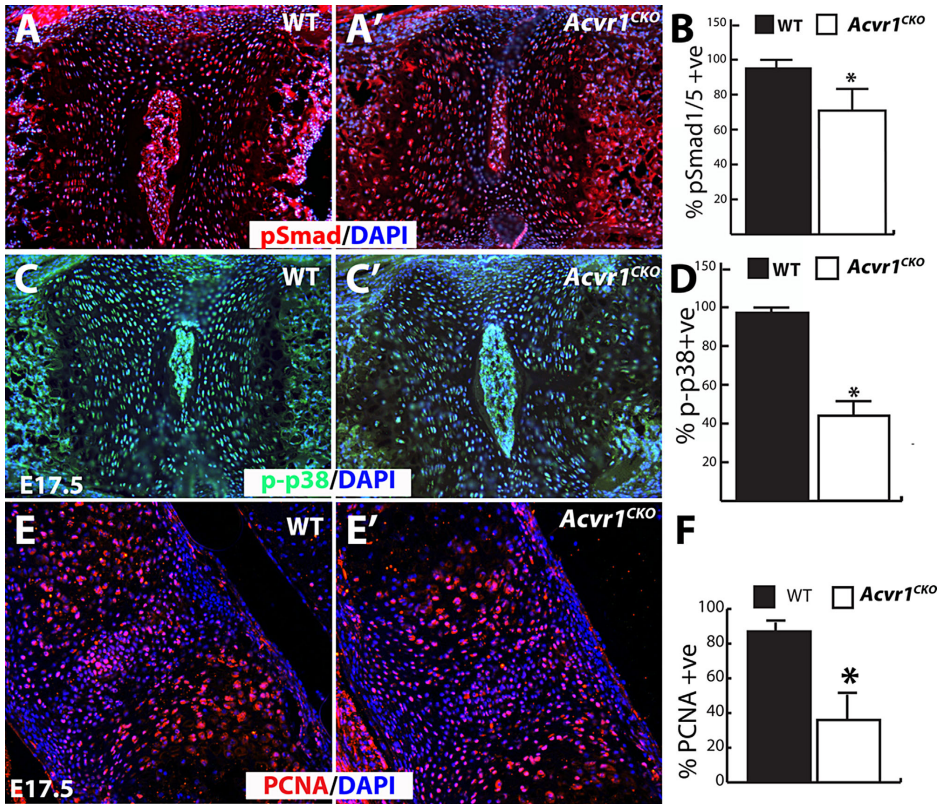

Fig. 3. Impaired BMP signaling in *Acvr1*$^{fx/fx}$;*Col2a1-Cre* (*Acvr1*^{CKO}) mutant axial elements. All images are sagittal sections through the vertebral column of E17.5 mice counterstained with DAPI. (*A*, *A*′) Immunofluorescence staining for pSmad1/5 in sections through E17.5 cervical vertebrae from WT and *Acvr1*^{CKO} littermate. (*B*) Quantitation revealed a reduction in *Acvr1*^{CKO} mice in the percentages of cells positive for pSmad1/5 compared to WT littermates ($n = 16$, $p < 0.0001$). (*C*, *C*′) Immunofluorescence staining for p-p38 in sections through E17.5 cervical vertebrae from WT and *Acvr1*^{CKO} littermate. (*D*) Quantitation revealed a reduction in *Acvr1*^{CKO} mice in the percentages of cells positive for p-p 38 compared to WT littermates ($n = 9$, $^*p < 0.0001$). (*E*, *E*′) PCNA immunofluorescence on E17.5 cervical vertebrae from WT and *Acvr1*^{CKO} littermate. (*F*) Quantitation of percentage of PCNA positive cells reveals a significant decrease in mutants. ($n = 6$, $^*p < 0.005$). Size differences in the nucleus pulposus for WT versus *Acvr1*^{CKO} mice in *A* and *C* are not real and are a result of the plane of section. DAPI = 4,6-diamidino-2-phenylindole; PCNA = proliferating cell nuclear antigen.

vertebral bodies appear smaller in *Alk2*^{CKO} mice at E17.5 (Supporting Fig. 6C, D). *Acvr1/Bmpr1a*^{CKO} axial elements are disorganized (Supporting Fig. 6C, E). There is a failure in segmentation and formation of nuclei pulposi.

Acvr1^{CKO}/*Bmpr1b*$^{-/-}$ P0 double mutants also exhibited craniofacial (data not shown) and vertebral abnormalities not seen in either single mutant strain. *Bmpr1b*$^{-/-}$ mice exhibited no ossification of the cervical centra at E17.5, but were otherwise normal (Fig. 4*E*, *E*′). This was also observed in *Acvr1*^{CKO}/*Bmpr1b* double mutants (Fig. 4*F*). All vertebrae were thinner than in *Bmpr1b*$^{-/-}$ or *Acvr1*^{CKO} mutants. Transverse processes were thin or discontinuous along the length of the vertebral column in *Acvr1/Bmpr1b* double mutants (Fig. 4*F*′). Vertebral fusions affecting thoracic vertebrae were occasionally observed in double mutants ($n = 2/6$). These were not seen in *Acvr1*^{CKO} or *Bmpr1b*$^{-/-}$ mice ($n = 9$).

As discussed, appendicular elements in *Acvr1*^{CKO} mutants were indistinguishable from those in WT littermates, except for a delay in ossification of digits (Fig. 5*A*, *B*). Forelimbs of *Bmpr1a*^{CKO} mice exhibit aplastic scapulae and shortened long bones[10] (Fig. 5*C*). The radius and ulna are shorter in *Acvr1/Bmpr1a*^{CKO} mice than in *Bmpr1a*^{CKO} mice ($n = 6$) (Fig. 5*D*). Similar findings were seen in hindlimbs (data not shown). Histological analysis revealed that growth plates from *Acvr1*^{CKO} mutants are

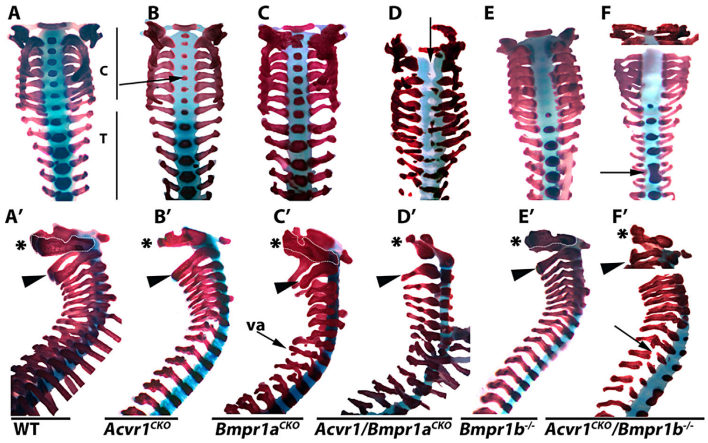

Fig. 4. ACVR1/ALK2 exhibits overlapping functions with BMPR1A and BMPR1B in axial elements. All images are cleared skeletal preparations of P0 spines (disarticulated from ribs) stained with Alcian blue/Alizarin red. (*A–F*) Dorsal views. (*A′–F′*) Lateral views. Arrow in *B* highlights reduced ossification of the centra in *Acvr1*^{CKO} mice. Arrow in *D* highlights lack of segmentation, evidenced by gaps in staining in regions where ossified centra should be located. Arrow in *F* highlights vertebral fusion. Arrow in *F′* highlights discontinuous vertebral arch. (*A′–F′*) Asterisks demarcate the axis (C_1); arrowheads demarcate the atlas (C_2). C = cervical; T = thoracic; va = vertebral arch.

indistinguishable from those of WT littermates (Fig. 5*E, F*). As shown,[10] *Bmpr1a*^{CKO} growth plates exhibit disorganized and short columnar zones (Fig. 5*G*). In *Acvr1/Bmpr1a*^{CKO} double mutants, the columnar zone is further reduced and disorganized (Fig. 5*H*). ACVR1 and BMPR1B also exhibited evidence of coordinated functions in appendicular elements (Fig. 6). As shown,[11] *Bmpr1b*$^{-/-}$ mice exhibit brachypodism accompanied by fusion and reduction of the proximal and middle phalanges, and delayed ossification of metacarpals/metatarsals (Fig. 6*A, C, E, F*). The reduction in ossification of the metacarpals/metatarsals is more severe in *Acvr1*^{CKO};*Bmpr1b*$^{-/-}$ mutants than in either single mutant strain (Fig. 6*A–H*).

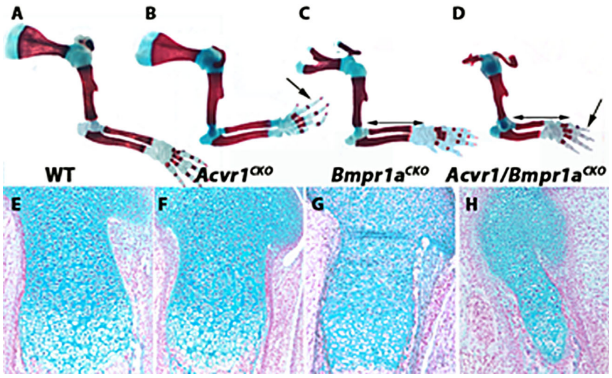

Fig. 5. Appendicular defects in *Acvr1*$^{fx/fx}$;*Bmpr1a*$^{fx/fx}$;*Col2a1-Cre* (*Acvr1/Bmpr1a*^{CKO}) mice. (*A–D*) Skeletal preparations from E17.5 forearms stained with Alcian blue/Alizarin red. Double-headed arrows in *C* and *D* highlight shortening of radius and ulna in *Acvr1/Bmpr1a*^{CKO} mice compared to *Bmpr1a*^{CKO} mice. Single-headed arrows in *B* and *D* highlight delayed ossification of digits in *Acvr1*^{CKO} mice, which is exacerbated in *Acvr1/Bmpr1a*^{CKO} mice. (*E–H*) Sagittal sections through proximal femurs of E17.5 mice of the indicated genotypes stained with Alcian blue/nuclear fast red.

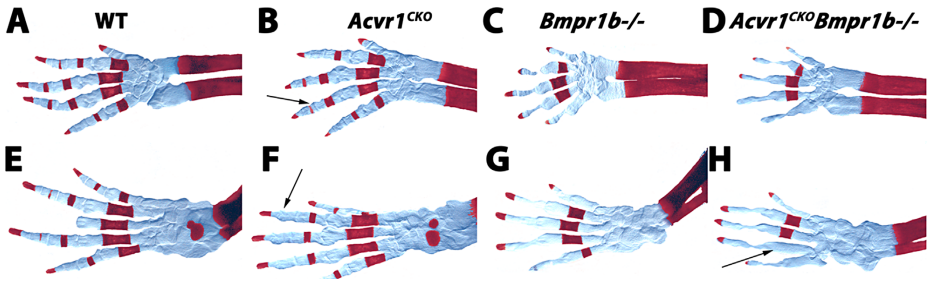

Fig. 6. Appendicular defects in *Acvr1*$^{fx/fx}$;*Bmpr1b*$^{-/-}$;*Col2a1-Cre* (*Acvr1*^{CKO}/*Bmpr1b*$^{-/-}$) mice. Cleared skeletal preparations from E17.5 autopods of forelimbs (*A–D*) and hindlimbs (*E–H*) stained with Alcian blue/nuclear fast red. A blue filter was applied in PhotoShop to the images to enhance visualization of Alcian blue–stained regions. Arrows in *B* and *F* point to reduced or absent ossification in phalangeal elements in *Acvr1*^{CKO} mice. Arrow in *H* highlights absence of ossification in the *Acvr1*^{CKO}/*Bmprb*$^{-/-}$ hindlimb compared to the *Acvr1*^{CKO} and *Bmpr1b*$^{-/-}$ single mutant strains.

Discussion

These studies demonstrate that ACVR1/ALK2 is essential for normal endochondral bone formation. Mice lacking *Bmpr1a* in cartilage exhibit lethal chondrodysplasia.[6] Loss of *Bmpr1b* in mice and humans is not lethal, and defects are most prominent in appendicular elements.[11,30,31] We show here that *Acvr1*^{CKO} mice are viable but exhibit craniofacial and axial defects. Thus, BMPR1A appears to have global functions, whereas ACVR1/ALK2 and BMPR1B have more restricted roles in committed chondrocytes in axial and appendicular elements, respectively. These differential roles may reflect differences in expression of these receptors or the BMP ligands that activate them.[11]

All three type I receptors are expressed to some extent in appendicular, axial, and craniofacial elements, raising the possibility of overlapping or coordinated functions. This was shown for BMPR1A and BMPR1B by the absence of cartilage in *Bmpr1a*^{CKO};*Bmpr1b*$^{-/-}$ mice.[6] Here we show that ACVR1 also exerts overlapping functions in committed chondrocytes with BMPR1A and BMPR1B. Combined loss of ACVR1 and either BMPR1A or BMPR1B leads to perinatal lethality and generalized chondrodysplasia.

FOP patients harbor an activating mutation in *Acvr1*.[15,16] However, there are few developmental effects of this activating mutation in cartilage, the most penetrant of which is malformation of the great toes. This has also been demonstrated in chimeric mice carrying the FOP mutation.[32] Although delayed ossification of digits was observed in *Acvr1*^{CKO} mice, there were no additional defects in the great toe. It is important to bear in mind, however, that in *Acvr1*^{CKO} mice, excision occurs only in committed chondrocytes. Therefore, limb patterning defects that might affect the great toe would not be expected. Some FOP patients exhibit congenital abnormalities in the cervical spine, the area most severely affected in *Acvr1*^{CKO} mice. In FOP patients, the cervical spine exhibits large spinous processes and progressive fusion of articular processes.[33,34] In *Acvr1*^{CKO} mice, cervical spinous and articular processes are hypoplastic. Thus, cervical vertebrae are sensitive to both gain and loss of ACVR1 function. The basis for the strong effects of ACVR1 on cervical elements in relation to other vertebrae is unclear, but might be related to the fact that cervical vertebrae are the earliest to be specified in mammals but the last to become ossified, thus requiring a longer period of growth and development.[35,36]

We show here that loss of ACVR1 also leads to craniofacial defects. Distinct facial defects have been reported in a subset of FOP patients, including a reduced mandible and underdevelopment of the supraorbital ridge.[37] Defective mandibular development was reported in mice lacking ACVR1 in cranial neural crest cells.[21] Distinct craniofacial defects were observed in the present study, which can be attributed to defects in chondrogenesis in the cranial base. It is thus conceivable that some of the facial features seen in FOP patients are a consequence of altered development of the cranial base. Similarly, conductive hearing loss is seen in about 50% of FOP patients.[34] It is conceivable that this is due to craniofacial defects affecting the inner ear.

We did not detect obvious changes in appendicular elements in *Acvr1*^{CKO} mice. However, proximal medial tibial osteochondromas and short broad femoral necks are common but variable features of FOP patients.[34] We cannot rule out the possibility that there are subtle defects in appendicular elements in *Acvr1*^{CKO} mice. The fact that the appendicular skeletons of both *Acvr1/Bmpr1a*^{CKO} and *Acvr1*^{CKO}/*Bmpr1b*$^{-/-}$ mice are more severely affected than those of *Bmpr1a*^{CKO} or *Bmpr1b*$^{-/-}$ mice demonstrates that ACVR1 is expressed in and plays a role in the development of appendicular elements.

The precise mechanisms by which ACVR1 exerts its effects during chondrogenesis are unknown. We found that loss of ACVR1 led to reduced canonical (pSmad1/5) and noncanonical (p-p38) activity in axial elements, as has also been seen in mice lacking BMPR1A and/or BMPR1B in cartilage.[10,11] The majority of the literature has focused on the ability of ACVR1 to activate canonical Smads 1/5/8. This has been demonstrated most clearly using constitutively active or FOP variants of ACVR1.[16,21] Our observation of a reduction in pSmad1/5 levels in *Acvr1*^{CKO} mutants is consistent with these findings. ACVR1/ALK2 can activate noncanonical pathways in addition to canonical ones. For example, it was reported that ACVR1 regulates cell proliferation during formation of the vertebrate lens in a Smad-independent manner.[38] Thus, the reduced p-p38 levels

in *Acvr1*^{CKO} mutants may contribute to the observed chondrocyte proliferation defects. These are not mutually exclusive possibilities. Regardless of the precise mechanism, the strong synergy in phenotype seen in *Acvr1/Bmpr1a*^{CKO} and *Acvr1*^{CKO}/*Bmpr1b*$^{-/-}$ double mutants strongly argues that ACVR1 exerts its effects through BMP signaling pathways.

The fact that *Acvr1/Bmpr1a*^{CKO} double mutants exhibit defects along the entire length of the spine indicates that ACVR1 and BMPR1A have coordinated functions in all axial elements. The *Acvr1/Bmpr1a*^{CKO} phenotype resembles that of *Pax1/9* double mutants, in which failure of sclerotomal cells to migrate ventrally leads to the loss of medial structures such as the centra.[39] This is consistent with the fact that *Col2a1-Cre* is expressed in the sclerotome.[19] The observation that rates of proliferation are reduced in committed chondrocytes in vertebral elements in *Acvr1*^{CKO} mice indicates that ALK2 plays a role at multiple stages of chondrogenesis.

The subtlety of the developmental limb phenotype in *Acvr1*^{CKO} mice can be attributed at least in part to overlapping functions with both BMPR1A and BMPR1B. It is also possible that the *Acvr1* limb phenotype is less severe than the axial one because *Col2a1-Cre* is first expressed in committed chondrocytes in appendicular elements.[19] It is conceivable that ACVR1 also has important functions in the limb at an earlier stage; studies utilizing *Prx1-Cre* would be very informative in this regard, although as discussed in Results, we (Fig. 1, Supporting Fig. 2) and others[26] did not detect high levels of ACVR1 expression in prechondrogenic condensations in the limb. Similarly, it is possible that ACVR1 plays a role in maintenance of articular cartilage. Although ACVR1 does not appear to be as highly expressed as BMPR1A or BMPR1B in articular cartilage,[40] extra-articular ankylosis of all major joints is a key feature of FOP.[41] Postnatal ablation of ACVR1 in cartilage would be required to address this question and to separate direct effects on articular cartilage from indirect effects resulting from abnormal development.

Finally, we show that ACVR1 is strongly expressed in the notochord and nucleus pulposus, raising the possibility that this receptor plays an essential role in the formation/maintenance of these structures. ACVR1 has been shown to regulate the rate of cell proliferation in the node, the transient embryonic structure that gives rise to the notochord.[42] The use of a notochord-specific Cre line will be required to address the function, if any, of ACVR1 in the notochord and its derivatives.

In summary, this study shows that all three type I BMP receptors play essential roles in committed chondrocytes. BMPR1A appears to have the most prominent function: *Bmpr1a*^{CKO} mutants exhibit generalized chondrodysplasia; defects in *Bmpr1b*$^{-/-}$ mice are seen primarily in appendicular elements; and defects in *Acvr1*^{CKO} mice are primarily found in axial and craniofacial elements. The extent to which ACVR1 transduces its signals in cartilage through the canonical Smad pathway versus noncanonical pathways is unknown; we show that loss of ACVR1 impacts levels of both canonical pSmads and noncanonical p-p38. However, we have shown previously that BMPs transduce the majority of their signals in committed chondrocytes through R-Smad pathways, and we have shown here genetically that ACVR1 exerts overlapping functions with BMPR1A and BMPR1B. These findings suggest that ACVR1 also transduces its effects in cartilage to a significant extent through R-Smad–mediated pathways, but future studies are needed to address this issue.

Disclosures

All authors state that they have no conflicts of interest.

Acknowledgments

This work was supported by NIH grant R01 AR044528 (to KML). We thank Austin M. Rike for technical assistance.

Authors' roles: Study design: DR performed the analysis of cleared skeletal preparations, histological analysis, and Western blots. SB performed the ACVR1 immunolocalization and X-ray studies. TA, JKK, and YJL assisted with the histological analyses. DR and KML analyzed and interpreted data. DR and KML designed experiments. DR and KML drafted and revised the manuscript. KML accepts responsibility for integrity of data analysis.

References

1. Chen D, Zhao M, Mundy GR. Bone morphogenetic proteins. Growth Factors. 2004;22(4):233–41.
2. Clarke TR, Hoshiya Y, Yi SE, Liu X, Lyons KM, Donahoe PK. Mullerian inhibiting substance signaling uses a bone morphogenetic protein (BMP)-like pathway mediated by ALK2 and induces SMAD6 expression. Mol Endocrinol. 2001;15(6):946–59.
3. Daly AC, Randall RA, Hill CS. Transforming growth factor beta-induced Smad1/5 phosphorylation in epithelial cells is mediated by novel receptor complexes and is essential for anchorage-independent growth. Mol Cell Biol. 2008;28(22):6889–902.
4. Luo J, Tang M, Huang J, et al. TGFbeta/BMP type I receptors ALK1 and ALK2 are essential for BMP9-induced osteogenic signaling in mesenchymal stem cells. J Biol Chem. 2010;285(38):29588–98.
5. Haas AR, Tuan RS. Chondrogenic differentiation of murine C3H10T1/2 multipotential mesenchymal cells: II. Stimulation by bone morphogenetic protein-2 requires modulation of N-cadherin expression and function. Differentiation. 1999;64(2):77–89.
6. Yoon BS, Ovchinnikov DA, Yoshii I, Mishina Y, Behringer RR, Lyons KM. Bmpr1a and Bmpr1b have overlapping functions and are essential for chondrogenesis in vivo. Proc Natl Acad Sci USA. 2005;102(14):5062–7.
7. Kronenberg HM. Developmental regulation of the growth plate. Nature. 2003;423(6937):332–6.
8. Minina E, Kreschel C, Naski MC, Ornitz DM, Vortkamp A. Interaction of FGF, Ihh/Pthlh, and BMP signaling integrates chondrocyte proliferation and hypertrophic differentiation. Dev Cell. 2002;3(3):439–49.
9. Kobayashi T, Lyons KM, McMahon AP, Kronenberg HM. BMP signaling stimulates cellular differentiation at multiple steps during cartilage development. Proc Natl Acad Sci USA. 2005;102(50):18023–27.
10. Yoon BS, Pogue R, Ovchinnikov DA, et al. BMPs regulate multiple aspects of growth-plate chondrogenesis through opposing actions on FGF pathways. Development. 2006;133(23):4667–78.
11. Yi SE, Daluiski A, Pederson R, Rosen V, Lyons KM. The type I BMP receptor BMPRIB is required for chondrogenesis in the mouse limb. Development. 2000;127(3):621–30.
12. Zhang D, Schwarz EM, Rosier RN, Zuscik MJ, Puzas JE, O'Keefe RJ. ALK2 functions as a BMP type I receptor and induces Indian hedgehog in chondrocytes during skeletal development. J Bone Miner Res. 2003;18(9):1593–604.
13. Fujii M, Takeda K, Imamura T, et al. Roles of bone morphogenetic protein type I receptors and Smad proteins in osteoblast and chondroblast differentiation. Mol Biol Cell. 1999;10(11):3801–13.
14. Kaplan FS, Hahn GV, Zasloff MA. Heterotopic ossification: Two rare forms and what they can teach us. J Am Acad Orthop Surg. 1994;2(5):288–96.

15. Shore EM, Xu M, Feldman GJ, et al. A recurrent mutation in the BMP type I receptor ACVR1 causes inherited and sporadic fibrodysplasia ossificans progressiva. Nat Genet. 2006;38(5):525–7.
16. Shen Q, Little SC, Xu M, et al. The fibrodysplasia ossificans progressiva R206H ACVR1 mutation activates BMP-independent chondrogenesis and zebrafish embryo ventralization. J Clin Invest. 2009;119(11):3462–72.
17. Medici D, Shore EM, Lounev VY, Kaplan FS, Kalluri R, Olsen BR. Conversion of vascular endothelial cells into multipotent stem-like cells. Nat Med. 2010;16(12):1400–6.
18. van Dinther M, Visser N, de Gorter DJ, et al. ALK2 R206H mutation linked to fibrodysplasia ossificans progressiva confers constitutive activity to the BMP type I receptor and sensitizes mesenchymal cells to BMP-induced osteoblast differentiation and bone formation. J Bone Miner Res. 2010;25(6):1208–15.
19. Ovchinnikov DA, Deng JM, Ogunrinu G, Behringer RR. Col2a1-directed expression of Cre recombinase in differentiating chondrocytes in transgenic mice. Genesis. 2000;26(2):145–6.
20. Mishina Y, Hanks MC, Miura S, Tallquist MD, Behringer RR. Generation of Bmpr/Alk3 conditional knockout mice. Genesis. 2002;32(2):69–72.
21. Dudas M, Sridurongrit S, Nagy A, Okazaki K, Kaartinen V. Craniofacial defects in mice lacking BMP type I receptor Alk2 in neural crest cells. Mech Dev. 2004;121(2):173–82.
22. Retting KN, Song B, Yoon BS, Lyons KM. BMP canonical Smad signaling through Smad1 and Smad5 is required for endochondral bone formation. Development. 2009;136(7):1093–104.
23. Luna L. Histopathological methods and color atlas of special stains and tissue artifacts. Gaithersburg, MD: American Histologics. Inc. 1992.
24. Estrada KD, Retting KN, Chin AM, Lyons KM. Smad6 is essential to limit BMP signaling during cartilage development. J Bone Miner Res. 2011;26(10):2498–510.
25. Estrada KD, Wang W, Retting KN, et al. Smad7 regulates terminal maturation of chondrocytes in the growth plate. Dev Biol. 2013;382(2):375–84.
26. Verschueren K, Dewulf N, Goumans MJ, et al. Expression of type I and type IB receptors for activin in midgestation mouse embryos suggests distinct functions in organogenesis. Mech Dev. 1995;52-(1):109–23.
27. Minina E, Schneider S, Rosowski M, Lauster R, Vortkamp A. Expression of Fgf and Tgfbeta signaling related genes during embryonic endochondral ossification. Gene Expr Patterns. 2005;6(1):102–9.
28. Yoshikawa SI, Aota S, Shirayoshi Y, Okazaki K. The ActR-I activin receptor protein is expressed in notochord, lens placode and pituitary primordium cells in the mouse embryo. Mech Dev. 2000;91(1–2):439–44.
29. Takae R, Matsunaga S, Origuchi N, et al. Immunolocalization of bone morphogenetic protein and its receptors in degeneration of intervertebral disc. Spine (Phila Pa 1976). 1999;24(14):1397–401.
30. Demirhan O, Turkmen S, Schwabe GC, et al. A homozygous BMPR1B mutation causes a new subtype of acromesomelic chondrodysplasia with genital anomalies. J Med Genet. 2005;42(4):314–7.
31. Lehmann K, Seemann P, Boergermann J, et al. A novel R486Q mutation in BMPR1B resulting in either a brachydactyly type C/symphalangism-like phenotype or brachydactyly type A2. Eur J Hum Genet. 2006;14(12):1248–54.
32. Chakkalakal SA, Zhang D, Culbert AL, et al. An Acvr1 R206H knock-in mouse has fibrodysplasia ossificans progressiva. J Bone Miner Res. 2012;27(8):1746–56.
33. Schaffer AA, Kaplan FS, Tracy MR, et al. Developmental anomalies of the cervical spine in patients with fibrodysplasia ossificans progressiva are distinctly different from those in patients with Klippel-Feil syndrome: clues from the BMP signaling pathway. Spine (Phila Pa 1976). 2005;30(12):1379–85.
34. Kaplan FS, Xu M, Seemann P, et al. Classic and atypical fibrodysplasia ossificans progressiva (FOP) phenotypes are caused by mutations in the bone morphogenetic protein (BMP) type I receptor ACVR1. Hum Mutat. 2009;30(3):379–90.
35. Bagnall KM, Harris PF, Jones PR. A radiographic study of the human fetal spine. 2. The sequence of development of ossification centres in the vertebral column. J Anat. 1977;124(Pt 3):791–802.
36. Sofaer JA. Developmental stability in the mouse vertebral column. J Anat. 1985;140(Pt 1):131–41.
37. Hammond P, Suttie M, Hennekam RC, Allanson J, Shore EM, Kaplan FS. The face signature of fibrodysplasia ossificans progressiva. Am J Med Genet A. 2012;158A(6):1368–80.
38. Rajagopal R, Huang J, Dattilo LK, et al. The type I BMP receptors, Bmpr1a and Acvr1, activate multiple signaling pathways to regulate lens formation. Dev Biol. 2009;335(2):305–16.
39. Peters H, Wilm B, Sakai N, Imai K, Maas R, Balling R. Pax1 and Pax9 synergistically regulate vertebral column development. Development. 1999;126(23):5399–408.
40. Muehleman C, Kuettner KE, Rueger DC, Ten Dijke, Chubinskaya P. Immunohistochemical localization of osteogenetic protein (OP-1) and its receptors in rabbit articular cartilage. J Histochem Cytochem. 2002;50(10):1341–50.
41. Kaplan FS, Chakkalakal SA, Shore EM. Fibrodysplasia ossificans progressiva: mechanisms and models of skeletal metamorphosis. Dis Model Mech. 2012;5(6):756–62.
42. Komatsu Y, Kaartinen V, Mishina Y. Cell cycle arrest in node cells governs ciliogenesis at the node to break left-right symmetry. Development. 2011;138(18):3915–20.

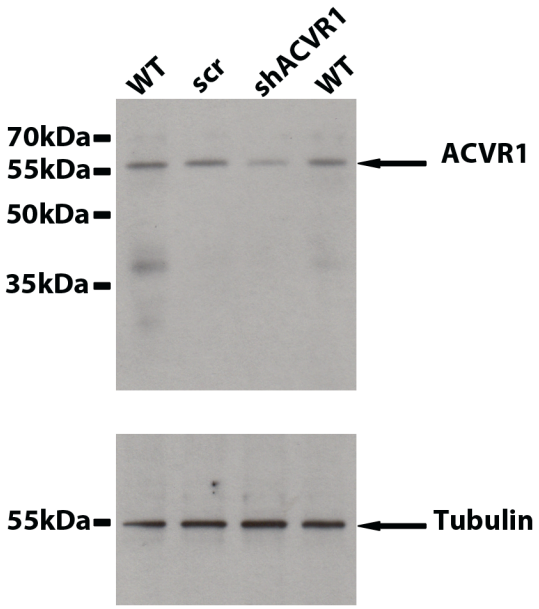

Supporting Figure 1. Western analysis of ACVR1 expression in primary chondrocytes. Primary sternal chondrocytes were isolated and maintained in chondrogenic medium and treated or not with scrambled (scr) or shACVR1 as described in Materials and Methods. A single band of the expected size was detected in lysates with anti-ACVR1 antibody (Sigma SAB1306388-40TST). Beta-Tubulin was detected as a loading control. The Western blot was performed three times with similar results. A representative blot is shown.

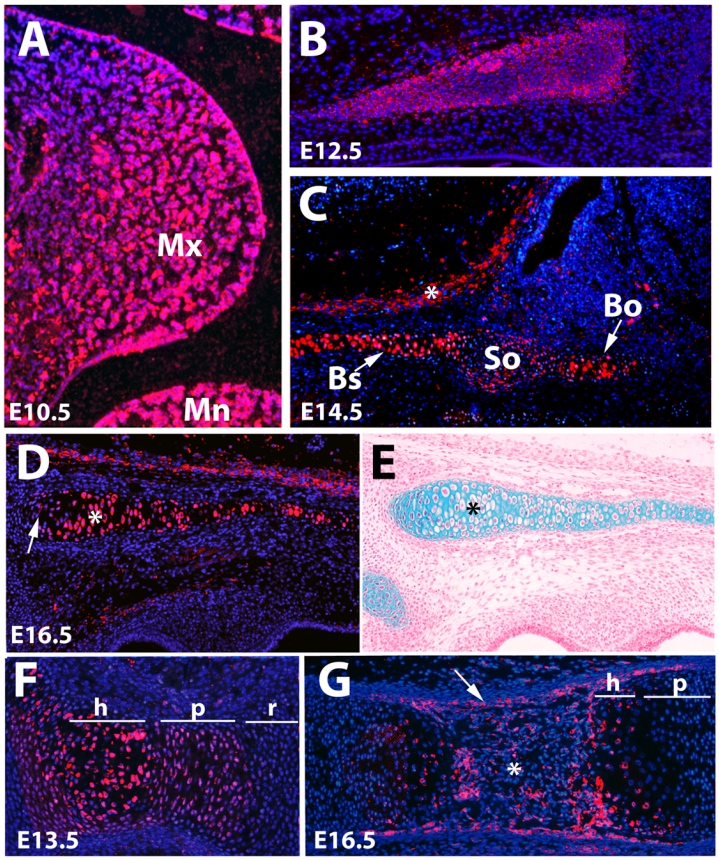

Supporting Figure 2. Expression of ACVR1/ALK2 protein in craniofacial and appendicular skeletal tissues. All images except (E) show immunofluorescent detection of ACVR1 counterstained with DAPI. (E) is stained with alcian blue-nuclear fast red A. Expression is seen in the E10.5 maxillary (Mx) and mandibular (Mn) mesenchyme. B. ACVR1 protein expression at E12.5 in the primordium of the basisphenoid bone. Expression is strongest in the perichondrium. C. ACVR1 protein expression in differentiated chondrocytes in the basisphenoid (Bs) and basioccipital (Bo) bones at E14.5. Lower levels are seen in less mature chondrocytes in the spheno-occipital synchondrosis (SO). ACVR1 protein is also expressed in arachnoid tissue (asterisk in C). D,E. Adjacent sections through the basioccipital bone

immunostained for ACVR1 (D) or stained with alcian blue (E). ACVR1 protein is expressed abundantly in differentiated (asterisk in D and E), and less mature (arrow in D and E)_chondrocytes. F. E13.5 femur showing ACVR1 protein expression throughout the proliferative and hypertrophic zones. G. E16.5 femur showing expression in hypertrophic chondrocytes, periosteum (arrow in G), and bone marrow (asterisk in G). h, hypertrophic; p, proliferative; r, resting.

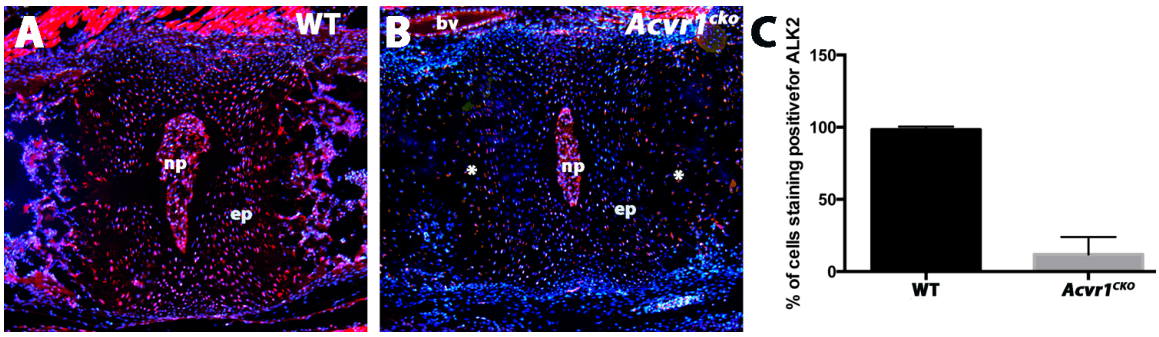

Supporting Figure 3. Efficient Cre-mediated recombination in *Acvr1*^{CKO} mice. A,B. Sections through vertebra of E17.5 WT (A) and *Acvr1*^{CKO} (B) mice showing immunofluoresecence staining for ACVR1 protein. In (A) immunofluorescence is detected in chondrocytes within the endplates (ep), and in the nucleus pulposus (np). In (B), ACVR1 protein is detected in the nucleus pulposus, derived from the notochord, but is diminished in endplate (ep) chondrocytes. Expression is also seen in the endothelial layer of an adjacent blood vessel (bv), demonstrating the specificity of recombination. Residual immunofluorescence is retained in hypertrophic chondrocytes (denoted by asterisks) in (B). It is unclear whether this reflects cross-reactivity of the antibody and/or incomplete recombination (C) Quantitation of recombination in proliferative chondrocytes ($n = 6$; $p < 0.0001$).

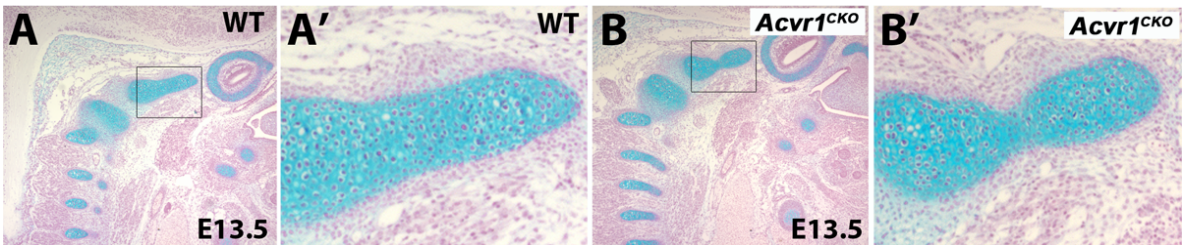

Supporting Figure 4. Histological examination of *Acvr1*^{CKO} vertebral elements. A,B. Sagittal sections through cervical regions of E13.5 WT and *Acvr1*^{CKO} littermate stained with alcian blue/nuclear fast red showing indistinguishable histology. A' and B' are higher magnifications of the boxed regions in A and B. The apparent difference in shape of the vertebral element is an artifact of the plane of section.

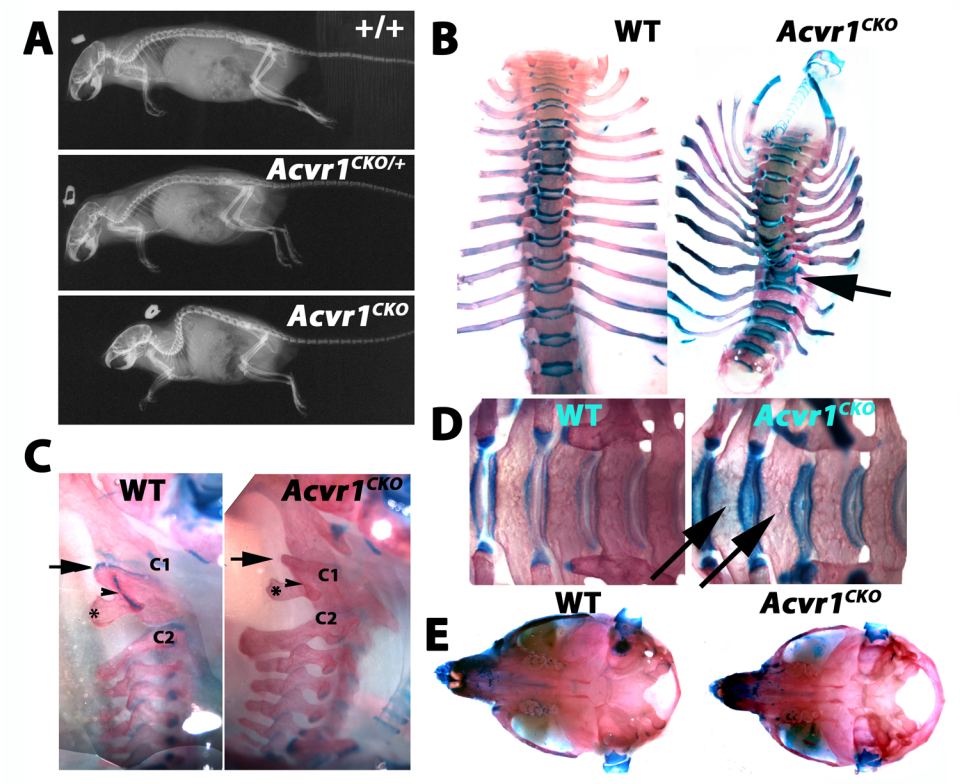

Supporting Figure 5. Craniofacial and axial defects in adult *Acvr1*^{CKO} mice. A, X-ray analysis of 7 month old mice revealing kyphosis. B-E, cleared skeletal preparations of 6-7 month old mice stained with alcian blue/alizarin red. B, Cleared skeletal preparations of 7 month old mice, showing wedging and herniation of T10 (arrow in B). C, Lateral views of cervical vertebrae in 6 month old mice. The *Acvr1*^{CKO} mutant exhibits a hypoplastic superior articular facet (arrows in WT and *Acvr1*^{CKO} littermate in C), and a hypoplastic transverse arch (arrowheads in C). The spinous process of the atlas (C1) (asterisks) is thinner in the mutant. The axis (C2) appears broader in the mutant in the image, but this is an artifact due to the angle of imaging. D, Ventral view of C2-T1. Several of the mutant vertebral bodies exhibit a "butterfly" configuration (arrows). E, Ventral views of skulls from 6 month old mice demonstrating shorter cranial base in mutants.

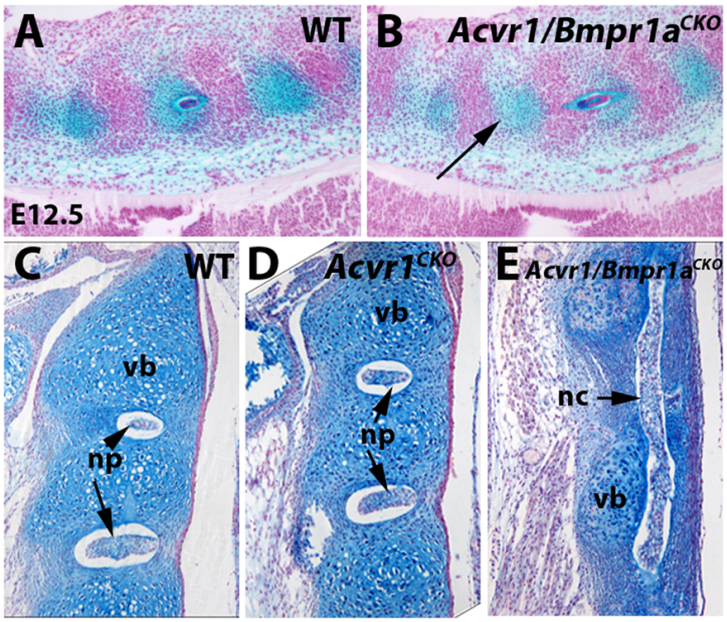

Supporting Figure 6. Histology of *Acvr1/Bmpr1a*^{CKO} cervical vertebrae. All images are sagittal sections stained with alcian blue/nuclear fast red. A,B. E12.5 WT and *Acvr1/Bmpr1a*^{CKO} littermate. Vertebral bodies (arrow in B) are smaller and less intensely stained in mutants. No differences were seen in *Acvr1*^{CKO} vs. WT littermates at this stage (Fig. 4). C-E, Sagittal sections through E17.5 cervical vertebrae. Vertebral bodies are slightly smaller in *Acvr1*^{CKO} mice compared to WT. E, In *Acvr1/Bmpr1a*^{CKO} mutants, the notochord persists, vertebral bodies are small, and cartilage matrix is sparse. nc, notochord; np, nucleus pulposus; vb, vertebral body.

CHAPTER FOUR:

Challenging the Dogma of Canonical BMP Signaling in the Absence of Smad4 during Endochondral Bone Formation

Abstract:

In the canonical BMP signaling pathway, the intracellular R-Smads 1, 5 and 8, transduce the signal by translocating to the nucleus in a complex with common Smad4, to activate or repress BMP target genes. The majority of studies to date indicate that Smad4 is an essential component of canonical BMP signaling. However, there is some evidence in the *Drosophila* literature that R-Smads transduce a limited amount of signaling in the absence of Smad4. To date, this has not been widely reported in vertebrates. Recent findings provide evidence that Smad1/5-dependent, Smad4 independent BMP signaling does occur in vertebrates. We find that cartilage-specific loss of Smads1/5/8 in results in severe chondrodysplasia yet cartilage-specific Smad4-knockout mice are viable and present with a much milder cartilage phenotype (Zhang et al., 2005; Retting et al., 2009). Therefore, in the context of the cartilage growth plate, Smad1/5-dependent, Smad4 independent BMP signaling may be the major mode of BMP signaling. A well-characterized BMP target gene, *Ihh*, albeit reduced, responds to BMP stimulation in isolated Smad4 deficient primary chondrocytes (Seki and Hata, 2004; Zhang et al., 2005). Smad4, however, is required for proper development of the zeugo- and autopodal skeletal elements before establishment of chondrogenic cell fate (Benazet and Zeller, 2013) and for activation of antagonistic pathways such as TGFβ signaling. Overall, these data exemplify that some systems may require Smad4 for canonical BMP transduction; however, Smad4 may be dispensable for

other systems, calling a re-evaluation of the putative BMP canonical pathway and the extent of BMP signaling.

Highlights: BMP, TGFβ; Smad; Mice; chondrocytes; dogma

Introduction:

Bone morphogenetic proteins (BMPs) and their receptors are essential for the formation of the axial and appendicular skeleton (Minina et al., 2001; Minina et al., 2002; Yoon et al., 2005). The formation of skeletal elements goes through a carefully regulated multistep process. BMPs are required for the initial formation of mesenchyme condensations, in which the cells express the Sox9 transcription factor, subsequently triggering differentiation into chondrocytes (Akiyama et al., 2002; Barna et al., 2007; Yoon et al., 2005). These chondrocytes undergo a program of differentiation mediated by Sox9 (Akiyama et al., 2002). This program coupled with BMPs promotes the formation and stratification of the growth plate, which is composed of resting, proliferating, pre- and terminal hypertrophic chondrocytes. The rapidly proliferating and hypertrophic chondrocytes secrete extracellular matrix proteins such as type II and X collagen, as well as aggrecan, that add substance and strength to the cartilage anlagen (Kronenberg, 2003; Song et al., 2009).

BMPs transduce their signaling by binding to complexes of type I and type II serine/threonine kinase receptors. Type II BMP receptors are constitutively active. Ligand binding triggers phosphorylation of the type I BMP receptors, which lead to phosphorylation at the C-terminal region of receptor regulated Smads (R-Smads 1/5/8) (Massague et al., 2005).

Signaling through the R-Smads is known as the canonical mode of BMP signaling. The R-Smads contain two distinct domains held together by a linker region. The N terminal domain (MHI) has DNA binding ability, while the C terminal domain (MH2) holds other Smad binding properties. The linker region of the protein is designed for proper regulation (activation and targeted degradation) of R-Smads (Alarcon et al., 2009; Fuentealba et al., 2007).

Overexpression of BMPs results in increased chondrocyte proliferation and fused skeletal elements (Brunet, 1998; Duprez, 1996). In contrast, loss of the type I receptor ALK3/BMPR1A and ALK6/BMPR1B leads to complete loss of cartilage formation (Rigueur et al., 2015; Yoon et al., 2005). Loss of R-Smads 1/5/8 result in a phenotype similar to the absence of ALK3 and ALK6 in cartilage, indicating that a canonical BMP pathway is essential to transduce BMP effects in the growth plate (Retting et al., 2009). In contrast to these severe phenotypes, Smad4 loss results in viability and only mild cartilage defects (Zhang et al., 2005). These divergent phenotypes show that in the context of the cartilage growth plate, the dominant mode of BMP signaling is mainly mediated through R-Smads in a Smad4-independent fashion. The exact mechanism by which this mode of signaling occurs is unknown.

BMPs also trigger non-Smad (noncanonical) pathways *in vivo* and *in vitro* through the TGFb-activated kinase TAK1/MAP3K7 which leads to p38 MAPK (MAPK1) activation (Greenblatt et al., 2010; Gunnell et al., 2010; Hoffmann et al., 2005; Shim et al., 2009). There are conflicting data that show that TAK1 can either promote or antagonize R-Smads in chondrocytes; however, the data suggest that Smad4 is not required for R-Smad-TAK1 interactions (Gunnell et al., 2010; Hoffmann et al., 2005).

The secreted factor Indian Hedgehog (IHH) is expressed in pre-hypertrophic chondrocytes and is required for maintenance of proliferation and thus growth of the cartilage growth plate. Moreover, *IHH* transcription is directly dependent on R-Smads 1/5/8 (Retting et al., 2009; Seki and Hata, 2004).

Here we investigate a mechanism underlying Smad1/5-dependent, Smad4-independent signaling in the growth plate. Cartilage-specific *Smad4* knockout mice (*Smad4CKO*) exhibit mild chondrodysplasia. Although Smad4CKO mice display lower levels of *Ihh* expression in the growth plate, the gene remains inducible by exogenous BMP ligand stimulation. *Ihh* may be one of the genes in the cartilage growth plate that requires Smads1/5/8 for induction, but remains in part, Smad4-independent. We also show that Smad4 is required for optimal levels of binding and responsiveness to BMP stimulation. However, we find that R-Smads do not require Smad4 for ability to bind to the *Ihh* promoter. We also show that Smad4 is indirectly required for crosstalk with the antagonistic TGFb pathway. Moreover, we show that Smad4 deficient chondrocytes display defects in phosphorylated Smad1/5/8 turnover that result in elevated levels and ectopic nuclear spatial positioning in chondrocytes. Furthermore, R-Smads and TAK1 may show enhanced cooperation to mediate BMP signaling in the absence of Smad4. Overall, we propose that a major mode of signaling during growth plate development occurs through R-Smad-mediated, Smad4-independent transcription.

Materials and Methods:

Mouse Strain

Smad4 cartilage-specific mutants were generated using the cre-loxP recombination system. The *Smad4* floxed allele was described by Chu et al., 2004. The recombination was driven by Cre expression under the control of the Collagen IIα1 promoter, *Col2a1-Cre*, a transgene described by Ovchinnikov et al., 2000. All mice were maintained on a mixed C57BL/6J/CD1 background, and were housed according to the National Institutes of Health (NIH) guidelines for care, and the use of the animals was under the approval of the UCLA Institutional Animal Care and Use Committee (IACUC), ARC #10095-018-52A. To obtain *Smad4CKO* mutants, a homozygous Smad4 floxed female was crossed with a heterozygous *Smad4* floxed; *Col2a1-Cre/+* male. We also crossed our mouse with Rosa-mTomato/mGFP reporter mice, which express constitutively red fluorescent protein prior to Conditional Cre expression, and subsequently green after Cre-mediated recombination (Muzumdar et al., 2007). WT and *Smad4fx/+; Col2a1-Cre* littermates were used as controls. There were no discernable differences between WT and *Smad4fx/+;Col2a1-Cre* mice.

Genotyping

A mixture of Phenol (Sigma-Aldrich, MO): Chloroform (Amresco, TX): Isoamyl Alcohol (Fisher Scientific, CA) (25:24:1 ratio) and a solution of ethanol (Decon Labs) were used to isolate and extract genomic DNA. Polymerase chain reaction (PCR) was performed using the following Cre recombinase and Smad4 primers from Invitrogen as follows: *Cre* Forward-TGGTCCTGGCATCGACATG, *Cre* Reverse-GGCTGCGGATGCTCTCAAT, *Smad4* Forward-

AAAATGGGAAAACCAACGAG and *Smad4* Reverse-TACAAGTGCTATGTCTTCAGCG. PCR products were then visualized on 1% or 2% agarose gels (Fisher Scientific).

Quantitative real-time Polymerase Chain Reaction (qRT-PCR).

RNA was extracted using the RNeasy kit (Qiagen, Valencia, CA, USA). Synthesis of cDNA was performed with the First Strand cDNA synthesis Kit (Fermenas, Glen Burnie, MD, USA). Quantitative real-time PCR reactions were performed with SYBR real-time PCR Master Mix (Fermentas) by sing a MX3005P qPCR system (Stratagene, Santa Clara, CA, USA). Reactions were run using a quantitative PCR (qPCR) machine (Agilent Technologies, Statagene MX3005P), with alternating annealing temperatures of 56°C and 55°C for multiple cycles. Gene expression was normalized to housekeeping genes such as actin. The primer sequences are as follows: *β-actin* forward-5'-CTGAACCCTAAGGCCAACCG-3', reverse-5'-GTCACGCACGATTTCCCTCTG-3'; *Ihh* forward-5'-GCTTCGACTGGGTGTATT-3', reverse-5' TGGCTTTACAGCTGACAG-3'; *Smad4* forward-5'-GACAAGGTGGGGAAAGTGAA-3', reverse-5'-CCTGAAGTCGTCCATCCAAT-3'.

Skeletal Preparation and Histology

Skeletal preparations were performed as described previously (Estrada et al., 2011; Rigueur et al., 2015). In brief, embryos were eviscerated and fixed in 95% EtOH over night at 4 °C, followed by Alcian Blue staining (0.01% Alcian Blue *GX (Sigma-Aldrich, A5268) w/v in 95% EtOH) overnight at room temperature. Samples were then stained with Alizarin Red (0.006% Alizarin Red S (Sigma-Aldrich, A5533) w/v in 1% KOH) for 3-4 hours and then cleared in a series of graded KOH in glycerol. Samples were stored in 100% glycerol indefinitely.

For histology embryos were fixed with 10% formalin (Fisher Scientific, SF100) overnight at 4°C, decalcified with Immunocal (Decal Chemical Corp., Tallman, NY, USA) overnight, embedded in paraffin, and cut at a thickness of 5-7 μm.

Immunofluorescence (IF)

Sections of embedded tissue were heated at 47˚C for 2 hours, left overnight in 100% xylene, and then rehydrated the following day through graded concentrations of EtOH (100%, 90%, 70%, 30%) and water. The slides were placed in citrate buffer (pH 6 Vector Laboratories, H-3300) boiled in the microwave for 1 minute and then in a water bath at 98˚C for 15 minutes.

For detection using the following primary antibodies; Smad1 (Cell Signaling, #9743), Smad5 (Cell Signaling, #9517), pSmad15/8 (Cell signaling, #9511), phospho Smad2/3 (Cell signaling, #8828), Smad4 (Santa Cruz, #7966; Abcam ab187094), pTAK1 (Cell signaling 4508), TAK1 (Abcam, #AB109526), TAK1 (Millipore, #2A12-ST1610) p38 and pp38 (Cell Signaling, #9212; #4511), Runx2 (Cell Signaling, #12556), ATF2 and ATF4 (Cell Signaling, #9221; #11815), Ihh (Abcam, #AB39634), sections were quenched in 3% hydrogen peroxide in methanol, blocked with 0.5% blocking reagent (TSA Biotin System, Perkin Elmer, NEL700A) in TBS (100mM Tris pH 7.5, 150mM NaCl) and incubated with primary antibody overnight at 4°C. Detection of binding was performed using the TSA Biotin System according to manufacturers instructions. Fluorescent detection was conducted using the streptavidin-AlexaFluor-594 or -488 (Invitrogen) secondary antibodies; sections were counterstained with DAPI (Invitrogen, D1306). Slides were washed and mounted with Fluoro-Gel (Electron Microscopy Sciences, #17985-30), coverslipped, and photographed under a fluorescent microscope.

Isolation of primary chondrocytes and treatment with Bone Morphogenetic Protein-2

Primary chondrocytes were isolated from *Smad4CKO* newborn mice and seeded at 1×10^5 cells/well in 12-well plates. Cells were maintained in chondrogenic medium for 3-4 days. Because mutants were rare, we opted to use *Smad4fx/fx* chondrocytes and drove recombination using adenoviral cre infection for the majority of our culture experiments. The primary chondrocytes from *Smad4fx/fx* cells were either infected for 24 hours with adenoviral Cre-recombinase (Ad-CRE) or adenovirus expressing GFP (Ad-GFP) as a control (University of Iowa Gene Transfer Vector Core, Iowa City, IA) at a multiplicity of infection of 150. DNA was isolated using aforementioned genotyping methods, and PCR was performed to verify *Smad4* excision as in Chu et al., 2004. Cells were treated with BMP2 for 1 hour, and lysates were collected for western blot analysis.

Western Blot

Lysates were prepared with NP-40 lysis buffer (25 mM Tris pH7.4, 150 mM NaCl, 2% NP-40, 0.1% SDS) supplemented with protease inhibitors (complete Mini Tablets, Roche Applied Science) and phosphatase inhibitors (Sigma-Aldrich, P5726). Whole cell lysates containing about 3-5 ug of protein and 1x Laemmli Sample buffer with 10% 1 M dichlorodiphenyltrichloroethane (DTT). The samples were heated at 90˚C for 5 minutes, run on a 10% SDS-PAGE gel, and then transferred onto a Polyvinylidene fluoride (PVDF) membrane. These membranes were then blocked in 5% BSA in Tris Buffered Saline with Tween 20 (0.2%) (TBST) and probed with Anti-pSmad1/5/8 (Cell Signaling, 1:2000, Cat. No.9511) and pSmad5 (Abcam, 1:2000, ab92698), and loading control antibodies tubulin (Sigma-Aldrich,T6793), b-actin (Sigma-Aldrich, A5316), for 1 hour. Membranes were washed and probed by a secondary goat anti-rabbit HRP-conjugated antibody (1:2000, Bio-Rad, Cat. No. 170-6515) for 30

minutes, followed by a 15-minute treatment in HRP substrate (Pierce ECL 2, 80196), and then left exposed for 1-30 seconds using the Bio-Rad-ChemiDoc Imager or film (Amersham Hyperfilm ECL, Cat No. 28906835). Blots were quantified using ImageJ, and averages and standard deviation were measured in Microsoft Excel in triplicates. A t-test (p-value<0.05) was used to validate significant differences in the data.

IHH promoter mutagenesis

Primers were used to implement the point mutations in the 740bp IHH luciferase promoter (Qiagen, CA). After PCR with this construct and the primers that implemented the nucleotide changes, bacteria were transformed via heat shock at 42˚C, plated, and incubated overnight on LB agar-ampicillin plates. Ten colonies were picked and grown overnight in LB medium containing ampicillin. Plasmid DNA was purified using Qiagen columns. Incorporation of the targeted mutations was confirmed by sequencing (Laragen, CA).

Results:

Efficient knockout of Smad4 in cartilage renders mild chondrodysplasia

Smad4fx/fx;Col2a1Cre cartilage-specific knockouts (*Smad4CKO*) were recovered at the expected Mendelian ratios and remained viable for a little over 2 months. As early as P0, *Smad4CKO* pups were smaller than wildtype (WT) littermates; the dwarfism, accompanied with a kinked spine, persisted until adulthood (Fig. 1A-D). At the age of 2 months, *Smad4CKO* mice displayed strong kyphosis at 100% penetrance (n=33), experienced difficulty eating, and therefore, were euthanized at an early adult age in accordance with UCLA's Animal Research Committee. The observations that *Smad4CKO* mice displayed mild chondrodysplasia and a

kinked spine are consistent with previous studies using a different *Smad4* conditional allele (Tan et al., 2007; Zhang et al., 2005). However, the degree of runting was greater in our *Smad4* mutants, and the kyphosis we observed was not reported by Zhang et al., 2005.

The allele we used to generate the *Smad4CKO* mice harbored loxP sites in exon 1, flanking the transcription start site of *Smad4*. This allele was well characterized and had previously been established as yielding a functional null upon Cre-mediated recombination (Chu et al., 2004); the Cre driver we used to ablate *Smad4* in cartilage was the same *Col2a1-Cre* transgenic allele used to generate both BMP receptor (BMPR1A/B) and Smad1/5/8 cartilage specific knockouts (Ovchinnikov et al., 2000; Retting et al., 2009; Yoon et al., 2005). A different *Smad4* floxed allele was used previously to carry out cartilage specific ablation of *Smad4*; the loxP sites flanked exon 8, and this mutant experienced *Smad4* nonsense mediated decay (Zhang et al., 2005), but the possibility remained that it was not a functional null. Moreover, the *Col2a1-Cre* mouse strain used for these studies has not been used by other groups.

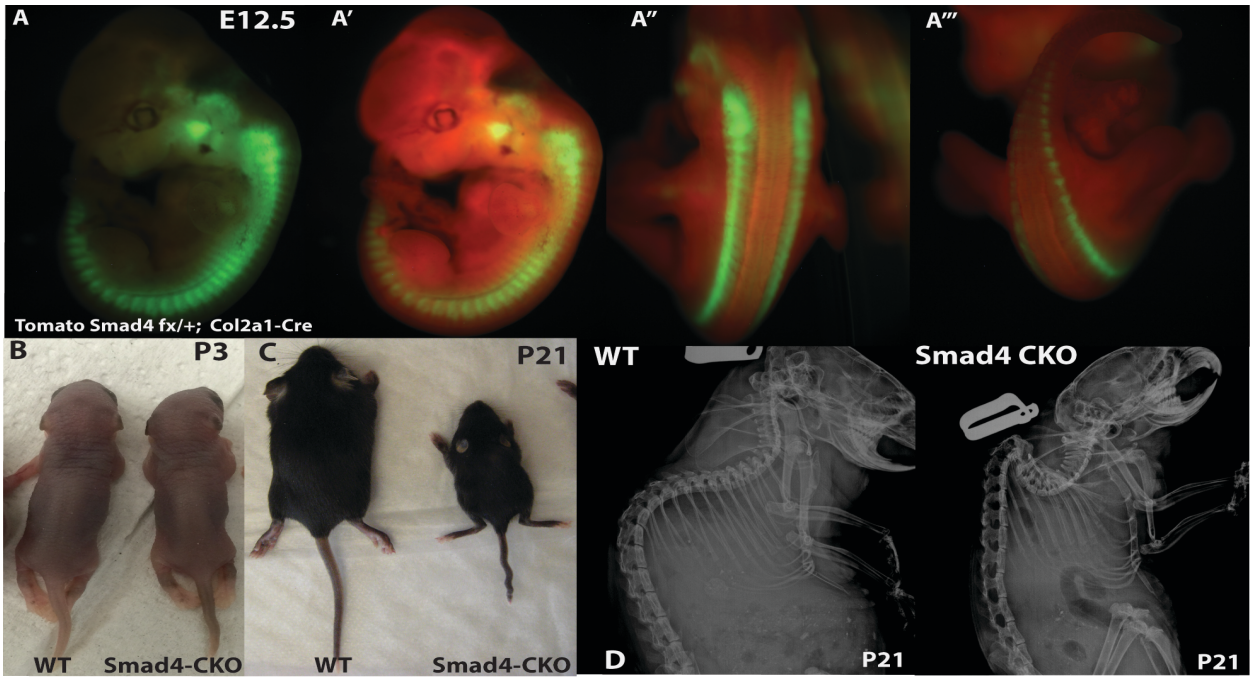

Figure 1. ***Smad4$^{fx/fx}$;Col2a1-Cre*** **(Smad4CKO) mutants exhibit mild chondrodysplasia.** Smad4CKO;tomato mice (**A-A'''**) show strong expression in cartilage elements at E12.5. WT and Smad4CKO mice display defects as early as P3 (**B)** and all the way to adult hood seen in P21 (**C**). X-ray analysis of kyphosis is observed strongly at age P21 (**D**).

Collagen II is expressed as early as embryonic day 10.5. A snapshot in time of Cre expression, at embryonic day 12.5, is shown (Fig. 1A). *Col2a1-Cre* mediated recombination in *Smad4fx/fx* mice was clearly seen in all the skeletal elements indicating that *Col2a1-Cre* activity is specific and efficient (Fig. 1A). Primary chondrocytes from Smad4fx/fx isolated from postnatal day 1 pups were infected with Adenovirus expressing GFP (Ad-GFP) or Cre-GFP (Ad-Cre-GFP) in order to test for efficiency of Smad4 excision and the potential generation of any isoforms and/or neomorphic variants of the Smad4 protein. The lysates were treated with or without TGFb (10 ng/mL) for 1 hour. We probed for Smad4 using antibodies that recognize

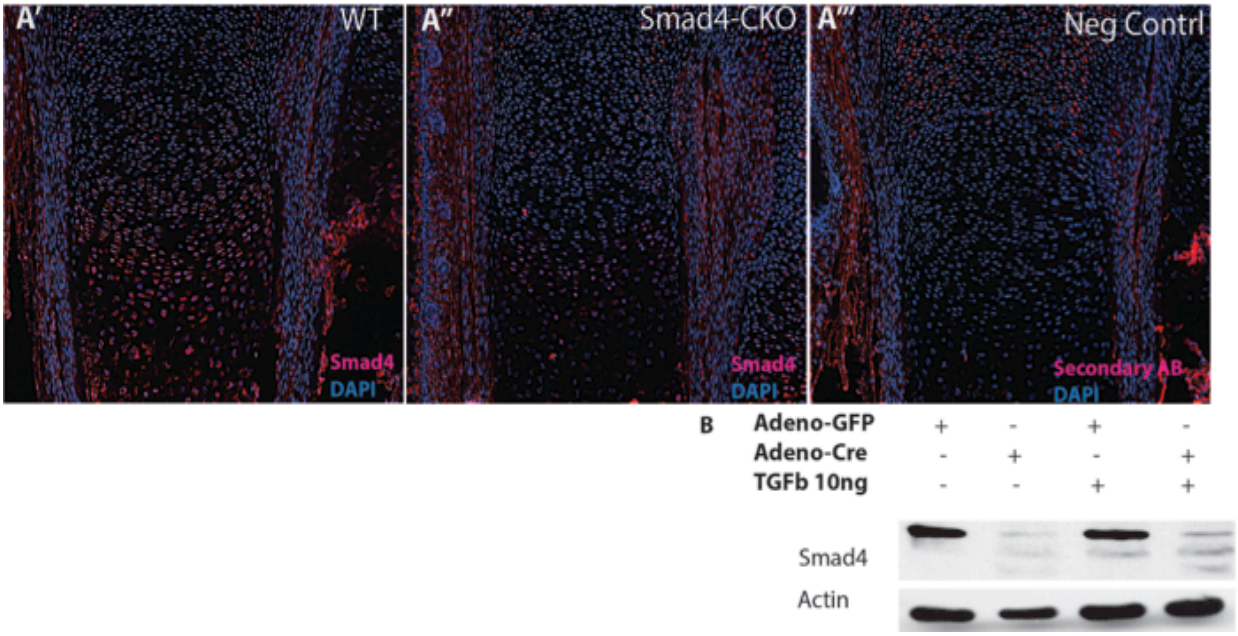

Figure 2. Efficient Cre-mediated recombination in Smad4CKO mice and in culture. Immunofluorescent staining (**A**) and westernblot analysis (**B**) for Smad4 demonstrate efficient deletion of total Smad4 protein via Cre mediated recombination in both growth plate and cultured primary chondrocytes. E18.5 tibias of (**A'**) WT, (**A''**) Smad4CKO, and (**A'''**) WT negative tibia control for 2° antibody staining.

either the N and C terminal regions of the protein to verify complete loss of the protein. We found that our Smad4 allele resulted in full ablation of the protein. The data also showed that no new products of Smad4 were made in response to recombination. It is visible through the western blot that Smad4 was efficiently ablated in *Smad4* floxed chondrocytes (Fig. 2).

Embryos at 18.5 days of gestation (E18.5) were collected, processed, embedded in paraffin and sectioned. Immunohistochemistry of tibial growth plates was performed for Smad4 in WT and *Smad4CKO* samples to assess efficient recombination of Smad4 in vivo (Fig. 2).

In comparison to sections from WT mice, Smad4 expression was efficiently ablated within the growth plate in *Smad4CKO* mice. The data showed that ablation of Smad4 in cartilaginous elements was efficient and that Smad4 is dispensable for some aspects of BMP signaling.

We proposed three different mechanisms by which BMP signaling could persist in the absence of Smad4. 1) BMP mediated transcription factors R-Smads 1/5/8 might regulate transcription of BMP target genes independently of Smad4. 2) There may be crosstalk between TAK1 and Smad1/5/8 that allowed enhanced compensatory signaling through the TAK1 arm of BMP signaling. 3) A Smad1/5/8-dependent, Smad4-independent mechanism, where R-Smads 1/5/8 play a role in microRNA maturation, had been described in endothelial cells. We surmised that perhaps R-Smad dependent microRNAs that selectively target BMP inhibitors might allow BMP signaling to persist in the absence of Smad4 (Davis, Hilyard, Lagna, & and Hata, 2008). However, mice lacking Drosha, a protein required for microRNA maturation, in cartilage displayed milder cartilage defects than those in mice lacking R-Smads 1/5/8 (Kobayashi et al., 2015; Retting, Song, Yoon, & Lyons, 2009). These data indicated that Smad1/5/8- mediated microRNA maturation is not the dominant mechanism for R-Smad1/5/8 signaling independently of Smad4.

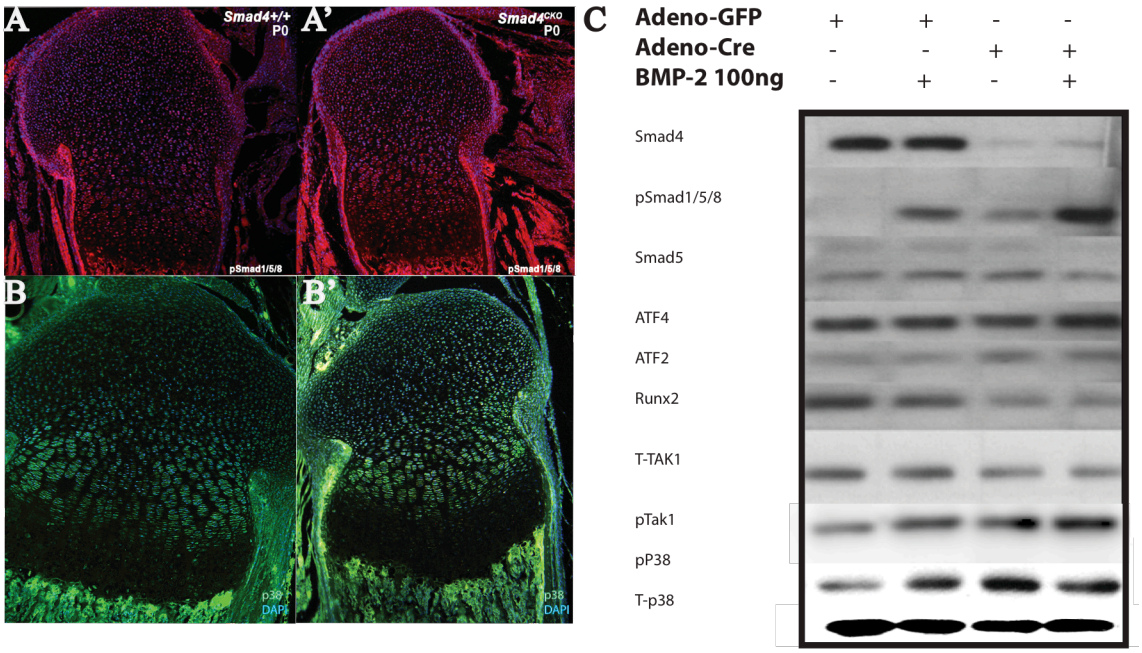

Figure 3. Loss of Smad4 results in ectopic phosphorylation in BMP R-Smad1/5/8 and MAPK pathways in vivo. Immunofluorescent staining of P0 WT and Smad4CKO growth plates for phospho-Smad1/5/8 (**A, A'**) and phospho-p38 (**B, B'**) show increased phosphorylation in Smad4CKO. Western blot analysis of R-Smads 1/5/8, TAK1, and downstream effectors of the noncanonical pathway are also elevated Smad4CKO in culture (**C**).

Loss of Smad4 affects both MAPK and R-Smad mediated BMP signaling pathways.

We then explored the first proposed mechanism, whereby R-Smads1/5/8 can regulate target gene expression independently of Smad4. According to this mechanism, R-Smads should be present in the nucleus in *Smad4*-deficient cells. We probed for pSmad1/5/8 protein in WT and *Smad4CKO* P0 tibia growth plates (Fig. 3). Overlapping staining of pSmad1/5/8 in red and the nucleus, in blue, indicated that Smad4CKO mice do not exhibit defects in Smad1/5/8 nuclear translocation.

Unexpectedly, in comparison to WT growth plates, *Smad4CKO* growth plates displayed an increase of Smad1/5/8 phosphorylation (Fig. 3A). We therefore tested whether this could be recapitulated in culture. *Smad4fx/fx* chondrocytes were plated and infected with adenovirus expressing either GFP or Cre-GFP. The chondrocytes were treated with BMP-2 and collected for western blot analysis of the BMP pathway transducers, the R-Smads 1/5/8 and the non-canonical signaling factors, TAK1 and p38. The data showed that like WT chondrocytes, *Smad4CKO* cells were responsive to BMP-2 stimulation, shown by the elevated levels of phosphorylated Smads1/5/8 (Fig. 3C). However, even in the absence of ligand stimulation, *Smad4CKOs* already showed elevated phosphorylation of R-Smads. Analysis of non-canonical signaling factors TAK1 and p38 mirrored the elevation of the R-Smads both in vivo and in culture (Fig. 3B and 3C).

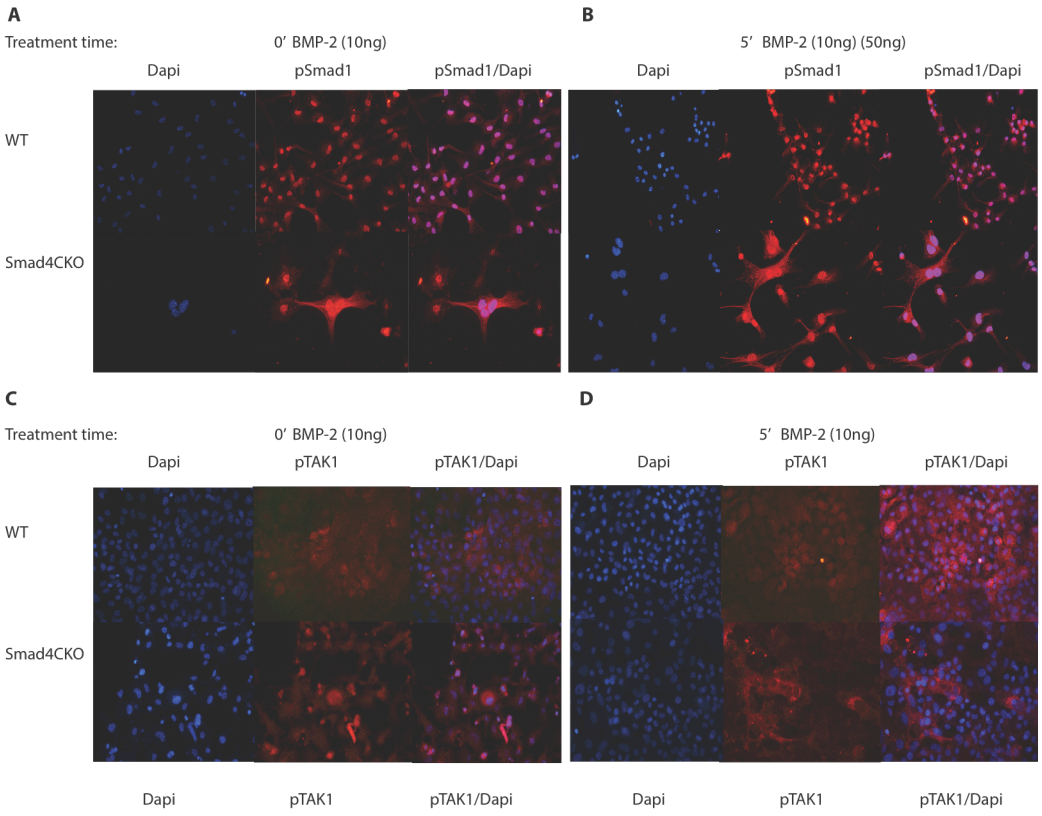

Figure 4. Loss of Smad4 leads to R-Smads 1/5/8 accumulation in the nucleus and perinuclear location of TAK1 is retained in Smad4 deficient chondrocytes. (A) Immunofluorescence of phosphorylated Smad1 location in WT and Smad4CKO sternal chondrocytes at **(A)** 0 minutes of BMP-2 stimulation **(B)** and 5 minutes after BMP-2 treatment**.** Immunofluorescence of phosphorylated levels of TAK1 in WT and Smad4CKO sternal chondrocytes at **(C)** time 0 and **(D)** 5 minutes after BMP-2 treatment.

R-Smads 1/5/8 are sequestered in the nucleus and perinuclear location of TAK1 is retained in Smad4 deficient chondrocytes.

Immunostaining of primary sternal chondrocytes for pSmad1 and pTAK1 was performed to evaluate their spatial expression in the absence of Smad4 upon BMP stimulation. In *Smad4CKO* cells, pSmad1 remained in the nucleus with or without BMP-2 ligand treatment (Fig. 4A and B). Lower levels of pSmad1 were seen WT compared to *Smad4CKO* chondrocytes, but expression was mainly nuclear expression with or without ligand stimulation (Fig. 4A and B). Interestingly, although WT and *Smad4CKO* cells were of similar size, the nuclei appeared to be enlarged in *Smad4CKO* cells because the cells adapted a flattened morphology compared to the rounded WT cells. Nonetheless, these results suggested that R-Smads1/5/8 have a function in the nucleus in the absence of Smad4. In WT chondrocytes, levels of phosphorylated TAK1 remained near the cell membrane without the BMP ligand stimulus, as expected. Moreover, low levels of active TAK1 migrated to a perinuclear location after a 5-minute ligand treatment (Fig. 4C and D top panel). In *Smad4* deficient chondrocytes, the phosphorylated levels of TAK1 remained perinuclear with and without BMP-2 ligand stimulation (Fig. 4C and D lower panel). These data suggests that Smad4 plays a small role in spatial regulation of the non-canonical arm of BMP signaling.

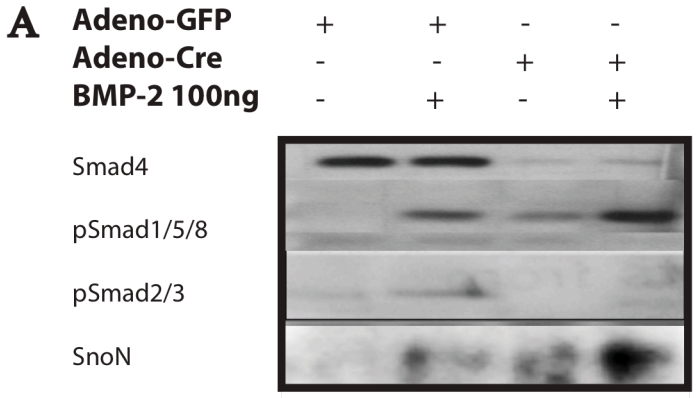

Figure 5. *Smad4* deficient chondrocytes show opposing effects on TGFβ R-Smads.
(A) Western blot analysis of pSmads 1/5/8, pSmads 2/3, and SnoN in *Smad4* deficient cells.

Smad4 has opposing effects on BMP and TGFb R-Smads

We tested the crosstalk between BMP and TGFb signaling by treating cells with BMP-2 and analyzing the levels of pSmad2/3 (Fig. 3C). In contrast to the elevated levels of pSmad1/5/8, the levels of pSmads 2/3 were reduced in *Smad4CKO* cells. Moreover, a TGFb pathway transcription inhibitor, SnoN, showed elevated levels in Smad4CKOs (Fig. 5A). The data suggest that the activity of the TGFb pathway is tempered in the absence of Smad4. However, further studies that address whether SnoN exhibits enhanced interactions with Smads 2/3 in Smad4CKO cells need to be conducted. Overall, loss of Smad4 has opposing effects on BMP and TGFb R-Smads.

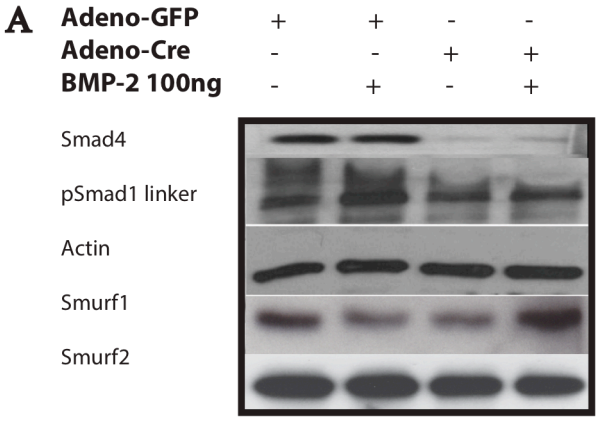

Figure 6. *Smad4* deficient chondrocytes display defects in R-Smad proteasome targeted degradation. Westernblot analysis shows protein levels of Smad1 linker phosphorylation, Smurf1, and Smurf2 in *Smad4* deficient chondrocytes.

***Smad4* deficient chondrocytes display defects in R-Smad proteasome targeted degradation.**

Elevated levels of pSmads could arise as a result of elevated rates of receptor-mediated phosphorylation, reduced rates of dephosphorylation, or increased stability of pSmads. Western blot analysis of Smad1 linker region phosphorylation was performed to detect defects in R-Smad proteasome targeted degradation that may account for the elevated levels of phosphorylated Smads. The data showed that *Smad4CKO* chondrocytes displayed decreased levels of Smad1 linker phosphorylation in response to BMPs; however no changes in Smurf1, an E3 ubiquitin ligase imperative for targeting Smad1 for degradation, were seen (Fig. 6A). Smad1 linker phosphorylation is required for Smurf1-Smad1 binding (Alarcon et al., 2009). The data suggest that Smad4 plays a role in rapid responsiveness to BMP stimulation and therefore in BMP-mediated degradation of R-Smads.

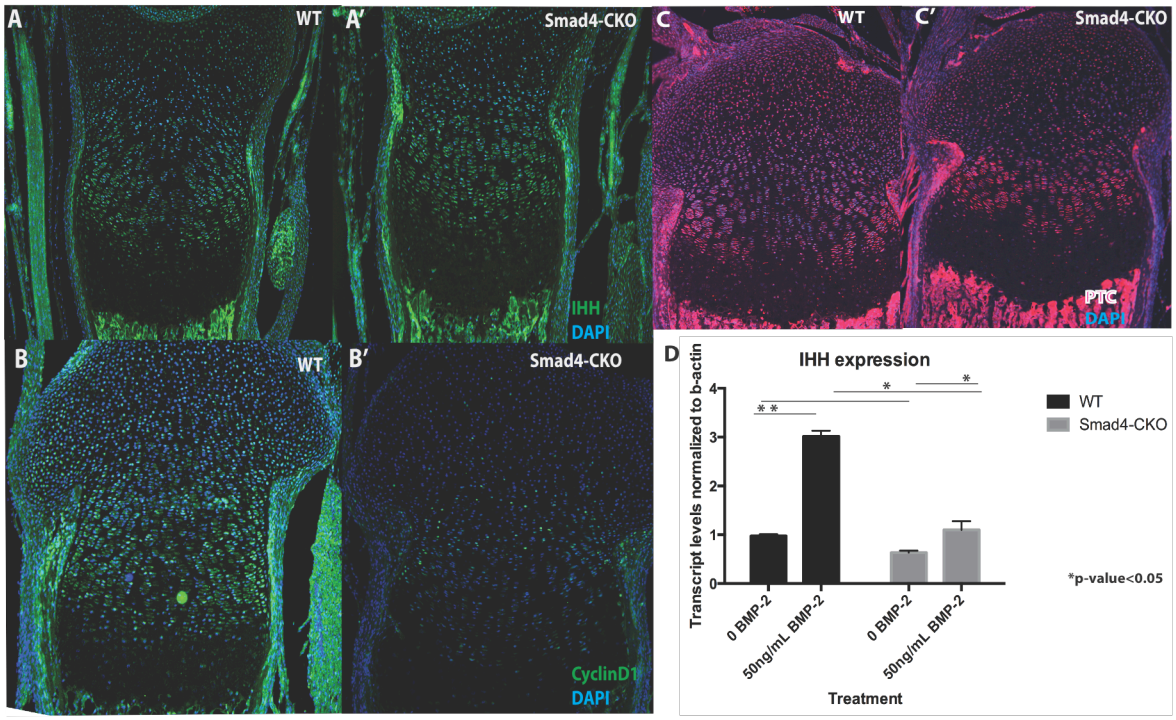

Figure 7. BMP target gene expression of *IHH* is retained in Smad4CKO growth plates. Immunofluorescent staining of IHH protein in WT **(A)** and Smad4CKO **(A')** is maintained in P0 growth plate. Immunostaining of an IHH and TGFβ target, Cyclin D1 is expressed mainly in the proliferative zone of WT growth plates **(B)** however, is abolished in Smad4CKOs **(B').** A direct target of IHH, its receptor Patched (PTC), shows comparable expression to WT **(C)** in Smad4CKO growth plates **(C').** The mRNA levels of IHH were measured via qRT-PCR in WT and Sma4CKO sternal chondrocytes **(D).**

Loss of Smad4 disrupts *Ihh* expression

We next investigated whether *Smad4CKO* chondrocytes are capable of BMP-induced Smad1/5/8 dependent transcription. Because the transcription of genes has never been characterized in the absence of Smad4, there are no known genes in the growth plate that are transcribed through a Smad1/5/8-dependent, Smad4 independent mechanism. A well-characterized BMP target gene known to be Smad1/5/8-dependent, *Ihh,* was chosen for these

studies (Retting et al., 2009; Seki & Hata, 2004). The transcription and production of IHH was analyzed in vivo through qRT-PCR and immunofluorescence (Fig. 7A, A', and D). The data showed that *Ihh* expression is reduced, but not abolished, in *Smad4CKO* cells, suggesting that *Ihh* does not absolutely require Smad4 for transcription. Immunofluorescence of IHH protein was examined in *Smad4CKO* P0 growth plates. There was no detectable difference in IHH protein secretion comparing WT and *Smad4CKO* growth plates, nor was a target gene of IHH, Patched, affected (Fig. 7 A, A', C, C'). However, an IHH and TGFb dependent gene, Cyclin D1 was greatly affected (Fig. 7B, B'). The low levels of Cyclin D1 may account for delays in growth plate cell proliferation.

Smads1/5/8 mediate transcription independent of Smad4.

Although R-Smads 1/5/8 were found in the nucleus of *Smad4CKO* chondrocytes, it was not clear the R-Smads were functional. Moreover, if R-Smads 1/5/8 are the main mediators of *Ihh* transcription, they should be able to bind to the *Ihh* promoter in the absence of Smad4. We therefore asked if Smads 1/5/8 can still bind to their putative sites in the *Ihh* promoter in *Smad4CKO* chromatin. Smads1/5/8 have been found to bind to 3 different sites, a BMP response element (CAGAGC), a GC rich sequence (GCCGNGC) and a GC-palindromic sequence (GGCGCC) (Fei et al., 2010; Seki and Hata, 2004). We conducted ChIP-PCR to test if the R-Smads 1) could bind to DNA, 2) were binding to their putative sites 3) and/or associated with known transcription factors, such Runx2, and their sites in *Smad4CKO* chromatin. The 1 kb proximal *Ihh* promoter was subdivided into 4 sections (Fig. 8A and B). The first section contained Runx2 and ATF4 binding sites. R-Smads have been known to interact with Runx2 at Runx2 binding sites to regulate osteoblast maturation (Morikawa et al., 2013). Although Smads

1/5/8 have not been shown to interact with the transcription factor ATF4, ATF4 expression is necessary for *Ihh* expression (Wang et al., 2009). The second promoter region did not contain any consensus BMP Smad binding elements. The third region contained one R-Smad binding site, and the forth region contained all the Smad1/5/8 binding sites characterized to be essential for BMP mediated activation of the *Ihh* gene (Seki and Hata, 2004). We predicted that in *Smad4CKO* chromatin, R-Smads1/5/8 would bind to these regions, but at lower levels than in WT chromatin.

After analysis of the sites where Smads1/5/8 were immunoprecipitated on the *Ihh* promoter, we found that in regions with Runx2 binding sites, regions 1 and 3, there were slightly elevated levels of Smads1/5/8 binding in *Smad4CKO* chromatin compared to WT, with and without BMP-2 ligand stimulation (Fig. 8D and F). However, in region 2, there was little to no R-Smad1/5/8 binding (Fig. 8E). In region 4, which contained the previously characterized Smad1/5/8 binding sites, we found the highest level of R-Smad binding, 3 orders of magnitude higher than in the other 3 regions. As expected, in the absence of BMP stimulation, there was a low level of binding of R-Smads in region 4 in WT cells. BMP-2 treatment induced binding 4 orders of magnitude higher than in the absence of stimulation (Fig. 8G). In *Smad4CKO* chromatin, even without treatment, there was significantly higher binding of R-Smads1/5/8 to the *Ihh* promoter. Upon BMP-2 stimulation, however, inducible binding of R-Smads was lost (Fig. 8G). The data show that Smad4 is not required for Smad1/5/8 binding to its putative sites on the *Ihh* promoter; however, it is required for optimal inducible transcription of the gene.

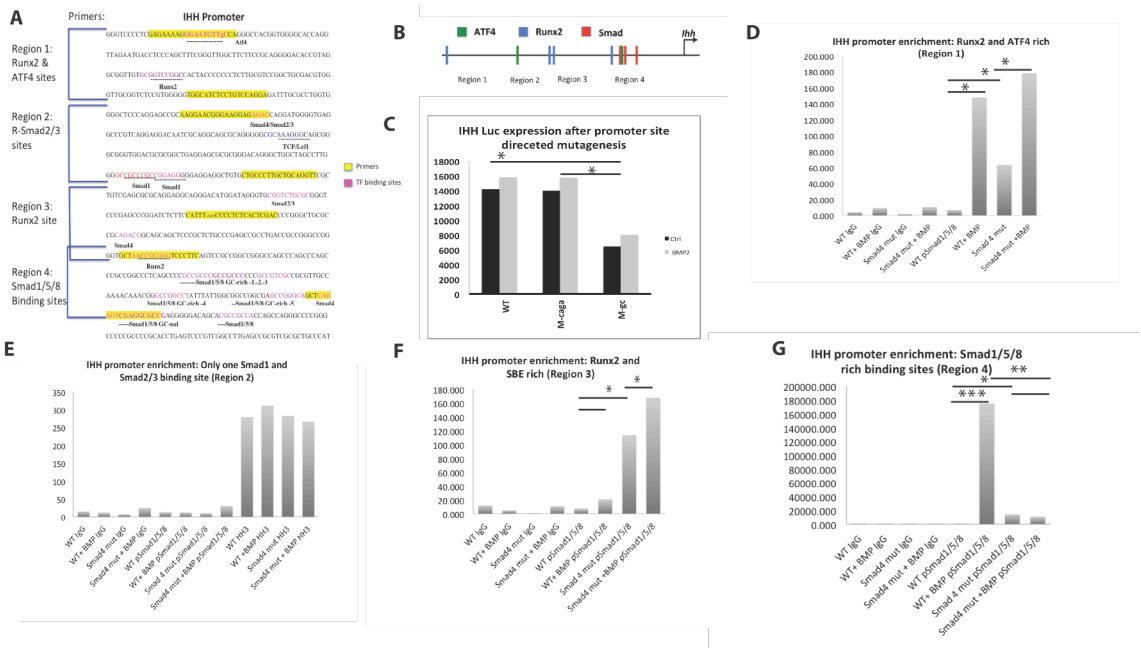

Figure 8. Chromatin Immunoprecipitation on the IHH promoter reveals R-Smad1/5/8 binding in *Smad4* deficient chondrocytes. A 1KB region of the IHH promoter upstream from the transcription start site displays Runx2, ATF4, R-Smad1/2/3/4/5/8 DNA binding sites **(A).** A schematic of transcription factors that bind to the IHH promoter are delineated in different colors **(B).** Site directed mutagenesis of the IHH promoter show dispensable SBE (CAGAGC) site for gene transcription **(C).** Promoter enrichment from Chromatin Immunoprecipitation of phosphorylated R-Smad1/5/8 on Runx2/ATF4 binding sites **(D),** pSmad2/3 binding sites (E), Runx2 binding sites **(F)** and Smad1/5/8 binding sites **(G)** on the IHH promoter. The graphs reveal preferable binding to pSmad1/5/8 palindrome and GCCGNGC sites on the IHH promoter **(G).**

R-Smad1/5/8 binding to the GGCGCC palindrome in IHH promoter mediates main gene transcription in the absence of Smad4.

In order to address if the majority of signaling that we observed in *Smad4CKO* chondrocytes was mediated through R-Smad1/5/8 transcription, we conducted site directed mutagenesis in two sites that were shown to be important for *Ihh* induction. An *Ihh* luciferase reporter containing the promoter sequence used by Seki and Hata, 2004, and directly 1Kb upstream of the transcription start site, was used. According to Seki and Hata, 2004, the most important transcription-binding site for *Ihh* expression was the palindrome GGCGCC, which rendered a 90% loss of expression when mutated to GGAACC. The CAGAGC site, also known as SBE, a site formerly known to have the highest binding affinity to Smad4 and Smad2/3 transcription factors in the TGFb signaling pathway (Fei et al., 2010; Morikawa, Koinuma, Miyazono, & Heldin, 2013) was found to be dispensable for *Ihh* expression (Seki and Hata, 2004). The fact that the CAGAGC site was dispensable for *Ihh expression* hinted that *Ihh* expression does not depend on the presence of Smad4. Our studies solidify the conclusion that Smad4 is dispensable at least in part for *Ihh* expression.

Promoter bashing experiments were conducted by Seki and Hata 2004 in a mouse embryonic carcinoma cell line. These studies identified the above palindrome GGCGCC and CAGAGC as essential for R-Smads 1/5/8-mediated transcription. However, these studies were conducted in the presence of Smad4. We first wanted to investigate if these effects were also observed in a chondrogenic cell line. Therefore we conducted site directed mutagenesis of the two sites (CAGAGC to CAAAGC and GGCGCC-GGAACC) and conducted the luciferase assays in the well-characterized chondrogenic cell line ATDC5 cells (Newton et al., 2012).

The preliminary results confirmed that the SBE element (CAGAGC-CAAAGC) had little affect on *Ihh* transcription, while mutations in the palindrome, GGCGCC to GGAACC led to stronger impairment. Although the reduction of *Ihh* expression was not as low as reported in Seki et al., the data still confirm that the palindrome GGCGCC holds a higher significance to *Ihh* transcription (Fig. 8C). We anticipate additional experiments will reveal that this site is required for Smad4-independent Smad1/5/8-dependent *Ihh* expression.

Discussion:

Previous studies of tissue-specific Smad4 knockout mice where Smad4 was ablated at early stages of skeletal formation demonstrated that Smad4 is essential for skeletal patterning and formation of condensations during the development of skeletal elements (Benazet and Zeller, 2013; Tan et al., 2007; Xu et al., 2008; Zhang et al., 2005). However, these studies do not explain the drastic differences between the *Smad1/5/8CKO* and *Smad4CKO* phenotypes (Retting et al., 2009; Zhang et al., 2005). Our studies show that BMP transduces signals through a 1/5/8-dependent, Smad4 independent transcriptional mechanism in cartilage, mediated in part by binding to GGCGCC palindromic site in the *Ihh* promoter. Our studies also show that Smad4 is required for the BMP-TGFb crosstalk. Further more our studies show that the mild chondrodysplasia in *Smad4CKO* mice is in part through reduced levels of Cyclin D1, a transcription factor necessary for G to S transition in proliferating cells (Tian et al., 2014). Thus, our studies provide the first in vivo molecular evidence that Smad4 deficient chondrocytes act through a Smad1/5/8 dependent mechanism in the murine cartilage growth plate.

The two Smad4 floxed alleles are functionally similar.

Mice lacking *Smad4* in cartilage through recombination of the exon1 or exon8 floxed allele both produced mild chondrodysplasia and growth defects. The differences in the generation of kyphosis with the exon1 floxed Smad4 allele may stem from differences in genetic backgrounds or in timing and efficiency of recombination. Although all the studies reported in this dissertation were conducted using the Smad4 exon1 floxed mice, we also obtained the Smad4 exon8 floxed mice from the JAX laboratory. Primary sternal chondrocytes isolated from Smad4 exon8 floxed mice that were exposed to Adenovirus Cre recombination also displayed elevated phosphorylation levels of both Smad1/5/8 and TAK1 (data not shown).

Loss of Smad4 affects R-Smad and MAPK mediated BMP pathways.

Loss of Smad4 in some cell types has been reported previously to result in an elevation of phosphorylated R-Smads1/5/8, although whether this had physiological consequences was unknown (Chu et al., 2004; Costello et al., 2009; Le Goff et al., 2012). Elevated levels of pSmads1/5/8 are also seen in patients with Myhre Syndrome, a condition characterized by dwarfism that is caused by a point mutation in Smad4. However, Smad4 levels are enhanced in Myhre syndrome. The mechanism by which this point mutation in Smad4 leads to elevated Smad4 and R-Smad levels is unknown (Le Goff et al., 2012). We speculate that the point mutation in Smad4 may stabilize Smad4, but impairs its interaction with R-Smads, enabling their accumulation. On the other hand, the loss of Smad4 in cancer cells like the human colon cancer cell line SW480 do not show elevated levels of pSmad1/5/8, and therefore pSmad1/5/8 elevation may be a cell type-dependent effect (Alarcon et al., 2009).

Loss of Smad4 leads to ectopic R-Smad1/5/8 nuclear accumulation and TAK1 perinuclear placement. One possibility is that without Smad4, R-Smads are less susceptible to

proteasome mediated protein turnover (Alarcon et al., 2009), as evidenced by the decreased level Smad1 linker phosphorylation we observed.

The ectopic location of TAK1 we observed may be related to its high affinity for phosphorylated R-Smad1/5/8. According to biochemical studies assessing R-Smad1/5/8-TAK1 interactions, TAK1 does not have a high affinity to Smad4, but has strong affinity for phosphorylated R-Smads. Because the BMP R-Smads in *Smad4* deficient chondrocytes are present in the nucleus, it is possible that the TAK1 bind to pSmads1/5/8, sequestering TAK1 in a perinuclear location.

R-Smads 1/5/8 mediate transcription independently of Smad4 by binding to putative GC-rich sites and the GGCGCC palindrome on the IHH promoter.

A striking aspect of the *Smad4* cartilage-specific knockouts is their viability compared to the lethal chondrodysplasia seen in Smad1/5 cartilage-specific knockouts. Thus, we examined whether R-Smads can bind to their consensus sites in a well-characterized BMP target gene, *Ihh,* independently of Smad4. Supportive to our hypothesis, we found 3 orders of magnitude higher binding of Smads1/5/8 to the Smad putative binding sites in the *Ihh* promoter in *Smad4* deficient chondrocytes even in the absence of BMP. Interestingly, we found that after BMP stimulation, *Smad4* deficient chondrocytes lost the ability to induce more Smad binding to these sites. WT cells displayed markedly higher binding to these sites in response to BMP treatment. Therefore, Smad4 is not required for Smad1/5/8 binding to all putative sites; however, Smad4 is necessary for optimal induction of R-Smad dependent BMP target genes. Site directed mutagenesis of the *Ihh* promoter showed that the CAGAGC (SBE) for Smad4 binding is dispensable for *Ihh* expression, and that the GGCGCC palindrome and GC-rich sites are necessary for *Ihh* induction,

and can do so independently of Smad4. We speculate that R-Smads1/5/8 can regulate the expression of multiple genes through binding to similar GC-rich sites. Future studies include transfecting the mutated *Ihh* promoters into *Smad4* deficient cells to address whether Smads1/5/8 mediate transcription through the palindrome independently of Smad4.

Conclusion:

The mechanism by which BMP signaling persists in *Smad4* growth plates is mediated through R-Smads1/5/8 transcriptional activity. Here we show that the loss of *Smad4* in mouse cartilage results in mild chondrodysplasia, resulting in part from persistent, unregulated BMP signaling and decreased TGFb responsiveness in chondrocytes. Hence, Smad4 is required for proper regulation of BMP and TGFb signaling during development, however, in comparison to Smad1/5/8 cartilage knockouts, is largely dispensable in chondrocytes. We suspect that chondrocytes require constant but relatively low levels of BMP signaling that can be maintained in the absence of Smad4. We expect that tissues whose development requires high levels of pSmad1/5/8 induction followed by rapid downregulation of BMP signaling will be highly dependent on Smad4.

References:

Akiyama, A., Chaboissier, M., Martin, J., Schedl, A., & and de Crombrugghe, B. (2002). The transcription factor Sox9 has essential roles in successive steps of the chondrocyte differentiation pathway and is required for xpression of Sox5 and Sox6. *Genes and Development, 16*, 2813-2828. doi:10.1101.

Alarcon, C., Zaromytidou, A. I., Xi, Q., Gao, S., Yu, J., Fujisawa, S., . . . and Massague, J. (2009). Nuclear CDKs drive Smad transcriptional activation and turnover in BMP and TGF-beta pathways. *Cell, 139*(4), 757-769. doi:10.1016/j.cell.2009.09.035

Barna, M., & Niswander, L. (2007). Visualization of cartilage formation: insight into cellular properties of skeletal progenitors and chondrodysplasia syndromes. *Developmental Cell, 12*(6), 931-941. doi:10.1016/j.devcel.2007.04.016

Benazet, J. D., and Zeller, R. (2013). Dual requirement of ectodermal Smad4 during AER formation and termination of feedback signaling in mouse limb buds. *Genesis, 51*(9), 660-666. doi:10.1002/dvg.22412

Brunet, L., McMahon, J.A., McMahon, A.P., Harland, R.M. (1998). Noggin, Cartilage Morphogenesis, and Joint Formation in the Mammalian Skeleton. *Science, 280*, 1455-1457.

Chu, G. C., Dunn, N. R., Anderson, D. C., Oxburgh, L., & Robertson, E. J. (2004). Differential requirements for Smad4 in TGFβ-dependent patterning of the early mouse embryo. *Development, 131*(15), 3501-3512. doi:10.1242/dev.01248

Costello, I., Biondi, C. A., Taylor, J. M., Bikoff, E. K., & and Robertson, E. J. (2009). Smad4-dependent pathways control basement membrane deposition and endodermal cell migration at early stages of mouse development. *BMC Dev Biol, 9*, 54. doi:10.1186/1471-213X-9-54

Davis, B. N., Hilyard, A. C., Lagna, G., & and Hata, A. (2008). SMAD proteins control DROSHA-mediated microRNA maturation. *Nature, 454*(7200), 56-61. doi:10.1038/nature07086

Derynck, H.-H. F. a. R. (2005). Specificity and versatility in TGFβ Signaling Through Smads. *Annual Review Cell Developmental Biology, 21*, 659-693. doi:10.1146/

Duprez, D., Bell, E.J., Richardson, M.K., Archer, C.W., Wolpert, L., Brickell, P.M., Francis-West, P.H. (1996). Overexpression of BMP-2 and BMP-4 alters the size and shape of developing skeletal elements in chick limb. *Mechanisms of Development, 57*, 145-157.

Estrada, K. D., Retting, K. N., Chin, A. M., & Lyons, K. M. (2011). Smad6 is essential to limit BMP signaling during cartilage development. *Journal of Bone and Mineral Research, 26*(10), 2498-2510. doi:10.1002/jbmr.443

Estrada, K. D., Wang, W., Retting, K. N., Chien, C. T., Elkhoury, F. F., Heuchel, R., & Lyons, K. M. (2013). Smad7 regulates terminal maturation of chondrocytes in the growth plate. *Dev Biol, 382*(2), 375-384. doi:10.1016/j.ydbio.2013.08.021

Fei, T., Xia, K., Li, Z., Zhou, B., Zhu, S., Chen, H., . . . Chen, Y. G. (2010). Genome-wide mapping of SMAD target genes reveals the role of BMP signaling in embryonic stem cell fate determination. *Genome Res, 20*(1), 36-44. doi:10.1101/gr.092114.109

Fuentealba, L. C., Eivers, E., Ikeda, A., Hurtado, C., Kuroda, H., Pera, E. M., & De Robertis, E. M. (2007). Integrating patterning signals: Wnt/GSK3 regulates the duration of the BMP/Smad1 signal. *Cell, 131*(5), 980-993. doi:10.1016/j.cell.2007.09.027

Greenblatt, M. B., Shim, J. H., & Glimcher, L. H. (2010). TAK1 mediates BMP signaling in cartilage. *Ann N Y Acad Sci, 1192*, 385-390. doi:10.1111/j.1749-6632.2009.05222.x

Gunnell, L. M., Jonason, J. H., Loiselle, A. E., Kohn, A., Schwarz, E. M., Hilton, M. J., & O'Keefe, R. J. (2010). TAK1 regulates cartilage and joint development via the MAPK

and BMP signaling pathways. *Journal of Bone and Mineral Research, 25*(8), 1784-1797. doi:10.1002/jbmr.79

Hino, K., Ikeya, M., Horigome, K., Matsumoto, Y., Ebise, H., Nishio, M., . . . and Toguchida, J. (2015). Neofunction of ACVR1 in fibrodysplasia ossificans progressiva. *Proc Natl Acad Sci U S A, 112*(50), 15438-15443. doi:10.1073/pnas.1510540112

Hoffmann, A., Preobrazhenska, O., Wodarczyk, C., Medler, Y., Winkel, A., Shahab, S., . . . Verschueren, K. (2005). Transforming growth factor-beta-activated kinase-1 (TAK1), a MAP3K, interacts with Smad proteins and interferes with osteogenesis in murine mesenchymal progenitors. *J Biol Chem, 280*(29), 27271-27283. doi:10.1074/jbc.M503368200

Kim, J., Johnson, K., Chen, H. J., Carroll, S., & and Laughon, A. (1997). Drosophila mad binds to DNA and directly mediates activation of vestigial by Decapentaplegic. *Nature, 388*(17), 304-308.

Kobayashi, T., Papaioannou, G., Mirzamohammadi, F., Kozhemyakina, E., Zhang, M., Blelloch, R., & Chong, M. W. (2015). Early postnatal ablation of the microRNA-processing enzyme, Drosha, causes chondrocyte death and impairs the structural integrity of the articular cartilage. *Osteoarthritis Cartilage, 23*(7), 1214-1220. doi:10.1016/j.joca.2015.02.015

Kronenberg, H. (2003). Developmental regulation of the growth plate. *Nature, 423*, 332-336.

Le Goff, C., Mahaut, C., Abhyankar, A., Le Goff, W., Serre, V., Afenjar, A., . . . Cormier-Daire, V. (2012). Mutations at a single codon in Mad homology 2 domain of SMAD4 cause Myhre syndrome. *Nat Genet, 44*(1), 85-88. doi:10.1038/ng.1016

Lehmann, K., Seemann, P., Stricker, S., Sammar, M., Meyer, B., Suring, K., . . . Mundlos, S. (2003). Mutations in bone morphogenetic protein receptor 1B cause brachydactyly type A2. *Proc Natl Acad Sci U S A, 100*(21), 12277-12282. doi:10.1073/pnas.2133476100

Massague, J., Seoane, J., & Wotton, D. (2005). Smad transcription factors. *Genes Dev, 19*(23), 2783-2810. doi:10.1101/gad.1350705

Morikawa, M., Koinuma, D., Miyazono, K., & Heldin, C. H. (2013). Genome-wide mechanisms of Smad binding. *Oncogene, 32*(13), 1609-1615. doi:10.1038/onc.2012.191

Newton, P. T., Staines, K. A., Spevak, L., Boskey, A. L., Teixeira, C. C., Macrae, V. E., . . . Farquharson, C. (2012). Chondrogenic ATDC5 cells: an optimised model for rapid and physiological matrix mineralisation. *Int J Mol Med, 30*(5), 1187-1193. doi:10.3892/ijmm.2012.1114

Retting, K. N., Song, B., Yoon, B. S., & Lyons, K. M. (2009). BMP canonical Smad signaling through Smad1 and Smad5 is required for endochondral bone formation. *Development, 136*(7), 1093-1104. doi:10.1242/dev.029926

Rigueur, D., Brugger, S., Anbarchian, T., Kim, J. K., Lee, Y., & Lyons, K. M. (2015). The type I BMP receptor ACVR1/ALK2 is required for chondrogenesis during development. *J Bone Miner Res, 30*(4), 733-741. doi:10.1002/jbmr.2385

Seki, K., & Hata, A. (2004). Indian hedgehog gene is a target of the bone morphogenetic protein signaling pathway. *J Biol Chem, 279*(18), 18544-18549. doi:10.1074/jbc.M311592200

Storm, E. E., Kingsley, D. M. (1999). GDF5 coordinates bone and joint formation during digit development. *Dev Biol, 209*, 11-27.

Tan, X., Weng, T., Zhang, J., Wang, J., Li, W., Wan, H., . . . Yang, X. (2007). Smad4 is required for maintaining normal murine postnatal bone homeostasis. *J Cell Sci, 120*(Pt 13), 2162-2170. doi:10.1242/jcs.03466

Tian, F., Wu, M., Deng, L., Zhu, G., Ma, J., Gao, B., . . . Chen, W. (2014). Core binding factor beta (Cbfbeta) controls the balance of chondrocyte proliferation and differentiation by upregulating Indian hedgehog (Ihh) expression and inhibiting parathyroid hormone-related protein receptor (PPR) expression in postnatal cartilage and bone formation. *J Bone Miner Res, 29*(7), 1564-1574. doi:10.1002/jbmr.2275

Urist, M. R. (1965). Bone: Formation by Autoinduction. *Science, 150*(3698), 893-899.

Wang, W., Lian, N., Li, L., Moss, H. E., Wang, W., Perrien, D. S., . . . Yang, X. (2009). Atf4 regulates chondrocyte proliferation and differentiation during endochondral ossification by activating Ihh transcription. *Development, 136*(24), 4143-4153. doi:10.1242/dev.043281

Wisotzkey, R. G., Mehra, A. Sutherland, D.J., Dobens, L. L., Liu, K., Dohrmann, C., Attisano, L., and Raftery, A. (1998). Medea is a Drosophila Smad4 homolog that is differentially required to potentiate DPP responsiveness. *Development, 125*, 1433-1445.

Yoon, B. S., Ovchinnikov, D. A., Yoshii, I., Mishina, Y., Behringer, R. R., & Lyons, K. M. (2005). Bmpr1a and Bmpr1b have overlapping functions and are essential for chondrogenesis in vivo. *Proc Natl Acad Sci U S A, 102*(14), 5062-5067. doi:10.1073/pnas.0500031102

Zhang, J., Tan, X., Li, W., Wang, Y., Wang, J., Cheng, X., & Yang, X. (2005). Smad4 is required for the normal organization of the cartilage growth plate. *Dev Biol, 284*(2), 311-322. doi:10.1016/j.ydbio.2005.05.036

CHAPTER FIVE:

Chapter 9

Whole-Mount Skeletal Staining

Diana Rigueur and Karen M. Lyons

Abstract

The first step in almost every investigation of skeletal phenotypes is analysis of whole-mount skeletal preparations. Whole-mount skeletal staining permits evaluation of the shapes and sizes of skeletal elements in their appropriate locations. The technique is thus the major method for detecting changes in skeletal patterning. Because cartilage and bone can be distinguished by differential staining, this technique is also a powerful means to assess the pace of skeletal maturation. This protocol covers staining of the pre- and postnatal mouse skeleton using Alcian blue and Alizarin red to identify cartilage and bone, respectively.

Key words Alcian blue, Alizarin red, Cartilage, Bone, Cleared skeletal preparation, Whole-mount

1 Introduction

The formation of bone occurs through two processes: endochondral and intramembranous. Endochondral bone formation occurs after cells in mesenchymal condensations differentiate into chondrocytes. These cells secrete a cartilaginous extracellular matrix rich in proteoglycans, glycosaminoglycans (GAGs), and collagen (types II and X). Chondrocytes undergo a process of stratified differentiation and apoptosis, enabling the replacement of cartilage by bone. In contrast, during intramembranous ossification, mesenchymal cells differentiate directly into bone-forming osteoblasts. Alcian blue and Alizarin red stain cartilage and bone, respectively. As a cationic dye, Alcian blue binds strongly to sulfated GAGs and glycoproteins, while Alizarin red, an anionic dye, binds to cationic metals such as calcium [1]. Because cartilage contains higher concentrations of GAGs than any other tissue, it binds more Alcian blue. However, other tissues, such as the skin, contain GAGs and other glycoproteins that bind Alcian blue. In contrast, because 99 % of the calcium in the body is localized in bone, Alizarin red is highly specific for bone. The selective staining properties of Alcian blue and Alizarin red and their use in whole-mount skeletal preparation

Matthew J. Hilton (ed.), *Skeletal Development and Repair: Methods and Protocols*, Methods in Molecular Biology, vol. 1130, DOI 10.1007/978-1-62703-989-5_9, © Springer Science+Business Media, LLC 2014

have been widespread for over a century [2]. The protocol has been refined over the years, and there are variations employing enzymatic steps and different fixatives [2–5]. The protocol described here is used in our laboratory. Most laboratories use very similar protocols.

As a brief overview of the process, specimens are prepared by removing skin, organs, and brown fat. They are then dehydrated and fixed in 95 % ethanol. For further removal of fatty tissue and tissue permeabilization, specimens are exposed to acetone and then consecutively transferred to Alcian blue and Alizarin red staining solutions. Concurrent with Alizarin red staining, exposure to potassium hydroxide (KOH) hydrolyzes soft tissue, leading to transparency and allowing visualization of stained skeletal elements. The procedure can be adjusted depending on the size/age of the specimens.

2 Materials

2.1 Solutions

Use analytical grade reagents.

1. Phosphate-buffered saline (PBS): 137 mM NaCl, 10 mM phosphate, 2.7 mM KCl, pH 7.4. To prepare 1 L of 1× PBS pour 800 mL of distilled water into a beaker. Add in order 8 g of NaCl, 0.2 g of KCl, 1.44 g of Na_2HPO_4, 0.24 g of KH_2PO_4. Adjust the pH to 7.4 with HCl. Add distilled water to a total volume of 1 L.
2. 100 % Ethanol (EtOH).
3. 100 % Acetone ($(CH3)_2CO$).
4. Glycerol ($C_3H_8O_3$).
5. 1 % Potassium hydroxide (KOH): 1 % (w/v) KOH, 99 % dH_2O. To make a 200 mL solution, weigh 2 g of KOH pellets. Gradually add to a beaker containing 200 mL of deionized water (*see* **Note 1**).
6. Alcian blue stain: 0.03 % (w/v), 80 % EtOH, 20 % (glacial) acetic acid. To make a 200 mL solution, weigh 0.06 g of Alcian blue 8GX and place in a beaker, add 160 mL of 100 % EtOH and 40 mL of 100 % glacial acetic acid (*see* **Notes 2** and **3**).
7. Alizarin red stain: 0.005 % (w/v) in 1 % (w/v) KOH. To make a 200 mL solution, weigh 10 mg of Alizarin red and add to 200 mL of 1 % KOH (*see* **Notes 4** and **5**).

2.2 Tools/Supplies

1. Dissecting microscope and photographic equipment.
2. Diapers.
3. Hot water bath.

4. Forceps.
5. Scalpel.
6. Glass scintillation vials, 15 mL, or 50 mL conical tubes.

3 Methods

3.1 Staining of Skeletal Elements: Mid-Gestation Stages (E12.5–E16.5)

1. Collect embryos following euthanization of timed pregnant females and place in 1× PBS.
2. Remove the extraembryonic membranes encircling the embryo. Remove the eyes while in PBS [3–7]. For early-stage embryos (E12.5–E14.5), it is not necessary to remove the skin or eviscerate the embryo. For older embryos, eviscerate as follows: initiate skin removal by creating a horizontal slit in the skin at the abdomen using dissecting scissors. Then pull apart using your fingers or forceps. Continue to tug the skin gently apart. Repeat by making a vertical slit in the dorsal skin of the embryo and pulling the edges apart. To remove skin from the arms, make a vertical slit on the ventral and dorsal surfaces of the fore and hind limbs. Peal the skin using forceps.
3. Place the embryos in glass scintillation vials containing 70 % ethanol to fix overnight at 4 °C (*see* **Note 6**).
4. Remove the 70 % EtOH and replace with 95 % EtOH for 1 h.
5. Remove the 95 % EtOH and replace with acetone overnight at room temperature (*see* **Note 7**).
6. Remove the acetone and replace with Alcian blue stain for 1–4 h (*see* **Note 8**).
7. Remove the Alcian blue stain and replace with Alizarin red stain for 3–4 h (*see* **Note 9**).
8. Remove the Alizarin red stain and replace with 1 % KOH for 12 h to overnight for clearing of the embryo [5, 7–9] (*see* **Note 10**).
9. Transfer the embryos to a 50 % glycerol:50 % (1 %) KOH solution at room temperature until tissue appears transparent.
10. Once cleared, transfer the specimen to 100 % glycerol for long-term storage [5, 7–9]. *See* Fig. 1.

3.2 Late-Gestation and Early-Postnatal Stages: E16.5–P21

1. Wash and then scald the specimen in hot tap water for 20–30 s at 65 °C to facilitate maceration (permeabilization) of the tissue and removal of skin [9] (*see* **Note 11**).
2. Remove eyes, all skin, internal organs, adipose tissue, and bubbles from the body cavity [7, 10] (*see* **Notes 12** and **13**).
3. Fix the embryos in 95 % EtOH overnight at room temperature [5, 7–9].

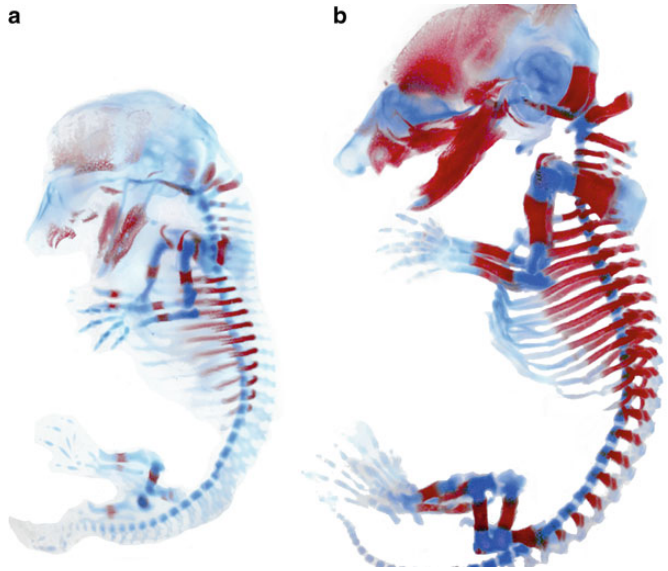

Fig. 1 Alcian blue and Alizarin red staining of (**a**) E14.5 and (**b**) E16.5 embryos. Images were taken using bright field optics. Following adjustment of color levels using Photoshop, the embryos were pasted onto a *white* background

4. Place the samples in acetone overnight at room temperature (*see* **Note 7**).
5. Stain for cartilage by submerging the embryo in a glass scintillation vial containing at least enough Alcian blue solution to cover the embryo. Incubate the sample overnight at room temperature [5, 7–9] (*see* **Note 14**).
6. Destain embryos by initially washing them in two changes of 70 % EtOH and then incubating them in 95 % EtOH overnight [5] (*see* **Note 15**).
7. To pre-clear the tissue, remove the 95 % EtOH and add 1 % KOH solution for 1 h at room temperature [7].
8. Then remove the KOH solution, and replace it with Alizarin red solution for 3–4 h at room temperature. To slow down the staining, place the samples at 4 °C overnight [5, 7, 9] (*see* **Note 16**).
9. Replace the Alizarin red solution with a 50 % glycerol:50 % (1 %) KOH solution. You can incubate the specimen in this solution at room temperature or 4 °C until the excess red color is removed and the specimen is cleared [7].
10. Transfer sample in 100 % glycerol for long-term storage [7–11]. *See* Fig. 2.

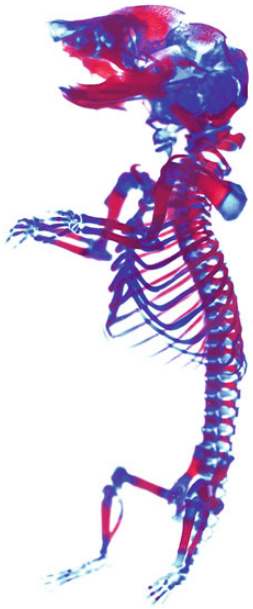

Fig. 2 Alcian blue and Alizarin red staining of a P0 pup. Image was processed as in Fig. 1

3.3 Later Postnatal and Adult Stages (3 Weeks Old and Over)

1. Euthanize the mouse and spray with 70 % EtOH.
2. Remove the skin (*see* Subheading 3.1, **step 2**, and **Notes 12** and **13**).
3. Remove eyes and visceral organs.
4. Remove as much adipose and other excess tissue as possible (*see* **Note 17**).
5. Place in two changes of 95 % EtOH overnight at room temperature to dehydrate and fix the specimen.
6. Replace the solution with 100 % acetone for 2 days to further fix the specimen and to remove adipose tissue (*see* **Note 7**).
7. Incubate the specimen in Alcian blue solution for 1–3 days (*see* **Notes 8** and **14**).
8. Destain embryos by initially washing them in two changes of 70 % EtOH and then incubating them in 95 % EtOH overnight [5, 7] (*see* **Note 15**).
9. Replace with 1 % KOH for 4 h at room temperature to overnight at 4 °C to pre-clear the specimens.
10. Replace the 1 % KOH with Alizarin red solution, and incubate the specimens for 2–5 days (*see* **Notes 16** and **17**).

Fig. 3 Alcian blue and Alizarin red staining of a 4-week-old postnatal mouse. The image was processed as in Fig. 1

11. Transfer the specimen into 1 % KOH as a clearing solution (*see* **Note 18**).
12. For long-term storage, keep the specimen in 100 % glycerol. *See* Fig. 3.

3.4 Preparing for Imaging

1. Carefully place the stained skeleton in a clear 60 mm or 10 cm plastic or glass dish using a scooping utensil (*see* **Note 19**).
2. Fill the plate with 100 % glycerol, and allow Schlieren patterns to settle (*see* **Note 20**).
3. Place the specimen under a dissecting microscope utilizing bright field optics and a white background.
4. If necessary, trim away excess tissue (*see* **Note 21**).

4 Notes

1. KOH is highly caustic to skin. Lab coat, gloves, and goggles should be worn when working with this chemical. KOH dissolves glass, so this solution should be stored in a plastic container or made fresh.
2. Mix the Alcian blue solution very well; this may take 30 min to an hour. Then filter the solution. Otherwise, unequal and

patchy distribution of the dye will lead to uneven staining of skeletal preparations.

3. This solution can be stored for several weeks but works best when freshly prepared. It should be filtered before each use.
4. To stain bone a purple–red appearance, use the formula stated above. If a more orange–red appearance is preferred, you can use Alizarin red diluted in EtOH: Alizarin red: 0.05 % (w/v) in 95 % (w/v) EtOH. Then digest in KOH until specimen clears.
5. Alizarin red solutions work best when prepared freshly.
6. The embryos can be transferred to 15 mL conical tubes or glass scintillation vials. We prefer the latter because it is easier to visualize the extent of staining.
7. Acetone acts as a fixative, permeabilizes cell membranes to permit penetration of the stain, and dissolves fat.
8. The skin of young embryos is porous enough to permit penetration of the Alcian blue stain following treatment with acetone. However, long-term exposure to Alcian blue stain will result in a nearly irreversible over-staining of skin and other soft tissues, making it difficult to see the underlying skeletal elements. If over-staining occurs, placing the embryo in 20 % glacial acetic acid can allow some leaching of the stain from soft tissues.
9. Incubate the specimens in Alizarin red until the bone turns red. Over-staining will lead to irreversible uptake of the stain by muscle.
10. If the sample is kept in KOH too long, the embryo will disintegrate and/or skeletal elements will disarticulate. The length of time the specimen should be maintained in KOH depends on its size, but at the end of the incubation, the specimen should be nearly transparent.
11. For older pups with hair, omit this step and just spray specimen generously with 70 % EtOH to dampen the hair to facilitate dissection.
12. One of the most commonly encountered problems with cleared skeletal preparations is insufficient staining of the digits due to failure to remove the skin around them. One way to remove the skin from hands and feet is to make a cut with a scalpel along the dorsal surface of the hand/foot and then along each finger. Then use the forceps to pinch the skin between the fingers to pull it off.
13. Ensure removal of fat, organs, and bubbles from the body cavity; they impair staining by Alcian blue. It is important to remove the brown fat behind the neck and between the scapulas because it is pigmented and does not clear well. Moreover, Alcian blue stains fat.

14. The entire specimen should turn blue, along with the cartilage. Weak staining can be attributed to improper evisceration, old solution, or inadequate exposure to Alcian blue. If weak staining is observed, keep the specimen in solution for a longer period of time, but this introduces a risk of over-staining.
15. Keep changing the 70 % EtOH until it shows no blue coloration. This dehydration will fix the Alcian blue solution in cartilage and help destain surrounding soft tissues.
16. Samples can be incubated in Alizarin red solution overnight at room temperature; however, avoid longer incubations as overstaining can occur, and the KOH can lead to disarticulation.
17. If the solution becomes murky, after its 2–3-day incubation, transfer the specimen to 1 % KOH solution. For an older mouse, 2 % KOH exposure is acceptable; however, beware that hydrolysis is faster. Change the solution daily until no longer murky and the tissue clears. Then place in a 50 % glycerol:50 % (1 %) KOH solution for complete clearance.
18. Decreasing gradients of 1 % KOH to glycerol can be used to further clear the specimen; however, for long-term storage, ensure that the specimen is stored in glycerol; otherwise, the KOH will cause the skeleton to disarticulate.
19. Take a plastic disposable 1 mL pipette and cut off the top half of the bulb lengthwise—this creates a scoop, with the dropper forming a handle.
20. The viscosity of glycerol facilitates positioning of the skeleton for imaging; however, Schlieren patterns result from differences in solution concentrations of glycerol or salt content. It can take several hours to overnight for these to disappear. Storing the specimens in a large enough volume of 100 % glycerol or graded concentrations of glycerol to EtOH, to completely submerge the specimen when the contents of the vial are transferred to the dish will eliminate this problem.
21. Removing excess tissue at this stage makes a big difference to the final quality of the image. For larger embryos and postnatal stages, forceps may be sufficient. For mid-gestation embryos, a set of 4-in. straight micro scissors is an excellent investment.

References

1. Horobin RW (2010) How do dyes impart color to different components of the tissues? In: Kumar GL (ed) Educational guide special stains and H & E, 2nd edn. Carpinteria, California, pp 159–166
2. Schultze O (1897) Ueber herstellung und conservirung durchsichtiger embryonen zum stadium der skeletbildung. Anat Anz 13:3–5
3. Nagy A, Gerstsenstein M, Vintersten K, Behringer R (2009) Alcian blue staining of the mouse fetal cartilaginous skeleton. Cold Spring Harb Protoc. doi: 10.1101/pdb.prot5169
4. Jegalian BC, De Robertis EM (1992) Homeotic transformations in the mouse induced by over expression of a human Hox3.3 transgene. Cell 71:901–910

5. Estrada K, Retting KN, Chin AM et al (2011) Smad6 is essential to limit bmp signaling during cartilage development. J Bone Miner Res 26(10):2498–2510
6. Nagy A, Gerstsenstein M, Vintersten K, Behringer R (2006) Isolating extraembryonic membranes. Cold Spring Harb Protoc. doi: 10.1101/pdb.prot4267
7. Hogan BLM, Beddington R, Costantini F, Lacy E (1994) Manipulating the mouse embryo: a laboratory manual. Cold Spring Harbor Laboratory Press, Cold Spring Harbor, NY
8. Retting KN, Song B, Yoon BS, Lyons KM (2009) BMP and Smad signaling through Smad1 and Smad5 is required for endochondral bone formation. Development 136(7): 1093–1104
9. Ovchinnikov D (2009) Alcian blue/Alizarin red staining of cartilage and bone in mouse. Cold Spring Harb Protoc. doi: 10.1101/pdbprot5170
10. Nagy A, Gerstsenstein M, Vintersten K, Behringer R (2009) Alizarin red staining of post-natal bone in mouse. Cold Spring Harb Protoc. doi: 10.1101/pdb.prot5171
11. Green MC (1952) A rapid method for clearing and staining specimens for the demonstration of bone. Ohio J Sci 52(1):31–33

CHAPTER SIX:

Conclusions and Future Directions

Summary

The studies presented in this dissertation describe the first investigations into the physiological roles of ALK2 in mammalian endochondral bone formation. Prior to our investigations, the pathological role of ALK2 was recognized in the disease fibrodysplasia ossificans progressiva (FOP), a condition that characterized by progressive ossification of connective tissues, resulting in early death of affected patients. Overexpression studies of different functional forms of the ALK2 receptor (WT, constitutively active, and an Activin A ligand-dependent hyperactive form) all recapitulate the FOP phenotype (Hino et al., 2015). However, the overexpression studies of ALK2 did not address the normal function of this receptor in skeletal tissues, or whether it held overlapping functions with BMP type I receptors BMPR1A (ALK3) and BMPR1B (ALK6) in endochondral bone formation. The results presented in this dissertation reveal that although ALK2 has a physiological role in both appendicular and axial elements, the receptor exhibits its strongest effects in the development of the axial skeleton. This is probably because the *Col2a1Cre* transgene is activated at an early stage of endochondral ossification in axial compared to appendicular elements. Moreover, ALK2 mediates its intracellular effects through the canonical and non-canonical pathways as phosphorylation of Smads1/5/8 and p38, respectively, are significantly decreased in ALK2 cartilage specific knockouts. Compound cartilage specific knockouts of BMP receptors ALK2;ALK3 and ALK2;ALK6 revealed some independent and overlapping functions in the developing skeleton.

Understanding the underlying mechanisms of endochondral bone formation is important as these processes are recapitulated in pathological conditions, to name a couple, osteoarthritis and FOP. Thus our findings may have important implications for understanding the underlying mechanisms that contribute to osteoarthritis and FOP. Detailed conclusions and future studies are presented below.

BMP type I receptors ALK2, ALK3, and ALK6 regulate dorsal ventral patterning.

Overall, these studies show that all three receptors are essential for endochondral bone formation, with distinct and overlapping functions in the axial and appendicular skeleton. These studies suggest that each BMP Type I receptor cannot sustain chondrogenesis on their own. Although they each have similar expression patterns in skeletal elements, the differences in each compound knockout may suggest differential signaling through different affinities to BMP or TGFb ligands (Hino et al., 2015; Rigueur et al., 2015; Yoon et al., 2005).

Future studies of the BMP Type I receptors include testing their physiological roles in maintenance of adult articular cartilage. Compound knockouts may address hidden regulatory functions of the receptors if single knockouts do not exhibit strong articular cartilage phenotypes, such as accelerated osteoarthritis. Other future studies should address the differences of BMP Type I receptor affinities to both BMP and TGFb ligands. Uncovering the effects of ligand binding to BMP and TGFb receptors may hint at different physiological combinations of Type I and Type II TGFb superfamily members that may address the differs phenotypic differences in receptor knockout studies.

Smad4 is dispensable in the developing cartilage growth plate

The studies presented in this dissertation describe the investigations of atypical Smad1/5/8 dependent, Smad4 independent BMP signaling. Prior to our investigations in the vertebrate mammalian skeleton, as early as 1998, Smad4/Medea-independent, R-Smad mediated BMP signaling was reported in *Drosophila melanogaster* (Wisotzkey, 1998), but had not been reported in vertebrates. Our data show that differential requirements for Smad4 is conserved across species. While investigations in *Smad4* deficient growth plates describe a more in-depth analysis of the molecular mechanisms by which the transcription factors Smad1/5/8 mediate BMP signaling in vertebrate systems, overall, future studies should include ChIP-sequencing experiments for phosphorylated Smads1/5/8 in *Smad4* deficient articular cartilage to uncover all BMP target genes that do not require Smad4 for transcription. Results from this study may shine light on various genes that are pathogenic in diseases associated with low levels of Smad4, such as various forms of cancer (prostate, epithelial, ovarian, etc) and therefore may identify targets for future therapeutics (Bandyopadhyay et al., 2013).

The physiological role of Smad4 in adult articular cartilage has not been investigated. Use of tissue and temporal specific transgenic mice, like Tamoxifen inducible Cre, to generate Smad4 deletions in articular cartilage may unravel its *in vivo* function as well as whether it affects progression of late onset osteoarthritis. These future studies may further elucidate the breadth of roles Smad4 plays in multiple stages of cartilage maintenance.

References:

Bandyopadhyay, A., Yadav, P. S., & Prashar, P. (2013). BMP signaling in development and diseases: a pharmacological perspective. *Biochem Pharmacol, 85*(7), 857-864. doi:10.1016/j.bcp.2013.01.004.

Hino, K., Ikeya, M., Horigome, K., Matsumoto, Y., Ebise, H., Nishio, M., . . . and Toguchida, J. (2015). Neofunction of ACVR1 in fibrodysplasia ossificans progressiva. *Proc Natl Acad Sci U S A, 112*(50), 15438-15443. doi:10.1073/pnas.1510540112

Rigueur, D., Brugger, S., Anbarchian, T., Kim, J. K., Lee, Y., & Lyons, K. M. (2015). The type I BMP receptor ACVR1/ALK2 is required for chondrogenesis during development. *J Bone Miner Res, 30*(4), 733-741. doi:10.1002/jbmr.2385

Wisotzkey, R. G., Mehra, A. Sutherland, D.J., Dobens, L. L., Liu, K., Dohrmann, C., Attisano, L., and Raftery, A. (1998). Medea is a Drosophila Smad4 homolog that is differentially required to potentiate DPP responsiveness. *Development, 125*, 1433-1445.

Yoon, B. S., Ovchinnikov, D. A., Yoshii, I., Mishina, Y., Behringer, R. R., & Lyons, K. M. (2005). Bmpr1a and Bmpr1b have overlapping functions and are essential for chondrogenesis in vivo. *Proc Natl Acad Sci U S A, 102*(14), 5062-5067. doi:10.1073/pnas.0500031102

APPENDIX A:

GATA4 Is Essential for Bone Mineralization via ERα and TGFβ/BMP

During the course of my graduate studies, I participated in a number of collaborations. The body of work described in appendix 1 (A1) was a collaboration with the Susie Krum Laboratory at UCLA. I was responsible for providing and performing the techniques and procedures for skeletal and tissue histology, as well as immunofluorescence, shown in figure 4, figure 6, and supplemental figure 6. I also advised and performed qRT-PCR and westernblot analysis for TGFβ and BMP targets shown in figure 8. Overall, the first two authors mainly performed the body of work; however, my unique expertise in the field of cartilage and bone as well as TGFβ /BMP signaling allowed me to play a pivotal role in this study.

ORIGINAL ARTICLE

JBMR®

GATA4 Is Essential for Bone Mineralization via ERα and TGFβ/BMP Pathways

Miriam Güemes,[1] Alejandro J Garcia,[1] Diana Rigueur,[1,2] Stephanie Runke,[3] Weiguang Wang,[1] Gexin Zhao,[1] Victor Hugo Mayorga,[3] Elisa Atti,[4] Sotirios Tetradis,[4] Bruno Péault,[1,5] Karen Lyons,[1,2] Gustavo A Miranda-Carboni,[3] and Susan A Krum[1]

[1]University of California, Los Angeles (UCLA)/Orthopaedic Hospital Department of Orthopaedic Surgery and the Orthopaedic Hospital Research Center, David Geffen School of Medicine at UCLA, Los Angeles, CA, USA
[2]Department of Molecular, Cell and Developmental Biology, UCLA, Los Angeles, CA, USA
[3]Department of Obstetrics and Gynecology, Jonsson Comprehensive Cancer Center, David Geffen School of Medicine at UCLA, Los Angeles, CA, USA
[4]Division of Diagnostic and Surgical Sciences, UCLA School of Dentistry, Los Angeles, CA, USA
[5]Centre for Cardiovascular Science and Centre for Regenerative Medicine, University of Edinburgh, Edinburgh, UK
[6]University of Tennessee Health Science Center, Department of Orthopaedic Surgery and Biomedical Engineering, Memphis, TN, USA

ABSTRACT

Osteoporosis is a disease characterized by low bone mass, leading to an increased risk of fragility fractures. GATA4 is a zinc-finger transcription factor that is important in several tissues, such as the heart and intestines, and has recently been shown to be a pioneer factor for estrogen receptor alpha (ERα) in osteoblast-like cells. Herein, we demonstrate that GATA4 is necessary for estrogen-mediated transcription and estrogen-independent mineralization in vitro. In vivo deletion of GATA4, driven by Cre-recombinase in osteoblasts, results in perinatal lethality, decreased trabecular bone properties, and abnormal bone development. Microarray analysis revealed GATA4 suppression of TGFβ signaling, necessary for osteoblast progenitor maintenance, and concomitant activation of BMP signaling, necessary for mineralization. Indeed, pSMAD1/5/8 signaling, downstream of BMP signaling, is decreased in the trabecular region of conditional knockout femurs, and pSMAD2/3, downstream of TGFβ signaling, is increased in the same region. Together, these experiments demonstrate the necessity of GATA4 in osteoblasts. Understanding the role of GATA4 to regulate the tissue specificity of estrogen-mediated osteoblast gene regulation and estrogen-independent bone differentiation may help to develop therapies for postmenopausal osteoporosis. © 2014 American Society for Bone and Mineral Research.

KEY WORDS: GATA4; ESTROGEN; TGF BETA, BMP, OSTEOBLAST

Introduction

Fifty percent of women over the age of 50 yr will experience an osteoporotic fracture in their lifetime.[1] The highest risk factor for osteoporosis is being postmenopausal. Thus, understanding the mechanism of action of estrogens in bone is key to preventing and treating osteoporosis. 17β-estradiol (E2) induces apoptosis in bone resorbing osteoclasts and is antiapoptotic in osteoblasts, leading to an overall building of bone.[2] Toward this end, we showed that E2, via estrogen receptor alpha (ERα), induces transcription of Fas ligand (FasL) in osteoblasts, resulting in a paracrine signal to induce osteoclast apoptosis.[3] E2 also induces transcription of alkaline phosphatase and *Bmp2* in osteoblasts, thereby regulating osteoblast differentiation.[4]

The GATA family of transcription factors is a conserved set of proteins that bind to the DNA sequence (A/T)GATA(A/G). *Gata4* is expressed early in embryogenesis and is a key regulator of mesodermal and endodermal development.[5] *Gata4* was recently described to be expressed in osteoblasts, and to be regulated by ERα.[6] However, a role for GATA4 in the commitment of bone progenitors, differentiation of preosteoblasts, or mineralization of bone has not been previously described.

TGFβ and BMP family members play important roles in skeletal development.[7] TGFβ-1, TGFβ-2, and TGFβ-3 are important in the maintenance and expansion of osteoblast progenitors, and BMP-2, BMP-4, BMP-5, BMP-6, and BMP-7 induce osteoblast differentiation.[8] TGFβ signaling leads to the phosphorylation of SMAD2/3, which then stimulates proliferation and early osteoblast differentiation, while inhibiting terminal differentiation.[9] BMP signaling leads to the phosphorylation of SMAD1/5/8 and activation of the expression and activity of *Runx2* and other genes[7] necessary for osteoblast differentiation. Although the

Received in original form January 28, 2014; revised form May 29, 2014; accepted June 12, 2014. Accepted manuscript online June 16, 2014.
Address correspondence to: Susan Krum Miranda, 19. S. Mansassas, Memphis, TN 38163, USA. E-mail: smirand5@uthsc.edu
The present address of Susan A Krum is University of Tennessee Health Science Center, Department of Orthopaedic Surgery and Biomedical Engineering, Memphis, TN, USA
Additional Supporting Information may be found in the online version of this article.
Journal of Bone and Mineral Research, Vol. 29, No. 12, December 2014, pp 2676–2687
DOI: 10.1002/jbmr.2296

actions of both TGFβ and BMP signaling in bone have been fairly well characterized, the mechanisms regulating their transcriptional regulation are poorly understood.

GATA4 and SMAD signaling pathways regulate transcription in the heart, gut, and ovaries. In heart development, BMP4 signaling regulates *Gata4* expression[10] and conversely, GATA4 regulates *Bmp4* expression.[11] Furthermore, GATA4 and SMADs co-activate transcription of heart-specific genes such as NKX2-5.[12] GATA4 and TGFβ signaling crosstalk in the gut, where they synergize to regulate epithelial gene expression[13]; similarly, in granulosa cells of the ovary, TGFβ upregulates *Gata4* and then GATA4 and SMAD3 cooperate to regulate inhibin-alpha.[14]

Global knockout of *Gata4* in the mouse reveals heart and gut defects and lethality between embryonic day 7.5 (E7.5) and E10.5.[15,16] Owing to the early embryonic lethality of these models, the importance of GATA4 for bone development in vivo was never studied. In order to investigate osteoblast-specific effects of GATA4, we analyzed the estrogen-dependent and estrogen-independent effects of GATA4 in vitro, and then selectively ablated GATA4 in osteoblasts in vivo. These results show that GATA4 in osteoblasts is necessary for survival and proper bone development. Furthermore, we demonstrate that GATA4 regulates TGFβ and BMP pathways in osteoblasts. Together, these studies identify GATA4 as a regulator of osteoblast commitment during early development via E2-dependent and E2-independent pathways.

Materials and Methods

Ethics statement

All animal work was approved by the Animal Research Committee at UCLA.

Reagents

E2 was purchased from Sigma-Aldrich Co (St. Louis, MO, USA). All E2 experiments were performed in media without phenol red and with 5% charcoal dextran-treated fetal bovine serum (CDT-FBS) (Omega Scientific, Dallas, TX, USA). The following antibodies were used: ERα (Thermo Fisher Scientific; clone Ab-16), GATA4 (Santa Cruz; Clone G4), RUNX2 (R&D Systems), and β-actin (Sigma-Aldrich Co.). SMAD antibodies were obtained from Cell Signaling (pSmad1/5/8 #9511; pSmad2: #3108; Smad2: #3122; Smad3: #9523; and Smad5: #9517).

Mice

Gata4 flox/flox mice were purchased from Jackson Laboratory (Gata4tm1.1Sad/J) and backcrossed for 10 generations to the FVB background. Type I collagen A1 (Col1A1) (2.3 kb)-Cre mice (FVB-Tg(Col1a1-cre)1Kry/Mmucd) were purchased from the Mutant Mouse Regional Resource Centers (MMRRC).

Primary calvarial osteoblasts

Neonatal CD1 calvaria were obtained 2 d after birth and incubated for 40 min in αMEM-1.0 mg/mL collagenase P-1.25% trypsin at 37°C. These were washed in αMEM, and transferred to αMEM-1.0 mg/mL collagenase P-1.25% trypsin for 1 hour at 37°C.[17] Digestion was stopped by addition of αMEM/10% FBS. The cells from the second digest were allowed to attach for 48 hours and then differentiated in mineralization medium with media replacement every 3 d. Differentiation was confirmed by quantitation of Col1A1, bone sialoprotein (BSP), and osteocalcin mRNA, alkaline phosphatase positivity, and Alizarin Red staining for mineralization.

Pericytes

Perivascular cells (pericytes) were obtained from human abdominal subcutaneous fat or lipoaspirate, fetal lung, fetal muscle, or fetal bone marrow as described.[18] Because specimens were obtained as anonymous and unidentifiable, the activities of the present research did not involve human subjects and therefore did not require IRB review according to UCLA IRB medical committee standards. For in vitro mineralization, cells were differentiated with the HyClone AdvanceSTEM Osteogenic Differentiation Kit (Fisher Scientific).

Lentiviral silencing

For shRNA-mediated knockdown of *Gata4* expression, cells were plated in six-well plates (1×10^5 cells per well) and infected 24 hours later with lentivirus. Cells were treated with virus in 2 mL MEM per well with a final concentration of 8 μg/mL polybrene. Plates were centrifuged at 1400*g* at 30°C for 45 minutes. The following day the media was replaced with mineralization medium with media replacement every 3 d. Knockdown of *Gata4* was confirmed by qPCR and immunoblotting. Two different shRNA from The RNAi Consortium (TRC) in pLKO vector were used to knockdown mouse *Gata4* (TRCN0000095215: CCGGCCCAATCTCGATATGTTTGATCTCGAGATCAAACATATCGAGATTGGGTTTTTG, and TRCN0000095217: CCGGCATCTCCTGTCACTCAGACATCTCGAGATGTCTGAGTGACAGGAGATGTTTTTG) and human *GATA4* (TRCN0000020424: CCGGCCAGAGATTCTGCAACACGAACTCGAGTTCGTGTTGCAGAATCTCTGGTTTTT, and TRCN0000020428: CCGGCCCGGCTTACATGGCCGACGTCTCGAGACGTCGGCCATGTAAGCCGGGTTTTT). pLKO-shGFP was used as a negative control for mouse experiments and pLKO-C (shC, with no mammalian target) was used for human experiments.

RNA and qPCR

Cells were hormone-deprived by culture for 3 d in phenol red-free medium (Life Technologies, Grand Island, NY, USA) supplemented with 5% CDT-FBS. Cells were treated with 10 nM E2 or ethanol as a vehicle control for 3 or 24 hours. Total RNA was converted to cDNA with Superscript III First Strand Synthesis Kit according to the manufacturer's instructions (Life Technologies). Primers were selected using Primer3[19]; the sequences are listed in Supporting Fig. 10. cDNA was subjected to quantitative PCR using SYBR Green Mastermix with roxithromycin (ROX). Each RNA sample was collected in triplicate and each PCR reaction was amplified in triplicate.

Microarray

Total RNA was analyzed using the MouseRef-8 v2.0 Expression BeadChips from Illumina (San Diego, CA, USA). Data was analyzed using GenomeStudio (Illumina). Gene ontology was performed by The Database for Annotation, Visualization and Integrated Discovery (DAVID) v6.7.[20] Upon acceptance, microarray data will be submitted to NCBI Geo Database.

Immunohistochemistry

Formalin-fixed paraffin-embedded samples were processed through standard deparaffinization protocols. The tissue was

then incubated in blocking buffer (5% normal goat serum, 2.5% bovine serum albumin [BSA] in PBS at pH 7.5) for 30 min. Primary antibodies were incubated overnight at 4°C in a humidified chamber followed by either the DAKO Envision+ visualization system and counterstaining with hematoxylin or by immunofluorescence with 4,6-diamidino-2-phenylindole (DAPI) counterstaining.

Protein and immunoblotting

Cells were hormone-deprived by culture for 3 d in phenol red–free medium (Invitrogen Corporation) supplemented with 5% CDT-FBS. Cells were treated with 10 nM E2 or ethanol as a vehicle control for 24 hours and then lysed in EBC buffer (50 mM Tris [pH 8], 120 mM NaCl, 0.5% Nonidet P-40) supplemented with a protease inhibitor mixture (Complete; Roche Applied Science, Indianapolis, IN, USA) for 30 min on ice. Proteins were subjected to SDS-PAGE and immunoblotting with antisera to the indicated proteins.

Alkaline phosphatase assay

Osteoblasts were differentiated for the indicated amount of time and then fixed with 3.7% formaldehyde, and stained for alkaline phosphatase activity with SigmaFast 5-bromo-4-chloro-3-indolyl phosphate/4-nitro blue tetrazolium (BCIP/NBT) (Sigma).

Mineralization assay

Osteoblasts were fixed in 50% ethanol for 15 min at 4°C, then 1% Alizarin Red S (wt/vol with 0.1% ammonium hydroxide) was added for 30 min. The stain was washed with water and photographed. The Alizarin Red was eluted with 10% cetylpyridinium chloride and the optical density (OD) was measured at 570 nm.

RNA in situ

Gata4 mRNA was detected by RNAscope technology (2.0 High Definition; Advanced Cell Diagnostics, Hayward, CA, USA) in wild-type FVB embryos according to the manufacturer's recommendations.

Recombination efficiency

The calvariae of postnatal day 0 (P0) mice were placed on a stainless steel grid in a 12-well tissue culture dish in differentiation media for 7 days. RNA from calvariae was obtained and cDNA was synthesized. Primers were designed to anneal to WT cDNA in exon 5 (which is excised by Cre recombinase) and exon 6 of *Gata4* (GCGGAAGGAGGGGATTCAAA and TGAATGTCTGGGACATGGAGC).

Skeletal preparations

Skeletal preparations were performed as described.[21] Briefly, embryos were eviscerated and fixed in 95% EtOH overnight at 4°C, followed by Alcian Blue staining (0.01% Alcian Blue 8GX [Sigma-Aldrich] [wt/vol] in 95% EtOH) overnight at room temperature. Samples were then stained for Alizarin Red (0.05% Alizarin Red S [Sigma-Aldrich] [wt/vol] in 1% KOH) for 3 to 4 hours and cleared in a series of graded KOH in glycerol.

Von Kossa

Deparaffinized sections were incubated with 1% silver nitrate solution under ultraviolet light for 30 minutes. Unreacted silver was removed with 5% sodium thiosulfate. The sections were counterstained with nuclear fast red.

Bone μCT scanning and analysis

Femurs, tibia/fibula, L_5 vertebrae, and skulls from a total of 9 P0 WT and *Gata4* conditional knockout (cKO) mice were dissected, cleaned of soft tissue, and stored in 70% ethanol before μCT scanning. μCT scanning was performed with a Skyscan 1172 scanner (Skyscan, Kontich, Belgium) with the X-ray energy equaling 30 KVp and 175 μA and a voxel isotropic resolution of 6 μm. Prior to scanning, bones were positioned with gauze in the sample holder. To compare femur measurements of trabecular bone microarchitecture and cortical bone morphology, 65 transaxial slices were reconstructed and measured for each sample covering 370 μm of the distal metaphysis starting 0.290 mm above the distal epiphysis and moving along the shaft, and 66 slices covering 380 μm (33 slices each above and below the mid-diaphysis), respectively. For trabecular bone measurements, contours were drawn in the medullar cavity at a fixed distance from the endosteum to define tissue volume. For L_5 vertebrae, 60 slices, covering ~345 μm, were analyzed. Bone volume fraction (BV/TV), trabecular number (Tb.N), trabecular thickness (Tb.Th), and trabecular separation (Tb.Sp) were measured for L_5 vertebrae and trabecular bone of the femur, using CTAn software (Skyscan, Kontich, Belgium). For cortical bone measurements, contours were drawn immediately adjacent to the periosteum bone perimeter to define the periosteal envelope. Total cross sectional area (T.Ar), cortical bone area (B.Ar), cortical area fraction (% B.Ar), and mean cortical thickness (Ct.Th) were measured using CTAn software.

Statistical analysis

All experiments represent both biological and experimental triplicates. Error bars represent mean ± SD; $^{**}p < 0.01$, $^{*}p < 0.05$ using a Student's *t* test.

Results

GATA4 regulates ERα and ERα target genes in osteoblasts

Maximal binding of GATA4 to osteoblast-specific target gene enhancers precedes ERα binding, and GATA4 is necessary for open chromatin (marked by histone 3 lysine 4 dimethylation) at ERα binding sites. In accordance, knockdown of GATA4 led to a reduction of ERα binding to DNA at these sites. Together, these results suggest that GATA4 is a pioneer factor (pioneer factors are a special class of transcription factor that can associate with compacted chromatin to facilitate the binding of additional transcription factors[22]) for ERα in osteoblast-like cells.[6] Therefore, we performed knockdown of *Gata4* in primary murine calvarial osteoblasts to determine the effects of GATA4 on ERα and ERα target gene regulation. *Gata4* can be successfully knocked down with lentivirally expressed short hairpins directed at *Gata4* mRNA. Two different short hairpins (designated #2 and #4) reduced the level of *Gata4* mRNA by more than two-thirds (Supporting Fig. 1A) compared to shGFP-infected cells. For consistency, all figures show shGATA4 #2 and supporting figures show shGATA4 #4. shGATA4 lentivirus induced apoptosis in 5.8% of the cells (Supporting Fig. 2) compared to 0% of the shGFP-infected cells. However, after 2 wk of differentiation, both the shGATA4 and shGFP-infected cells were at confluence (data not shown). In vehicle (ethanol, EtOH)-treated cells, shGATA4 reduced the basal levels of ERα mRNA and protein (Fig. 1*A*, *B*). Additionally, shGATA4 affected the E2 response of ERα in these

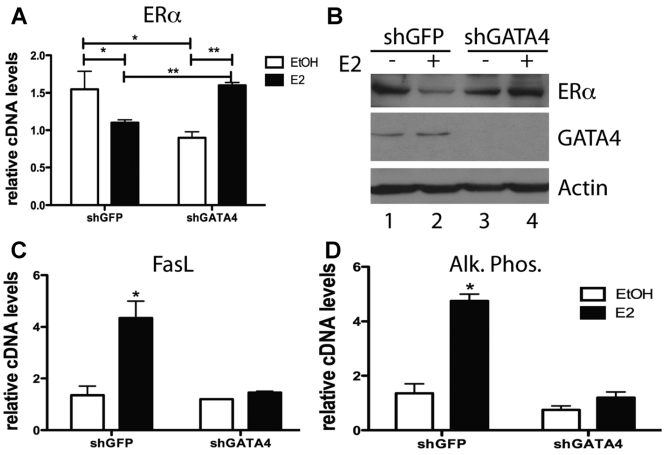

Fig. 1. GATA4 regulates ERα and E2 target genes. (*A*) Calvarial osteoblasts were infected with lentivirus expressing either shGFP or shGATA4. Cells were then differentiated for 2 wk and RNA was obtained. qPCR was performed for ERα and normalized to actin mRNA. (*B*) Calvarial osteoblasts were infected with lentivirus expressing either shGFP or shGATA4. Cells were then differentiated for 2 wk and then treated with 10 nM E2 for 24 hours. Protein was obtained and immunoblots for ERα, GATA4, and actin were performed. (*C*) RNA was obtained as in *A*, and qPCR was performed with primers to FasL and normalized to actin mRNA. (*D*) RNA was obtained as in *A*, and qPCR was performed with primers to alkaline phosphatase and normalized to actin mRNA. $^{*}p < 0.05$; $^{**}p < 0.001$. Alk. Phos. = alkaline phosphatase.

cells. ERα protein and mRNA levels are negatively regulated following E2 treatment in E2-treated shGFP calvarial osteoblasts, as observed in other cell types.[23,24] Loss of GATA4 in primary calvarial osteoblasts treated with E2 led to an increase in ERα mRNA and protein compared to vehicle-treated cells (Fig. 1*A*, *B*). Together, these data demonstrate a misregulation of ERα signaling in GATA4-ablated cells.

FasL and alkaline phosphatase are two important targets of ERα in osteoblasts[3,25] (Fig. 1*C*, *D*). When GATA4 is knocked down, E2 can no longer induce FasL and alkaline phosphatase mRNA (Fig. 1*C*, *D*), suggesting that GATA4 protein is necessary for expression of E2-mediated gene targets in primary calvarial osteoblasts. E2 also increases *Gata4* mRNA, and after shGATA4, *Gata4* mRNA is not increased (Supporting Fig. 1B). Therefore, GATA4 is necessary to regulate E2 targets in primary osteoblasts, regulating both osteoblast differentiation (via alkaline phosphatase) and osteoclast apoptosis (via FasL).

ERα-independent roles for GATA4 in bone mineralization

Because GATA4 regulates osteoblast differentiation genes such as alkaline phosphatase (Fig. 1*D*), we hypothesized that GATA4 may be necessary for proper differentiation and mineralization. To test this, primary calvarial osteoblasts were differentiated for 14 d following *Gata4* knockdown, and alkaline phosphatase activity and mineralization were quantitated (Fig. 2*A*, *B*). Knockdown of *Gata4* reduced the amount of alkaline phosphatase activity as early as 3 d after differentiation and throughout the time course of differentiation (Fig. 2*A*). Furthermore, knockdown of *Gata4* led to a greater than twofold reduction in mineralization, as compared to control shGFP ($p < 0.001$; Fig. 2*B*). An independent shRNA targeting of *Gata4* (shGATA4 #4) confirmed a significant reduction in mineralization (Supporting Fig. 3). The data suggest an essential role for GATA4 in differentiation and/or mineralization in primary osteoblasts. Interestingly, E2 does not increase mineralization in calvarial osteoblast cultures in vitro (data not shown and Almeida and colleagues[26]). In addition, E2 treatment does not increase expression of bone differentiation markers such as bone sialoprotein (BSP (*Spp1*)), osteocalcin (OCN (*Bglap*)), Col1A1, or RUNX2 (Fig. 2*C*–*F*). However, knockdown of *Gata4* significantly reduced the levels of BSP, OCN, Col1A1, and RUNX2 mRNA, corresponding to the differentiation and mineralization assays, indicating E2-independent effects for GATA4 in osteoblast differentiation.

GATA4 is necessary in mesenchymal stem cells for osteoblast differentiation

The expression of *Gata4* during osteoblast differentiation was further investigated in order to determine if GATA4 has stage-specific effects on osteoblast formation and/or activity. *Gata4* mRNA is reduced by fivefold after 1 d of osteoblast differentiation, and by more than 10-fold after 16 d of differentiation (Fig. 3*A*). However, mature osteoblasts still express significantly more *Gata4* mRNA than mammary gland cells used as the control tissue for the absence of *Gata4* expression. This suggests that GATA4 might influence early stage "precursor" decisions upstream of mature terminally differentiated osteoblast cells. To assess the translational potential of the model, we next verified that *Gata4* is expressed more highly in human mesenchymal stem cells (MSCs) than in differentiated osteoblasts. Human fat adventitial cells, fetal lung pericytes, fetal muscle pericytes, and fetal bone marrow pericytes (the native

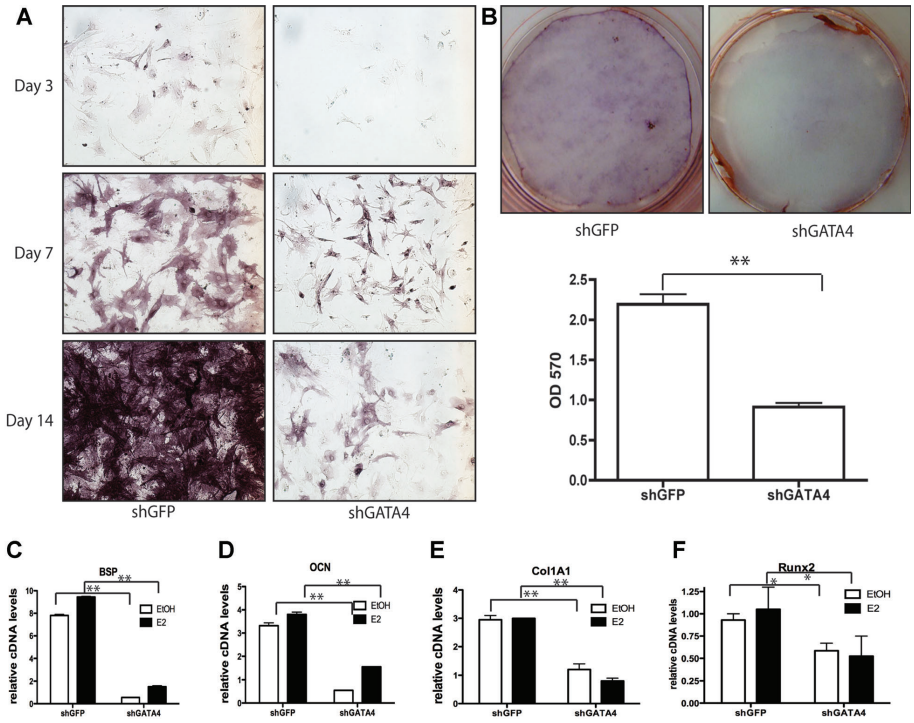

Fig. 2. GATA4 regulates differentiation and mineralization in vitro. (*A*) Primary calvarial osteoblasts were infected with lentivirus expressing an shRNA directed to GFP (shGFP) or to *Gata4* (shGATA4). The following day the cells were placed in mineralization media and allowed to differentiate for 3, 7, or 14 d. Cells were then fixed and assayed for alkaline phosphatase. (*B*) Primary calvarial osteoblasts were infected with lentivirus expressing an shRNA directed to GFP (shGFP) or to *Gata4* (shGATA4). The following day the cells were placed in mineralization media and allowed to differentiate for 2 wk. Cells were then fixed and stained using Alizarin Red. Alizarin Red was eluted and the mineral content was measured at an OD of 570 nm. Silencing was performed in three wells and the average OD is displayed. (*C–F*) Calvarial osteoblasts were infected with lentivirus expressing either shGFP or shGATA4. Cells were then differentiated for 2 wk and RNA was obtained. qPCR was performed for the indicated genes and normalized to actin mRNA. $^{*}p < 0.05$; $^{**}p < 0.001$. BSP = bone sialoprotein; OD = optical density; OCN = osteocalcin; Col1A1 = type I collagen A1; Runx, Runt-related transcription factor.

ancestors of MSCs) were left undifferentiated or differentiated into osteoblasts.[18] *Gata4* mRNA was significantly lower in terminally differentiated osteoblasts than in undifferentiated cells (Fig. 3*B*, *C*). There is an inverse relationship between osteoblast differentiation markers (*Col1A1* and alkaline phosphatase mRNA) and *Gata4* mRNA expression (Fig. 3*C*). Therefore, *Gata4* is expressed more highly in mesenchymal stem-like cells than in differentiated, mineralizing osteoblasts.

The observation that *Gata4* expression is higher prior to differentiation raises the possibility that GATA4 plays a critical role at the phase of osteoblast commitment. To test this, *Gata4* was either knocked down "early" (in undifferentiated pericytes) or "late" in differentiating osteoblasts (1 wk after initiating differentiation; Fig. 3*D*). The corresponding alkaline phosphatase levels, indicating the amount of differentiation of WT pericytes, is demonstrated in Fig. 3*E*. The cells were selected with puromycin to ensure efficient lentiviral infection, and then induced to mineralize. Cells infected with control lentivirus showed efficient mineralization, as visualized by Alizarin Red staining, whether infected early or late (Fig. 3*F*, *G*). In contrast, cells infected with shGATA4 before differentiation exhibited a significant reduction in the amount of mineralization compared to control infected cells. However, osteoblasts infected with shGATA4 "late" in differentiation showed no loss of mineralization, suggesting that GATA4 plays a role in either osteoblast progenitors or early in differentiation. Taken together, the above results suggest that in vitro in both human and mouse osteoblasts, GATA4 elicits its strongest effects on "early" progenitor and/or precursor cells.

GATA4 expression in vivo

GATA4 has been described in detail in the developing heart, intestines, and several other tissues.[5] Indeed, analysis of *Gata4* mRNA in E18.5 embryos reveal highest expression in these

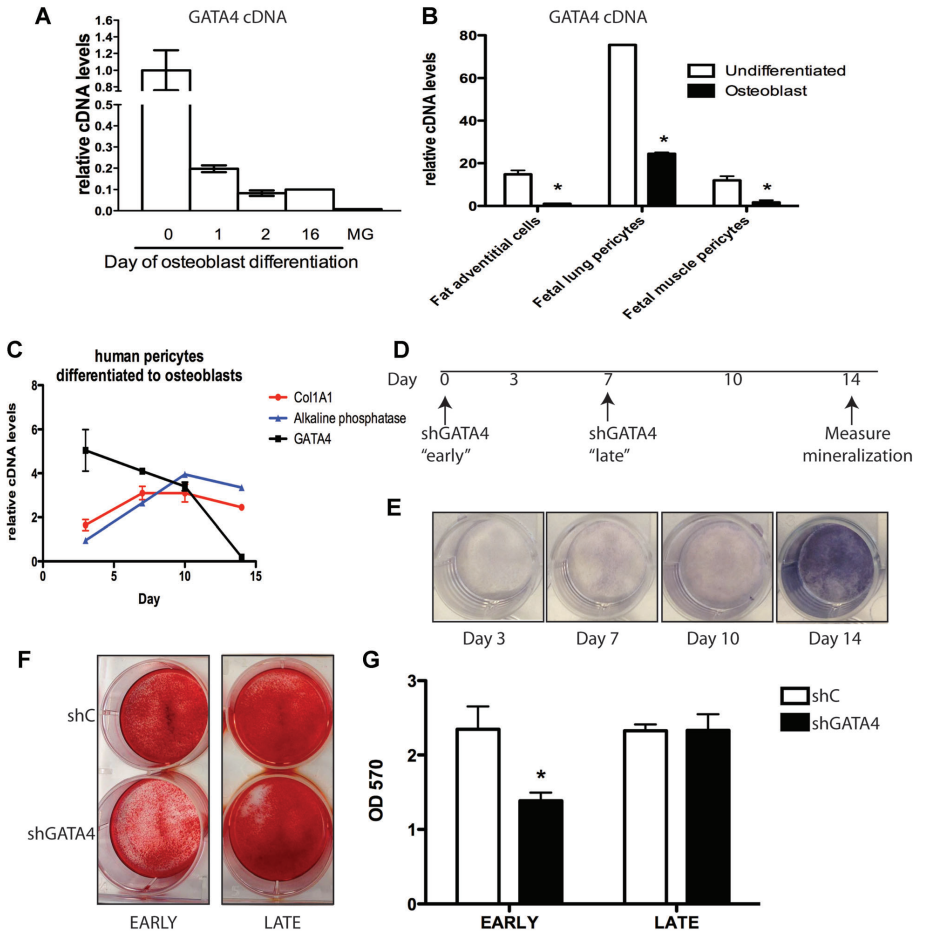

Fig. 3. GATA4 regulates bone mineralization early in the differentiation process. (*A*) Bone marrow stromal cells were differentiated for 0, 1, 2, or 16 d. RNA was obtained and qPCR was performed for *Gata4* and normalized to actin mRNA. MG RNA was also obtained for comparison. (*B*) Fat adventitial cells, fetal lung pericytes, and fetal muscle pericytes were left undifferentiated or differentiated to mineralizing osteoblasts. RNA was obtained and qPCR was performed for *Gata4* and normalized to actin mRNA. (*C*) Human fetal bone marrow CD146+ cells (pericytes) were cultured in osteoblast differentiation media for 3, 7, 10, and 14 d. RNA was obtained and qPCR was performed for *Gata4*, *Col1A1*, and alkaline phosphatase cDNA and normalized to actin mRNA. (*D*) Design of experiment for parts *E*–*G*. (*E*) Human fetal bone marrow CD146+ cells (pericytes) were cultured in osteoblast differentiation media for 3, 7, 10, and 14 d. At the indicated times cells were fixed and assayed for alkaline phosphatase. (*F*) Pericytes were infected with lentivirus expressing shC or shGATA4 either "early" at day 0 or "late" at day 7. All cells were placed in mineralization media at day 1 and allowed to differentiate for 2 wk. Cells were then fixed and stained using Alizarin Red. (*G*) Alizarin Red from part *F* was eluted and the mineral content was measured at an OD of 570 nm. Silencing was performed in three wells and the average OD is displayed. $^{*}p < 0.05$. OD = optical density; Col1A1 = type I collagen A1; MG = mammary gland.

tissues (Supporting Fig. 4, and data not shown). However, based on the in vitro data described above, *Gata4* expression was analyzed in the developing skull and hind limb. Using highly sensitive in situ RNA hybridization (RNAscope technology), *Gata4* mRNA is shown to be abundant in the ventricular zone of the developing brain in E13.5, E14.5, and E16.5 mice, before ossification of the skull (Fig. 4). At E18.5 *Gata4* mRNA has decreased significantly in the brain and is present near and/or within the ossifying skull. *Gata4* mRNA is also present in proliferating chondrocytes in E13.5, E14.5, and E16.5 hind limbs,

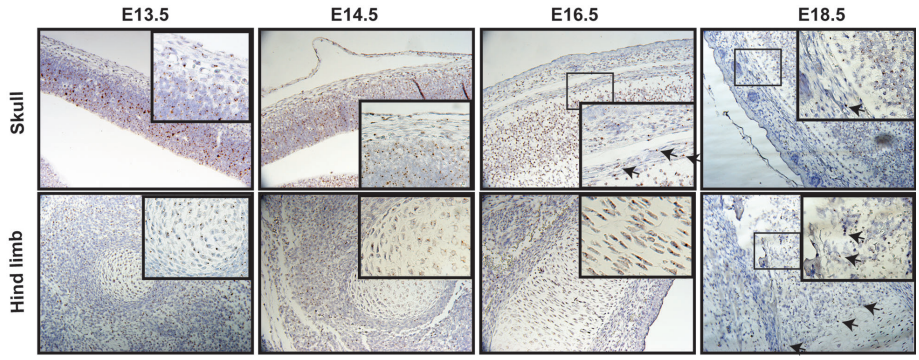

Fig. 4. In situ analysis of *Gata4* expression. Sagittal sections of E13.5, E14.5, E16.5, and E18.5 wild-type FVB embryos were probed for *Gata4* expression (brown) and counterstained with hematoxylin (blue). Arrows indicate *Gata4* expression in bone.

which has not been previously reported. At E18.5 *Gata4* mRNA is expressed at the ossification front of the growth plate and periosteum. Although the precise identity of the *Gata4*-positive cells in these locations is as yet unclear, the data are consistent with a direct role for GATA4 at various times and stages in normal embryonic bone development.

GATA4 is necessary for bone development in embryogenesis in vivo

To determine the role of GATA4 in vivo, *Gata4* floxed (GATA4Fl/Fl) mice were crossed with mice expressing Cre recombinase under control of a 2.3-kb fragment of the rat *Col1a1* gene.[27] Previous studies have shown that Cre-mediated deletion of exons 3, 4, and 5 of the *Gata4* gene converts the floxed allele into a recombined allele no longer capable of encoding a functional GATA4 protein.[28] *Gata4* recombination efficiency in osteoblasts was determined in vivo by qPCR of mRNA, using primers that cannot detect recombined *Gata4* mRNA. *Gata4* mRNA was reduced by over 75% in differentiated calvarial organs of GATA4Fl/FlCre+ mice (cKO) (Fig. 5*A*). The actual recombination of *Gata4* in osteoblasts is probably significantly higher, because the calvarial organs consist of other cell types, such as stromal cells.

Gata4 cKO mice were not present at Mendelian ratios after E16.5 (Fig. 5*B*). Mutants were morphologically indistinguishable from control littermates' appearance at any age, including E18.5 (Fig. 5*C*) or P1 (Fig. 5*D*), or by weight (Fig. 5*E*). The mice did not exhibit any obvious heart defects, as might be predicted from leaky Col1a1-Cre expression. Whole hearts and H&E-stained sections of left and right ventricles from P0 animals revealed normal septal structure, and a well-developed myocardium (Supporting Fig. 5, and data not shown). In addition, heart weight–body weight ratios were the same in wild-type and cKO littermate animals (Supporting Fig. 5). Thus, although we cannot at present determine the cause of death of cKO mice, we have no evidence that heart defects are responsible.

Skeletal preparations of E18.5 mice revealed no gross abnormalities (Fig. 6*A*, *B*). However, closer examination revealed multiple skull defects (Fig. 6*C–J*, Supporting Fig. 5), including smaller zygomatic bones (Fig. 6*C*, *D*; red arrows), a more mineralized occipital one (Fig. 6*D*, *F*) and decreased thickness of cranial bone (Fig. 6*G*, *H*; red lines). Furthermore, Von Kossa staining and μCT analysis demonstrate a reduced mineralization of the skull in the cKO mice (Fig. 6*I*, *J*; Supporting Fig. 5F, G).

In addition to cranial defects, we also observed vertebral and appendicular defects. Individual lumbar vertebrae were larger and misshapen (Fig. 6*K*, *L*), leading to an overall increase in spine length of cKO mice (Fig. 6*M*). The vertebral bodies of the cKO mice have a decrease in hypertrophic chondrocytes (Fig. 6*N*, *O*) and irregular mineralization (Fig. 6*P*, *Q*). There is a lack of fusion of the distal tibia and fibula in cKO mice as observed by both skeletal preparations (Fig. 6*R*, *S*) and μCT (Fig. 6*T*, *U*). There is also a decrease in hypertrophic chondrocytes and mineralization in the femurs of cKO mice (Fig. 6*V–Y*).

To quantify the mineralization effects in Fig. 6, μCT analysis was performed on the femurs and vertebrae of WT and cKO newborn mice, which demonstrated that cKO mice had reduced trabecular bone (Fig. 7*A–L*). The trabecular bone volume (BV/TV), trabecular number (Tb.N), and trabecular thickness (Tb.Th) were significantly reduced in cKO femurs compared to wild-type littermates (Fig. 7*C–E*). Trabecular spacing was increased in the cKO mice, although it did not reach statistical significance (Tb.Sp; Fig. 7*F*). Cortical bone parameters (total cross-sectional area, cortical bone area, cortical bone area fraction, or cortical thickness) were not statistically different between wild-type and cKO littermate animals (Supporting Fig. 7). μCT analysis of lumbar vertebrae (L_5) confirmed the irregular shape of cKO vertebrae (Fig. 7*G*, *H*) and revealed a significant reduction in the BV/TV and Tb.Th (Fig. 7*I*, *K*). Tb.N was decreased in the cKO mice, although it did not reach statistical significance (Fig. 7*J*). Together, the skeletal preparations, histology, and μCT analysis indicate defects in intramembranous and endochondral bone formation.

GATA4 regulates TGFβ and BMP pathways

To investigate mechanisms underlying the role of GATA4 in osteoblasts, we examined global gene expression changes

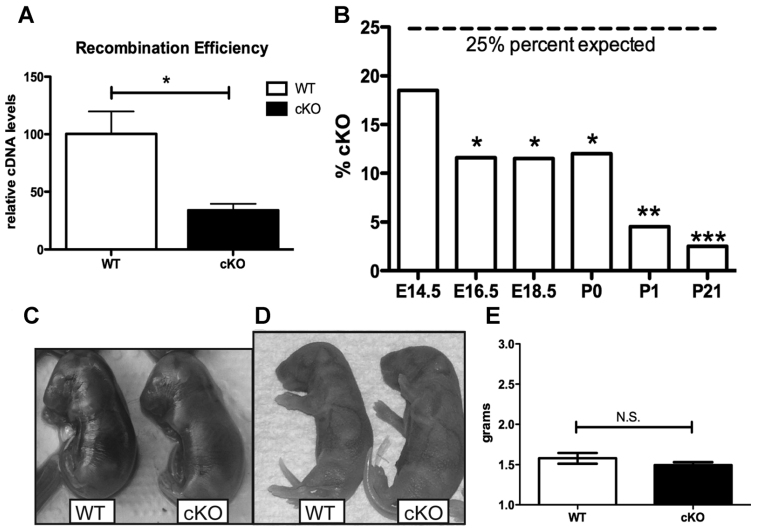

Fig. 5. GATA4 cKO mice are not born at expected Mendelian ratios. (*A*) The recombination efficiency of Cre-mediated excision was measured by qPCR from cDNA from differentiated WT and cKO calvarial organ cultures. (*B*) Tail DNA was obtained from mice at E14.5, E16.5, E18.5, P0, P1, and P21. Genotyping was performed for the presence of Floxed *Gata4* and for Cre recombinase. The percent of mice that were GATA4 Fl/Fl/Cre+ (% cKO) is graphed. $^{*}p < 0.05$; $^{**}p < 0.001$; $^{***}p < 0.0001$. (*C*) Photograph of representative WT and cKO mice at E18.5. (*D*) Photograph of representative WT and cKO mice at P1. (*E*) Weight, in grams, of newborn WT and cKO mice. cKO = conditional knockout; N.S. = not significant.

following *Gata4* knockdown in primary murine calvarial osteoblasts (Supporting Fig. 1A). Osteoblasts were differentiated for 2 wk and RNA was analyzed by genomewide expression profiling (MouseRef-8 v2.0 Expression BeadChips; Illumina). Loss of *Gata4* resulted in a decrease in expression of 1610 genes by twofold or greater and an increase in expression of 2399 genes by twofold or greater. Gene ontology analysis by DAVID software revealed several categories of differentially expressed genes.[20] The most downregulated genes in shGATA4 cells encode extracellular matrix proteins ($p = 3.2 \times 10^{-16}$) and drive bone development ($p = 3.6 \times 10^{-8}$), thereby confirming a role for GATA4 in osteoblasts.

Loss of *Gata4* resulted in misregulation of a large number of TGFβ superfamily pathway genes (Supporting Figs. 8 and 9). Key upregulated genes in this pathway were TGFβ2 and TGFβ3, whereas both BMP pathway genes were downregulated. Analysis of mRNA expression in shGATA4-infected calvarial osteoblasts confirmed decreased expression of two BMP ligands (*Bmp4* and *Bmp6*), a receptor (*Bmpr1A*), and a downstream effector SMAD (*Smad5*) (Fig. 8*A*). Because of the downregulation of BMP pathway genes, BMP pathway activation (phosphorylated SMAD [pSMAD] 1/5/8 as a downstream target for BMP-mediated signaling[7]) was analyzed with a pSMAD1/5/8 antibody by immunoblotting. Indeed, shGATA4 cells had a reduced amount of pSMAD1/5/8, illustrating that BMP-mediated signal transduction has been severely attenuated. E2 had no effect on the regulation of pSMAD1/5/8 (Fig. 8*B*). Conversely, TGFβ2 and TGFβ3 were significantly upregulated in shGATA4 cells (Fig. 8*C*). Consistent with the upregulation of the ligands, pSMAD2/3 were increased in shGATA4 cells (Fig. 8*D*), demonstrating activation of the TGFβ pathway. E2 induced phosphorylation of SMAD2 and SMAD3 in shGFP cells, but not in shGATA4 cells.

To investigate the possibility of an in vivo role for GATA4 regulation of the TGFβ and BMP pathways, the femurs of control (Fl/Fl) and cKO mice were analyzed by immunohistochemistry (IHC) for pSMAD1/5/8 and pSMAD2/3. cKO bones exhibited a decrease in the amount of pSMAD1/5/8 in the trabecular bone (Fig. 8*E*). Conversely, pSMAD2/3 was increased in the trabecular bone from cKO mice, as compared to WT bone (Fig. 8*F*). Our findings thus indicate that GATA4 is critical for the maintenance of osteoblast function, and raise the possibility that this is in part through regulating the balance between BMP and TGFβ pathway activity.

Discussion

We previously identified GATA4 as a pioneer factor for estrogen receptor in osteoblasts.[6] Here we demonstrate that GATA4 is important for the regulation of several E2 targets in osteoblasts, but that GATA4 also has E2-independent functions.

Knockout of GATA4 specifically in osteoblasts leads to embryonic and/or perinatal lethality. Because cKO mice were physically indistinguishable from their WT littermates at all stages of development, the cause of death remains under investigation. The Col1A1 2.3-kb promoter is expressed as early

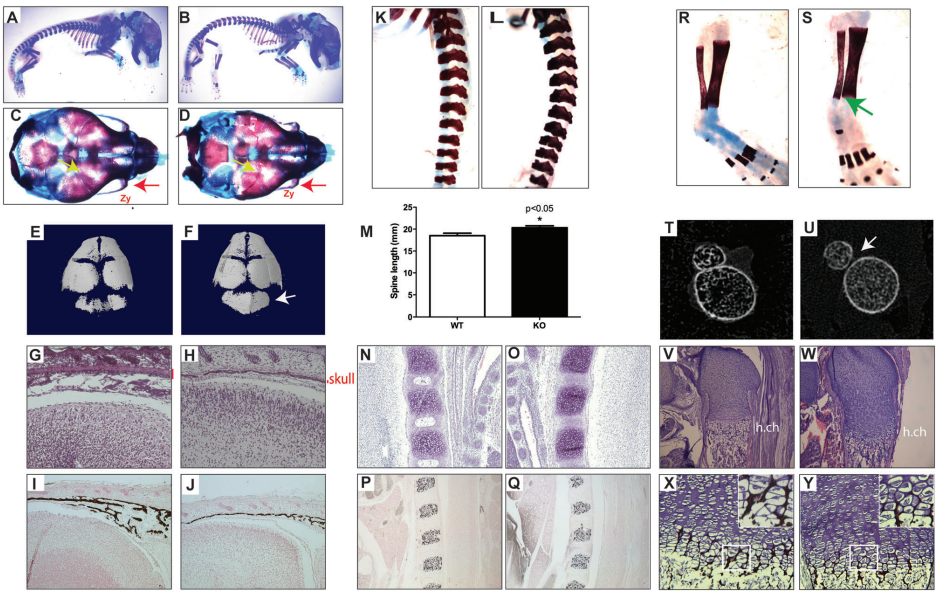

Fig. 6. GATA4 cKO mice have skeletal defects. (*A–D*) Skeletal preparations of E18.5 WT (*A*, *C*) and cKO (*B*, *D*) mice. (*A*, *B*) Whole body. (*C*, *D*) Superior view of skull. Red arrow indicates decreased zygomatic bone size in cKO mice. Yellow arrows highlight a suture defect in the cKO skull. (*E*, *F*) μCT images of WT (*E*) and cKO (*F*) skulls. Arrow points to occipital bone. (*G*, *H*) H&E staining of sagittal sections of WT (*G*) and cKO (*H*) heads. Red line indicates thickness of skull bone. (*I*, *J*) Von Kossa staining of sagittal sections of WT (*I*) and cKO (*J*) heads. (*K*, *L*) Skeletal preparations of spine from WT (*K*) and cKO (*L*). (*M*) Total spine length of $n = 7$ mice. $^{*}p < 0.05$. (*N*, *O*) H&E staining of sagittal sections of WT (*N*) and cKO (*O*) vertebrae. (*P*, *O*) Von Kossa staining of sagittal sections of WT (*P*) and cKO (*Q*) vertebrae. (*R*, *S*) Skeletal preparations of tibia and fibula from WT (*R*) and cKO (*S*). Green arrow indicates lack of fusion of tibia and fibula. (*T*, *U*) μCT images of WT (*T*) and ckO (*U*) tibia and fibula at their closest distance. (*V*, *W*) H&E staining of sagittal sections of WT (*V*) and cKO (*W*) femurs. (*X*, *Y*) Von Kossa staining of sagittal sections of WT (*X*) and cKO (*Y*) femurs. Zy = zygomatic bone; h.ch = hypertrophic chondrocytes. KO = knockout; cKO = conditional knockout.

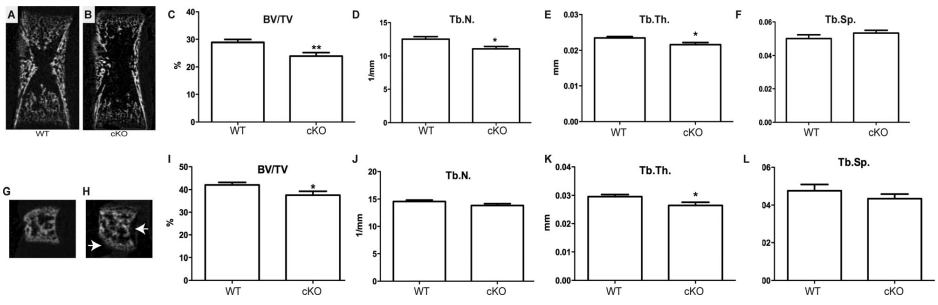

Fig. 7. Comparison of trabecular bone structure in P0 WT and cKO mice assessed by μCT. (*A*, *B*) Representative μCT images of WT and cKO femurs. (*C*) BV/TV, (*D*) Tb.N, and (*E*) Tb.Th were decreased in femurs of cKO mice. (*F*) There was no statistical increase in Tb.Sp in cKO mice. (*G*, *H*) Representative μCT images of WT and cKO L_5 vertebrae. Arrows indicate defects in shape. (*I*) BV/TV, (*J*) Tb.N, (*K*) Tb.Th, and (*L*) Tb.Sp of L_5 vertebrae in WT and cKO L_5 vertebrae. $n = 9$; $^{*}p < 0.05$. cKO = conditional knockout; BV/TV = bone volume/total volume; Tb.N = trabecular number; Tb.Th = trabecular thickness; Tb.Sp = trabecular spacing.

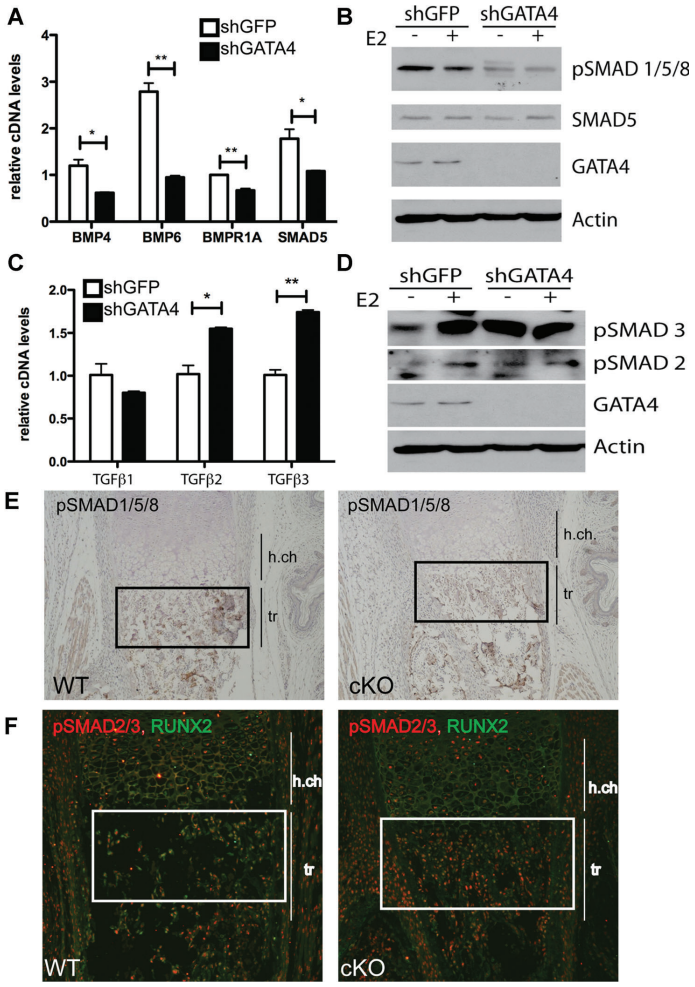

Fig. 8. GATA4 regulates the TGFβ and BMP pathways in osteoblasts. (*A*) Calvarial osteoblasts were infected with lentivirus expressing either shGFP or shGATA4. Cells were then differentiated for 2 wk and RNA was obtained. qPCR was performed for the indicated genes and normalized to actin mRNA. (*B*) Calvarial osteoblasts were infected with lentivirus expressing either shGFP or shGATA4. Cells were then differentiated for 2 wk and then treated with E2 for 24 hours. Protein was obtained and immunoblots for pSMAD1/5/8, SMAD5, GATA4, and actin were performed. (*C*) RNA was obtained as in *A*, and qPCR was performed for the indicated genes and normalized to actin mRNA. (*D*) Protein was obtained as in *B*, and immunoblots for pSMAD3, pSMAD2, GATA4, and actin were performed. (*E*) IHC with an antibody to pSMAD1/5/8 was performed on femurs from P0 WT (Fl/Fl) and cKO (Fl/Fl; Cre+) mice. (*F*) Immunofluorescence with an antibody to pSMAD1/5/8 was performed on femurs from P0 WT (Fl/Fl) and cKO (Fl/Fl; Cre+) mice. $^{*}p < 0.05$; $^{**}p < 0.001$. cKO = conditional knockout; h.ch = hypertrophic chondrocytes; tr = trabecular bone; IHC = immunohistochemistry.

as E14.5, when analyzed by crossing the Col1A1-Cre mouse with the ROSA26 reporter mouse (R26R).[29] The Col1A1-Cre;R26R mouse demonstrates a high level of bone-specific expression of Cre recombinase,[29] as does mRNA from many tissues.[27] Furthermore, the *Col1a1* (2.3-kb)-GFP transgene was not detected in the heart or intestines,[30] which are two tissues with high *Gata4* expression. However, it is possible that expression could occur at a different age, or at a level below

the detection of a Northern blot. The *Col1a1* 2.3-kb promoter might be active in some growth plate chondrocytes,[27] and the extent of this effect needs to be investigated.

Although rare, Col1A1-Cre–mediated deletion has led to embryonic death.[31] Crossing the *Gata4* Fl/Fl mouse with a mouse that expresses Cre later in the osteoblast lineage, such as the osteocalcin promoter,[32] could reveal a role for GATA4 in adult mice and potential roles in estrogen-deficient osteoporosis. Similarly, crossing the *Gata4* Fl/Fl mouse with a mouse that expresses Cre earlier in development could further define the "early" role for GATA4 suggested by the above data.

Total *Gata4* knockout mice exhibit embryonic lethality from E7.5 to E10.5,[15,16] which is much earlier than for the osteoblast-specific knockout described here. Interestingly, specific knockouts of GATA4 in the heart with Cre-recombinase controlled by the β-myosin heavy promoter (β-MHC) or α-MHC promoter were generated at predicted Mendelian ratios and mice were viable up to 16 wk of age.[33] *Gata4* deletion from the developing intestinal epithelium,[34] pancreas,[35] testicular somatic cells,[36] or granulosa cells[37] also resulted in mice born at the expected Mendelian ratios, but with tissue-specific effects.

These results demonstrate that GATA4 is essential for bone mineralization both in vitro and in vivo. μCT analysis shows a decrease in trabecular bone measurements in the cKO mice. Furthermore, the skeletal preparations and μCT show defects, including those in the skull, legs, and spine, in these mice.

Mouse models for TGFβ and BMP signaling in bone have been generated (reviewed in Chen and colleagues[8]). TGFβ2 overexpression leads to lower bone mineral density, in agreement with the *Gata4* cKO mice.[38] TGFβ2-null mice have a lack of occipital bone formation,[39] corresponding with the increase in occipital bone formation in *Gata4* cKO mice and the suppression of TGFβ2 by GATA4. A limb mesenchyme double KO of both BMP2 and BMP4 (driven by Prx1-cre) leads to severe bone malformation. Interestingly, the tibia and fibula in the BMP4 KO are not fused,[40] as is seen in the *Gata4* cKO. Furthermore, an osteoblast-specific KO of SMAD1 leads to an osteopenic phenotype.[41] Together, these mouse models are in agreement with a role for GATA4 in regulating TGFβ and BMP signaling. Genetic epistasis experiments will be required to test the physiological relevance of the altered BMP and TGFβ pathway activity we have observed in *Gata4* cKO mice.

GATA4 is currently being used for gene therapy in the heart in combination with heart-specific transcription factors.[42] MSCs show potential for the treatment of osteoporosis, and their optimization could be realized by estrogens, selective estrogen receptor modulators (SERMs), and/or GATA4 to better induce osteoblast formation. In conclusion, GATA4 in osteoblasts plays a key role in the regulation of TGFβ and BMP pathways to control bone differentiation and/or mineralization.

Disclosures

All authors state that they have no conflicts of interest.

Acknowledgments

This work was supported by an ASBMR Junior Faculty Osteoporosis Research Award and 1R56DK090231-01 to SAK and AR044528 to KL. The UCLA Vector Core is supported by JCCC/P30 CA016042 and CURE/P30 DK041301. The funders had no role in study design, data collection and analysis, decision to publish, or preparation of the manuscript.

Authors' roles: Study conduct: MG, AJG, DR, SR, WW, GZ, VHM, EA, GAMC, and SAK. Study design: AJG, ST, BP, KL, GAMC, and SAK. MG, AJG, ST, BP, KL, GAMC, and SAK participated in drafting the manuscript or revising it critically for important intellectual content. MG, AJG, DR, SR, WW, GZ, ST, BP, KL, GAMC, and SAK approved the final version of the submitted manuscript. SAK agrees to be accountable for all aspects of the work.

References

1. United States Bone and Joint Decade: The Burden of Musculoskeletal Diseases in the United States. Rosemont, IL: American Academy of Orthopaedic Surgeons; 2008. Available from: http://www.boneandjointburden.org/chapter_downloads/index.htm.
2. Kousteni S, Bellido T, Plotkin LI, et al. Nongenotropic, sex-nonspecific signaling through the estrogen or androgen receptors: dissociation from transcriptional activity. Cell. 2001;104(5):719–30.
3. Krum SA, Miranda-Carboni GA, Hauschka PV, et al. Estrogen protects bone by inducing Fas ligand in osteoblasts to regulate osteoclast survival. EMBO.J. 2008;27(3):535–45.
4. Krum SA. Direct transcriptional targets of sex steroid hormones in bone. J Cell Biochem. 2011;112(2):401–8.
5. Molkentin JD. The zinc finger-containing transcription factors GATA-4, -5, and -6. Ubiquitously expressed regulators of tissue-specific gene expression. J Biol Chem. 2000;275(50):38949–52.
6. Miranda-Carboni GA, Guemes M, Bailey S, et al. GATA4 regulates estrogen receptor-{alpha}-mediated osteoblast transcription. Mol Endocrinol. 2011;25(7):1126–36.
7. Song B, Estrada KD, Lyons KM. Smad signaling in skeletal development and regeneration. Cytokine Growth Factor Rev. 2009;20(5–6):379–88.
8. Chen G, Deng C, Li YP. TGF-beta and BMP signaling in osteoblast differentiation and bone formation. Int J Biol Sci. 2012;8(2):272–88.
9. Alliston T, Choy L, Ducy P, Karsenty G, Derynck R. TGF-beta-induced repression of CBFA1 by Smad3 decreases cbfa1 and osteocalcin expression and inhibits osteoblast differentiation. EMBO J. 2001;20(9):2254–72.
10. Rojas A, De Val S, Heidt AB, Xu SM, Bristow J, Black BL. Gata4 expression in lateral mesoderm is downstream of BMP4 and is activated directly by Forkhead and GATA transcription factors through a distal enhancer element. Development. 2005;132(15):3405–17.
11. Nemer G, Nemer M. Transcriptional activation of BMP-4 and regulation of mammalian organogenesis by GATA-4 and -6. Dev Biol. 2003;254(1):131–48.
12. Brown CO 3rd, Chi X, Garcia-Gras E, Shirai M, Feng XH, Schwartz RJ. The cardiac determination factor, Nkx2-5, is activated by mutual cofactors GATA-4 and Smad1/4 via a novel upstream enhancer. J Biol Chem. 2004;279(11):10659–69.
13. Belaguli NS, Zhang M, Rigi M, Aftab M, Berger DH. Cooperation between GATA4 and TGF-beta signaling regulates intestinal epithelial gene expression. Am J Physiol Gastrointest Liver Physiol. 2007;292(6):G1520–33.
14. Anttonen M, Parviainen H, Kyronlahti A, et al. GATA-4 is a granulosa cell factor employed in inhibin-alpha activation by the TGF-beta pathway. J Mol Endocrinol. 2006;36(3):557–68.
15. Kuo CT, Morrisey EE, Anandappa R, et al. GATA4 transcription factor is required for ventral morphogenesis and heart tube formation. Genes Dev. 1997;11(8):1048–60.
16. Molkentin JD, Lin Q, Duncan SA, Olson EN. Requirement of the transcription factor GATA4 for heart tube formation and ventral morphogenesis. Genes Dev. 1997;11(8):1061–72.
17. Ducy P, Zhang R, Geoffroy V, Ridall AL, Karsenty G. Osf2/Cbfa1: a transcriptional activator of osteoblast differentiation. Cell. 1997;89(5):747–54.

18. Crisan M, Yap S, Casteilla L, et al. A perivascular origin for mesenchymal stem cells in multiple human organs. Cell Stem Cell. 2008;3(3):301–13.
19. Rozen S, Skaletsky H. Primer3 on the WWW for general users and for biologist programmers. Methods Mol Biol. 2000;132:365–86.
20. Huang da W, Sherman BT, Lempicki RA. Systematic and integrative analysis of large gene lists using DAVID bioinformatics resources. Nat Protoc. 2009;4(1):44–57.
21. Retting KN, Song B, Yoon BS, Lyons KM. BMP canonical Smad signaling through Smad1 and Smad5 is required for endochondral bone formation. Development. 2009;136(7):1093–104.
22. Jozwik KM, Carroll JS. Pioneer factors in hormone-dependent cancers. Nat Rev Cancer. 2012;12(6):381–5.
23. Nawaz Z, Lonard DM, Dennis AP, Smith CL, O'Malley BW. Proteasome-dependent degradation of the human estrogen receptor. Proc Natl Acad Sci U S A. 1999;96(5):1858–62.
24. Read LD, Greene GL, Katzenellenbogen BS. Regulation of estrogen receptor messenger ribonucleic acid and protein levels in human breast cancer cell lines by sex steroid hormones, their antagonists, and growth factors. Mol Endocrinol. 1989;3(2):295–304.
25. Krum SA, Miranda-Carboni GA, Lupien M, Eeckhoute J, Carroll JS, Brown M. Unique ER{alpha} cistromes control cell type-specific gene regulation. Mol Endocrinol. 2008;22(11):2393–406.
26. Almeida M, Martin-Millan M, Ambrogini E, et al. Estrogens attenuate oxidative stress and the differentiation and apoptosis of osteoblasts by DNA-binding-independent actions of the ERalpha. J Bone Miner Res. 2010;25(4):769–81.
27. Liu F, Woitge HW, Braut A, et al. Expression and activity of osteoblast-targeted Cre recombinase transgenes in murine skeletal tissues. Int J Dev Biol. 2004;48(7):645–53.
28. Watt AJ, Battle MA, Li J, Duncan SA. GATA4 is essential for formation of the proepicardium and regulates cardiogenesis. Proc Natl Acad Sci U S A. 2004;101(34):12573–8.
29. Dacquin R, Starbuck M, Schinke T, Karsenty G. Mouse alpha1(I)-collagen promoter is the best known promoter to drive efficient Cre recombinase expression in osteoblast. Dev Dyn. 2002;224(2):245–51.
30. Kalajzic I, Kalajzic Z, Kaliterna M, et al. Use of type I collagen green fluorescent protein transgenes to identify subpopulations of cells at different stages of the osteoblast lineage. J Bone Miner Res. 2002;17(1):15–25.
31. Gaur T, Hussain S, Mudhasani R, et al. Dicer inactivation in osteoprogenitor cells compromises fetal survival and bone formation, while excision in differentiated osteoblasts increases bone mass in the adult mouse. Dev Biol. 2010;340(1):10–21.
32. VanKoevering KK, Williams BO. Transgenic mouse strains for conditional gene deletion during skeletal development. IBMS Bonekey. 2008;5:151–70.
33. Oka T, Maillet M, Watt AJ, et al. Cardiac-specific deletion of Gata4 reveals its requirement for hypertrophy, compensation, and myocyte viability. Circ Res. 2006;98(6):837–45.
34. Battle MA, Bondow BJ, Iverson MA, et al. GATA4 is essential for jejunal function in mice. Gastroenterology. 2008;135(5):1676–86.e1.
35. Xuan S, Borok MJ, Decker KJ, et al. Pancreas-specific deletion of mouse Gata4 and Gata6 causes pancreatic agenesis. J Clin Invest. 2012;122(10):3516–28.
36. Kyronlahti A, Euler R, Bielinska M, et al. GATA4 regulates Sertoli cell function and fertility in adult male mice. Mol Cell Endocrinol. 2011;333(1):85–95.
37. Kyronlahti A, Vetter M, Euler R, et al. GATA4 deficiency impairs ovarian function in adult mice. Biol Reprod. 2011;84(5):1033–44.
38. Erlebacher A, Derynck R. Increased expression of TGF-beta 2 in osteoblasts results in an osteoporosis-like phenotype. J Cell Biol. 1996;132(1–2):195–210.
39. Sanford LP, Ormsby I, Gittenberger-de Groot AC, et al. TGFbeta2 knockout mice have multiple developmental defects that are non-overlapping with other TGFbeta knockout phenotypes. Development. 1997;124(13):2659–70.
40. Bandyopadhyay A, Tsuji K, Cox K, Harfe BD, Rosen V, Tabin CJ. Genetic analysis of the roles of BMP2, BMP4, and BMP7 in limb patterning and skeletogenesis. PLoS Genet. 2006;2(12):e216.
41. Wang M, Jin H, Tang D, Huang S, Zuscik MJ, Chen D. Smad1 plays an essential role in bone development and postnatal bone formation. Osteoarthritis Cartilage. 2011;19(6):751–62.
42. Hartung S, Schwanke K, Haase A, et al. Directing cardiomyogenic differentiation of human pluripotent stem cells by plasmid-based transient overexpression of cardiac transcription factors. Stem Cells Dev. 2013 Apr 1;22(7):1112–25.

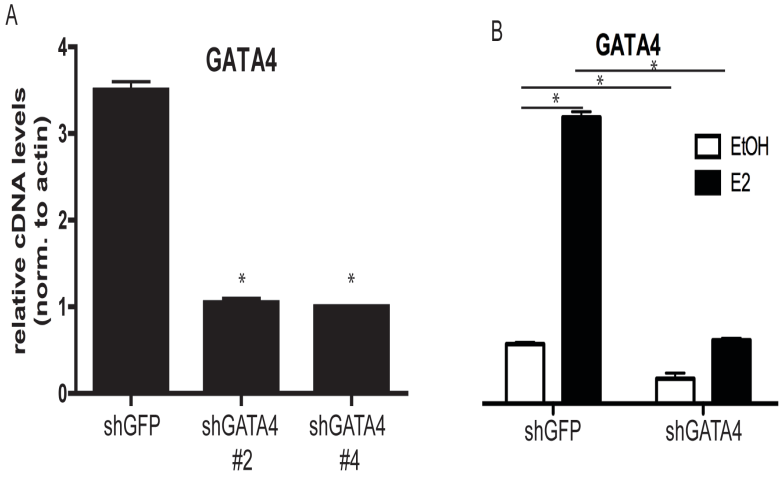

Supplemental Figure 1. GATA4 lentiviral shRNA successfully knocks down *Gata4* gene expression.

(A) Two different lentiviruses successfully knockdown *Gata4* mRNA. Calvarial osteoblasts were infected with lentivirus expressing either shGFP or shGATA4 clone #2 or #4. Cells were then differentiated for two weeks and RNA was obtained. qPCR was performed for *Gata4* and normalized to actin mRNA.

(B) Calvarial osteoblasts were infected with lentivirus expressing either shGFP or shGATA4 clone #2. Cells were then differentiated for two weeks, treated with 10 nM E2 for 24 hours, and then RNA was obtained. qPCR was performed for *Gata4* and normalized to actin mRNA.

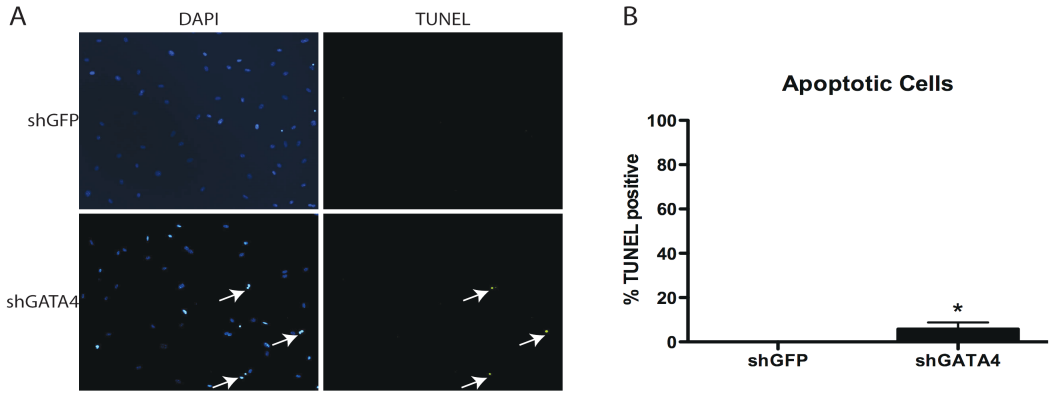

Supplemental Figure 2. Apoptosis in shGATA4 calvaria osteoblasts.
(A) Calvarial osteoblasts were infected with lentivirus expressing either shGFP or shGATA4. TUNEL was performed and cells were counterstained with DAPI.
(B) Multiple wells from part (A) were quantified.

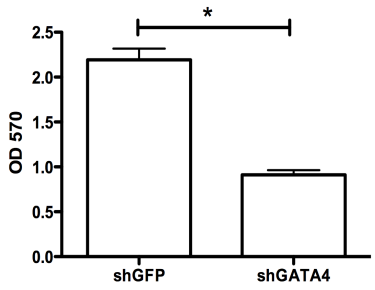

Supplemental Figure 3. Mineralization in shGATA4 calvaria osteoblasts.
An independent shRNA targeting of *Gata4 (*shGATA4 #4) also yielded a significant reduction in mineralization. Calvarial osteoblasts were infected with lentivirus expressing either shGFP or shGATA4 clone #4. Cells were then differentiated for two weeks. Cells were then fixed and stained using alizarin red. Alizarin red was eluted and the mineral content was measured at an OD of 570. Silencing was performed in three wells and the average OD is displayed. Experiments were then performed in triplicate.
* $P < .05$.

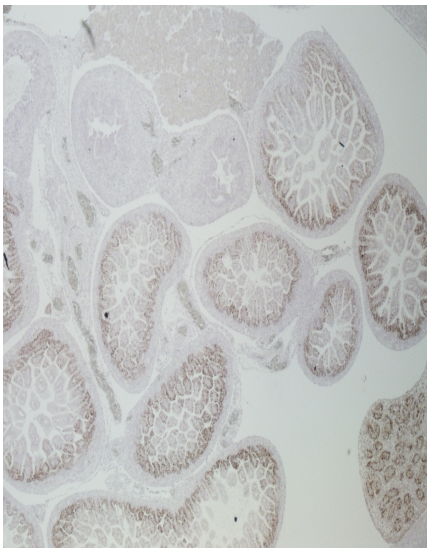

Supplemental Figure 4. GATA4 *in situ* analysis.
E18.5 embryos were probed for *Gata4* expression. The highest level of staining was seen in the intes9nes shown here.

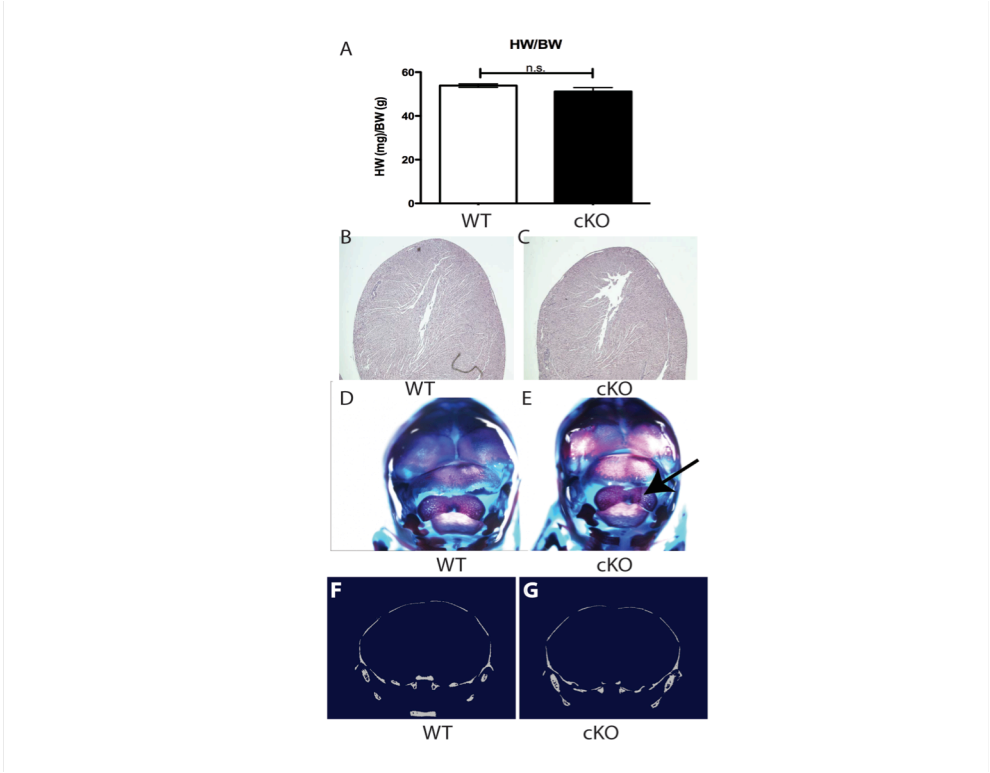

Supplemental Figure 5. Heart and cranial defects in *GATA4 cKO* mice.
(A) Heart weight/body weight (HW/BW) in wildtype (WT) and cKO mice.
(B and C) H&E staining of hearts from WT and cKO mice.
(D and E) Skeletal preparations of E18.5 mice reveal skull defects (arrow) in cKO mice.
(F and G) microCT images of WT (F) and cKO (G) skulls.

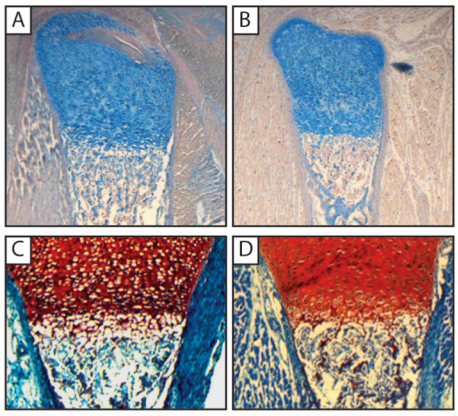

Supplemental Figure 6. Alcian Blue and Safranin O staining of femurs from WT and cKO mice.

(A---B) Alcian Blue staining of femurs from WT (A) and cKO (B) P0 mice.
(C---D) Safranin O staining of femurs from WT (C) and cKO (D) P0 mice.

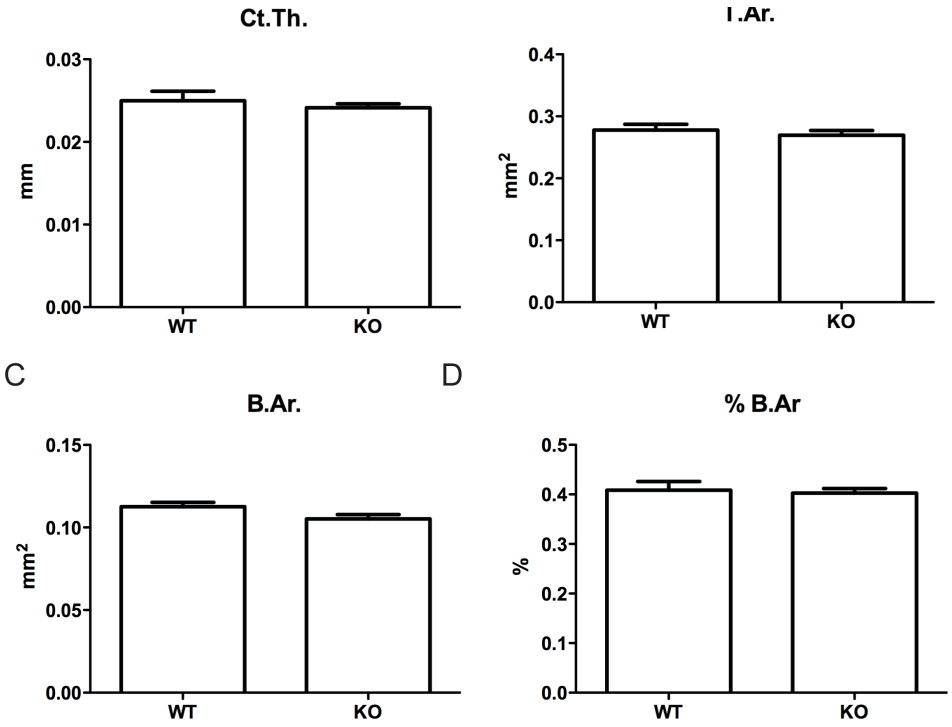

Supplemental Figure 7. Comparison of cortical bone structure in P0 WT and cKO mice assessed by μC.
(A) Cor9cal thickness (Ct.Th.), (B) Total Area (T. Ar.), (C) Bone Area (B.Ar.) and (D) percent bone area (% B.Ar.). N=9

Supplemental Fig. 8

Most decreased after shGATA4

Gene	Gene Name	DiffScore
Ibsp	integrin binding sialoprotein	-347.0
Akp2	alkaline phosphatase, liver/bone/kidney (Alpl)	-346.4
Prss35	protease, serine, 35	-346.4
Bglap	bone gamma carboxyglutamate protein (osteocalcin)	-265.0
Phex	Phosphate regulating gene with homologies to endopeptidases on the X chromosome	-200.9
Bmp3	bone morphogenetic protein 3	-194.8
Igfbp3	insulin-like growth factor binding protein 3	-126.2
Igfbp5	insulin-like growth factor binding protein 5	-93.0
Dlk1	delta-like 1 homolog	-65.4
Chrd	chordin	-59.1
Sox9	SRY-box containing gene 9	-57.1
Foxc1	forkhead box C1	-47.7
Rbp4	retinol binding protein 4	-43.9
Fgfr2	fibroblast growth factor receptor 2	-35.3
Kazald1	Kazal-type serine peptidase inhibitor domain 1	-31.2
Col11a1	collagen, type XI, alpha 1	-27.1
Sort1	sortilin 1	-27.0
Insig2	insulin induced gene 2	-26.7
BmpR1a	bone morphogenetic protein receptor, type 1A	-20.4
Smad5	MAD homolog 5	-17.3
Mmp13	matrix metallopeptidase 13	-15.4
Thra	thyroid hormone receptor alpha	-14.7
Sp7	Sp7 transcription factor 7 (osterix)	-13.1
Ror2	receptor tyrosine kinase-like orphan receptor 2	-11.4
Bmp4	bone morphogenetic protein 4	-11.3
Smad3	MAD homolog 3	-10.3
Insig1	insulin induced gene 1	-10.3
Smo	smoothened homolog	-10.2
Tgfbr1	transforming growth factor, beta receptor I	-9.6
Msx1	homeobox, msh-like 1	-9.3
Cbfb	core binding factor beta	-8.9
Mef2c	myocyte enhancer factor 2C	-8.4
Hspg2	perlecan (heparan sulfate proteoglycan 2)	-7.0
Tgfbr2	transforming growth factor, beta receptor II	-6.4
Ltbp3	latent transforming growth factor beta binding protein 3	-6.0
Osr2	odd-skipped related 2	-6.0
Bmp6	bone morphogenetic protein 6	-5.9
Fgfr1	fibroblast growth factor receptor 1	-5.7
Foxc2	forkhead box C2	-5.6
Znrd1	zinc ribbon domain containing, 1	-5.2
Col9a1	collagen, type IX, alpha 1	-3.2
Bcl2	B-cell leukemia/lymphoma 2	-3.2

Less decreased after shGATA4

Supplemental Figure 8. Most decreased and increased gene expression in shGATA4 calvaria osteoblasts.

Gene	Gene Name	DiffScore
Bmp3	bone morphogenetic protein 3	-194.8
BmpR1a	bone morphogenetic protein receptor, type 1A	-20.4
Smad5	MAD homolog 5	-17.3
Tgfbr3	transforming growth factor, beta receptor II	-16.3
Bmp4	bone morphogenetic protein 4	-11.3
Smad3	MAD homolog 3	-10.3
Tgfbr1	transforming growth factor, beta receptor I	-9.6
Tgfbr2	transforming growth factor, beta receptor II	-6.4
Bmp6	bone morphogenetic protein 6	-5.9
Bmp8a	bone morphogenetic protein 8a	-2.0
TGFB1I1	Transforming growth factor beta 1 induced transcript 1	3.4
Bmp1	bone morphogenetic protein 1	3.6
Tgfb1	Transforming growth factor, beta 1	4.3
BMPER	BMP binding endothelial regulator	10.8
Tgfb2	Transforming growth factor, beta 2	10.9
Bmpr1b	bone morphogenetic protein receptor, type 1B	11.2
Tgfb3	Transforming growth factor, beta 3	69.4

Supplemental Figure 9. Differential gene expression in shGATA4 calvaria osteoblasts.

HUMAN mRNA PRIMERS

SEQUENCE	FORWARD PRIMER 5′ TO 3′	REVERSE PRIMER 5′ TO 3′
B-ACTIN	GGACTTCGAGCAAGAGATGG	AGCACTGTGTTGGCGTACAG
GATA4	TCCCTCTTCCCTCCTCAAAT	TCAGCGTGTAAAGGCATCTG
RUNX2	TTTGCACTGGGTCATGTGTT	TGGCTGCATTGAAAAGACTG
COL1A1	ACGTCCTGGTGAAGTTGGTC	ACCAGGGAAGCCTCTCTCTC
Alkaline phosphatase	CCACGTCTTCACATTTGGTG	AGACTGCGCCTGGTAGTTGT

MOUSE mRNA PRIMERS

SEQUENCE	FORWARD PRIMER 5′ TO 3′	REVERSE PRIMER 5′ TO 3′
B-ACTIN	AGCCATGTACGTAGCCATCC	CTCTCAGCTGTGGTGGTGAA
GATA4	GTTGTGGTGGTGGGTTTTTC	CCCCAGGAAGCATTCAGTAA
COL1A1	ACGTCCTGGTGAAGTTGGTC	CAGGGAAGCCTCTTTCTCCT
ALP1	GTTGCCAAGCTGGGAAGAACAC	CCCACCCCGCTATTCCAAAC
RUNX2	CACGGTGACTCCCGTTACTT	ATACGTGTGACCCAGTGCAA
ERα	GCCAAGGAGACTCGCTACTG	CTCCGGTTCTTGTCAATGGT
FASL	CTGGGTTGTACTTCGTGTATTCC	TGTCCAGTAGTGCAGTAGTTCAA
EAP	GACGCAGAGTCCCTTCAGAC	CACCCCTACTCCCCATACCT
BSP	AAAGTGAAGGAAAGCGACGA	GTTCCTTCTGCACCTGCTTC
OCN	GGCCCTGAGTCTGACAAAGC	GCGCCGGAGTCTGTTCACT
BMP4	GCGGGACTTCGAGGCGACAC	CGGGACGCTCCGGGTACTCA
BMP6	GCGGTGACGGCTGCTGAGTT	GCACGGGGGTTGACGTGGAG
BMPR1A	CACCGAAAGCCCAGCTACGCA	GGGGGCAGTGTAGGCTGCAA
SMAD5	TCACCTGCGAGCCACGCTTT	TGCTTGGCTGTCCTGGGCTG
TGFB1	AGGGCTACCATGCCAACTTC	CCACGTAGTAGACGATGGGC
TGFB2	CTGCCTTCGCCCTCTTTACA	CCCCAGCACAGAAGTTAGCA
TGFB3	ATGACCCACGTCCCCTATCA	ACTCAGACTCCGAGGTCTCC

Supplemental Figure 10. Human and mouse mRNA primers.

APPENDIX B:

TGFβ and BMP Dependent Cell Fate Changes Due to Loss of Filamin B Produces Disc Degeneration and Progressive Vertebral Fusions

During the course of my graduate studies, I participated in a number of collaborations. The body of work described in Appendix B was a collaboration with our neighbors, the Deborah Krakow Laboratory at UCLA. I was responsible for providing and performing the techniques and procedures for skeletal and tissue histology, as well as immunofluorescence, shown in figures 1-4, 6, 8, 9, and supplemental figures 1-3. I characterized all the antibodies used for immunofluorescence and westernsblot analysis for fibroblast and vertebral cartilage signaling, with the exception of Filamin B. I also helped with the fractionation, TUNEL, and luciferase assays performed in this study. Furthermore, I advised on observing specific downstream targets that are affected in the TGFβ and BMP signaling pathway. The majority of work was performed by the Krakow group; however, my unique expertise in the field of cartilage and bone as well as TGFβ/BMP signaling allowed me to play an important role in this study.

PLOS | GENETICS

RESEARCH ARTICLE

TGFβ and BMP Dependent Cell Fate Changes Due to Loss of Filamin B Produces Disc Degeneration and Progressive Vertebral Fusions

Jennifer Zieba[1,2], Kimberly Nicole Forlenza[2], Jagteshwar Singh Khatra[2], Anna Sarukhanov[2], Ivan Duran[2], Diana Rigueur[3], Karen M. Lyons[2,3], Daniel H. Cohn[2,3], Amy E. Merrill[4,5], Deborah Krakow[1,2,6]*

1 Department of Human Genetics, David Geffen School of Medicine at the University of California at Los Angeles, Los Angeles, California, United States of America, **2** Department of Orthopaedic Surgery, David Geffen School of Medicine at the University of California at Los Angeles, Los Angeles, California, United States of America, **3** Department of Molecular, Cell, and Developmental Biology, University of California at Los Angeles, Los Angeles, California, United States of America, **4** Center for Craniofacial Molecular Biology, Ostrow School of Dentistry, University of Southern California, Los Angeles, California, United States of America, **5** Department of Biochemistry and Molecular Biology, Keck School of Medicine, University of Southern California, Los Angeles, California, United States of America, **6** Department of Obstetrics and Gynecology, David Geffen School of Medicine at the University of California at Los Angeles, Los Angeles, California, United States of America

* dkrakow@mednet.ucla.edu

Abstract

Spondylocarpotarsal synostosis (SCT) is an autosomal recessive disorder characterized by progressive vertebral fusions and caused by loss of function mutations in *Filamin B* (*FLNB*). FLNB acts as a signaling scaffold by linking the actin cytoskleteon to signal transduction systems, yet the disease mechanisms for SCT remain unclear. Employing a *Flnb* knockout mouse, we found morphologic and molecular evidence that the intervertebral discs (IVDs) of $Flnb^{-/-}$mice undergo rapid and progressive degeneration during postnatal development as a result of abnormal cell fate changes in the IVD, particularly the annulus fibrosus (AF). In $Flnb^{-/-}$mice, the AF cells lose their typical fibroblast-like characteristics and acquire the molecular and phenotypic signature of hypertrophic chondrocytes. This change is characterized by hallmarks of endochondral-like ossification including alterations in collagen matrix, expression of Collagen X, increased apoptosis, and inappropriate ossification of the disc tissue. We show that conversion of the AF cells into chondrocytes is coincident with upregulated TGFβ signaling via Smad2/3 and BMP induced p38 signaling as well as sustained activation of canonical and noncanonical target genes *p21* and *Ctgf*. These findings indicate that FLNB is involved in attenuation of TGFβ/BMP signaling and influences AF cell fate. Furthermore, we demonstrate that the IVD disruptions in $Flnb^{-/-}$mice resemble aging degenerative discs and reveal new insights into the molecular causes of vertebral fusions and disc degeneration.

OPEN ACCESS

Citation: Zieba J, Forlenza KN, Khatra JS, Sarukhanov A, Duran I, Rigueur D, et al. (2016) TGFβ and BMP Dependent Cell Fate Changes Due to Loss of Filamin B Produces Disc Degeneration and Progressive Vertebral Fusions. PLoS Genet 12(3): e1005936. doi:10.1371/journal.pgen.1005936

Editor: John F Bateman, Murdoch Childrens Research Institute, AUSTRALIA

Received: August 25, 2015

Accepted: February 24, 2016

Published: March 28, 2016

Data Availability Statement: All relevant data are within the paper and its Supporing Information files.

Funding: This work is supported by NIH grant 1F31AR066487-01A1 to JZ. We also thank the March of Dimes (http://www.marchofdimes.org) and the Joseph Drown Foundation (http://www.jdrown.org) for their support to DK. We are grateful to the CNSI Advanced Light Microscopy/Spectroscopy Shared Resource Facility at UCLA, supported with funding from NIH-NCRR shared resources grant (CJX1-443835-WS-29646), and NSF Major Research Instrumentation grant (CHE-0722519), for their

assistance. The research was supported by NIH/National Center for Advancing Translational Science (NCATS) UCLA CTSI Grant Number UL1TR000124 and by NIH/National Institute of Arthritis Musculoskeletal and Skin (NIAMS). The funders had no role in study design, data collection and analysis, decision to publish, or preparation of the manuscript

Competing Interests: The authors have declared that no competing interests exist.

Author Summary

Whereas there is a large foundation of knowledge concerning skeletal formation and development, identifying the molecular changes behind Intervertebral Disc (IVD) aging and degeneration has been a challenge. The loss of Filamin B, a protein component of the cell's cytoskeletal structure, gives rise to Spondylocarpotarsal Synostosis, a rare genetic disorder characterized by fusions of the vertebral bodies. Similarly, mice lacking the Filamin B protein show fusions of the vertebral bodies. We found that these fusions are caused by the early degeneration and eventual ossification of the IVDs. Our study demonstrates that this degeneration is caused by the increase in TGFβ and BMP activity, developmental pathways essential in bone and cartilage formation. These findings represent a significant step forward in our understanding of the molecular basis of IVD degeneration. as well as revealing filamin B's role in TGFβ/BMP signaling regulation. Moreover, we demonstrate that the study of the rare disease spondylocarpotarsal synostosis in a model organism can uncover mechanisms underlying more common diseases. Finally, our findings provide a model system that will facilitate further discoveries regarding disc degeneration, which affects a significant proportion of the population.

Introduction

Skeletal dysplasias are a heterogeneous group of more than 450 disorders characterized by abnormalities in patterning, development, and maintenance of the skeleton [1]. Congenital vertebral deformities in some of these disorders, particularly those that lead to progressive fusions, cause chronic pain and deformity and the mechanisms underlying the development of these fusions are poorly understood. Spondylocarpotarsal synostosis (SCT) syndrome is a recessively inherited disorder caused by nonsense mutations in *Filamin B (FLNB);* it is characterized by progressive vertebral, carpal, and tarsal bone fusions, short stature, and scoliosis [2]. The vertebral fusions can occur prenatally, leading to the appearance of an ectopic bar of bone spanning multiple vertebral bodies at birth [3].

Development of the axial skeleton, including the vertebral bodies, occurs via the process of endochondral bone formation, in which a cartilage template is replaced by bone. Endochondral bone growth occurs through the cartilage growth plate, a stratified tissue consisting of reserve, resting, proliferating, and hypertrophic chondrocytes which ultimately undergo apoptosis, leaving voids that become inhabited by osteoblasts forming the primary spongiosa. Vertebral bodies of the axial skeleton develop through endochondral ossification and are separated from each other by intervertebral discs (IVDs). The IVD forms a fibrous joint that functions as a shock absorber for the spine and allows for slight flexion. Each IVD consists of two functional domains: the inner gel-like center of the nucleus pulposus and the outer fibrous tissue of the annulus fibrosus (AF). At the interface between the IVD and the vertebral body lies the endplate, a transitional tissue of mineralized matrix surrounding hypertrophic-like chondrocytes.

The process of endochondral ossification requires the coordination of multiple signaling pathways. TGFβ/BMP signaling is essential for early cartilage and bone formation as well as postnatal growth [4, 5]. The BMP and TGFβ pathways signal via their canonical receptor phosphorylated Smads (R-Smads) [6, 7]. The TGFβ pathway signals through R-Smads 2 and 3 while the BMP pathway utilizes R-Smads 1, 5, and 8. Upon ligand binding the receptors phosphorylate and activate the R-Smads. The activated R-Smads translocate to the nucleus and form complexes with additional proteins to induce or repress target gene transcription. Both pathways also utilize the MAPK/ERK and TAK1/p38 pathways as non-canonical signaling

pathways. Misregulation of TGFβ and BMP signaling affects many aspects of skeletal development, including formation of the IVD [8], and over-activation of these pathways has been shown to cause ectopic bone formation in several tissues [9–11]. The IVD AF, as well as cartilage, ligament, and tendon tissues, are derived from progenitor pools consisting of distinct cell populations with unique expression profiles. While TGFβ and BMP signaling are critically important in musculoskeletal tissues, studies have recently shown that each of these distinct cell populations responds differently to changes in these respective signaling pathways [12].

Filamins are cytoskeletal proteins that stabilize actin filament networks and link them to the cellular membrane, thus forming a scaffold for integrating cell mechanics and signaling [13]. Filamins have also been shown to interact directly with Smads 2 and 3, as well as 1 and 5, central mediators of canonical TGFβ and BMP signaling, respectively [14, 15]. FLNB is expressed throughout the cartilage growth plate as well as in the cartilaginous condensations of developing vertebrae [16]. Biallelic loss of function mutations leading to loss of FLNB cause SCT, while heterozygosity for missense mutations in *FLNB* produces a spectrum of autosomal dominant skeletal disorders including boomerang dysplasia (OMIM 112310); Larsen syndrome (OMIM 150250); and atelosteogenesis I and III (AOI, OMIM 108720; AOIII, OMIM 108721).

In this study we used mice homozygous for a gene trapped *Flnb* allele ($Flnb^{-/-}$) [17]. We previously showed that $Flnb^{-/-}$mice phenocopy SCT and show progressive vertebral, carpal, tarsal, and sternal fusions as well as smaller overall body size, making this an ideal animal model for studying progressive vertebral fusions [17]. Mice heterozygous for the gene trap are unaffected. FLNB is expressed in the developing skeleton, throughout the growth plate, in the developing limb buds and between the neural arches of the vertebrae [17] as well as in the somites, which include the cells destined to become the vertebral bodies and IVDs of the spine. It was initially hypothesized that SCT vertebral fusions resulted from failure to segment the vertebrae properly [18, 19], but analysis of the *Flnb* knockout mouse model demonstrated that the vertebrae form normally but subsequently fuse [17]. In this study, we seek to explain how absence of FLNB produces spinal fusions, the most compelling phenotypic finding in both humans and mice. We demonstrate that in the absence of FLNB, TGFβ and BMP signaling is increased both *in vitro* and *in vivo*, demonstrating that FLNB is required for the attenuation of TGFβ/BMP signaling. We also show that the mutant AF undergoes ectopic differentiation toward a chondrogenic lineage in the IVD, leading to abnormal endochondral ossification. The phenotypic findings resemble those seen in aging disc degeneration and therefore provide a developmental model for degenerative disc disease.

Results

Absence of FLNB causes progressive fusions and abnormalities in the postnatal vertebral growth plate and IVD

In SCT patients, vertebral abnormalities are seen early in infancy, frequently presenting as scoliosis before eventually progressing to the fusion phenotype. Our previous study demonstrated initially normal formation of the IVD, but did not determine the precise time points at which ectopic ossifications and fusions occur. To investigate the spinal phenotype, $Flnb^{-/-}$and $Flnb^{+/+}$ skeletal preparations were stained with alcian blue (to stain cartilage proteoglycans) and alizarin red (to stain mineralized bone) (Fig 1). Ectopic bone formations are seen between the neural arches of the thoracic region of the spine beginning at E17.5 and progressing through P7 (Fig 1A–1C, 1A′–1C′, arrows). These formations likely represent the ossification of the interspinous ligaments. Development of thoracic vertebral fusions (T7, T8, and T9) began later, at P5, and progressed as shown in P15 vertebrae (n = 5) (Fig 1D and 1D′). Lumbar vertebrae (T13, L1, and L2) are nearly completely fused by P19 (Fig 1E and 1E′). By P21 IVDs have

completely disappeared at the thoracic and lumbar fusion sites (Fig 1F and 1F′). These observations show that the spinal phenotype is indeed progressive and begins in the thoracic area of the spine before progressing to the lumbar vertebrae.

We demonstrated FLNB expression in the AF and nucleus pulposus of E14.5 mice via X-gal staining, indicating that FLNB plays a role in the development of these tissues (S1 Fig). Histological analysis of sagittal IVD sections from P1 to P15 showed that the IVDs developed apparently normally until P1 but IVD disruptions were evident by P5 (Fig 2). Within the *Flnb*$^{-/-}$vertebral body growth plates there was an initial increase in size of the proliferative zone at P1, followed by an increased zone of hypertrophic chondrocytes at P5 and P7 (Fig 2A′–2C′) as compared with control animals (Fig 2A–2C). By P15 this increase in hypertrophy was less evident as the vertebral growth plate reached its final stage of differentiation (Fig 2E and 2E′). In addition, the vertebral body heights were significantly shorter in *Flnb*$^{-/-}$mice (S2 Fig). This was likely due to the accelerated chondrocyte differentiation observed in the growth plate that removed chondrocytes from the proliferative pool, resulting in decreased longitudinal growth. Investigation of the nucleus pulposus showed that beginning at P5, the nucleus pulposus became compressed and the disruption became more severe as the IVD aged as demonstrated in P7, P11, and P15 IVDs (Fig 2B′–2E′).

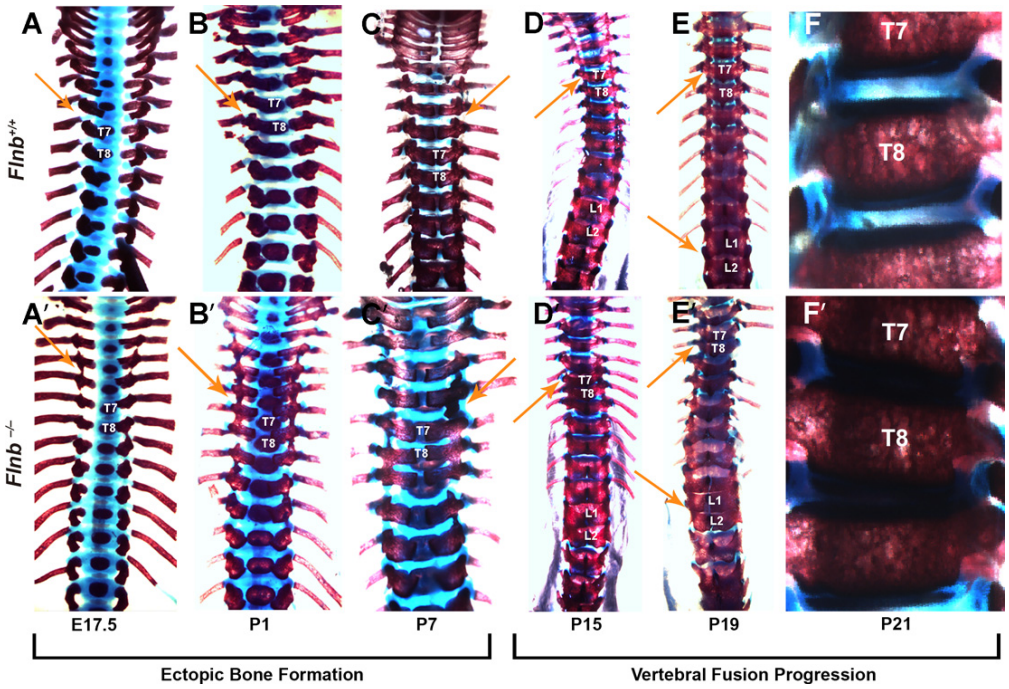

Fig 1. *Flnb*$^{-/-}$vertebrae progressively fuse in the thoracic and lumbar areas of the spine. Posterior view of mouse spines stained for cartilage proteoglycans (blue) and mineralized bone (red). (A-C, A′-C′) The *Flnb*$^{-/-}$mouse spine exhibited ectopic ossifications between the neural arches of the thoracic area (arrows). (D, D′) P15 image depicts representative vertebral fusions between thoracic vertebrae in the *Flnb*$^{-/-}$mouse spine (arrows). (E, E′) At P19, vertebral fusions and ectopic ossifications have progressed into the lumbar area (arrows). (F, F′) Anterior view. Multiple discs have disappeared and mineralized to bone in the P21 *Flnb*$^{-/-}$mouse spine. N = 3 for each timepoint.

doi:10.1371/journal.pgen.1005936.g001

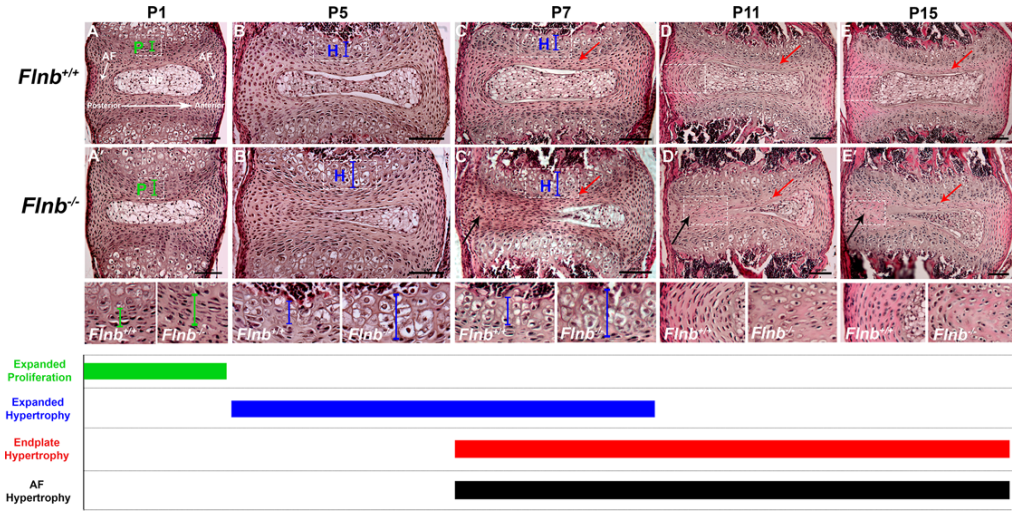

Fig 2. Absence of FLNB progressively affects vertebral growth plate and IVD tissue morphology. H&E staining of (A-E) *Flnb*$^{+/+}$ and (A′-E′) *Flnb*$^{-/-}$T7 thoracic IVDs and vertebral growth plates. Left: posterior, Right: anterior. (A, A′) *Flnb*$^{-/-}$P1 vertebral growth plates showed an enlarged proliferative zone compared with *Flnb*$^{+/+}$ (green brackets). (B, B′) *Flnb*$^{-/-}$P5 vertebral growth plates showed enlarged hypertrophic zones compared with *Flnb*$^{+/+}$ (blue brackets). (C, C′) *Flnb*$^{-/-}$P7 vertebral growth plates showed increased hypertrophic zones (blue brackets). *Flnb*$^{-/-}$P7 AF tissues exhibited rounder cell morphologies (black arrows) at the same time point as the initiation of endplate mineralization (red arrows). (D, D′, E, E′) *Flnb*$^{-/-}$P11 and P15 AF tissues exhibited similar morphology (black arrows) to the now mineralized endplate tissues (red arrows).

doi:10.1371/journal.pgen.1005936.g002

Absence of FLNB induces ectopic differentiation towards chondrogenic lineages in AF tissue

Using sagittal sections of the vertebral spine in both *Flnb*$^{+/+}$ and *Flnb*$^{-/-}$, we observed starting at P7 the cells of the AF begin to exhibit a change in morphology by becoming rounder and more hypertrophic in appearance as demonstrated in P7, P11, and P15 IVDs (Fig 2C–2E, 2C′–2E′, black arrows). These findings suggest that a process of cell transformation occurred in the AF cells of *Flnb*$^{-/-}$mouse spines rather than solely the encroachment of the existing growth plate. A closer examination of P15 IVDs in Fig 3A–3D revealed that *Flnb*$^{-/-}$mice exhibited a developing front of chondrocyte-like cells and an expanding acellular matrix that overtook the cells of the nucleus pulposus leading to a fissure (Fig 3D, asterisk). This expanding front of cells led to a narrowing of the nucleus pulposus (Fig 3D). In the posterior AF of *Flnb*$^{-/-}$IVDs, the cells became rounder, resembling the hypertrophic-like cells normally found in the cartilaginous endplate (Fig 3C, arrows).

Because hypertrophy is associated with changes in matrix composition, we examined AF matrix structure and composition [20]. Loss of polarized birefringence visualized with picrosirius red staining indicated a severe disruption of the collagen structure with the fibers becoming thinner and more irregular in the *Flnb*$^{-/-}$IVD, indicating matrix disorganization (Fig 3E–3H). Additionally, the *Flnb*$^{-/-}$mouse IVD spaces exhibited markedly increased alcian blue staining indicating greater proteoglycan content (Fig 3I and 3J, arrow). To further investigate the *Flnb*$^{-/-}$IVD matrix, we probed for specific collagen distributions and demonstrated an increase in type II collagen staining in the outer AF (Fig 3K and 3L, arrows) as well as a decrease in type I

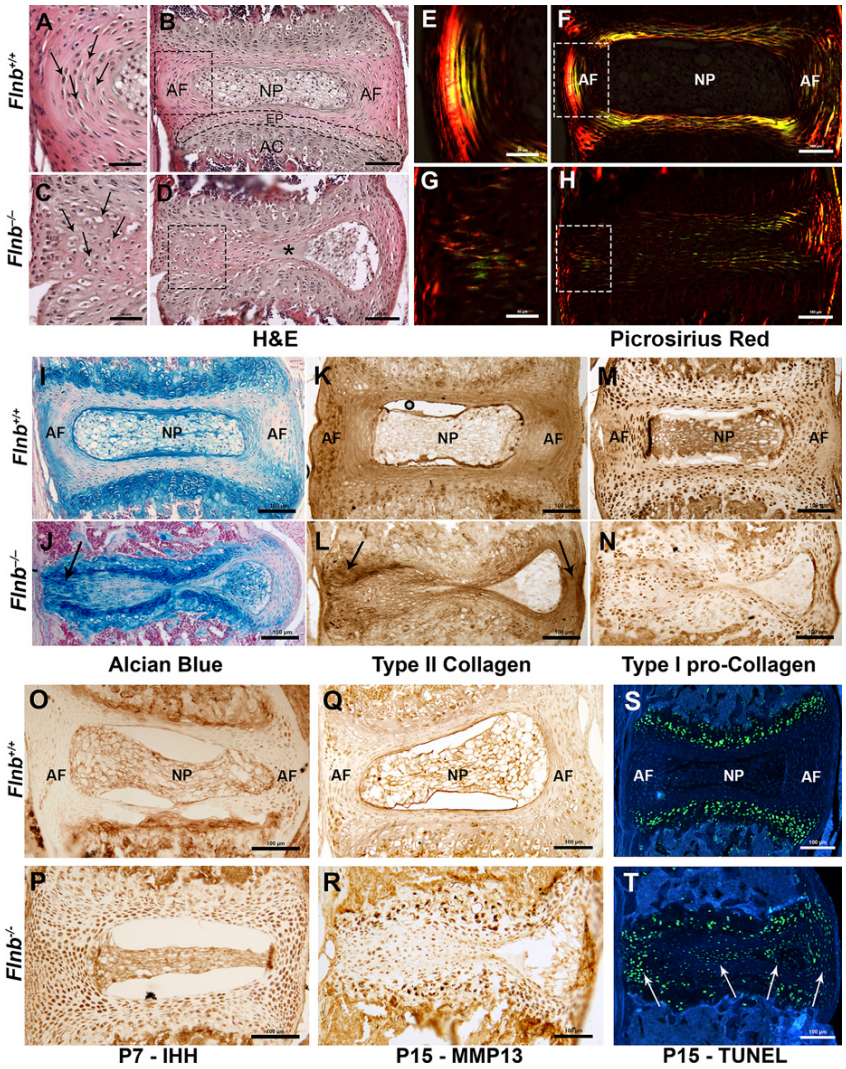

Fig 3. *Flnb*$^{-/-}$IVDs exhibit disruptions in AF cell morphology; show altered ECM and markers of enhanced chondrocyte differentiation. Left: posterior, Right: anterior. (A-D) H&E staining of P15 T7 IVDs. The IVD is composed of: NP = Nucleus Pulposus, AF = Annulus Fibrosus, EP = Endplate, AC = Articular Cartilage. (A-C) P15 *Flnb*$^{+/+}$ AF cells had a fibroblast-like appearance while *Flnb*$^{-/-}$AF cells were enlarged and exhibited more hypertrophic-like qualities (arrows). (D) The *Flnb*$^{-/-}$IVD showed a disruption of the AC hypertrophic zone as well as a fissure within the NP/AF boundary (shown by *). (E-H) Polarized imaging of picrosirius red staining of P15 mouse IVD paraffin sections. (E) *Flnb*$^{+/+}$ IVDs exhibited a distinct structure of collagen bundles forming the lamellae of the AF. (G) The *Flnb*$^{-/-}$collagenous matrix of the posterior AF lacked an organized structure. (I,J) P15 disc tissue stained with alcian blue. The posterior AF of the *Flnb*$^{-/-}$disc contained increased proteoglycan deposition compared with *Flnb*$^{+/+}$ (black arrow). (K,L) IHC against type II collagen.

Type II collagen was increased in the anterior and posterior AF of the *Flnb*$^{-/-}$IVD (black arrows). (M,N) IHC against type I pro-collagen. Pro-type I collagen protein expression was decreased throughout the AF, end-plate and nucleus pulposus of the *Flnb*$^{-/-}$IVD. (O,P) IHC against IHH in P7 T7 IVD. The *Flnb*$^{-/-}$disc contained increased IHH protein expression in the AF compared with *Flnb*$^{+/+}$. (Q,R) IHC against MMP13 in P15 T7 IVD. The *Flnb*$^{+/+}$ AF exhibited some MMP13 expression in both the posterior and anterior AF regions. MMP13 protein expression was increased throughout the AF and endplate in the absence of FLNB. (S,T) TUNEL staining of P15 T7 IVD to detect apoptotic activity. *Flnb*$^{+/+}$ discs exhibit apoptosis almost exclusively in the hypertrophic zone of the vertebral body growth plate. In *Flnb*$^{-/-}$discs, the apoptotic zone seen in *Flnb*$^{+/+}$ discs was no longer present and there was an increase in apoptotic cells visible within the posterior and anterior AF as well as the nucleus pulposus. Blue background represents auto-fluorescence and is shown for orientation only.

doi:10.1371/journal.pgen.1005936.g003

collagen staining in the AF of *Flnb*$^{-/-}$mice compared with *Flnb*$^{+/+}$ (Fig 3M and 3N). This change in the type II: type I collagen ratio, as well as an increased proteoglycan content, is indicative of a change from a fibrous to a more cartilaginous matrix.

To investigate whether there were cell fate changes in the AF cells, we examined the AF and nucleus pulposus regions of *Flnb*$^{-/-}$mouse spines for expression of the chondrocyte specific markers Indian Hedgehog (IHH) for prehypertophic chondrocytes and Matrix Metalloproteinase-13 (MMP13) for hypertrophic chondrocytes. There was an early increase in IHH expression within the AF of P7 *Flnb*$^{-/-}$IVDs (Fig 3O and 3P). We also observed a subsequent increase in MMP13 expression throughout *Flnb*$^{-/-}$P15 IVDs (Fig 3Q and 3R) compared with *Flnb*$^{+/+}$. These findings are consistent with the gradual inappropriate and premature differentiation of AF cells to a hypertrophic chondrocyte phenotype. Additionally, we carried out TUNEL staining to detect apoptotic activity characteristic of terminally differentiated hypertrophic chondrocytes (Fig 3S and 3T). Whereas in the *Flnb*$^{+/+}$ section, apoptotic activity is restricted to the hypertrophic region of the vertebral growth plate (Fig 3S), there is evidence of increased apoptotic activity in the AF as well as the nucleus pulposus of *Flnb*$^{-/-}$IVDs (Fig 3T, arrows). We also performed RNA *in situ* hybridization on frozen sagittal sections of the mouse spine at P15 using a Collagen X (*ColX*) riboprobe to detect *in vivo ColX* expression, a known specific marker of hypertrophic chondrocytes. While the *Flnb*$^{+/+}$ IVD showed *ColX* expression restricted to the hypertrophic region of the vertebral body growth plate, the *Flnb*$^{-/-}$IVD showed *ColX* expression within the AF of the collapsing IVD (Fig 4). These data confirms the transformation of fibroblastic AF cells to hypertrophic chondrocytes in *Flnb*$^{-/-}$IVDs.

Although we have shown that AF cells adopt gene expression patterns of hypertrophic chondrocytes in the *Flnb*$^{-/-}$IVDs, we further sought to determine if these findings result from transformation of AF cells as opposed to invasion by chondrocytes. Thus, we crossed *Flnb*$^{-/-}$mice with mice containing a GFP reporter driven by the *Scleraxis (Scx)* promoter. SCX expression is used as a marker for tendons, ligaments, and AF tissue, but not chondrocytes [21]. Using paraffin embedded spine sections, we stained for GFP expression in the IVD. At ages P7 and P15, the *Flnb*$^{+/+}$ IVDs showed SCX expression in the AF tissues (Fig 5A and 5B, white arrows). Importantly, SCX expression was also observed in the inappropriately transformed hypertrophic cells of *Flnb*$^{-/-}$IVDs at P7 and P15 (Fig 5A′ and 5B′, white arrows). Co-expression of SCX in cells that also express genetic markers of hypertrophic chondrocytes indicated that AF cells become hypertrophic chondrocytes. These findings show that the AF cells differentiate from a fibroblast-like cell to prehypertrophic then hypertrophic-like chondrocytes, leading to destruction of the nucleus pulposus through apoptosis.

FLNB attenuates TGFβ signaling pathway activation in the annulus fibrosus

Since FLNB has been shown to interact with Smad3, a component of canonical TGFβ signaling in cultured primary chondrocytes [15], we chose to investigate whether there are further changes in the TGFβ signaling pathway in chondrocytes and the IVD. Protein extracts from *Flnb*$^{-/-}$IVDs demonstrated increased endogenous levels of phospho-Smad3 and phospho-ERK

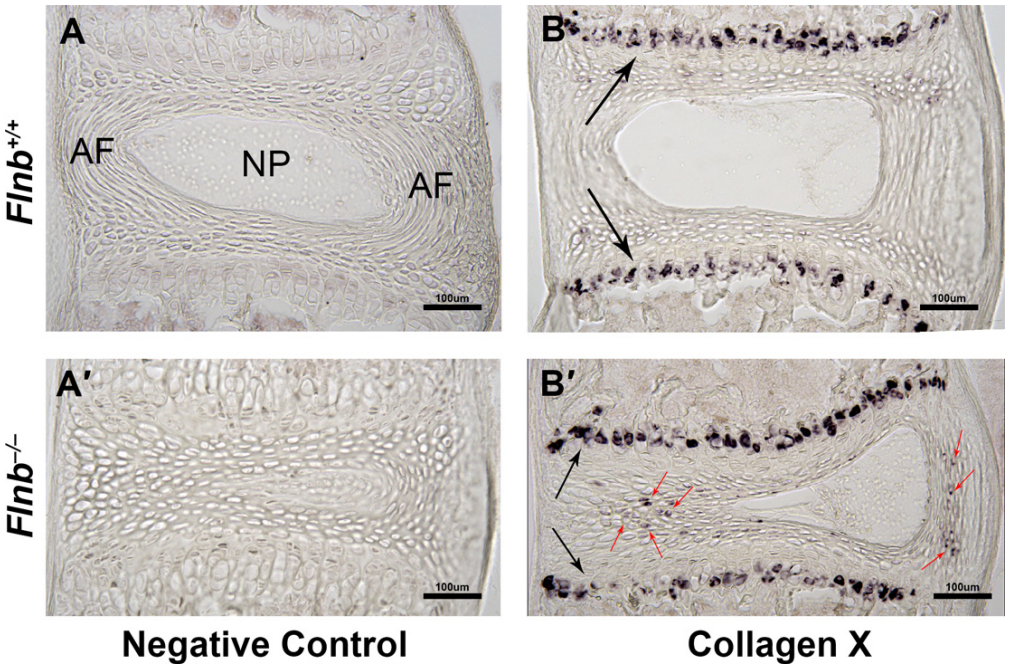

Fig 4. *Flnb*$^{-/-}$AF tissues exhibit Collagen X expression. Left: posterior, Right: anterior. (A, A′, B, B′) RNA *in situ* staining of P15 T7 IVD sagittal sections. (A, A′) *Flnb*$^{+/+}$ and *Flnb*$^{-/-}$*in situ* sections using sense riboprobe as a negative control. (B) *Flnb*$^{+/+}$ *in situ* section using antisense riboprobe against ColX. ColX expression is exhibited in the hypertrophic zone of the *Flnb*$^{+/+}$ vertebral body growth plate (black arrows) and not in the IVD. (B′) *Flnb*$^{-/-}$*in situ* section using antisense riboprobe against ColX. ColX expression is exhibited in both the vertebral body growth plate hypertrophic zone (black arrows) as well as the transformed hypertrophic *Flnb*$^{-/-}$AF cells (red arrows).

doi:10.1371/journal.pgen.1005936.g004

in the AF compared with *Flnb*$^{+/+}$ (Fig 6A). The sterna of *Flnb*$^{-/-}$mice, similar to vertebrae, also exhibit fusions [17] and sternal chondrocytes were used to further interrogate the TGFβ pathway. To determine the *in vitro* responsiveness of *Flnb*$^{-/-}$cells to TGFβ pathway activation, primary sternal chondrocytes were isolated from P1 *Flnb*$^{+/+}$ and *Flnb*$^{-/-}$mice and stimulated with TGFβ-1 ligand. In both unstimulated and stimulated *Flnb*$^{-/-}$primary chondrocytes, TGFβ signaling activity was upregulated as measured by increased phosphorylation of Smad3 (Fig 6B), as well as Smad2 (Fig 6C). Additionally, with TGFβ-1 stimulation, we found increased phospho-ERK signaling indicating a noncanonical pathway signaling response (Fig 6D) [22]. To further define the increase in TGFβ signaling activity, we quantified the *in vivo* expression of TGFβ signaling targets including *Connective Tissue Growth Factor (CTGF)* and *p21*, both of which are highly expressed in cartilage, by qPCR of RNA derived from *Flnb*$^{+/+}$ and *Flnb*$^{-/-}$P1 sternal cartilage as well as P15 IVD AF tissue [23–25]. *Flnb*$^{-/-}$sternal cartilage showed a statistically significant increase in *Ctgf* (Fig 7A) and *p21* expression (Fig 7B). We also observed statistically significant increases in both *Ctgf* (Fig 7C) and *p21* (Fig 7D) in P15 IVDs indicating that the observed increase in TGFβ signaling activation also results in increases in TGFβ target transcription *in vivo*.

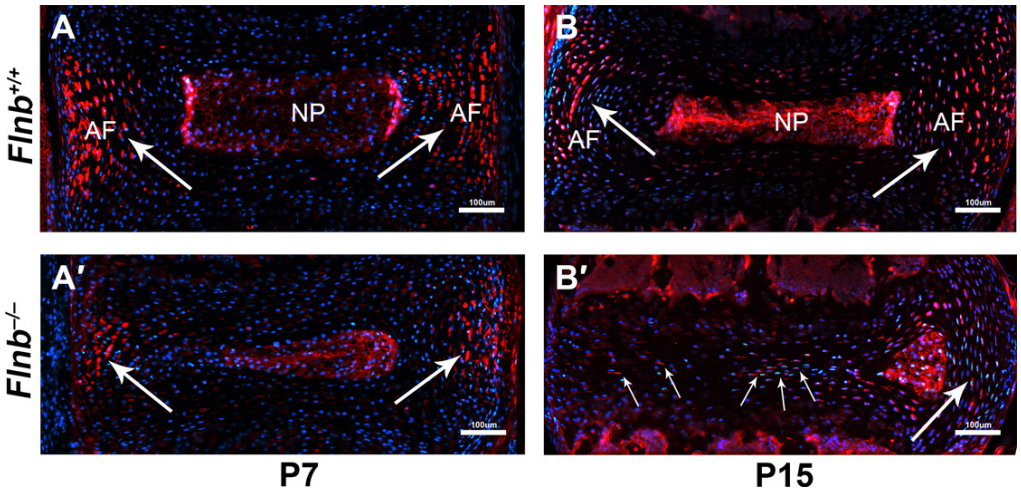

Fig 5. Transformed hypertrophic AF cells continue to express AF marker Scleraxis in *Flnb*$^{-/-}$IVDs. (A-D) IHC analysis of Scleraxis-GFP expression in P15 mouse disc tissue paraffin sections. (A,B) *Flnb*$^{+/+}$ IVDs at P7 and P15 show SCX expression in the AF tissues (white arrows). (A',B') *Flnb*$^{-/-}$IVDs at P7 and P15 exhibit continued SCX expression in the transformed hypertrophic AF cells.

doi:10.1371/journal.pgen.1005936.g005

Loss of FLNB up-regulates BMP mediated TAK1/p38 signaling in the postnatal IVD affecting homeostasis

The BMP signaling pathway is an inducer of chondrocyte differentiation. Therefore, observed ectopic ossification of IVDs seen in *Flnb*$^{-/-}$mice suggested a possible increase in BMP signaling activation. Similar to the *in vitro* TGFβ experiments, we stimulated primary sternal chondrocytes with BMP-2 ligand. Although the data indicated a trend towards increased phosphorylation of receptor Smad1,5,8, we did not see a statistically significant change in treated mutant versus *Flnb*$^{+/+}$ primary sternal chondrocytes (Fig 8A). We therefore tested whether there was an alteration in non-canonical signaling within the mutant chondrocytes. We detected a significant increase in the phosphorylation of p38 in both unstimulated and BMP-2 stimulated mutant sternal chondrocytes (Fig 8B). A previous study by Liu et al. demonstrated that increases in BMP activated TAK1/p38 result in inhibition of the MAPK/ERK pathway [26]. We therefore tested whether the increase in p-p38 in our mutant chondrocytes exhibited the same inhibitory effect. Similar to the TGFβ stimulation experiments, *Flnb*$^{-/-}$cells have increased p-ERK at baseline (Fig 8C), adding complexity to the *in vitro* analyses of p-ERK. However, although there was an endogenous increase of ERK phosphorylation levels in *Flnb*$^{-/-}$chondrocytes, these levels were no longer increased after 10 minutes and significantly decreased after 30 minutes of BMP-2 stimulation in mutant versus *Flnb*$^{+/+}$ chondrocytes (Fig 8C). Our finding supports that increased BMP-2 activation of p38 results in inhibition of ERK phosphorylation and shows non-canonical up-regulation of the BMP pathway in the absence of FLNB. The Liu et al. study also demonstrated that p38 inhibition of ERK had the ability to increase Smad1 nuclear activity and localization [26]. To determine if there was augmented pathway activation through increased p-p38 and decreased ERK, we performed a *Msx2* luciferase assay in primary sternal chondrocytes using a p-Smad1,5 reporter construct to test for

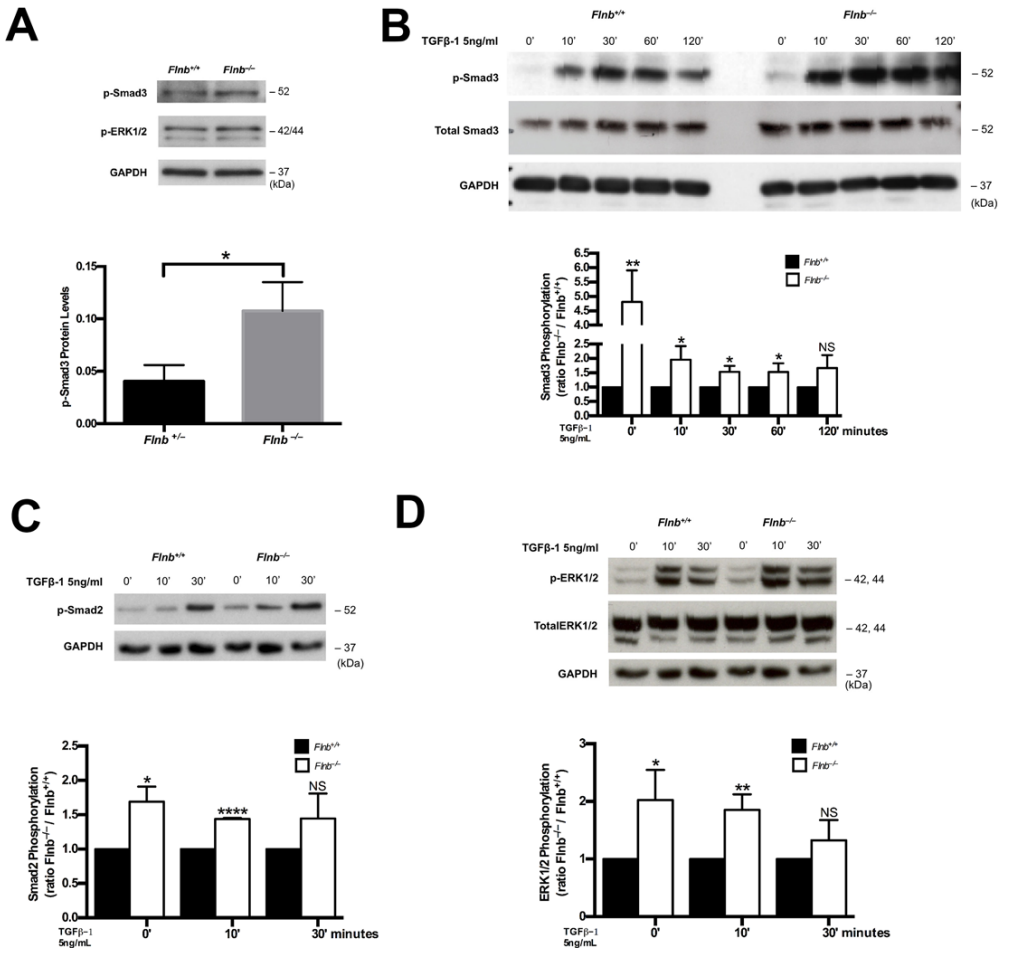

Fig 6. TGFβ signaling increased in absence of FLNB *in vitro* and *in vivo*. (A) Western blot analysis of protein lysates extracted from AF tissue of P15 pups. (B-D) Western blot analysis of protein lysates extracted from cultured primary mouse chondrocytes. (B) P-Smad3 and p-ERK levels are significantly increased both with and without TGFβ-1 (5ng/mL) stimulation in mutant cells whereas total Smad3 levels are unchanged, N = 6. (C) P-Smad2 levels are significantly increased both with and without TGFβ-1 stimulation in mutant cells, N = 6. (D) P-ERK levels are significantly increased endogenously as well as after 10 minutes of TGFβ-1 stimulation whereas total ERK levels remain unchanged, N = 6.

doi:10.1371/journal.pgen.1005936.g006

potential increased R-Smad1,5,8 nuclear activity. *Msx2* is a direct target of Smad mediated BMP signaling [27]. We observed an endogenous increase of *Msx2* transcription in $Flnb^{-/-}$ chondrocytes compared with $Flnb^{+/+}$ (Fig 8D). Further, to determine if BMP signaling pathway targets are inappropriately activated in $Flnb^{-/-}$IVDs, we interrogated by western blot analysis

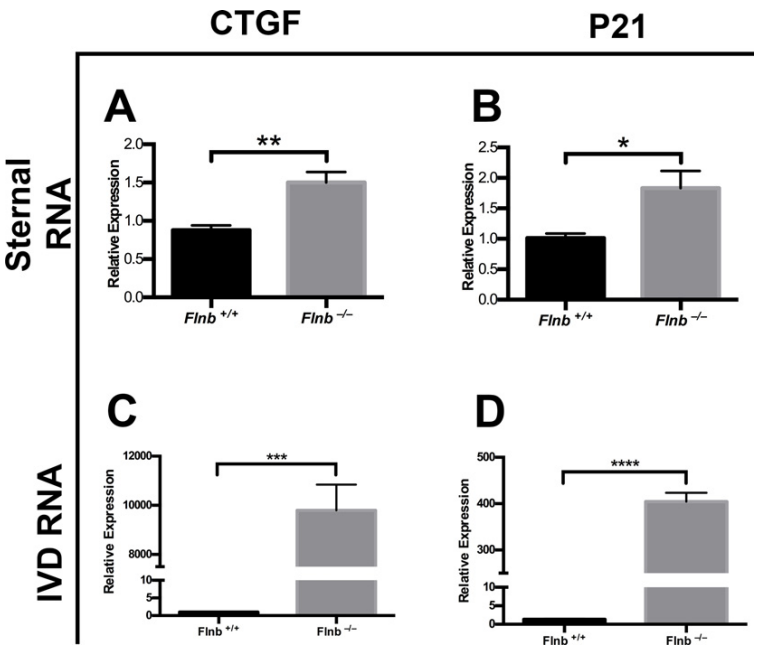

Fig 7. TGFβ nuclear target RNA expression increased in absence of FLNB *in vivo*. (A,B) RT-qPCR analysis results using RNA derived from P1 mouse sternums. The expression levels of the TGFβ nuclear targets *CTGF* and *p21*, are both significantly increased in *Flnb*$^{-/-}$mouse sternums, N = 6. * = p<0.05, ** = p<0.01, data are represented as mean ± SEM. (C,D) RT-qPCR analysis results using RNA derived from P15 mouse IVDs. The expression levels of the TGFβ nuclear targets, *CTGF* and *p21*, are significantly increased in *Flnb*$^{-/-}$mouse IVDs, N = 3. *** = p<0.001, **** = p<0.0001, NS = not significant, data are represented as mean ± SEM.

doi:10.1371/journal.pgen.1005936.g007

whole tissue IVD lysates for expression of BMP-2, a target of the pathway, as well as p-Smad1/5/8 and p-p38 levels. There was a statistically significant increase in BMP-2 expression and an increase of p-p38 in the IVDs of *Flnb*$^{-/-}$mice with no change in p-Smad1/5/8 levels (Fig 8E). Increased total BMP-2 and *Msx2* transcription are consistent with increased BMP pathway output.

We subsequently tested whether an increase in Smad1 nuclear localization can be directly visualized in the AF of *Flnb*$^{+/+}$ and *Flnb*$^{-/-}$mice. In the *Flnb*$^{+/+}$ discs, p-Smad1,5,8 proteins were found in both the cytoplasm and the nucleus of AF cells (Fig 9A–9D, arrow). However, in the *Flnb*$^{-/-}$AF, p-Smad1,5,8 predominantly demonstrated nuclear localization (Fig 9A′–9D′, arrow) with very little cytoplasmic staining. Consistent with our earlier TGFβ experiments, we demonstrated the same increased nuclear localization of p-Smad3 in *Flnb*$^{-/-}$AF cells (Fig 9E–9H, 9E′–9H′, arrows). To confirm these findings we determined nuclear versus cytoplasmic levels of p-Smad1,5,8 and p-Smad3 by western blot analysis of stimulated primary chondrocytes (Fig 9I–9L). As previously demonstrated, this data set also showed an increase in both cytoplasmic and nuclear p-Smad3 (Fig 9K and 9L). Similar to the previous BMP-2 stimulated *in vitro* experiments, total cytoplasmic p-Smad1,5,8 levels were unchanged in *Flnb*$^{+/+}$ versus mutant chondrocytes, yet the nuclear fraction showed increased Smad1,5,8 phosphorylation

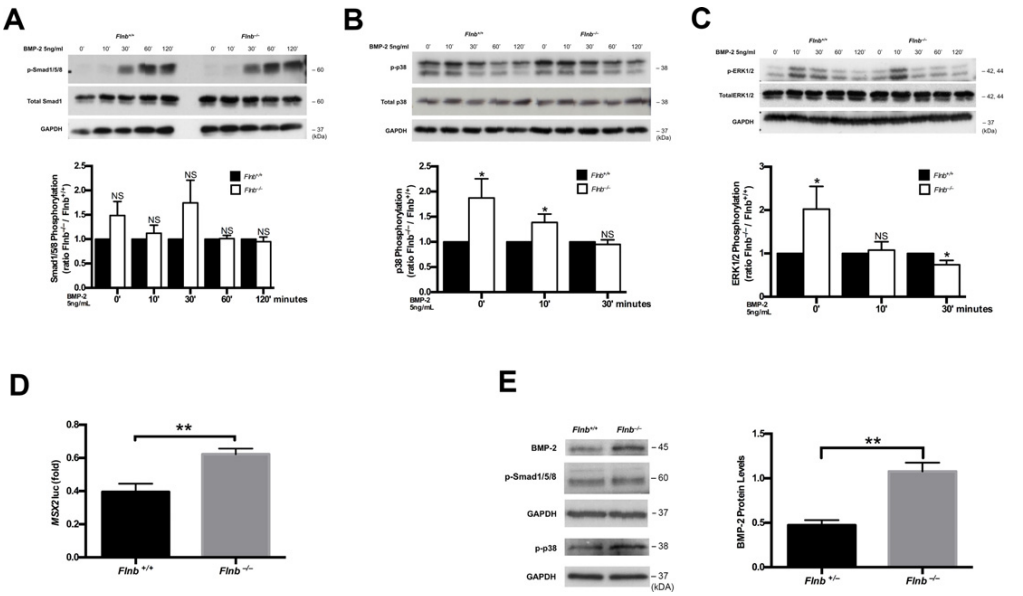

Fig 8. BMP non-canonical pathway activation is increased in the absence of FLNB *in vivo* and *in vitro*. (A-C) Western blot analysis of protein lysates extracted from cultured primary mouse chondrocytes. (A) P-Smad1,5,8 levels remain unchanged in *Flnb*$^{-/-}$when compared with *Flnb*$^{+/+}$, N = 6. (B) P-p38 levels are increased endogenously as well as upon BMP-2 (10ng/mL) stimulation in mutant versus *Flnb*$^{+/+}$ chondrocytes, N = 3. (C) p-ERK levels are upregulated endogenously but are subsequently decreased in mutant chondrocytes following 30 minutes of BMP-2 stimulation. N = 4. (D) Luciferase assay measuring *Msx2* promoter activity in primary mouse chondrocytes. *Msx2* promoter activity is increased in *Flnb*$^{-/-}$chondrocytes, N = 3. * = p<0.05, ** = p<0.01, data are represented as mean ± SEM. (E) Western blot analysis of protein lysates extracted from AF tissue of P15 pups. BMP-2 and p-p38 protein expression levels are increased in *Flnb*$^{-/-}$IVDs with no change in p-Smad1/5/8 levels, N = 7.

doi:10.1371/journal.pgen.1005936.g008

(Fig 9I and 9J). Taken together, these findings are consistent with a model in which the levels of canonical BMP signaling are not impacted by loss of *Flnb*, but the increase in non-canonical phosphorylation of p38 results in increased Smad1 nuclear activity due to the inhibition of ERK.

Discussion

Our *Flnb* knockout model shows that absence of FLNB leads to progressive fusions of the thoracic and lumbar vertebrae with patterns directly phenocopying those seen in SCT patients. We focused on the spine because it is the most severely affected region of the skeleton in both SCT patients and *Flnb*$^{-/-}$mice. Our results indicate that the spinal fusions in *Flnb*$^{-/-}$mice initiate in the thoracic vertebrae before progressing into the lumbar region. Within the *Flnb*$^{-/-}$cartilage growth plates of the vertebral body flanking the IVD space, there was an initial expansion of proliferative chondrocytes at P1, followed by an expansion of the hypertrophic zone at later stages. This change in growth plate morphology suggests that the growth plate chondrocytes undergo an accelerated differentiation cycle in the absence of FLNB, as has been seen in the growth plates of appendicular elements [28].

Further, in the posterior AF of *Flnb*$^{-/-}$IVDs, the cells are rounder and enlarged, resembling the cartilaginous cells normally found only in the endplate. The findings of altered collagen

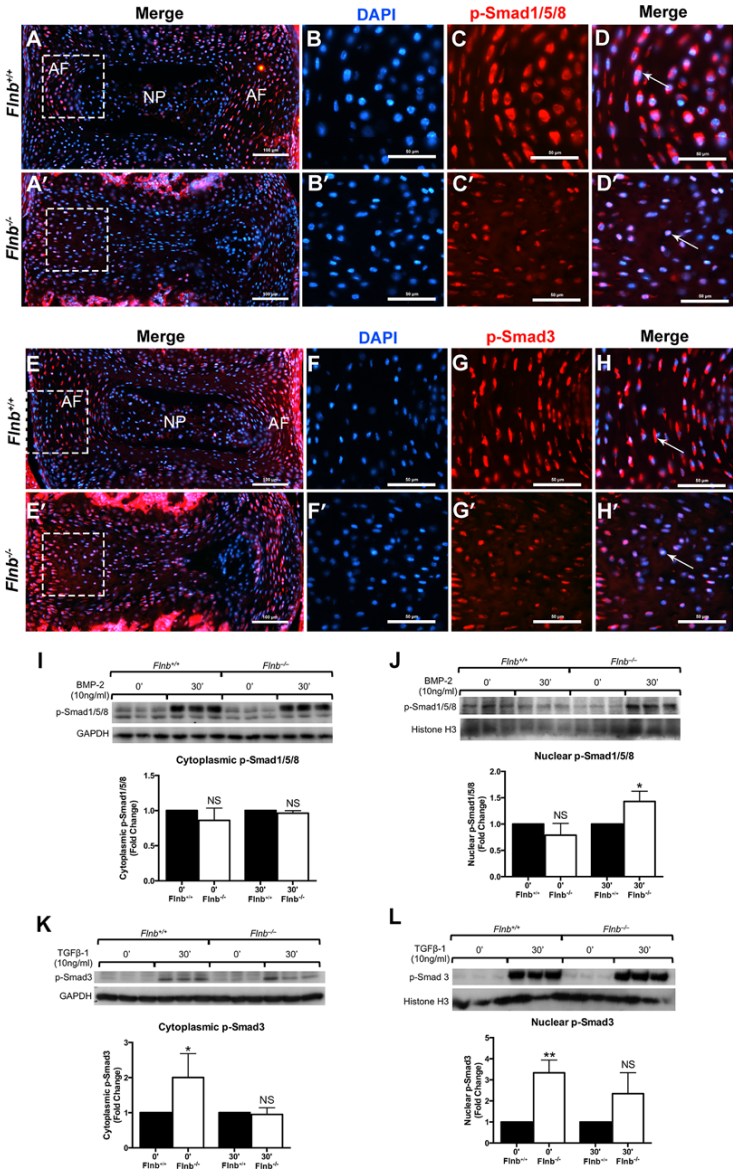
Merge
DAPI
p-Smad1/5/8
Merge
A
B
C
D
AF
NP
AF
Flnb+/+
A′
B′
C′
D′
Flnb−/−
Merge
DAPI
p-Smad3
Merge
E
F
G
H
AF
NP
AF
Flnb+/+
E′
F′
G′
H′
Flnb−/−
I
Flnb+/+
Flnb−/−
BMP-2 (10ng/ml)
0′
30′
0′
30′
p-Smad1/5/8
GAPDH
Cytoplasmic p-Smad1/5/8
Cytoplasmic p-Smad1/5/8 (Fold Change)
NS
NS
J
Flnb+/+
Flnb−/−
BMP-2 (10ng/ml)
0′
30′
0′
30′
p-Smad1/5/8
Histone H3
Nuclear p-Smad1/5/8
Nuclear p-Smad1/5/8 (Fold Change)
NS
*
K
Flnb+/+
Flnb−/−
TGFβ-1 (10ng/ml)
0′
30′
0′
30′
p-Smad3
GAPDH
Cytoplasmic p-Smad3
Cytoplasmic p-Smad3 (Fold Change)
*
NS
L
Flnb+/+
Flnb−/−
TGFβ-1 (10ng/ml)
0′
30′
0′
30′
p-Smad 3
Histone H3
Nuclear p-Smad3
Nuclear p-Smad3 (Fold Change)
**
NS

Fig 9. TGFβ and BMP pathway components exhibit nuclear localization in *Flnb*$^{-/-}$AF. IHC analysis of P15 mouse disc tissue paraffin sections. (A, A′, E, E′) Whole IVDs shown for orientation. (B, B′, F, F′) DAPI channel only showing nuclear staining. (C, C′, G, G′) Red channel only showing protein localization. (D) P-Smad1,5,8 (red) has a cytoplasmic localization in the *Flnb*$^{+/+}$ AF. (D′) P-Smad1,5,8 (red) exhibits a nuclear localization as it co-localizes with the nucleus (blue) In the AF of *Flnb*$^{-/-}$mice. (H) P-Smad3 (red) has a cytoplasmic localization in the *Flnb*$^{+/+}$ AF. (H′) P-Smad3 (red) exhibits a nuclear localization as it co-localizes with the nucleus (blue) in the AF of *Flnb*$^{-/-}$mice. (I-L) Western blot analysis of fractionated protein lysates extracted from cultured primary mouse sternal chondrocytes. (I,J) p-Smad1,5,8 levels remain unchanged in the cytoplasm but are significantly higher in the nuclei of stimulated primary chondrocytes. (K,L) p-Smad3 levels are significantly upregulated in both the cytoplasm and the nucleus without stimulation. (K,L) N = 3. NS = Not Significant, * = p<0.05, ** = p<0.01, data are represented as mean ± SEM.

doi:10.1371/journal.pgen.1005936.g009

composition and structure, along with increases in sulfated proteoglycans, type II collagen, IHH, MMP13 expression, *ColX* expression, and apoptosis are indicative of advancing chondrocyte maturation in *Flnb*$^{-/-}$AF. The transforming *Flnb*$^{-/-}$cells also continue to express the AF marker SCX, showing that the observed hypertrophic cells are inappropriately transformed AF cells. This suggests that the AF cells in the IVD of *Flnb*$^{-/-}$mice undergo an inappropriate transition from fibroblast-like to chondrocytic cells, culminating in transition to terminally differentiated chondrocytes that undergo apoptosis. Whereas MMP13 is used as a marker for late hypertrophic chondrocytes, it also plays a role in matrix degradation as it degrades collagens and cleaves aggrecan [29]. While its' inappropriate expression in the AF may be due to the changes in AF cell fate, the consequences of its expression likely results in matrix disruption and decreased ability of the IVD to absorb mechanical forces. It is likely that changing cellular characteristics and the disruption of the extracellular matrix (ECM) reduces the ability of the IVD to absorb mechanical stress, resulting in the collapse of the IVD. The final consequence of these changes is that the IVD transitions through endochondral ossification to bone, producing vertebral fusions (Fig 10). In our model, the IVD fusions progress posteriorly to anteriorly and these changes in IVD morphology are temporal with spinal fusions and disappearance of the IVD by P21.

TGFβ/BMP signaling has long been implicated in ectopic bone formation and the combination of both TGFβ and BMP up-regulation produces more ectopic bone formation than BMP up-regulation alone [30]. Our findings of increased canonical and noncanonical TGFβ signaling supports previous findings by Zheng et al. that demonstrated up-regulated TGFβ signaling through increased p-Smad3 in a different *Flnb*$^{-/-}$mouse model that also exhibited vertebral fusions [15]. Supporting our findings of enhanced TGFβ signaling activity, we showed increased *in vivo* RNA expression of the TGFβ transcriptional targets *Ctgf* and *p21*. p21 protein acts as an inhibitor of cyclin-dependent kinase CDKs 2, 3, 4, and 6 and participates in cell cycle

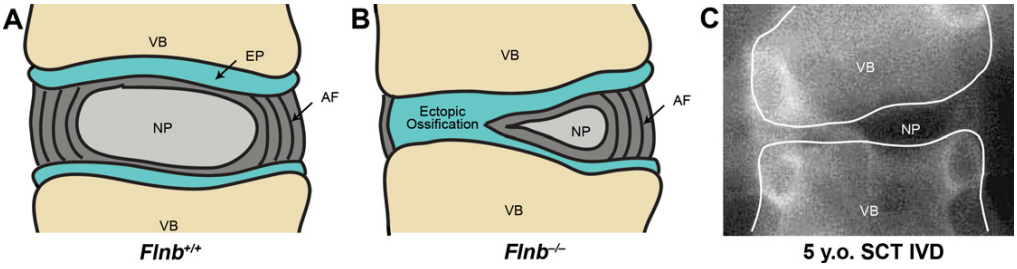

Fig 10. Illustration of tissue morphology change in *Flnb*$^{-/-}$IVD. (A) *Flnb*$^{+/+}$ IVD illustration. (B) *Flnb*$^{-/-}$IVD illustrating transition of AF to hypertrophic-like state resembling the mineralized endplate. Flanking vertebral bodies shift in position as IVD degenerates resulting in inappropriate spinal curvature. (C) IVD of 5 year old SCT patient. Positions of flanking vertebrae suggest compression of the IVD identical to those observed in *Flnb*$^{-/-}$mouse spines.

doi:10.1371/journal.pgen.1005936.g010

inhibition through the TGFβ pathway. Its up-regulation is associated with increased hypertrophic differentiation in chondrocytes [31, 32]. The premature onset of chondrocyte hypertrophy observed in the vertebral growth plates of *Flnb*$^{-/-}$mice may result from premature cell cycle exit coupled with accelerated differentiation caused by increased p21 expression. Additionally, *Hu et al*. described a decrease in CDK phosphorylation as well as enhanced chondrocyte differentiation after FLNB knockdown, which supports our data [28]. Interestingly, a study conducted by Sohn et al. elegantly demonstrated (using a knockdown model of the TGFβ receptor TGFβR2 under the control of a Col2a1cre promoter) that the consequences of loss of TGFβ signaling in the embryonic sclerotome results in disruption of IVD development [8]. This study showed that TGFβ signaling is essential to IVD embryonic development and our findings further show the importance of TGFβ signaling on postnatal IVD homeostasis.

BMP signaling has been consistently implicated as one of the primary inducers of chondrocyte differentiation. We did not observe increased p-Smad1,5,8 levels in response to BMP-2 stimulation either *in vitro* or *in vivo*. However, BMP-2 stimulation did increase BMP activated p38 phosphorylation, a component of TAK1/p38 non-canonical signaling. Further, in *Flnb*$^{-/-}$chondrocytes after BMP-2 stimulation there was diminished ERK phosphorylation at 30 minutes consistent with previous work that showed p38 functions in the inhibition of the MAPK/ERK pathway (Liu at al., 2012). This p38 induced inhibition of ERK results in increased Smad1 nuclear activity and localization [26]. Our findings of enhanced *in vitro* activation of *Msx2*, a direct target of BMP Smad mediated signaling [27] and increased nuclear localization of p-Smad1,5,8 supports that in the absence of FLNB, there is activation of the BMP pathway through the p38 and subsequent inhibition of ERK. The aforementioned *Hu et al*. study showed no change in p-ERK levels in their ATDC5 cell model. This difference may result in part from different outcomes in knockout versus knock-down models.

FLNB is expressed throughout the developing skeleton [17], yet the increase in TGFβ/BMP signaling has a profound effect specifically on the AF and the vertebrae growth plate. The vertebral body growth plate, endplate and annulus fibrosus are all derived from the same mesenchymal tissues arising in the sclerotome [33]. The morphological fate of these tissues is governed by the differential levels and ratios of pathway activation and gene expression. A recent study showed that cartilage, ligament/tendon, and IVD tissues develop from distinct progenitor pools that express Sox9, an SRY related transcription factor that is important in the regulation of cartilage development, and/or Scleraxis (Scx), a basic helix-loop-helix transcription factor highly expressed in tendons and ligaments as well as the IVD [12, 21]. Whereas tendon progenitors are mainly derived from Scx^{+}/Sox9^{-} progenitor pools, short ligaments and the IVD AF are derived from Scx^{+}/Sox9^{+} progenitor pools. Cartilage is derived from Scx^{-}/Sox9^{+} progenitor cells. An additional study showed that knockdown of BMP signaling in Scx^{+}/Sox9^{+} (ligament/IVD) expressing progenitor cells inhibits tissue development and differentiation indicating that Scx^{+}/Sox9^{+} expressing cells are more sensitive to changes in TGFβ/BMP signaling whereas Scx^{-}/Sox9^{+} and Scx^{+}/Sox9^{-} expressing progenitor cells are less sensitive [34]. In human SCT as well as our mouse model, the affected tissues include cartilage, ligaments, and the IVD. We have demonstrated FLNB expression in the developing annulus fibrosus and nucleus pulposus of E14.5 mice, implying that the absence of FLNB may have a more profound effect on these Scx^{+}/Sox9^{+}, TGFβ/BMP sensitive cell populations. In our model, the persistent up-regulation of TGFβ/BMP signaling occurring throughout postnatal development of the axial skeleton is likely to disrupt the normal molecular balance in signaling and induce a change in cell fate. These findings suggest that a crucial role of FLNB is to regulate and attenuate TGFβ/BMP signaling in these tissues in order to maintain normal morphological boundaries during postnatal tissue development.

In the postnatal IVD, it is vital that signaling and matrix integrity be maintained within the disc, and degeneration is caused by a loss of homeostasis. In aging disc degeneration, the cells of the AF go from a spindle shape to a more rounded chondrocyte-like shape [35], collagen fibers become thinner and more irregular [36], and IVDs exhibit a fissure between the nucleus pulposus and AF boundary as well as increased apoptotic activity within the nucleus pulposus and the AF [37]. An increase in MMP13 production has also been shown in degenerated discs and identified as one of the causative factors in the reorganization of the matrix due to its tendency to cleave aggrecan and collagens [29]. These morphologic and molecular findings are those seen in the IVDs of *Flnb*$^{-/-}$mice. Previous work in aging disc degeneration has shown increases in BMP and TGFβ signaling [35, 38]. Additionally, patients harboring activating Smad3 mutations exhibited increased Smad3 phosphorylation levels coupled with disc degeneration beginning as early as 12 years of age [39]. These findings further support that inappropriate and increased TGFβ and BMP signaling due to the absence of FLNB is phenotypically and molecularly similar to aging degenerating discs and suggests that our model may be useful in dissecting the molecular mechanisms underlying this common disease process.

Conclusions

In our study, we demonstrated that loss of FLNB in a mouse models produces an alteration in AF cells from a fibrous to a cartilaginous fate and disruption of the nucleus pulposus, leading to degeneration, subsequent collapse of the disc followed by fusion of the flanking vertebral bodies. This phenotype results from inappropriate up-regulation of the TGFβ canonical and BMP non-canonical pathways. Previous studies have interpreted that the observed increases in TGFβ/BMP signaling within degenerative discs occur as an effort to repair the extracellular matrix [40]. Because elevated p-Smad2 and 3 were observed in chondrocytes prior to IVD disc degeneration, our model suggests that increased TGFβ and BMP signaling as a consequence of loss of FLNB initiates the cascade of cell fate changes including differentiation, subsequent IVD degeneration and bony fusions. This study has revealed the cascade of some molecular mechanisms governing the development of vertebral fusions and postnatal disc maintenance and degeneration, providing insights which may direct studies that lead to rationale targets for therapeutic solutions.

Materials and Methods

Generation of mice

Mice used in these experiments were generated and characterized previously [17]. Briefly, The 129/Ola ES cell line (BayGenomics RRF239) contained the gene-trap vector pGT0Lxf inserted into intron 3 of *Flnb*. The gene trap contains a splice acceptor site and a β-gal Neomycin cassette causing loss of functional protein expression and production of a short fusion transcript. The cells were microinjected into C57BL/6 blastocysts and chimeras were mated with C57BL/6 mice to generate *Flnb*$^{+/-}$mice. The mice used in this study were maintained on a mixed genetic background. *Scx/GFP-Cre* mice were a generous gift from the Ronen Schweitzer laboratory.

Histological analyses and immunohistochemistry

Tissues were fixed in 10% neutral buffered formalin, decalcified using Immunocal decalcification solution and then paraffin embedded. Paraffin blocks were sectioned sagitally at 5–10 μm, and stained with Alcian Blue/Nuclear Fast Red, Hematoxylin/Eosin, and Picrosirius Red. Additional paraffin sections were stained for apoptotic activity using the In Situ Cell Death Detection Kit, Fluorescein (Roche). Sections used for staining were taken from the middle of the

spine and each staining and IHC protocol was repeated with at least three biological replicates and three technical replicates for each biological replicate. Whole skeletal preparations were prepared and stained with Alcian Blue and Alizarin Red as previously described [41].

Staining protocols: For Alcian Blue/Nuclear Fast Red staining, deparaffinized and rehydrated sections were incubated in 3% acetic acid solution and subsequently stained in 10% Alcian Blue (Sigma, A5268)/3% Acetic Acid solution. This was followed by counter staining in a 0.1% Nuclear Fast Red (Sigma, N8002)/5% Aluminum Sulfate (Sigma, A7523) solution. For Hematoxylin/Eosin staining, deparaffinized and rehydrated sections were stained with Hematoxylin QS (Vector H-3404), rinsed in tap water and then destained in 0.5% Acid EtOH. Sections were then counterstained with a 0.1% Eosin Y (Sigma E4009)/90% EtOH/0.5% Glacial Acetic Acid solution. For Picrosirius Red staining, deparaffinized and rehydrated sections were stained in a 0.1% Direct Red 80 (Sigma, 43665)/Saturated Picric Acid (Sigma, P6744) solution followed by counterstaining Hematoxylin QS. Additional paraffin sections were stained for apoptotic activity using the In Situ Cell Death Detection Kit, Flourescein (Roche, 11684795910).

For immunohistochemistry, paraffin sections were boiled for 20 minutes in Antigen Unmasking Solution (Vector) and subsequently stained using a Rabbit Specific HRP/DAB (ABC) Detection IHC Kit (Abcam). Beta-galactosidase staining was carried out on 10 mm thick frozen sections following fixation in 10% PBF for two minutes and three washes in 1x PBS. Sections were stained for beta-gal activity using X-gal in the staining solution (5 mM K3Fe(CN)6,5 mM K4Fe(CN)6, 2 mM MgCl2, 1 mg/mL X-gal made in 1x PBS) at 37°C overnight. After washing twice in PBS the slides were counterstained with nuclear fast red (N3020, Sigma) and mounted. All experiments were performed with at least three biological replicates and four sections per replicate.

Primary Antibodies used for IHC: Phospho-Smad3 (Cell Signaling, cs 9520, 1:50), Phospho-Smad1/5/8 (Cell Signaling, cs 9511, 1:25), Collagen II (Abcam, 34712, 1:50), Pro-Collagen I (Santa Cruz, 8787, 1:50), MMP13 (Abcam, 39012, 1:25), Indian Hedgehog (Abcam, 39634, 1:50), and GFP (Abcam, ab290, 1:100).

RNA *in situ* hybridization

P15 mouse spines were dissected, immediately placed in 4% paraformaldehyde, and rotated at 4°C for three days. Tissue was washed in PBS at 4°C for thirty minutes, then transferred to 0.48M EDTA DEPC treated pH 7.4 decalcification solution and rotated at 4°C for three days. Samples were checked via X-ray for proper decalcification and, if necessary, decalcification solution was replaced and samples were rotated for an additional day. Samples were transferred to 30% sucrose/PBS solution and rotated at 4°C overnight. Samples were finally embedded in OCT compound.

Riboprobes were generated using the DIG RNA labeling kit (Roche, 111750259100). Probes were purified using an RNEasy mini kit (Qiagen, 74104). 16 μm sagittal spine sections were collected on slides and fixed for 10 minutes in 4% formaldehyde in PBS. All steps were performed at room temperature unless otherwise noted. Sections were washed 3×3 minutes in PBS, immersed in 0.2M HCl for 10 minutes, washed 2×5 minutes in PBS, immersed in Proteinase K buffer for 10 minutes (40ug/mL proteinase K, 6.25mM EDTA in 0.05M Tris, pH 7.5), washed 2×5 minutes in PBS, immersed in 4% paraformaldehyde for 20 minutes, washed 2×5 minutes in PBS, immersed in Acetic Anhydride buffer for 10 minutes (0.1M triethanolamine pH8.0 + 1/400 acetic anhydride), washed 5 minutes in PBS, washed with 2x SSC for 5 minutes, dehydrated, then incubated with hybridization buffer for at least 5 mins (50% formamide, 5x SSC, 5x Denhardt's solution, 0.25 mg/mL baker's yeast RNA, 0.5 mg/mL single stranded fish sperm

DNA). DIG labeled probes were diluted to 1–4 ug/ml in hybridization buffer and applied to sections, which were then covered with plastic coverslips and incubated in a humidified chamber containing 50% formamide/5x SSC for 18–20 hours at 52°C. Sections were washed in 35% Formamide/5X SSC/0.1% Tween-20 for 15 minutes at 52°C 3 times, then washed in 50% Formamide/2X SSC at 52°C for 15 minutes 3 times, then washed in Maleic Acid Buffer (0.1M Maleic Acid, 0.15M NaCl, pH 7.5) + 1% Tween-20 (MABT) 10 minutes at room temperature 2 times, then blocked in 1X MABT + 10% goat serum + 2% BMB (blocking agent, Roche) for 1 to 4 hours. Sections were incubated with 1:2500 anti-DIG AB-Alkaline phosphatase ALP conjugated antibody for DIG (Roche) in 1X MABT + 2% goat serum + 1% BMB overnight at 4°C in a humidified chamber.

Sections were washed with MABT 15 minutes 4-5X + levamisole (0.048g/100mL), then washed with Detection buffer (0.1M Tris-HCl, 0.1M NaCl pH 9.5) + 0.1% TWEEN for 10 minutes 3 times, then slides were immersed in Color Reaction reagent (300ul NBT/BCIP (Roche, cat# 11175041910) in 15mL Detection buffer) and left in the dark at room temperature until color appears. Sections were washed in PBS for 5 minutes, washed in water for 5 minutes, and mounted with Hydro-Matrix.

Cell culture and tissue extraction

Mouse primary chondrocytes were extracted from the ribcages of P1 mice. Ribcages were digested in 1mg/ml Type II Collagenase (Life Technologies)/serum free DMEM solution (GIBCO) for two hours in a 37°C/5% CO_2 incubator. The liberated cells were subsequently filtered through a 40um sterile cell strainer and plated in DMEM + 10% FBS (GIBCO). Primary chondrocytes were stimulated at multiple time points using recombinant human TGFβ-1 (R&D, 10ng/ml) ligand and then lysed in RIPA buffer. Six biological replicates were performed for stimulation experiments. Cytoplasmic and nuclear fractions were isolated using the Subcellular Protein Fractionation Kit for Cultured Cells (Thermo Scientific). Three biological replicates were performed for stimulated cell fractionation experiments.

IVD discs were dissected from P15 mouse spines in PBS using a dissecting microscope. IVDs were placed in DMEM + 10% FBS (GIBCO) until dissections were complete. Discs were then washed with PBS, transferred to a 15mL conical tube containing a 10mL solution of DMEM + 0.03% Type II Collagenase (Life Technologies) and incubated overnight in a 37°C/5% CO_2 incubator. The next day, the Collagenase was neutralized with DMEM +10% FBS, the cells collected by centrifugation at 1,000 rpm for 7 minutes, washed with PBS and the solution was passed through a 40um filter to removed larger particulates. For protein lysates, after centrifugation again at 1,000 rpm for 7 minutes, the resulting cell pellet was resuspended in RIPA buffer supplemented with phosphatase inhibitors (Sigma, P0044) and protease inhibitors (Sigma, P8340). We used discs T5 through T11 for protein analysis.

Western blot analysis

Stimulated primary chondrocytes were rinsed with phosphate buffered saline. The monolayer cells in each well were lysed in RIPA buffer supplemented with phosphatase inhibitors (Sigma, P0044) and protease inhibitors (Sigma, P8340). Both AF tissue and primary chondrocyte lysates were incubated at 4°C for 30 minutes and centrifuged for 10 minutes at 10,000 rpm. The protein concentration was determined using a BCA protein assay, and equivalent amounts of protein (20 μg) were separated by electrophoresis on 10% SDS-polyacrylamide gels and transferred onto polyvinylidene fluoride membranes. After blocking for 1 hour with 5% milk in Tris-buffered saline-Tween (TBST), membranes were incubated with primary antibodies in 3% BSA/TBST solution at 4°C with gentle shaking overnight. Membranes were incubated with

horseradish peroxidase-conjugated secondary antibody at a concentration of 1:2000 at room temperature for 1 hour and detected using an ECL plus kit (Cell signaling, 7071). The band intensities were demonstrated to be in the linear range and their intensities were captured using a digital image scanner, quantified using imageJ (NIH, Bethesda, MD) and the data subjected to statistical analysis.

Primary Antibodies used for Western Blots: Phospho-Smad3 (Cell Signaling, cs 9520, 1:1000), Smad3 (Cell Signaling 9523, 1:1000), Phospho-Smad1/5/8 (Cell Signaling, cs 9511, 1:1000), Smad1 (Cell Signaling, 9743, 1:1000), Phospho-Erk p44/42 MAPK (Cell Signaling, cs 9101, 1:1000), Erk p44/42 MAPK (Cell Signaling 9102, 1:1000), Phospho-p38 (Cell signaling, cs 9211, 1:1000), Beta-Actin (Cell Signaling, cs 4967, 1:1000), BMP2 (Abcam, ab 141933, 1:750), GAPDH (Cell Signaling, cs 2118, 1:1000), and Histone-H3 (Abcam, 1:1000).

Each primary chondrocyte cell experiment was repeated with at least 6 biological replicates. $Flnb^{+/+}$ and $Flnb^{-/-}$IVD protein lysates were derived from three pooled IVD tissue samples each containing six IVDs from each of three mice. Quantified bands were normalized to housekeeping gene levels (GAPDH). Because western blots for each biological replicate were performed separately, $Flnb^{-/-}$samples were analyzed as ratios against $Flnb^{+/+}$ samples, $Flnb^{+/+}$ samples were at a value of 1. Data were analyzed by Student's T-test; the results are shown as the mean ± standard error of a given number of trials (n) as noted in the Fig legend. $P \leq 0.05$ was considered statistically significant.

RT-qPCR

RNA was extracted from isolated mouse sternal tissue and IVD AF tissue using TRIzol reagent (Life Technologies). cDNA was prepared from 1 ug of RNA using RevertAid First strand cDNA synthesis kit (Thermo Scientific) and amplified using Maxima SYBR Green/ROX qPCR Master Mix. Expression levels were calculated using the 2^deltaCT-method of analysis against the stable housekeeping gene beta-2-microglubulin (B2M) [42]. Significance was determined via Student's T-test. Biological replicates were performed six times each for sternal tissue and three times each for AF tissue with three technical replicates.

Primer Sequences: B2M (Forward) tggtgcttgtctcactgacc; (Reverse) tatgttcggcttcccattct, CTGF (Forward) CTGCTATGGGCCAGGACT; (Reverse) CGTCACACACCCACTCCTC; MMP13 (Forward) GGA CAA GCA GTT CCA AAG GC; (Reverse) CTTCATCGCCTGGAC CATAAAG; p21 (Forward) CGGTGGAACTTTGACTTCGT; (Reverse) CACACAGAGTGA GGGCTAAGG.

Ethics statement

UCLA institutional animal care and use committee (IACUC) Approval Number 2010-082-13C. Animals underwent euthanasia with isoflurane and then cervical dislocations as approved by the institutional review board.

Supporting Information

S1 Fig. FLNB is expressed in the developing IVD. Distribution of FLNB in the E14.5 mouse IVD. (A) FLNB expression (blue stain) in a sagittal spinal section of E14.5 embryos. FLNB is expressed in the early developing annulus fibrosus (white arrows), nucleus pulposus (red arrow), and strongly in the developing vertebral body tissues (VBC). (B) Negative control for the X-gal stain of an E14.5 mouse sagittal section. Nuclei are stained red, VBC = Vertebral Body Cartilage.
(TIF)

S2 Fig. *Flnb*$^{-/-}$vertebral bodies exhibit decreased height. Cleared P15 vertebral bodies stained stained for cartilage proteoglycans (blue) and mineralized bone (red). *Flnb*$^{-/-}$vertebral bodies exhibit decreased height when compared with *Flnb*$^{+/+}$. N = 3, ** = $p<0.01$.
(TIF)

S3 Fig. Negative and IgG controls for immunohistochemistry. Left: posterior, Right: anterior. (A, A′) Negative control IHC in P15 T7 IVD. (B, B′) IHC using rabbit whole IgG. (C, C′) IHC using goat whole IgG.
(TIF)

Author Contributions

Conceived and designed the experiments: DK JZ AEM KML DHC. Performed the experiments: JZ KNF JSK ID DR AEM AS. Analyzed the data: JZ AEM DK KML. Contributed reagents/materials/analysis tools: DK KML. Wrote the paper: DK JZ KML AEM DHC.

References

1. Krakow D, Rimoin DL. The skeletal dysplasias. Genetics in medicine: official journal of the American College of Medical Genetics. 2010; 12(6):327–41. doi: 10.1097/GIM.0b013e3181daae9b PMID: 20556869.
2. Mitter D, Krakow D, Farrington-Rock C, Meinecke P. Expanded clinical spectrum of spondylocarpotarsal synostosis syndrome and possible manifestation in a heterozygous father. American journal of medical genetics Part A. 2008; 146A(6):779–83. doi: 10.1002/ajmg.a.32230 PMID: 18257094.
3. Al Kaissi A, Ghachem MB, Nassib N, Ben Chehida F, Kozlowski K. Spondylocarpotarsal synostosis syndrome (with a posterior midline unsegmented bar). Skeletal radiology. 2005; 34(6):364–6. doi: 10.1007/s00256-004-0869-4 PMID: 15891931.
4. Lories RJ, Luyten FP. Bone morphogenetic protein signaling in joint homeostasis and disease. Cytokine & growth factor reviews. 2005; 16(3):287–98. doi: 10.1016/j.cytogfr.2005.02.009 PMID: 15993360.
5. Yang X, Chen L, Xu X, Li C, Huang C, Deng CX. TGF-beta/Smad3 signals repress chondrocyte hypertrophic differentiation and are required for maintaining articular cartilage. The Journal of cell biology. 2001; 153(1):35–46. PMID: 11285272; PubMed Central PMCID: PMC2185521.
6. Shi Y, Massague J. Mechanisms of TGF-beta signaling from cell membrane to the nucleus. Cell. 2003; 113(6):685–700. PMID: 12809600.
7. Miyazono K, Kusanagi K, Inoue H. Divergence and convergence of TGF-beta/BMP signaling. Journal of cellular physiology. 2001; 187(3):265–76. doi: 10.1002/jcp.1080 PMID: 11319750.
8. Sohn P, Cox M, Chen D, Serra R. Molecular profiling of the developing mouse axial skeleton: a role for Tgfbr2 in the development of the intervertebral disc. BMC developmental biology. 2010; 10:29. doi: 10.1186/1471-213X-10-29 PMID: 20214815; PubMed Central PMCID: PMC2848151.
9. Harradine KA, Akhurst RJ. Mutations of TGFbeta signaling molecules in human disease. Annals of medicine. 2006; 38(6):403–14. doi: 10.1080/07853890600919911 PMID: 17008304.
10. Li J, Yoon ST, Hutton WC. Effect of bone morphogenetic protein-2 (BMP-2) on matrix production, other BMPs, and BMP receptors in rat intervertebral disc cells. Journal of spinal disorders & techniques. 2004; 17(5):423–8. PMID: 15385883.
11. Wang EA, Rosen V, D'Alessandro JS, Bauduy M, Cordes P, Harada T, et al. Recombinant human bone morphogenetic protein induces bone formation. Proceedings of the National Academy of Sciences of the United States of America. 1990; 87(6):2220–4. PMID: 2315314; PubMed Central PMCID: PMC53658.
12. Sugimoto Y, Takimoto A, Akiyama H, Kist R, Scherer G, Nakamura T, et al. Scx+/Sox9+ progenitors contribute to the establishment of the junction between cartilage and tendon/ligament. Development. 2013; 140(11):2280–8. doi: 10.1242/dev.096354 PMID: 23615282.
13. Stossel TP, Condeelis J, Cooley L, Hartwig JH, Noegel A, Schleicher M, et al. Filamins as integrators of cell mechanics and signalling. Nature reviews Molecular cell biology. 2001; 2(2):138–45. doi: 10.1038/35052082 PMID: 11252955.

14. Sasaki A, Masuda Y, Ohta Y, Ikeda K, Watanabe K. Filamin associates with Smads and regulates transforming growth factor-beta signaling. The Journal of biological chemistry. 2001; 276(21):17871–7. doi: 10.1074/jbc.M008422200 PMID: 11278410.

15. Zheng L, Baek HJ, Karsenty G, Justice MJ. Filamin B represses chondrocyte hypertrophy in a Runx2/Smad3-dependent manner. The Journal of cell biology. 2007; 178(1):121–8. doi: 10.1083/jcb.200703113 PMID: 17606870; PubMed Central PMCID: PMC2064428.

16. Krakow D, Robertson SP, King LM, Morgan T, Sebald ET, Bertolotto C, et al. Mutations in the gene encoding filamin B disrupt vertebral segmentation, joint formation and skeletogenesis. Nature genetics. 2004; 36(4):405–10. doi: 10.1038/ng1319 PMID: 14991055.

17. Farrington-Rock C, Kirilova V, Dillard-Telm L, Borowsky AD, Chalk S, Rock MJ, et al. Disruption of the Flnb gene in mice phenocopies the human disease spondylocarpotarsal synostosis syndrome. Human molecular genetics. 2008; 17(5):631–41. doi: 10.1093/hmg/ddm188 PMID: 17635842; PubMed Central PMCID: PMC2680151.

18. Langer LO Jr., Gorlin RJ, Donnai D, Hamel BC, Clericuzio C. Spondylocarpotarsal synostosis syndrome (with or without unilateral unsegmented bar). American journal of medical genetics. 1994; 51 (1):1–8. doi: 10.1002/ajmg.1320510102 PMID: 8030662.

19. Seaver LH, Boyd E. Spondylocarpotarsal synostosis syndrome and cervical instability. American journal of medical genetics. 2000; 91(5):340–4. PMID: 10766994.

20. Dahia CL, Mahoney EJ, Durrani AA, Wylie C. Postnatal growth, differentiation, and aging of the mouse intervertebral disc. Spine. 2009; 34(5):447–55. doi: 10.1097/BRS.0b013e3181990c64 PMID: 19247165.

21. Pryce BA, Brent AE, Murchison ND, Tabin CJ, Schweitzer R. Generation of transgenic tendon reporters, ScxGFP and ScxAP, using regulatory elements of the scleraxis gene. Developmental dynamics: an official publication of the American Association of Anatomists. 2007; 236(6):1677–82. doi: 10.1002/dvdy.21179 PMID: 17497702.

22. Lee MK, Pardoux C, Hall MC, Lee PS, Warburton D, Qing J, et al. TGF-beta activates Erk MAP kinase signalling through direct phosphorylation of ShcA. The EMBO journal. 2007; 26(17):3957–67. doi: 10.1038/sj.emboj.7601818 PMID: 17673906; PubMed Central PMCID: PMC1994119.

23. Ivkovic S, Yoon BS, Popoff SN, Safadi FF, Libuda DE, Stephenson RC, et al. Connective tissue growth factor coordinates chondrogenesis and angiogenesis during skeletal development. Development. 2003; 130(12):2779–91. PMID: 12736220; PubMed Central PMCID: PMC3360973.

24. Leivonen SK, Hakkinen L, Liu D, Kahari VM. Smad3 and extracellular signal-regulated kinase 1/2 coordinately mediate transforming growth factor-beta-induced expression of connective tissue growth factor in human fibroblasts. The Journal of investigative dermatology. 2005; 124(6):1162–9. doi: 10.1111/j.0022-202X.2005.23750.x PMID: 15955090.

25. Pardali K, Kowanetz M, Heldin CH, Moustakas A. Smad pathway-specific transcriptional regulation of the cell cycle inhibitor p21(WAF1/Cip1). Journal of cellular physiology. 2005; 204(1):260–72. doi: 10.1002/jcp.20304 PMID: 15690394.

26. Liu C, Goswami M, Talley J, Chesser-Martinez PL, Lou CH, Sater AK. TAK1 promotes BMP4/Smad1 signaling via inhibition of erk MAPK: a new link in the FGF/BMP regulatory network. Differentiation; research in biological diversity. 2012; 83(4):210–9. doi: 10.1016/j.diff.2011.12.007 PMID: 22387344.

27. Brugger SM, Merrill AE, Torres-Vazquez J, Wu N, Ting MC, Cho JY, et al. A phylogenetically conserved cis-regulatory module in the Msx2 promoter is sufficient for BMP-dependent transcription in murine and Drosophila embryos. Development. 2004; 131(20):5153–65. doi: 10.1242/dev.01390 PMID: 15459107.

28. Hu J, Lu J, Lian G, Zhang J, Hecht JL, Sheen VL. Filamin B regulates chondrocyte proliferation and differentiation through Cdk1 signaling. PloS one. 2014; 9(2):e89352. doi: 10.1371/journal.pone.0089352 PMID: 24551245; PubMed Central PMCID: PMC3925234.

29. Stickens D, Behonick DJ, Ortega N, Heyer B, Hartenstein B, Yu Y, et al. Altered endochondral bone development in matrix metalloproteinase 13-deficient mice. Development. 2004; 131(23):5883–95. doi: 10.1242/dev.01461 PMID: 15539485; PubMed Central PMCID: PMC2771178.

30. Tachi K, Takami M, Sato H, Mochizuki A, Zhao B, Miyamoto Y, et al. Enhancement of bone morphogenetic protein-2-induced ectopic bone formation by transforming growth factor-beta1. Tissue engineering Part A. 2011; 17(5–6):597–606. doi: 10.1089/ten.TEA.2010.0094 PMID: 20874259.

31. Harper JW, Elledge SJ, Keyomarsi K, Dynlacht B, Tsai LH, Zhang P, et al. Inhibition of cyclin-dependent kinases by p21. Molecular biology of the cell. 1995; 6(4):387–400. PMID: 7626805; PubMed Central PMCID: PMC301199.

32. Stewart MC, Farnum CE, MacLeod JN. Expression of p21CIP1/WAF1 in chondrocytes. Calcified tissue international. 1997; 61(3):199–204. PMID: 9262510.

33. O'Rahilly R, Müller F. Human embryology & teratology. 3rd ed. New York: Wiley-Liss; 2001. xii, 505 p. p.

34. Blitz E, Viukov S, Sharir A, Shwartz Y, Galloway JL, Pryce BA, et al. Bone ridge patterning during musculoskeletal assembly is mediated through SCX regulation of Bmp4 at the tendon-skeleton junction. Developmental cell. 2009; 17(6):861–73. doi: 10.1016/j.devcel.2009.10.010 PMID: 20059955; PubMed Central PMCID: PMC3164485.

35. Tolonen J, Gronblad M, Vanharanta H, Virri J, Guyer RD, Rytomaa T, et al. Growth factor expression in degenerated intervertebral disc tissue. An immunohistochemical analysis of transforming growth factor beta, fibroblast growth factor and platelet-derived growth factor. European spine journal: official publication of the European Spine Society, the European Spinal Deformity Society, and the European Section of the Cervical Spine Research Society. 2006; 15(5):588–96. doi: 10.1007/s00586-005-0930-6 PMID: 15980999; PubMed Central PMCID: PMC3489346.

36. Colombier P, Clouet J, Hamel O, Lescaudron L, Guicheux J. The lumbar intervertebral disc: from embryonic development to degeneration. Joint, bone, spine: revue du rhumatisme. 2014; 81(2):125–9. doi: 10.1016/j.jbspin.2013.07.012 PMID: 23932724.

37. Smith LJ, Nerurkar NL, Choi KS, Harfe BD, Elliott DM. Degeneration and regeneration of the intervertebral disc: lessons from development. Disease models & mechanisms. 2011; 4(1):31–41. doi: 10.1242/dmm.006403 PMID: 21123625; PubMed Central PMCID: PMC3008962.

38. Clouet J, Pot-Vaucel M, Grimandi G, Masson M, Lesoeur J, Fellah BH, et al. Characterization of the age-dependent intervertebral disc changes in rabbit by correlation between MRI, histology and gene expression. BMC musculoskeletal disorders. 2011; 12:147. doi: 10.1186/1471-2474-12-147 PMID: 21726455; PubMed Central PMCID: PMC3150337.

39. van de Laar IM, Oldenburg RA, Pals G, Roos-Hesselink JW, de Graaf BM, Verhagen JM, et al. Mutations in SMAD3 cause a syndromic form of aortic aneurysms and dissections with early-onset osteoarthritis. Nature genetics. 2011; 43(2):121–6. doi: 10.1038/ng.744 PMID: 21217753.

40. Hadjipavlou AG, Tzermiadianos MN, Bogduk N, Zindrick MR. The pathophysiology of disc degeneration: a critical review. The Journal of bone and joint surgery British volume. 2008; 90(10):1261–70. doi: 10.1302/0301-620X.90B10.20910 PMID: 18827232.

41. McLeod MJ. Differential staining of cartilage and bone in whole mouse fetuses by alcian blue and alizarin red S. Teratology. 1980; 22(3):299–301. doi: 10.1002/tera.1420220306 PMID: 6165088.

42. Meller M, Vadachkoria S, Luthy DA, Williams MA. Evaluation of housekeeping genes in placental comparative expression studies. Placenta. 2005; 26(8–9):601–7. doi: 10.1016/j.placenta.2004.09.009 PMID: 16085039.

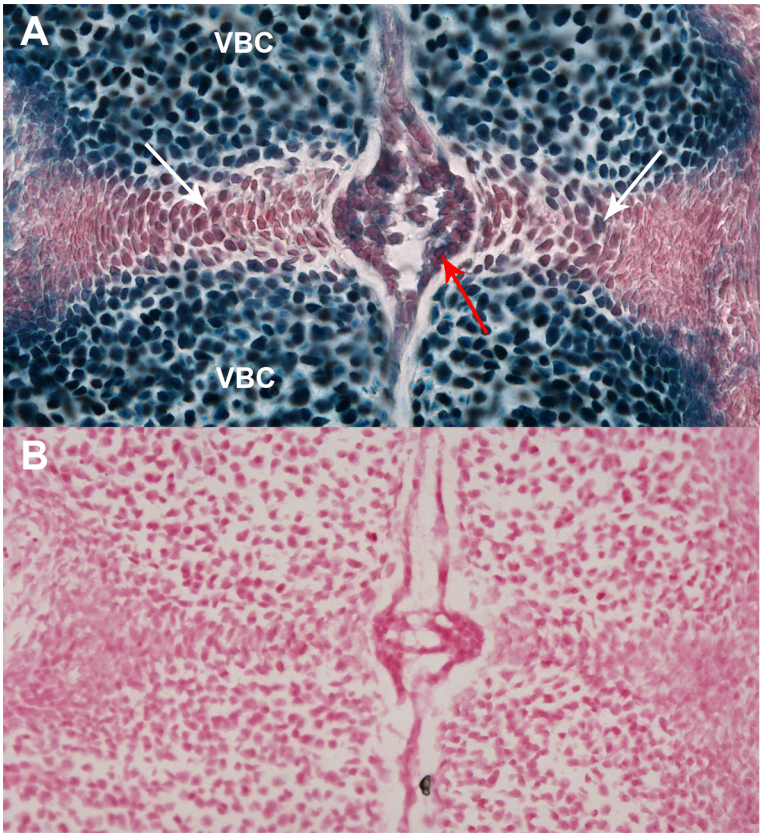

Supporting Figure 1. FLNB is expressed in the developing IVD. Distribution of FLNB in the E14.5 mouse IVD. (A) FLNB expression (blue stain) in a sagittal spinal section of E14.5 embryos. FLNB is expressed in the early developing annulus fibrosis (white arrows), nucleus pulposus (red arrow), and strongly in the developing vertebral body tissues (VBC). (B) Negative control for the X-gal stain of an E14.5 mouse sagittal section. Nuclei are stained red, VBC = Vertebral Body Cartilage.

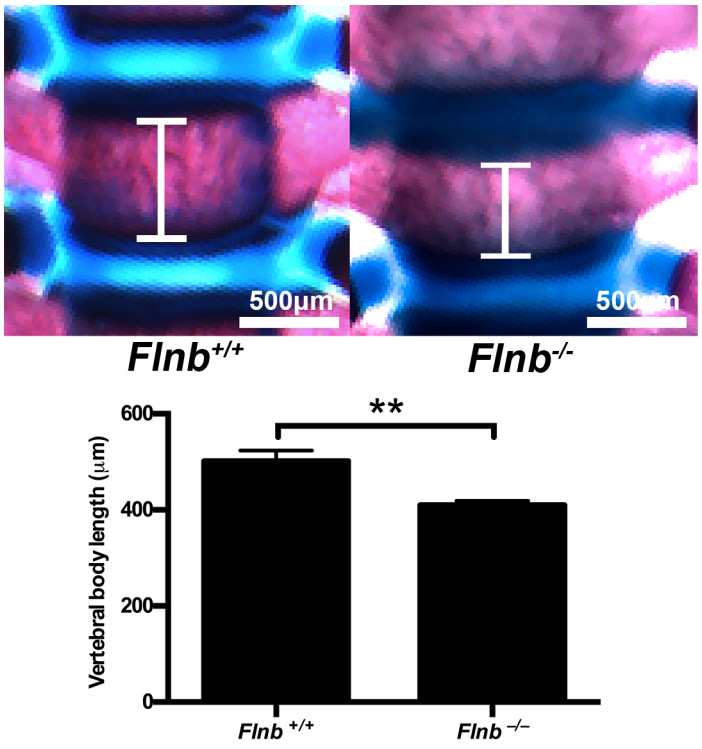

Supporting Figure 2. *Flnb*$^{-/-}$vertebral bodies exhibit decreased height. Cleared P15 vertebral bodies stained stained for cartilage proteoglycans (blue) and mineralized bone (red). *Flnb*$^{-/-}$ vertebral bodies exhibit decreased height when compared with *Flnb*$^{+/+}$. N = 3, ** = p<0.01.

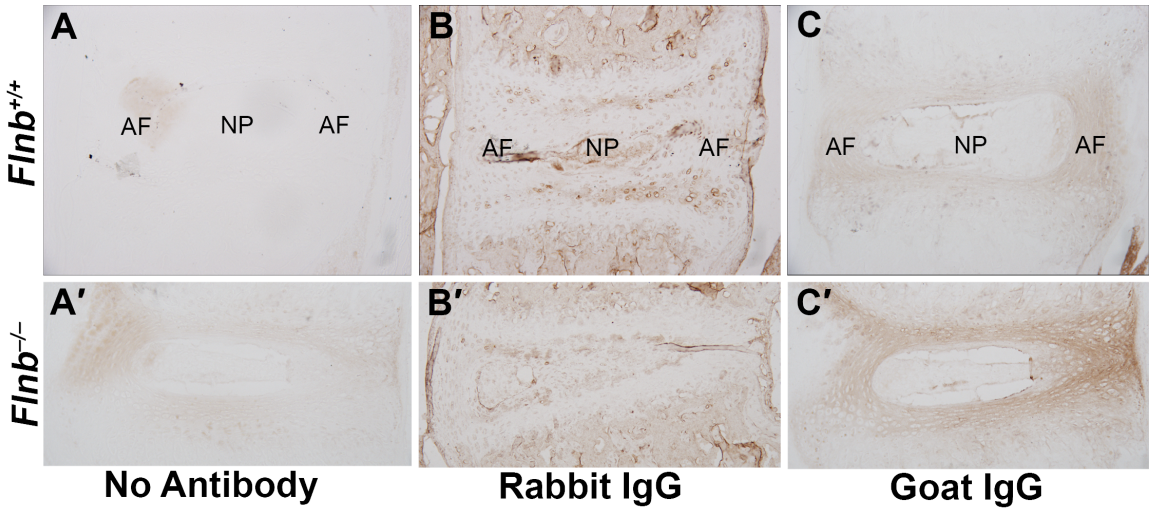

Supporting Figure 3. Negative and IgG controls for immunohistochemistry. Left: posterior, Right: anterior. (A, A′) Negative control IHC in P15 T7 IVD. (B, B′) IHC using rabbit whole IgG. (C, C′) IHC using goat whole IgG.